

The Evolution of Body Shape and Locomotion in Archosauria

Thesis submitted in accordance with the
requirements of the University of Liverpool for the
degree of Doctor of Philosophy

by

Sophie Macaulay

September 2018

ACKNOWLEDGMENTS

First and foremost, I must thank Karl, without whom this project (and certainly this thesis) wouldn't have happened. Your expertise and enthusiasm were never far away, but equally you gave me the freedom to find my own way. Between the speedy feedback and the Starbucks sessions, we've both managed to survive the last four years relatively unscathed. Here's to another 6 months! Thanks also to my secondary supervisors, for the provision of specimens and wide-ranging support - John Hutchinson, Emma Schachner and Phil Cox.

Much of this thesis could not have happened without inputs from various co-authors and collaborators who have all provided practical assistance in their own way. My thanks go to: Susie Maidment, Tom Maddox, Kayleigh Rose, Mary Blanchard, Robin Crompton, Charlotte Brassey, Bill Sellers, Jamie Gardiner, Vivian Allen, David Hone, Philip Brophy, Twycross Zoo, the World Museum Liverpool and my funder - ACCE.

Huge thanks to my PhD partners in crime - Abby and Ali. The PhD experience wouldn't have been the same without all the crazy antics, you kept me (in)sane through it all. The last four years would have been much duller without you both! Thanks also to all the other members of EMB through my time here.

I must also thank my family near and far for supporting me along the way. You were always keen to lend a hand, and you often succeeded (or at least listened attentively). Now you know far more about the biomechanics of bricks than you ever wanted to!

And last but not least thanks to all the other critters - the Sea Slugs, Unicorns and a brown bear. You know who you are, and I hope you know I couldn't have wished for better distractions!

ABSTRACT

The Evolution of Body Shape and Locomotion in Archosauria

Sophie Macaulay

Locomotion is essential to the survival of all organisms. Extant animals display a broad range of adaptations to a wide range of locomotor behaviours. Locomotion can be observed directly in living animals, but this is not the case for fossil taxa which are known from only skeletal material. An indirect route is therefore required to access this information on locomotor capabilities. Centre of mass is a key biomechanical parameter which effectively summarises body shape. Body shape influences, and is influenced by, the locomotor capabilities of an organism. Due to these close links, centre of mass has considerable potential value as an indirect route to information on locomotion in extinct species. One group of particular interest is Archosauria, which contains a host of unusual animals such as *Diplodocus*, *Pterodactylus* and *Tyrannosaurus*.

However, there are several obstacles which currently prevent centre of mass being used to its full potential in investigations of fossil taxa. Firstly, existing methods for estimating centre of mass position in fossils are limited either by substantial subjectivity, or by a lack of data on extant archosaurs. Additionally, the interpretation of any resulting predictions of centre of mass is hindered by a poor understanding of the links between centre of mass and specific locomotor behaviours, especially in volant organisms. It is therefore recognised that in order for the field to progress, more data are required on extant archosaurs.

This thesis seeks to address this issue by collecting a series of novel datasets on living archosaurs which are used as the foundation for improved predictions and interpretations of centre of mass data in extinct archosaurs. Three commonly used methods for centre of mass estimation in physical specimens were assessed in order to determine their absolute accuracies. The scales and digital methods were found to have high levels of accuracy and repeatability. Due to method specific limitations when applied to biological specimens, I concluded that the digital method is the preferred solution for this thesis. One benefit of digital modelling is the ease of alteration; small details can be added to models, but this is a time consuming process. This thesis examined the impact of different levels of model detail on whole body centre of mass. For example, air cavities (included as standard in current models), were found to exert less influence on centre of mass than a feathered integument (which has never before been quantified), calling standard modelling practices into question. Using digital models of 27 bird species, links were explored between centre of mass position and locomotor type. Species using volant behaviours were found to have more ventral centres of mass than their terrestrial counterparts; though this difference was not significant after accounting for phylogeny. This would provide greater manoeuvrability in flight. Finally, a new method for centre of mass estimation in fossils was developed and applied to fossil taxa. Compared to previous work, this method produced different centres of mass, with greater error margins. This is despite the fact that this new method benefits from greater objectivity and a quantitative grounding based on data from extant archosaurs. This suggests that previous studies have underestimated the biological variation present and their results should therefore be interpreted with caution.

This thesis provides the foundation for further work to continue to build towards better methods for centre of mass estimation in extinct taxa, and more confident biological interpretations of the resulting predictions.

LAY ABSTRACT

The Evolution of Body Shape and Locomotion in Archosauria

Sophie Macaulay

Locomotion is essential to the survival of all organisms. Living animals display a variety of locomotor behaviours, from swimming to running and flying. Locomotion can be observed directly in living animals, but this is not the case for extinct species which are only known from fossilised skeletons. An alternative route to information on their locomotion is therefore required. Many extinct animals are unlike anything alive today and, as such, they capture the imagination of scientists and the general public alike. One group of particular interest is Archosauria, which contains a host of unusual animals such as *Diplodocus*, *Pterodactylus* and *Tyrannosaurus*. Centre of mass is a key biomechanical parameter which summarises body shape. Body shape influences, and is influenced by, the locomotor capabilities of an organism. Due to these close links, centre of mass has considerable potential value as an indirect route to information on locomotion in extinct species.

However, there are several obstacles which currently prevent centre of mass being used to its full potential in investigations of extinct species. Firstly, existing methods for estimating centre of mass position in fossils are limited either by substantial subjectivity, or by a lack of data on their living relatives. Additionally, the interpretation of any resulting predictions of centre of mass is hindered by a poor understanding of the links between centre of mass and specific locomotor behaviours, especially in flying organisms. It is therefore recognised that in order for the field to progress, more information is required on living archosaurs (crocodylians and birds).

This thesis seeks to address this issue by collecting a series of novel datasets on living archosaurs which are then used as the foundation for improved predictions and interpretations of centre of mass data in extinct archosaurs. Three commonly used methods for centre of mass estimation in physical specimens were assessed in order to determine their absolute accuracies. The scales and digital methods were found to have high levels of accuracy and repeatability. Due to method specific limitations when applied to biological specimens, I concluded that the digital method is the best solution for this thesis. One benefit of digital modelling is the ease of alteration; small details can be added to models, but this is a time consuming process. This thesis examined the impact of different levels of model detail on whole body centre of mass. For example, air cavities (included as standard in current models), were found to exert less influence on centre of mass than the feathers of birds (which has never before been included). This calls standard modelling practices into question. Using digital models of 27 bird species, links were explored between centre of mass position and locomotor type. Species reliant on flight were found to have centres of mass which are closer to the spine than to the breast bone, in comparison to their terrestrial counterparts. This would provide greater manoeuvrability in flight. Finally, a new method for centre of mass estimation was developed and applied to extinct species. Compared to previous work, this method produced different centres of mass, with greater error margins. This is despite the fact that this new method benefits from greater objectivity and a host of data on living archosaurs. This suggests that previous studies have underestimated the biological variation present and their results should therefore be interpreted with caution.

This thesis provides the foundation for further work to continue to build towards better methods for centre of mass estimation in extinct species, and more confident biological interpretations of the resulting predictions.

TABLE OF CONTENTS

ACKNOWLEDGMENTS	i
ABSTRACT.....	ii
LAY ABSTRACT	iii
TABLE OF CONTENTS	iv
LIST OF TABLES.....	x
LIST OF FIGURES.....	xi
LIST OF EQUATIONS	xvi
LIST OF SUPPLEMENTARY INFORMATION	xvii
LIST OF APPENDICES.....	xix
CHAPTER 1 - INTRODUCTION AND BACKGROUND	1
1.1. Thesis introduction and overview.....	1
1.2. Background	2
1.2.1. <i>Mass properties and avian locomotion</i>	2
1.2.1.1. <i>CoM and locomotor biomechanics</i>	2
1.2.1.2. <i>Other mass properties and locomotor biomechanics</i>	6
1.2.1.3. <i>Mechanics of flight</i>	7
1.2.2. <i>Methods for CoM estimation</i>	11
1.2.2.1. <i>Physical methods</i>	11
1.2.2.2. <i>Digital methods</i>	16
1.2.3. <i>CoM and evolutionary studies</i>	26
1.2.4. <i>Systematics</i>	31
1.2.5. <i>Background summary</i>	34
1.3. Aims and Objectives.....	35

1.4.	Thesis Structure	36
1.4.1.	<i>Chapter 2</i>	36
1.4.2.	<i>Chapter 3</i>	36
1.4.3.	<i>Chapter 4</i>	37
1.4.4.	<i>Chapter 5</i>	37
1.5.	References	38

CHAPTER 2 - A quantitative evaluation of physical and digital approaches to centre of mass estimation 44

2.1.	Abstract.....	45
2.2.	Introduction	46
2.3.	Methodology.....	51
2.3.1.	<i>Specimens and background</i>	51
2.3.2.	<i>Physical CoM - suspension methodology</i>	55
2.3.3.	<i>Physical CoM - scales methodology</i>	58
2.3.4.	<i>Digital CoM - digital modelling</i>	63
2.3.5.	<i>Geometric centres</i>	64
2.4.	Results.....	67
2.4.1.	<i>Overview</i>	67
2.4.2.	<i>Bricks</i>	74
2.4.2.1.	<i>Geometric centres</i>	74
2.4.2.2.	<i>Suspension method</i>	74
2.4.2.3.	<i>Scales method</i>	75
2.4.2.4.	<i>Digital modelling</i>	75
2.4.2.5.	<i>Overview</i>	75
2.4.3.	<i>Birds</i>	76
2.4.3.1.	<i>Suspension method</i>	76

2.4.3.2. <i>Scales method</i>	76
2.4.3.3. <i>Digital modelling</i>	77
2.4.3.4. <i>Quantifying posture change</i>	77
2.4.3.5. <i>Overview</i>	78
2.5. Discussion.....	78
2.5.1. <i>Overview</i>	78
2.5.2. <i>Suspension methodology</i>	80
2.5.3. <i>Scales methodology</i>	82
2.5.4. <i>Digital modelling</i>	85
2.6. Conclusion.....	87
2.7. Supplementary Information.....	89
2.1. Appendices.....	95
2.2. References	98
CHAPTER 3 - Linking integument and body shape evolution in archosaurs	103
3.1. Abstract.....	104
3.2. Introduction	105
3.3. Methodology.....	106
3.3.1. <i>Integument mass property data</i>	106
3.3.2. <i>Statistical analysis of integument data</i>	110
3.3.3. <i>Digital modelling</i>	110
3.4. Results.....	114
3.4.1. <i>Do integument mass properties correlate with ecology and locomotion in archosaurs?</i>	114
3.4.2. <i>How does integument impact mass distribution in extant archosaurs?</i>	119
3.4.3. <i>How did feather evolution impact CoM position during theropod evolution?</i>	
	122

3.5. Discussion.....	123
3.5.1. <i>Ecological and functional adaptations in integumentary structures</i>	123
3.5.2. <i>Functional consequences of the evolution of body shape and integument</i>	125
3.6. Conclusion.....	128
3.7. Supplementary Information.....	130
3.8. References	160
CHAPTER 4 - Body shape and the evolution of locomotor diversity in birds.....	165
4.1. Abstract.....	166
4.2. Introduction	167
4.3. Methodology.....	170
4.3.1. <i>Digital modelling: calculating body segment mass properties and whole body CoM</i>	170
4.3.2. <i>Density data</i>	176
4.3.3. <i>Statistical analyses</i>	178
4.4. Results.....	179
4.4.1. <i>CoM position across Aves</i>	179
4.4.1.1. <i>Does CoM correlate with locomotor style?</i>	179
4.4.1.2. <i>What drives differences in whole body CoM position?</i>	182
4.4.1.3. <i>Does CoM correlate with body mass?</i>	187
4.4.2. <i>Avian body density</i>	190
4.4.2.1. <i>Segment specific density data</i>	190
4.4.2.2. <i>Whole body density in 25 bird species</i>	190
4.4.3. <i>Assessing modelling approaches</i>	190
4.4.3.1. <i>Segment closing technique - validity assessment</i>	190
4.4.3.2. <i>Comparing mass property estimates from heterogeneous and homogeneous models</i>	195

4.5.	Discussion.....	197
4.5.1.	<i>Does whole body CoM position differ between forelimb and hindlimb dominated species?.....</i>	197
4.5.2.	<i>Do birds specialised for novel behaviours possess unique CoM positions? .</i>	202
4.5.3.	<i>Does density assignment affect the ability of models to predict mass properties?.....</i>	203
4.6.	Conclusion.....	206
4.7.	Supplementary Information.....	207
4.8.	References	209
CHAPTER 5 - A new method for predicting mass distribution in extinct archosaurs.....		212
5.1.	Abstract.....	213
5.2.	Introduction	214
5.3.	Methodology.....	219
5.3.1.	<i>Determining ratio of skeletal volume to skin volume in extant taxa</i>	219
5.3.2.	<i>Application to extinct taxa</i>	221
5.4.	Results.....	227
5.4.1.	<i>Establishing relationships between skeletal volume and skin volume in extant taxa</i>	227
5.4.2.	<i>Method validation - predicting CoM in extinct taxa using convex hulling... </i>	228
5.4.2.1.	<i>Segment CoM positions.....</i>	228
5.4.2.2.	<i>CoM estimates versus Allen et al. (2013)</i>	231
5.5.	Discussion.....	233
5.5.1.	<i>Segment specific relationships between skeletal volume and skin volume .</i>	233
5.5.2.	<i>Method validation - predicting CoM in extinct taxa using extant-based convex hulling</i>	234
5.5.2.1.	<i>Using convex hull CoMs as segment CoM positions</i>	234

5.5.2.2.	<i>Selection of segment ‘types’ for extinct taxa</i>	236
5.5.2.3.	<i>Comparisons to existing work and future steps</i>	236
5.6.	Conclusion.....	238
5.7.	Supplementary Information.....	240
5.8.	Appendices.....	248
5.9.	References	252
CHAPTER 6 - DISCUSSION		256
6.1.	Overview	256
6.2.	Methods for CoM estimation.....	257
6.2.1.	<i>Physical methods for CoM estimation</i>	257
6.2.2.	<i>Digital method for CoM estimation</i>	258
6.2.3.	<i>Exploring refinements of digital methods - integument</i>	259
6.3.	CoM position and locomotion	262
6.4.	Improving CoM estimation in extinct taxa.....	264
6.5.	References	267
CHAPTER 7 - CONCLUSION		268
THESIS REFERENCES		270

LIST OF TABLES

Table 2.1: Data on body mass and approximate dimensions for the six specimens studied here.....	52
Table 2.2: Details of the density data used in the sensitivity analysis.....	65
Table 2.3: 3D distances from brick geometric centre (CoM_G) to the centres of mass predicted by the methodologies examined here for the three brick specimens.....	72
Table 2.4: 3D distances from the digital centre of mass predicted by our original model (CoM_{D1}) to the centres of mass predicted by the methodologies examined here for the three bird specimens.....	73
Table 4.1: Details on the 27 specimens modelled here, including measured whole body mass (kg) and locomotor category.....	171
Table 4.2: Details on the five bird specimens for which segment specific densities were derived.....	177
Table 4.3: Table showing the results of Spearman's rank test, assessing the correlations of various segment mass properties with whole body centre of mass in the dorso-ventral direction. p^2 indicates the percentage of CoM variation which is accounted for by a given variable. Significant results (at $p < 0.05$) are highlighted in red.....	185
Table 4.4: Table showing the results of Spearman's rank test, assessing the correlations of various segment mass properties with whole body centre of mass in the crano-caudal direction. p^2 indicates the percentage of CoM variation which is accounted for by a given variable. Significant results (at $p < 0.05$) are highlighted in red.....	186
Table 4.5: Table showing the body density (kgm^{-3}) values calculated by dividing measured body mass by model skin volume.....	192
Table 4.6: Table showing segment volumes (mm^3), segment CoMs (mm) and whole-body CoM estimates (mm) when all body segments are closed using three alternative methods (Geomagic, alpha shapes and convex hulls). Where +x is right, +y is dorsal, +z is caudal. See Figure 4.9 for visualisation of these differences.....	194
Table 5.1: Details on the reptile specimens used in extant dataset here, including measured whole body mass (kg) where available.....	220

LIST OF FIGURES

- Figure 1.1:** A: Taken from Google Images. Showing differences in areas of support for quadrupeds versus bipeds. The centre of mass (indicated as black circle) must lie within the base of support in order for an organism to be stable at rest. B: Taken from Carrano and Biewener (1999). For an organism to maintain stability in walking, whole body centre of mass must be positioned over the supporting foot during the stance phase. This is shown in a natural state in chickens in (a). Alterations of whole body CoM position must result in postural changes (e.g. b and c) in order to maintain stability. C: Taken from Gatesy (2009). Showing possible limb postures for *Tyrannosaurus* (b & d), as determined by constraint based mapping of joint angles (a). The combined effects of centre of mass position and muscle moment arms result in differences to locomotor ability, as indicated by ground reaction force (GRF) (c). 3
- Figure 1.2:** A: Taken from Thomas (2001). In aerial locomotion, rotation can occur about 3 axis which produce pitch, yaw and roll movements. B: Taken from Thomas (2001). Centre of mass position (circle) along the crano-caudal axis varies across species. The majority of species have been found to have CoMs which are cranial to the wing centre (cross). The relationship between centre of mass and wing position determines stability in pitching motions. C: Schematic of an organism in lateral view showing the influence of dorso-ventral centre of mass position. A greater distance between the shoulder joint (white circle) and the centre of mass (crossed circle) means a larger moment arm (red arrow) and therefore greater inertial resistance to rolling motions. This 'pendulum' effect can be observed in paragliders and ships, and acts to provide passive roll stability..... 5
- Figure 1.3:** A: Schematic showing the forces acting on a bird in flight. B: Bird wings from three species scaled to the same length (from Kardong, 2012). The different locomotor modes of the hummingbird and the albatross are reflected in the relative length of the various wing segments. C: Two bird species with different aspect ratios (modified from Rayner, 1988). The high aspect ratio wing of the albatross facilitates soaring, while the lower aspect ratio wing of the eagle provides greater manoeuvrability in flight. 8
- Figure 1.4:** Taken from Ozkaya (2012). Showing three physical methods for determining centre of mass position. A: suspension method, when the object is suspended from points O and Q, the centre of mass (C) is located at the intersection of lines aa and bb. B: balance board method. C: scales technique, where the object (exerting force W_p) is placed on a board (exerting force W_b) balanced on a knife edge (A) and a scale (B) which are a known distance (l) apart. The distance from the end of the board to the centre of mass (x_{cg}) can then be calculated..... 13
- Figure 1.5:** Taken from Henderson (1999). Showing the stages of the mathematical slicing method. Body outline is created (A) and split into sections (B) from which the final model is constructed and whole body centre of mass (indicated by '+') can be calculated (C). 17
- Figure 1.6:** Taken from Hutchinson et al. (2011). Showing the stages of the manual shape fitting method using octagonal hoops in this case. The skeletal material is digitalised and put into a standard posture (A), hoops are applied around the skeleton to define the soft tissue outline (B) and air spaces (C) and a final skin outline is created by lofting a surface between the hoops (D). 19
- Figure 1.7:** Taken from Sellers et al. (2012) and Brassey and Gardiner (2015). A: The stages of the 'mathematical shape fitting' method using convex hulls. The original skeletal material

(Aa) is digitalised (Ab) and convex hulls are applied around the skeletal material for each segment (Ac). **B**: A ‘family’ of alpha shapes for the 2D object in (Be). A infinite alpha value gives a convex hull (Ba), while reducing alpha relaxes the outer boundary of the alpha shape, producing gradually more detailed representations of the original object (Bb-d).22

Figure 1.8: **A-C:** Taken from Allen et al. (2013). 16 specimens across Archosauria (**A**) were modelled using a manual shape fitting approach to predict “best guess” CoM positions, along with CoMs skewed maximally in the cranio-caudal and dorso-ventral directions in order to generate error margins (**B & C**). **D & E:** Taken from Bates et al. (2016). 22 specimens covering the sauropod radiation (**D**) were modelled using a mathematical shape fitting approach to predict “best guess” CoM positions, along with CoMs skewed maximally in the cranio-caudal direction in order to generate error margins (**E**).28

Figure 1.9: Schematic displaying the phylogenetic relationships between the three extant groups and the fossil species which are studied in this thesis.32

Figure 2.1: Pictures showing marker positions (silver balls indicated by white arrows) in bricks (**A**), and birds (**B**) as well as the standardised posture used for all bird specimens.54

Figure 2.2: Stages of the suspension methodology performed in this study. **A:** Suspension of object for Qualisys capture, at least three different suspension positions were captured for each object. **B:** After the multiple Qualisys runs for the same specimen were matched, the specimen markers are aligned, and the various lines of suspension are now distributed around the specimen. **C & D:** Two hypothetical 3D lines plotted in two, 2D graphs. Note that in (**C**), the lines have equal x values at y=0.5, but at y=0.5 in (**D**), they have different z values, and therefore do not intersect in 3D space. **E:** Two hypothetical, non-intersecting curves, highlighting the point of closest approach (CPoA) on each line, and the resulting mean CPoA.56

Figure 2.3: Stages of the scales methodology performed in this study. **A:** Photograph of the experimental set-up, with the duck specimen. **B:** Schematic of experimental set-up, showing specimen resting on plank, lying on the two scales. The distance between supports (L) and distance from proximal plank edge to proximal support (ΔL) are indicated. These data combined with mass readings from the two scales enable calculations of CoM position. **C:** Rendering of Brick1, after marker data from three data captures was matched, showing the position of the three planks aligned with the three axes, and the three, 1D CoM positions plotted. These are then combined to give a 3D, final CoM prediction from the method.....59

Figure 2.4: Render of Brick1 from the top (**A**), left side (**B**) and front (**C**) depicting the method for calculating the geometric centre (CoM_G). This was calculated by taking the mean of three pairs of Qualisys markers, one pair per axis. CoM_x , CoM_y and CoM_z then combine to give the final xyz co-ordinates for a 3D CoM_G66

Figure 2.5: Predicted CoM positions displayed on renders of Brick1 (**A-C**), Brick2 (**D-F**) and Brick3 (**G-I**), shown from the left (**A, D, G**), front (**B, E, H**) and top (**C, F, I**). Predicted CoM positions are shown for each methodology, coloured according to the key. In cases where multiple CoM positions were available for the initial suspension and scales methods, only the CoM from the first runs are displayed here, for clarity.68

Figure 2.6: Predicted CoM positions displayed on renders of chicken (**A-C**), buzzard (**D-F**) and duck (**G-I**), shown in cranial view (**A, D, G**), left lateral view (**B, E, H**) and dorsal view (**C, F, I**). Predicted CoM positions are shown for each methodology, coloured according to the key. In the chicken and buzzard, multiple suspension CoMs are shown along with multiple scales CoMs in the chicken.....69

Figure 2.7: **A:** Graph displaying 3D distances from brick geometric centre (CoM_G) to the CoM positions predicted by the methodologies listed on the x axis. **B:** Graph displaying 3D distances from our ‘best guess’ bird digital CoM (CoM_{D1}) to the CoM positions predicted by the methodologies listed on the x axis. **(C)** 3D differences between geometric centre (bricks)/best guess digital CoM (birds) and CoM predictions produced by the methods studied here, normalised by maximum side length (bricks)/cranio-caudal body length (birds).70

Figure 2.8: Renders of Brick1 (**A-C**), chicken (**D-F**) and buzzard (**G-I**) displaying the broad spread of centre of mass positions predicted by the suspension methodology with three repeats (orange) and ten repeats (red).83

Figure 3.1: **A:** Diagrammatic representation of data collection protocol for integument mass properties. Mass and thickness measures were taken for the whole sample, and retaken after plucking of body feathers. Surface area calculated for remaining skin sample. **B:** Digital model of iguana model in standardised posture. Shown from left to right as: skeleton with air cavities (in blue), overlying skin, and skin with centre of mass positions indicated. **C:** Digital model of *Microraptor* model in standardised posture. Shown from left to right as: skeleton with air cavities (in blue), overlying skin, and skin with centre of mass positions indicated. **D:** Schematic representing the phylogenetic relationships of the species modelled in this study (not to scale).107

Figure 3.2: Flight feather properties (**A:** density, **B:** length, **C:** thickness, **D:** surface area) showing differences between birds of different locomotor types. Significant differences were determined and are indicated by text over each bar (where * indicates significant difference to all other groups, and letters indicate significant differences to another group - B: Burst-adapted flight, C: Continuous flapping, F: Flap-gliding, S: Soaring, T: Terrestrial). N = 140 flight feathers from 22 specimens.115

Figure 3.3: Integument properties (**A:** scaly skin density, **B:** feather density, **C & D:** feather thickness, **E & F:** skin thickness) showing differences between different taxonomic groups (**A, D, E**), different feather types (**B, C**) and different locomotor types (**F**). Significant differences were determined and are indicated by text over each bar (where * indicates significant difference to all other groups, and letters indicate significant differences to another group). Abbreviations for taxonomic groups in **D & E** - A: Accipitriformes, Ca: Casuariiformes, Co: Columbiformes, F: Falconiformes, Ga: Galliformes, Gr: Gruiformes, Pa: Passeriformes, Ps: Psittaciformes, Su: Struthioniformes. N = 152 scaly skin samples from 22 specimens; 155 feathered skin samples from 27 specimens.117

Figure 3.4: CoM positions for all models, normalised by body mass^{0.33}, with convex hulls around specimens from the same groups. Displayed **A:** relative to flesh CoM (displayed as ‘x’, set to 0 0 0 in x y z coordinates for all models) and **B:** relative to right hip (displayed as ‘x’, at 0 0 0 in xyz coordinates for all models). Different colours represent different taxa as per the

legend. Lightly shaded icons: flesh only models; hollow icons: flesh and air cavities; filled icons: flesh, air cavities and integument. 120

Figure 3.5: Digital models showing skin outlines (grey) and air cavities (blue) for *Cœlophysis* (maximum model) (**A**), *Microraptor* (maximum model) (**B**), *Yixianornis* (maximum model) (**C**), alligator (**D**) and duck (**E**). Centre of mass positions indicate by coloured spheres, see key for detail. Models are not to scale. 121

Figure 4.1: Tinamou model shown in the standardised posture used in this study, shown as skeletal material and associated skin outlines. 174

Figure 4.2: Phylogeny representing the 27 specimens used in this study, labelled with the names of their respective Orders. Based on Jetz et al. (2012). 180

Figure 4.3: Size corrected centre of mass data for 27 bird species, grouped by locomotor type. Centre of mass position is expressed relative to the right hip (at 0, 0)..... 181

Figure 4.4: First mass moment data in the crano-caudal direction plotted on the y-axis for each of the 27 specimens on the x-axis (see Table 4.1 for specimen numbers), for each body segment. A positive FMM indicates a cranial pull, negative FMM indicates a caudal pull. 183

Figure 4.5: First mass moment data in the dorso-ventral direction plotted on the y-axis for each of the 27 specimens on the x-axis (see Table 4.1 for specimen numbers), for each body segment. A positive FMM indicates a ventral pull, negative FMM indicates a dorsal pull. 184

Figure 4.6: Whole body mass plotted against raw data on crano-caudal (left), and dorso-ventral (right) centre of mass position. Negative values indicate shifts in a cranial and ventral direction respectively. Data points are colour coded according to locomotor categories: terrestrial (green), diving (blue) and volant (orange). Data points of interest are labelled with specimen names. 188

Figure 4.7: Whole body mass plotted against size normalised data on crano-caudal (left), and dorso-ventral (right) centre of mass position. Negative values indicate shifts in a cranial and ventral direction respectively. Trendlines are for the whole dataset. Data points are colour coded according to locomotor categories: terrestrial (green), diving (blue) and volant (orange). Data points of interest are labelled with specimen names. 189

Figure 4.8: Segment specific and whole body density data measured from the cadavers of five specimens..... 191

Figure 4.9: **A & B:** Example skin segments closed in Geomagic (left), using an alpha shape (centre) and using convex hulling (right). The segments shown are the upper arm (**A**) and thigh (**B**) of a buzzard. **C:** Three alternative whole body CoM predictions produced by applying the three alternative methods for closure to all body segments of a buzzard (red: closed segments, yellow: alpha-shaped segments, green: hulled segments). 193

Figure 4.10: Raw centre of mass position plotted relative to the right hip (at 0, 0) for homogeneous and heterogeneous version of models (see key)..... 196

Figure 4.11: Difference between measured body mass, and predicted body mass, displayed as a percentage of measured body mass. All differences shown as positive changes, in enable easier comparison of error magnitudes.198

Figure 5.1 (i): Plots showing the relationship between skeletal hull volume and skin volume for individual body segments. **A:** head, **B:** neck, **C:** torso, **D:** tail, **E:** arm, **F:** forearm, **G:** hand, **H:** thigh, **I:** shank, **J:** tarsometatarsal/metatarsals, **K:** toes.....224

Figure 5.1 (ii): Plots showing the relationship between skeletal hull volume and skin volume for individual body segments. **A:** head, **B:** neck, **C:** torso, **D:** tail, **E:** arm, **F:** forearm, **G:** hand, **H:** thigh, **I:** shank, **J:** tarsometatarsal/metatarsals, **K:** toes.....225

Figure 5.1 (iii): Plots showing the relationship between skeletal hull volume and skin volume for individual body segments. **A:** head, **B:** neck, **C:** torso, **D:** tail, **E:** arm, **F:** forearm, **G:** hand, **H:** thigh, **I:** shank, **J:** tarsometatarsal/metatarsals, **K:** toes.....226

Figure 5.2: Differences between whole body CoMs derived from skeletal segment CoMs (blue spheres) and skin segment CoMs (red spheres), shown in the context of each specimen (**A:** iguana, **B:** alligator, **C:** rhea, **D:** buzzard).229

Figure 5.3: Renders in lateral view of the skeletal convex hulls of five fossils species studied here. Showing whole body CoM positions estimated using: best guess models (coloured spheres), error from predictive equations (lighter coloured spheres), maximum cranio-caudal spread (black spheres) and maximum cranio-caudal spread from models of Allen et al. (2013) (white spheres) to estimate segment volumes. **A:** *Plateosaurus*, **B:** *Coelophysis*, **C:** *Allosaurus*, **D:** *Microraptor*, **E:** *Yixianornis*.232

LIST OF EQUATIONS

Equation 2.1.....	61
Equation 2.2.....	64
Equation 3.1.....	113
Equation 3.2.....	139
Equation 4.1.....	176
Equation 4.2.....	179
Equation 5.1.....	223

LIST OF SUPPLEMENTARY INFORMATION

Supplementary Information 2.1	89
Supplementary Information 2.2	90
Supplementary Information 2.3	91
Supplementary Information 2.4	92
Supplementary Information 2.5	93
Supplementary Information 2.6	94
Supplementary Text 3.1	130
Supplementary Text 3.2	133
Supplementary Text 3.3	136
Supplementary Text 3.4	139
Supplementary Figure 3.1	144
Supplementary Figure 3.2	146
Supplementary Table 3.1	147
Supplementary Table 3.2	156
Supplementary Table 3.3	157
Supplementary Table 3.4	158
Supplementary Table 3.5	159
Supplementary Information 4.1	207
Supplementary Information 4.2	208
Supplementary Information 5.1	240
Supplementary Information 5.2	241
Supplementary Information 5.3	242

Supplementary Information 5.4 (i)	243
Supplementary Information 5.4 (ii)	244
Supplementary Information 5.4 (iii)	245
Supplementary Information 5.5	246
Supplementary Information 5.6	247

LIST OF APPENDICES

Appendix 2.1.....	95
Appendix 5.1.....	248

CHAPTER 1 - INTRODUCTION AND BACKGROUND

1.1. Thesis introduction and overview

Locomotion is fundamentally important to all organisms, enabling a host of essential behaviours - such as feeding, reproduction and survival. It determines the interactions between organisms and subsequently whole ecosystem dynamics. The evolution of locomotor behaviours is therefore intertwined with the evolution of all vertebrate species. Locomotor behaviours frequently place harsh demands on the vertebrate skeleton, meaning locomotor demands are reflected in organisms' anatomy. In extant species, locomotion and whole organism morphology can be quantified directly, and thus the links between form and function can be directly tested. However, in extinct taxa, locomotion cannot be observed directly. One factor influencing, and influenced by, the locomotor mode of an organism is mass distribution. Mass distribution, summarised by whole body centre of mass (CoM), represents an indirect route to information on locomotor capabilities in fossil species (e.g. Henderson, 2018, Sellers et al., 2017, Snively et al., 2018). However, in fossil taxa, mass properties must be estimated from skeletal material only, which is far from a simple task.

CoM is a fundamentally important biomechanical parameter. At the level of the whole organism, it is a key determinant of stability at rest and in motion. Through its impact on a host of factors, including posture, CoM has a substantial impact on the locomotor capabilities of an organism. CoM has been estimated using a variety of methods across a wide range of extant and extinct species, but no comprehensive review of these methods currently exists. A range of digital methods have been developed with the aim of improving mass property (body mass, CoM etc) estimates in fossil species. However, these methods bring their own limitations, which are currently poorly explored. The primary issue is a reliance on subjectively generated skin outlines, and a lack of data on modern species to enable

interpretation of resulting CoM predictions. When existing digital methods are applied in an evolutionary context, they are therefore accompanied by considerable error margins. This undermines any conclusions drawn, and potentially obscures more subtle trends in body shape evolution.

This thesis will examine the relationship between whole body morphology and CoM, and the links to the evolution of locomotion diversity present in modern birds. This chapter provides background information on previously published work in this field, outlining past successes and weaknesses. In my subsequent review of previous work, I identify key gaps in the area related to CoM estimation and interpretation of the resulting CoM data. From a methodological perspective there is currently considerable uncertainty regarding the accuracy of frequently used methods for CoM estimation, in addition to the effects of heterogeneous density and explicit inclusion of key organ systems. From a biological and evolutionary perspective, there is currently limited understanding of how adaptations to whole body shape are correlated to locomotion in living birds. This hinders our understanding of living birds, but also undermines our ability to predict body shape and locomotion in closely related fossil species. A literature review in Section 1.2 culminates in a series of specific research objectives (Section 1.3) which form the basis for the novel independent research carried out in Chapters 2-5 of this thesis.

1.2. Background

1.2.1. Mass properties and avian locomotion

1.2.1.1. CoM and locomotor biomechanics

The CoM of an object can be thought of as the point at which all its mass is concentrated (Özkaya et al., 2012). In a terrestrial organism, the CoM must lie over the area of support

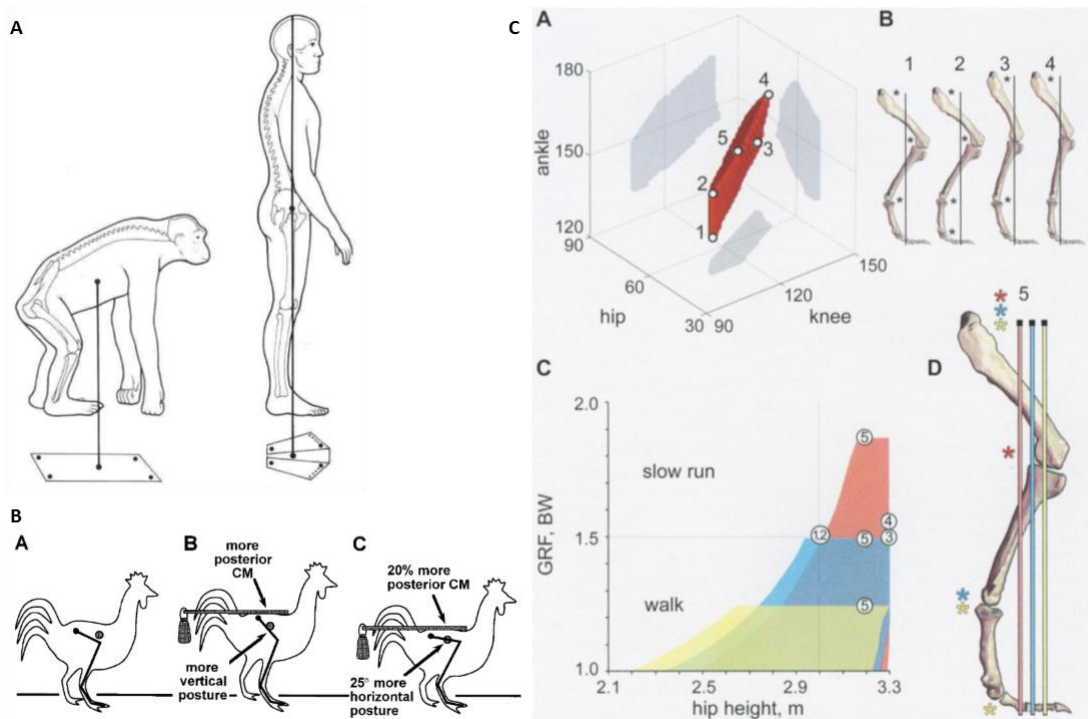


Figure 1.1: **A:** Taken from Google Images. Showing differences in areas of support for quadrupeds versus bipeds. The centre of mass (indicated as black circle) must lie within the base of support in order for an organism to be stable at rest. **B:** Taken from Carrano and Biewener (1999). For an organism to maintain stability in walking, whole body centre of mass must be positioned over the supporting foot during the stance phase. This is shown in a natural state in chickens in (a). Alterations of whole body CoM position must result in postural changes (e.g. b and c) in order to maintain stability. **C:** Taken from Gatesy (2009). Showing possible limb postures for *Tyrannosaurus* (b & d), as determined by constraint based mapping of joint angles (a). The combined effects of centre of mass position and muscle moment arms result in differences to locomotor ability, as indicated by ground reaction force (GRF) (c).

defined by the limbs in order for the organism to be stable at rest (Figure 1.1A). For example, a CoM located far cranial to the hindfeet requires a quadrupedal posture to be adopted; while if the hindfeet can be placed under the CoM, bipedal behaviours are possible (Figure 1.1A). Because of this, CoM exerts a substantial influence over the posture of an organism at rest and in motion. This is especially true in bipeds, where the area of support defined by the feet is much smaller, and CoM therefore imposes stricter constraints on posture (Figure 1.1A). This principle is exemplified by the extreme posture shift which occurred alongside drastic changes to CoM position in bird line archosaurs. Along the ancestral bird line, within non-avian theropods, body plan underwent drastic changes - the forelimbs, head and neck complexes were enlarged, while the tail was reduced - resulting in a cranial CoM shift (Allen et al., 2013). In association with this CoM shift, hindlimb posture changed from a relatively straight-legged stance, to that seen in modern birds - a virtually horizontal femur and flexed hip and knee joints (Alexander, 2006, Gatesy and Biewener, 1991) (Figure 1.1B). In this way, the gait kinematics and kinetics seen in extant birds came to evolve, in which locomotion is driven by flexion-extension at the knee and ankle, rather than at the hip as it was in their extinct, long tailed bipedal ancestors (Gatesy, 1990).

The CoM shift seen in bird line archosaurs has been relatively well studied, and the repercussions of this shift for terrestrial locomotion have been explored. For example, the downstream effects of whole body CoM position have been quantitatively examined in factors such as posture (Gatesy et al., 2009) and locomotor ability (Bates et al., 2010), highlighting the non-trivial effects CoM has on higher level biological conclusions (see Figure 1.1C for example, and Section 1.2.3 for further discussion). This underlines the importance of producing and utilising correct CoM estimates in studies of fossil taxa. However, studies investigating links between CoM and aerial locomotion are rare (with the exception of Henderson, 2010, Thomas and Taylor, 2001). CoM position informs the stability and

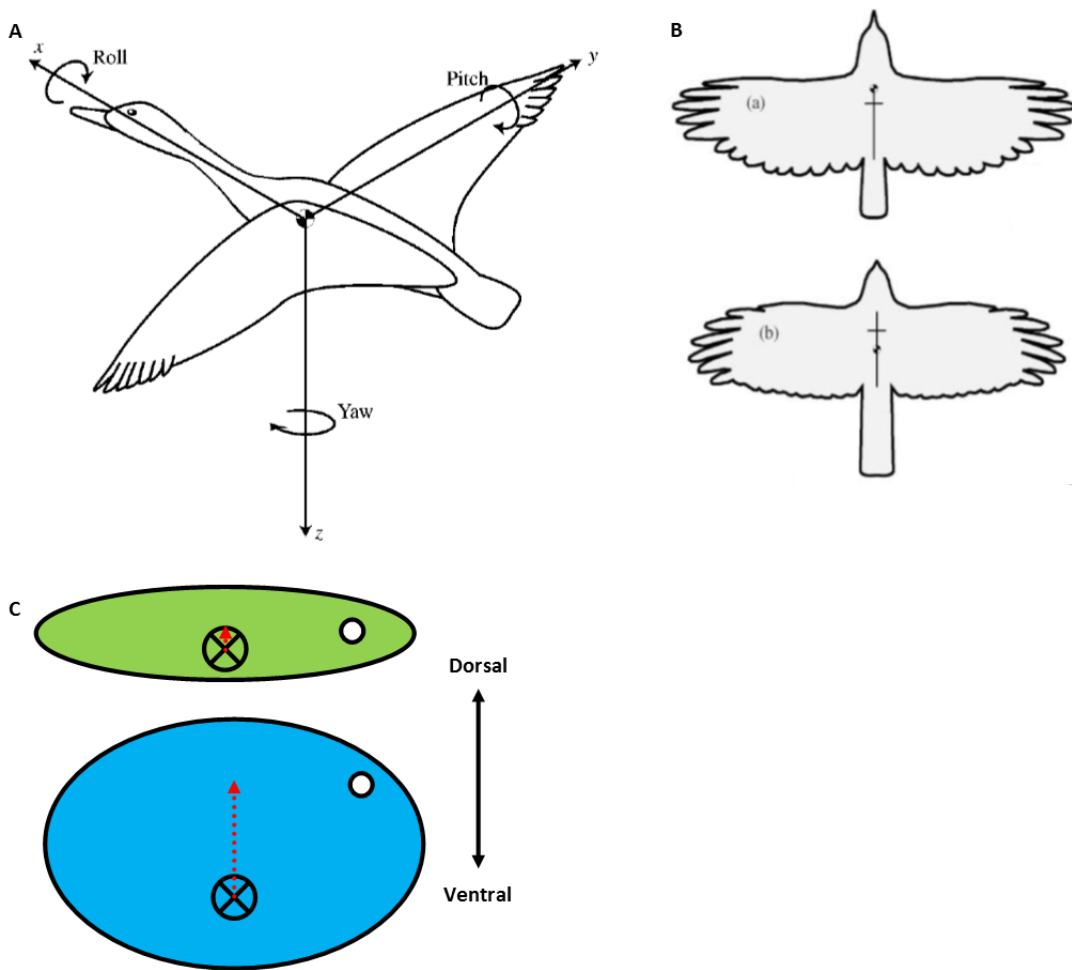


Figure 1.2: **A:** Taken from Thomas (2001). In aerial locomotion, rotation can occur about 3 axis which produce pitch, yaw and roll movements. **B:** Taken from Thomas (2001). Centre of mass position (circle) along the cranio-caudal axis varies across species. The majority of species have been found to have CoMs which are cranial to the wing centre (cross). The relationship between centre of mass and wing position determines stability in pitching motions. **C:** Schematic of an organism in lateral view showing the influence of dorso-ventral centre of mass position. A greater distance between the shoulder joint (white circle) and the centre of mass (crossed circle) means a larger moment arm (red arrow) and therefore greater inertial resistance to rolling motions. This ‘pendulum’ effect can be observed in paragliders and ships, and acts to provide passive roll stability.

manoeuvrability of an organism in-flight (Figure 1.2). Any turning moments generated about the centre of lift of the wings must be countered in order for a bird to maintain steady locomotion in the air. A CoM which lies close to the wings, minimises the active inputs required to correct for any undesired rotations (Thomas and Taylor, 2001). However, in the dorso-ventral direction, a CoM which is more distant to the wing centre can provide passive benefits - a greater inertial resistance to motion results in greater stability at the expense of manoeuvrability (Figure 1.2C). Extant bird species vary considerably in the amount of time they spend flying, and the way in which they fly. Some birds have taken this to the extreme, having reverted back to the ancestral state of terrestrial bipedalism (e.g. ratites), but still retain the characteristic avian flexed hindlimb posture suggestive of a more cranial CoM. However, previous studies (Henderson, 2010, Thomas and Taylor, 2001) suggest that CoM position varies within Aves, potentially reflecting differences in locomotor capabilities.

If links between CoM position and locomotor style could be established in extant birds, CoM could be used as an indirect route to information about both the terrestrial and aerial locomotor capabilities of extinct ‘transitional’ species, such as *Microraptor* and *Archaeopteryx*. The locomotion, and particularly the flight capabilities, of these taxa have been extensively debated and remain controversial (e.g. Alexander et al., 2010, Chatterjee and Templin, 2007, Dyke et al., 2013, Koehl et al., 2011). However, at present more work is required in order for CoM position to make a significant contribution to this debate.

1.2.1.2. Other mass properties and locomotor biomechanics

It should be noted that CoM, though the main focus of this thesis (see Section 1.2.1.1), it is only one of a host of mass property which all act to determine the locomotor capabilities of an organism. For example, the simple metric of whole body mass determines the force generation required for take-off, and for sustained flight. In combination with wing area,

body mass determines wing loading which in turn determines the locomotor behaviours an individual is capable of (see Section 1.2.1.3 for more detail). Moment of inertia (Mol) is a more detailed mass property, which describes the distance between the centre of mass and the pivot point of a segment. A CoM close to the pivot produces a low Mol, meaning that for a given force input the resulting angular velocity of the segment will be greater. Alternatively, for an organism which must generate a set angular velocity (e.g. in order to move a segment in order to achieve a given locomotor behaviour), a low Mol means less force is required to be generated. Through Mol, segment CoM position therefore directly impacts the locomotor capabilities of an individual.

1.2.1.3. *Mechanics of flight*

Birds are one of only three vertebrate groups to have evolved powered flight, alongside the pterosaurs and bats. Flight is a complex, energy intensive locomotor behaviour which places a wide range of demands on an organism, and requires a suite of specialisations. The successful development of flight was a key factor in enabling the extensive radiation of birds into over 10,000 species, occupying a diverse range of niches across all seven continents.

For powered flight to be successful, an organism must generate sufficient lift and thrust in order to counter the forces of gravity and drag respectively (Figure 1.3A). These forces are inherently linked to morphology and mass properties. Bird wings are a biological aerofoil, their anatomy forces air to travel faster over the upper surface than the lower surface of the wing (Kardong, 2012). This generates a pressure difference between the upper and lower surfaces of the wing, which produces lift. This aerofoil is achieved by a combination of soft tissue and flight feather morphology. Lift is required to counter the force of gravity, and enables birds to stay aloft. Birds with lower body masses are subjected to lower forces by gravity, and therefore need less lift to fly. Birds must also generate thrust in order to move

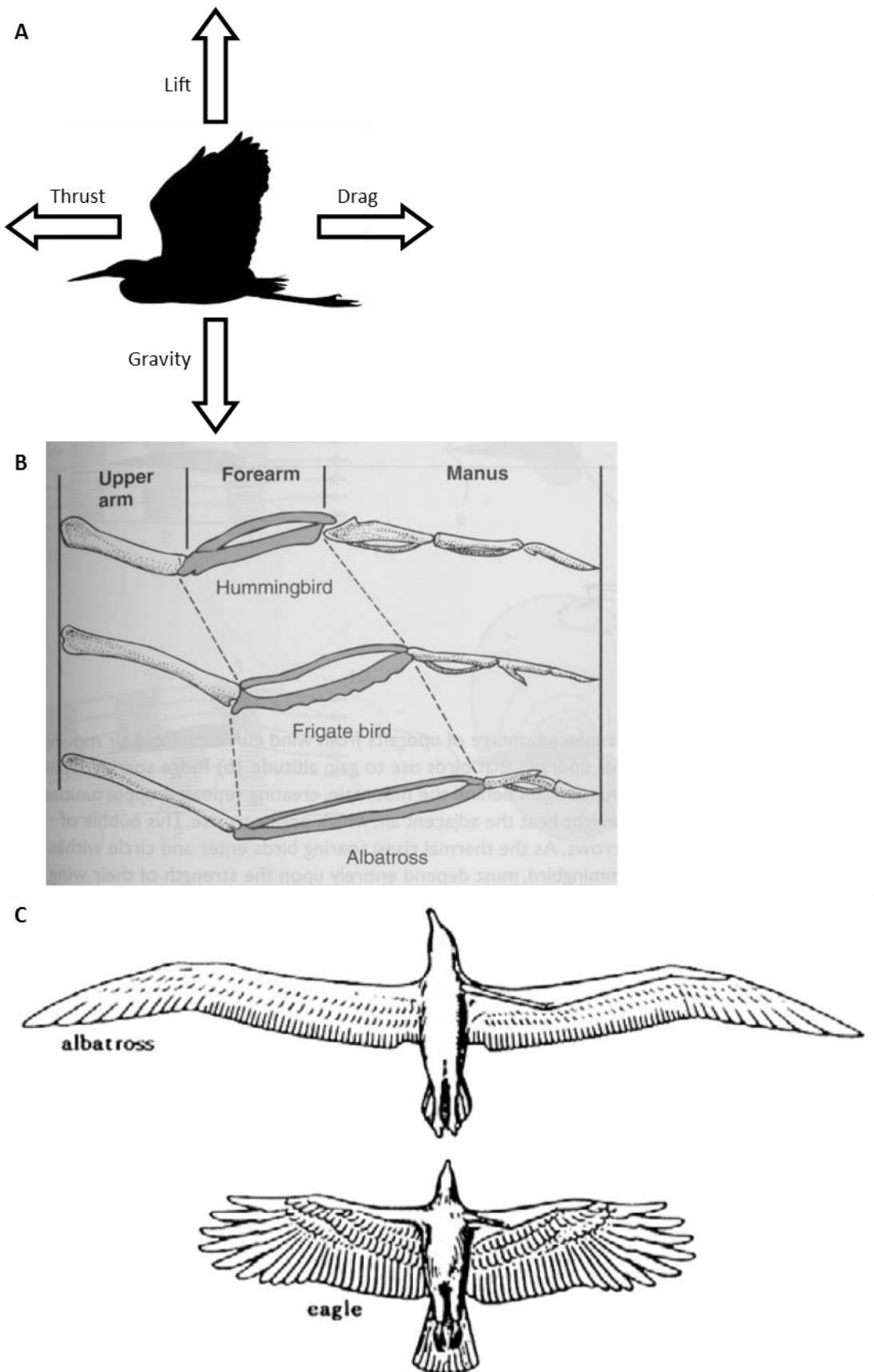


Figure 1.3: A: Schematic showing the forces acting on a bird in flight. B: Bird wings from three species scaled to the same length (from Kardong, 2012). The different locomotor modes of

Chapter 1 - Introduction and background

the hummingbird and the albatross are reflected in the relative length of the various wing segments. **C:** Two bird species with different aspect ratios (modified from Rayner, 1988). The high aspect ratio wing of the albatross facilitates soaring, while the lower aspect ratio wing of the eagle provides greater manoeuvrability in flight.

through the air and maintain flight. For the majority of volant birds, sufficient lift can be generated passively by the wings in order to stay aloft, however the majority of thrust must be actively generated. Thrust is generated by the wingbeat, which is powered by the flight musculature. The flight musculature attaches onto the pectoral girdle of birds, and is dominated by the large pectoralis major. The pectoral muscles attach onto the highly keeled sternum, and make up a considerable proportion of whole body mass (Hartman, 1961, Tobalske, 2007). Thrust acts to counter drag, which birds have reduced with covering of contour feathers and many have minimised drag further by altering their body profile to be more aerodynamic (Kardong, 2012).

The flight capabilities of an organism are intrinsically linked to various aspects of their morphology and mass properties. For example, lift and thrust generation are dependent on energy generated by the flight musculature, which in turn affect the size and shape of their attachment sites (e.g. pectoralis major on the sternal keel), which impacts body mass and mass distribution across the organism. Additionally, the relative proportions of wing segments give indication of locomotor requirements of an organism, as does wing shape. The primary flight feathers, attached to the manus, are responsible for producing thrust; while the secondary flight feathers, attached to the forearm, produce lift (Kardong, 2012). Reflecting this, birds which require high manoeuvrability (e.g. hummingbird), have an elongate manus segment; while soaring birds (e.g. albatross) possess elongate forearms to support a larger area of secondary feathers, facilitating greater lift generation (Figure 1.3B). The aspect ratio of a wing refers to the relationship between wing span to wing area (Lindhe Norberg, 2002, Savile, 1957) (Figure 1.3C). This relationship informs the locomotor capabilities of an organism, with different wing morphologies offering different benefits. For example, the relatively short and elliptical wings of woodland birds offer enhanced manoeuvrability at low speeds; while swept-back wings enable higher top speeds for hunting

or migrating species; and long, slender wings generate large amounts of lift, as seen in many sea birds (Kardong, 2012, Savile, 1957, Warham, 1977) (Figure 1.3C). Wing loading describes the relationship between body mass and wing area (Lindhe Norberg, 2002). Birds which have low wing loadings can generate sufficient lift to stay aloft at slower speeds, which has impact on take-off and landing speeds (Lindhe Norberg, 2002). Wing loading also determines turning abilities in flight (Lindhe Norberg, 2002). High wing loading and high wing aspect ratio are both energetically expensive, a further consideration which informs trade-offs for different wing morphologies and functions (Lindhe Norberg, 2002).

1.2.2. Methods for CoM estimation

1.2.2.1. Physical methods

CoM position has long been estimated using a range of physical experimentation techniques, on various species of interest, to tackle a range of research questions (e.g. Alexander, 1985, Clemente, 2014, Crompton et al., 1996, Dempster, 1955, Henderson, 2006). Three methods are primarily utilised, each of which will be discussed in more detail here (see Özkaya et al., 2012 for summary).

In suspension methods (see Figure 1.4A), objects are suspended from a single point and either allowed to come to rest naturally (Alexander, 1983, Alexander, 1985, Chandler et al., 1975, Dempster, 1955, Dempster and Gaughran, 1967, Fedak et al., 1982, Rubenson and Marsh, 2009), or they are repositioned until they come to rest aligned with a set axis (Nauwelaerts et al., 2011). When the system reaches equilibrium, the CoM of the object lies along the same line as the line of suspension. To determine CoM in more than one dimension, as is required for 3D biological specimens, it is necessary to use multiple points of suspension. The results of these multiple runs can then be overlain, and the point at which the lines of suspension intersect is then taken as the CoM position for that specimen. This

method requires no specialist equipment for small to medium sized specimens, but is difficult for large specimens and not feasible for *in vivo* experimentation.

The balance board uses the same principal as suspension (see Figure 1.3B). This technique can be applied to whole organisms or to individual segments (e.g. Crompton et al., 1996, Dempster, 1955, Dempster and Gaughran, 1967, Goetz et al., 2008, Hutchinson, 2004a, Myers and Steudel, 1997, Vilensky, 1979). In this method, a board is balanced on a knife-edge which acts as a pivot for the system. The object of interest is then placed on the balance board, and repositioned until the board returns to its balanced state. When the board-object system is at this point of equilibrium, the CoM of the object lies directly over the pivot of the balance board. For three-dimensional objects such as a biological specimen, it is necessary to repeat this process for each of the three axes, in order to give a final, 3D CoM. This method offers no substantial benefits over the suspension method, and requires the construction of specialist equipment for each specimen, if not each segment.

The scales technique (or ‘reaction board’ technique) (see Figure 1.4C) uses a set-up with scales at one end only (Lephart, 1984, Sprigings and Leach, 1986, Walter and Carrier, 2002, Willey et al., 2004), or with scales at both ends (Clemente, 2014, Henderson, 2003, Henderson, 2006, Kilbourne, 2013). This method determines a 1D CoM position by enabling calculation of the moment arm of the specimen’s weight which is acting on the scales at the ends of the system. This method is accessible as it only requires basic lab equipment for small to medium sized specimens. However, as for other physical methods it is difficult to apply *in vivo*, and requires a series of 1D CoM positions to be combined.

Few studies which calculate CoM position using physical methods include an investigation into the accuracy of their respective methods, with some notable exceptions. This, along

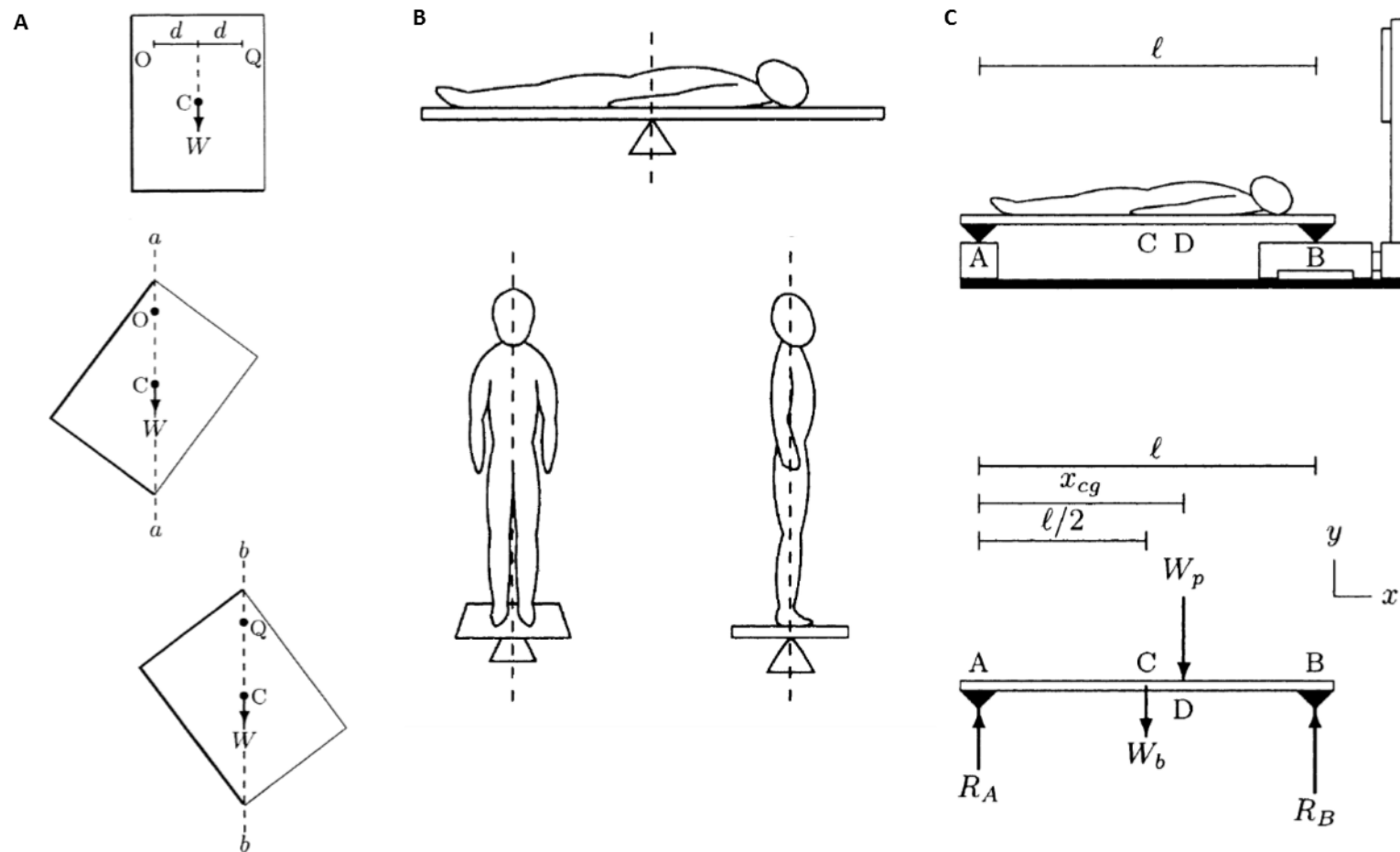


Figure 1.4: Taken from Ozkaya (2012). Showing three physical methods for determining centre of mass position. **A:** suspension method, when the object is suspended from points O and Q , the centre of mass (C) is located at the intersection of lines aa' and bb' . **B:** balance board method. **C:** scales technique, where

the object (exerting force W_p) is placed on a board (exerting force W_b) balanced on a knife edge (A) and a scale (B) which are a known distance (l) apart. The distance from the end of the board to the centre of mass (x_{cg}) can then be calculated.

with a lack of detail on the exact methods used, and infrequent reporting of the geometries of studied objects, makes a rigorous comparison of methods challenging. Lephart (1984) assessed the accuracy of a variation of the scales technique which had samples positioned on a plate, which by means of two metal blades, rested on a set of scales at one end and an adjustable height stand at the other. Lephart (1984) found mean absolute percentage errors of 0.03% in his estimations of CoM position. This accuracy test was performed on a range of 37 test objects ranging from 0.3 to 30kg, all with standard geometries, including hollow and filled metal cylinders. This error was within the error margin of the balance used ($\pm 1g$), leading Lephart to label this method “a very accurate procedure indeed”. The balance board technique of Sprigings and Leach (1986) predicted a CoM within 2mm of the measured, geometric centre of their test object (Olympic weightlifting disc: 20kg, 450mm diameter). The suspension method used by Nauwelaerts et al. (2011) was able to predict CoM to within approximately 1cm of the ‘true’ CoM. They found that this accuracy was dependent on the length and radius of their test objects, though do not specific the dimensions or number of these test items. Additionally, the method of Nauwelaerts et al. (2011) represents an usual application of the suspension technique, and therefore this error may not be representative of that present in more traditional methods. Though the theoretical principles behind all of these techniques is correct, any experiment has the potential to introduce error at various stages of testing. Aspects of these errors will undoubtedly be unique to specific studies, and researchers, further hindering the comparison of published studies in order to assess the accuracies of physical methodologies relative to one another, as well as their practical limitations for biological specimens.

Furthermore, all of these techniques are of limited use to palaeontologists. They have been employed to look at dinosaurs (e.g. Alexander, 1985). But these methods are then reliant on the accurate creation of scale models of the specimen of interest. Even for specimens where

there is largely complete skeletal material for one individual, there is substantial uncertainty on the amount of soft tissue to include around the skeleton. This inherent subjectivity undoubtedly results in discrepancies. Any errors made in the original scale models will be magnified when calculating the mass properties of the whole organism, resulting in large differences in CoM positions from small changes to the original model (Farlow et al., 1995).

1.2.2.2. Digital methods

To combat the significant challenges posed by use of physical methodologies when applying to dinosaurs, various computational approaches have been developed which are capable of estimating mass properties in extinct taxa. These methods share common benefits over physical models, including ease of alteration and distribution and the fact that they can be based directly on the original skeletal material. However, they are all sensitive to the effects of errors in the original reconstructions of the skeletal material (Brassey et al., 2013). These methods must also tackle the major issue surrounding work on mass properties of extinct taxa - the question of how much flesh to add around the skeletal material. Some take a qualitative approach to reconstructing this skin outline; while later studies apply quantitative methods in attempts to improve accuracy, and to give objectively constrained error margins. The main digital methods for computing mass properties are discussed below.

Mathematical slicing

The first computational method - mathematical slicing - was developed by Henderson (1999), and the methodology has since been refined and applied to a variety of taxa to address a wide range of questions (e.g. Henderson, 2006, Henderson, 2010, Henderson, 2018, Henderson and Snively, 2004, Henderson and Nicholls, 2015, Jones et al., 2000b, Maidment et al., 2014) (see Figure 1.5 for summary of this method). This method reconstructs the skin outline of the specimen of interest from a dorsal and ventral perspective, commonly taken

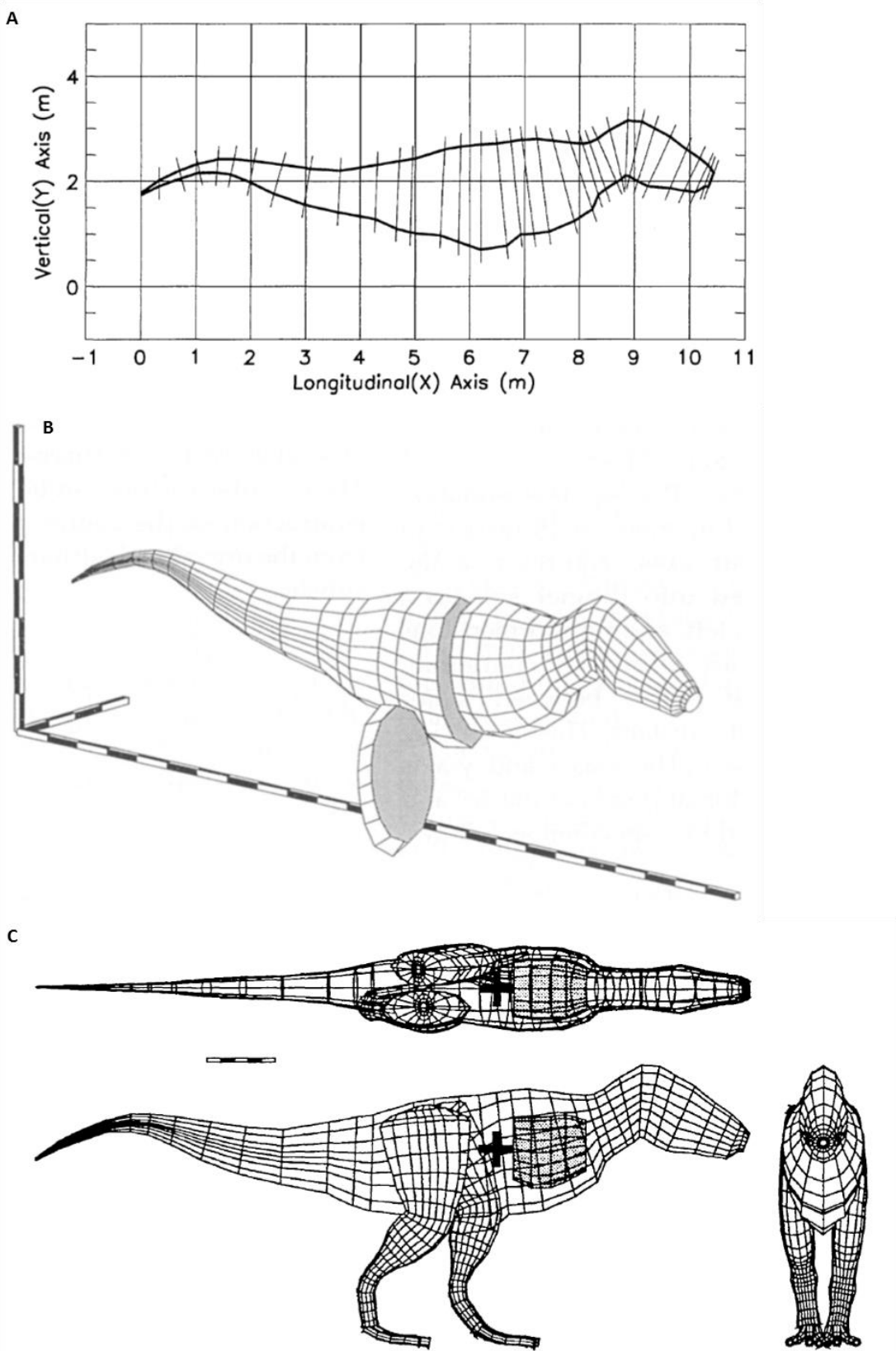


Figure 1.5: Taken from Henderson (1999). Showing the stages of the mathematical slicing method. Body outline is created (**A**) and split into sections (**B**) from which the final model is constructed and whole body centre of mass (indicated by '+') can be calculated (**C**).

directly from pre-existing artistic reconstructions, with the exception of Maidment et al. (2014) who created their own reconstructions based two 2D pictures of the articulated skeletal material directly. The resulting 2D skin outlines are then extrapolated into 3D, and the model is split into a series of thin sections which run along the cranio-caudal axis of the animal. Areas of zero density, such as the lungs or air cavities can be modelled in the same way. Additional heterogeneity in the composition of an organism can be accounted for by altering the density value for each individual cylinder as deemed appropriate. From these data on segment volumes and densities, mass and subsequently CoM can be calculated. The validity of this method has been tested in large mammals, crocodylians and birds, with model estimates found to correspond closely to the expected (Henderson, 1999, Henderson, 2010) or experimentally measured (Henderson, 2003, Henderson, 2006) CoM values. However, this method suffers from uncertainty around construction of skin outlines. Though it uses skeletal material to an extent, reduction of the material to 2D means it is not used to its full potential. It also assumes elliptical cross sections of all body segments, which has been found to introduce varying degrees of error across a range of vertebrates (Motani, 2001).

Manual shape fitting

Later digital volumetric methodologies improved on Henderson's technique by utilising the whole 3D skeleton when constructing their own skin outlines, and using techniques which enabled easier manipulation of the shape of each body segment. This has been achieved using B-splines (Hutchinson et al., 2007), NURBs (Bates et al., 2009a, Bates et al., 2009b, Mallison, 2010) and octagonal hoops (Allen et al., 2013, Allen et al., 2009, Hutchinson et al., 2011). The basis of all the studies is similar and they yield similar results (see Figure 1.6 for summary). Firstly, a fully 3D representation of the skeletal material is generated, for example by laser surface scanning, computed tomography or digital photogrammetry. A series of shapes are fitted to the skeletal material along the cranio-caudal axis of the articulated

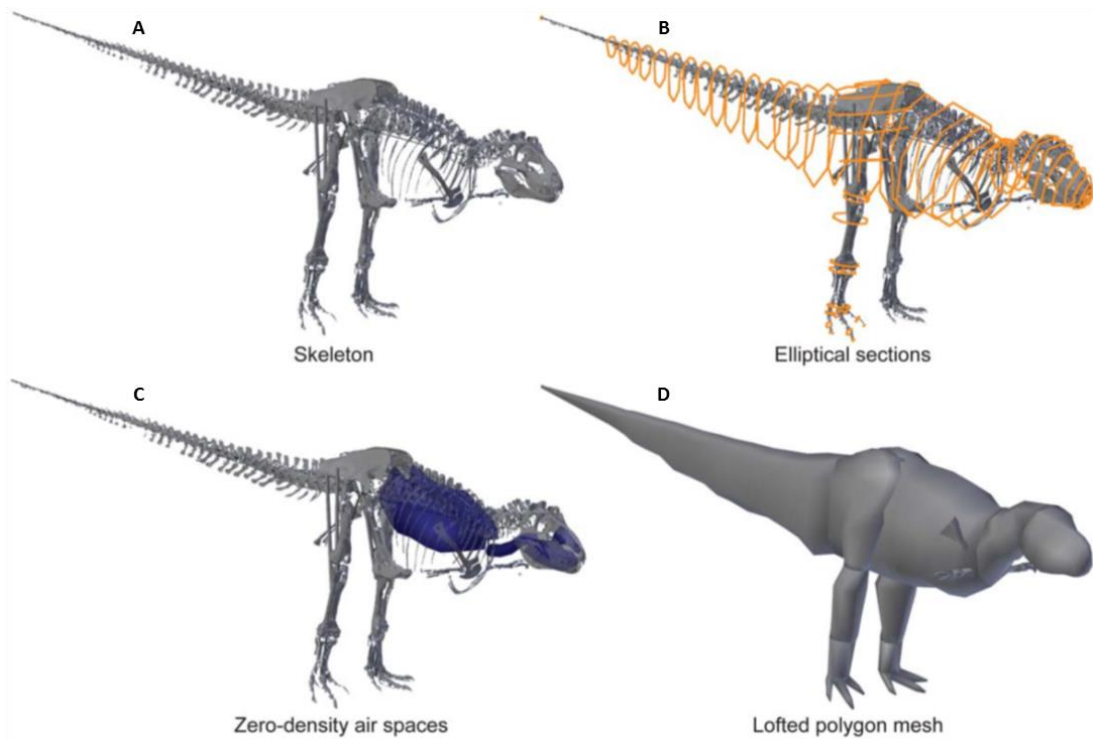


Figure 1.6: Taken from Hutchinson et al. (2011). Showing the stages of the manual shape fitting method using octagonal hoops in this case. The skeletal material is digitalised and put into a standard posture (**A**), hoops are applied around the skeleton to define the soft tissue outline (**B**) and air spaces (**C**) and a final skin outline is created by lofting a surface between the hoops (**D**).

skeleton. These shapes are subsequently inflated in order to accommodate soft tissue around the skeletal material, based on reference to soft tissue anatomy in closely related extant taxa. Joining these shapes produces a final skin outline for the specimen, from which whole body CoM can be calculated.

By using data from the whole 3D skeleton, these manual shape fitting methods maximise the amount of biological information available to inform their reconstructions. However, their soft tissue reconstructions contain the same inherent subjectivity as in the creation of a physical model, or a model for mathematical slicing. In several cases, the validity of these manual shape fitting methods has been tested, by application to extant archosaur(s) in addition to application to fossil material (e.g. Allen et al., 2009, Bates et al., 2009b, Hutchinson et al., 2007). In these cases, the method was found to produce a CoM in close agreement with expected values for the extant specimen. However, the ability to generate a good reconstruction of a living animal, with a relatively familiar morphology, does not speak to the ability of observers to accurately recreate the skin outline of a long-extinct species, especially those with a body plan unlike anything alive today (Bates et al., 2009b). The uncertainty and subjectivity associated with these methods has been acknowledged by extensive sensitivity analyses. By creating ‘maximal’ and ‘minimal’ versions of their skin outlines, within bounds deemed to be biologically realistic, a spread of plausible CoM positions have been calculated in the cranio-caudal and dorso-ventral directions (e.g. Allen et al., 2013, Bates et al., 2009b, Bates et al., 2016, Hutchinson et al., 2011). The ‘true’ CoM position of an organism is assumed to lie within these bounds, and these maximum brackets inform any higher conclusions being drawn.

Mathematical shape fitting - convex hulls and alpha shapes

In an attempt to eliminate the need for subjective reconstructions of skin outlines in extinct species, mathematical shape fitting methods have been developed which are grounded in quantitative data from extant taxa (Brassey and Gardiner, 2015, Sellers et al., 2012) (see Figure 1.7 for summary). These methods were originally developed to predict whole body mass, and have been widely applied in this context (Basu et al., 2016, Bates et al., 2015, Brassey and Gardiner, 2015, Brassey et al., 2015, Brassey et al., 2016, Brassey et al., 2018, Brassey and Sellers, 2014, Sellers et al., 2012). The original relationship derived by Sellers et al. (2012) has also been used to derive estimates for whole body CoM (Bates et al., 2016, Sellers et al., 2013, Sellers et al., 2017).

These mathematical shape fitting methods take digitised skeletal material from specimens, either whole (e.g. Brassey and Gardiner, 2015) or split into segments (e.g. Brassey et al., 2016, Sellers et al., 2012). 3D shapes are then wrapped around the skeletal material using automated, mathematical shape fitting. A convex hull is formed by wrapping a 3D surface around the points at the outer extremes of an object, like an elastic band (see Figure 1.7B). An alpha shape with an infinitely high α value is a convex hull. Decreasing the α value relaxes the shape, allowing it to wrap to increasingly more internal points, creating a shrink-wrap of the original object (see Figure 1.7B). Alpha shapes undoubtedly have the potential to produce volumes which are closer to the true value for the object under consideration. However, they require selection of an appropriate α value for each object, which is a time consuming, subjective process. While convex hulls are coarser representations of the skeletal volume; they can be generated faster, more objectively and with greater repeatability than alpha shapes.

By mathematically deriving skin outlines, these methods offer improved repeatability and

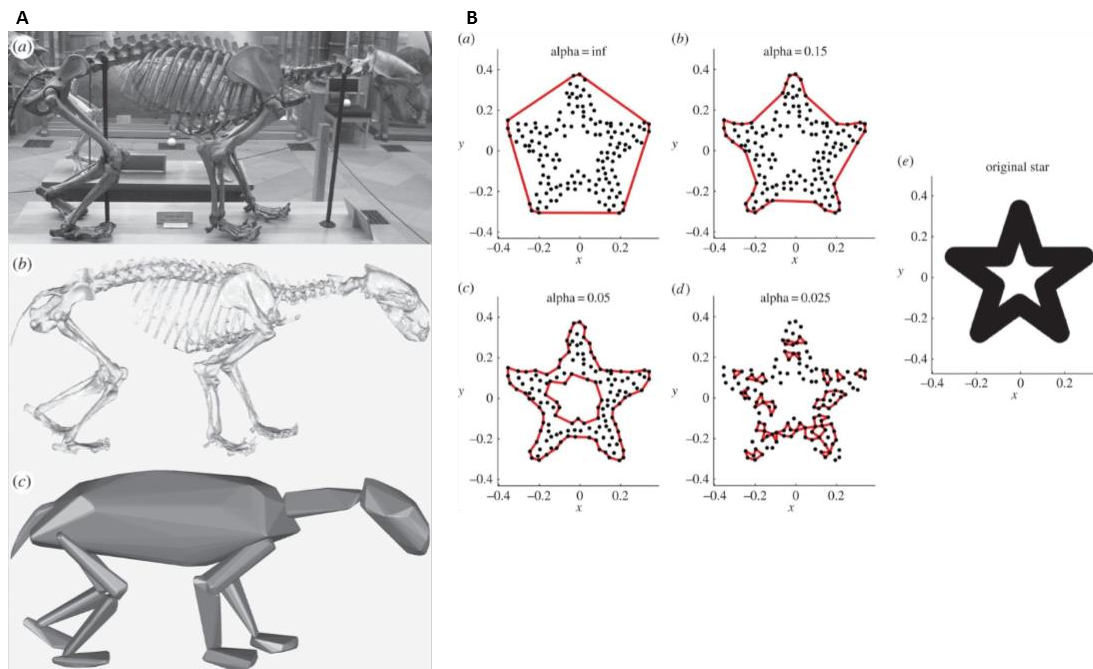


Figure 1.7: Taken from Sellers et al. (2012) and Brassey and Gardiner (2015). **A:** The stages of the ‘mathematical shape fitting’ method using convex hulls. The original skeletal material (**Aa**) is digitalised (**Ab**) and convex hulls are applied around the skeletal material for each segment (**Ac**). **B:** A ‘family’ of alpha shapes for the 2D object in (**Be**). A infinite alpha value gives a convex hull (**Ba**), while reducing alpha relaxes the outer boundary of the alpha shape, producing gradually more detailed representations of the original object (**Bb-d**).

greater objectivity in the derivation of segment mass properties (mass and CoM). Additionally, their grounding in data from living animals enables the error contained within the method to be confidently quantified. However, all previously published methods of this type focus solely on the relationship between whole body mass and skeletal mass/volume. In their application, they therefore assume a homogeneous expansion of skeletal material across an organism. It is reasonable to hypothesise based on visual examination of organisms' morphology that soft tissue is rarely, if ever, distributed evenly across the body relative to the skeletal material. This has been recognised as an area requiring future work (Brassey and Gardiner, 2015), as assuming a homogeneous expansion will impact on the accuracy of any resulting CoM estimates. Additionally, existing relationships using this methodology are based on limited sample sizes, on groups of taxa which are unlikely to be the best proxies for dinosaurs, and frequently use museum specimens which have been subjectively mounted and have unknown body masses.

Extant CoMs using digitised skin outlines

Though not applicable to extinct taxa, studies have also used digital skin outlines from living species to derive CoM estimates (Allen et al., 2013, Allen et al., 2009, Clemente et al., 2018). By using real skin outlines, these studies represent significant improvements over previous work on extant taxa using mathematical slicing and manual shape fitting (e.g. Henderson, 1999, Henderson, 2010, Ren and Hutchinson, 2008). These newer studies using real skin outlines are able to offer an insight into the maximum potential accuracy of any methods, in a best case scenario which is unachievable for extinct taxa. These studies extract skin outlines from CT data (Allen et al., 2009, Clemente et al., 2018), which also enables capture of relevant internal geometry (e.g. air cavities). This eliminates the major problem faced in paleontological work where a soft tissue outline must be generated subjectively based only on skeletal geometry. The ability of the segmenting process in producing a consistent skin

outline was assessed by Allen et al. (2009) and found to produce insignificant differences to CoM position. Other factors, such as density assignment also impact on final CoM position predicted, these are discussed below.

Digital models - model detail

Digital methods offer a host of advantages over physical approaches to CoM estimation, including easy data sharing, sensitivity analyses and replication of results. Digital approaches make it possible to incorporate extremely high levels of detail into models, particularly in the case of extant taxa. Researchers using these techniques must therefore make decisions on how much detail to include in models, constrained mainly by researcher time (Allen et al., 2009). There are multiple factors which have the potential to influence estimates of whole body CoM, but the extent of their impact is generally poorly quantified in extant and extinct taxa.

Air cavities have been included as standard in models since the advent of digital modelling approaches (Henderson, 1999), and long before (e.g. Alexander, 1985). As a minimum this involves the low density structures of the lungs in the torso cavity (e.g. Alexander, 1985, Henderson, 2018), alternatively more detailed representations include more pneumatic cavities across the model segments (e.g. Allen et al., 2013, Bates et al., 2016, Hutchinson et al., 2007). Physical representations, assumed to have zero density, can be incorporated into models, or the density of the relevant segments can be reduced to an appropriate degree in order to account for the presence of pneumaticity.

Aside from air cavities, other organ systems are very rarely explicitly included in volumetric models, instead being represented by the different density values assigned to segments. One system which has the potential to influence whole body CoM is the integument. Various

types of integumentary coverings are present across the animal kingdom which serve a variety of functions, including insulation from heat and water loss, as well as for display. Modern birds have evolved a unique integument in the form of feathers which not only represent a significant proportion of whole body mass (up to 19% (Summers et al., 1992)), but which also has a non-uniform distribution across the body. These factors combine to suggest that a feathered integument may exert a significant influence on CoM position in modern birds, an influence which would have appeared gradually through time culminating in crown Aves. However, there is currently a lack of published data on the integument mass properties required to test this hypothesis in birds. The effect of integument has been assessed in various ornithischian species (Maidment et al., 2014, Mallison, 2014), which possess extremely derived integumentary features such as cranial frills and extensive dermal armour. These studies found that highly modified integument with uneven distribution significantly influenced whole body CoM position (Maidment et al., 2014).

In order to derive whole body CoM positions, density data are required for application to the skin outlines of the model. Some data are published on whole body density in birds and a few in crocodylians, but no segment specific data are available for extant archosaurs. Previous volumetric modelling studies use a wide range of data, some based on published studies, others based on ‘common sense’ conclusions about the relative proportions of tissue types in extinct taxa (e.g. Alexander, 1985, Allen et al., 2013, Henderson, 2004, Henderson, 2006). Generally, density is modelled heterogeneously, accounting for different ratios of tissue types of different densities in the different segments. For other taxa (e.g. horse - Buchner et al., 1997, and human - Dempster and Gaughran, 1967), segment specific density data are available, which enable measured biological data and observed biological variability to be incorporated into models. Currently, there is limited assessment of the impact of these

decisions on density assignment make on whole body CoM. Again, the lack of data from extant species is a major problem, hindering confident application to extinct taxa.

Digital methods - summary

The best digital methodologies seek to incorporate as much of the data available from fossils into models, while generating quantitative, minimally subjective predictions which are grounded in data from living animals. However, existing methods drastically underuse the broad range of data obtainable from extant archosaurs; producing relationships at the whole body level only which are based on narrow ranges of taxa. These methods are currently therefore limited when it comes to the derivation of CoM estimates for fossil archosaurs. The amount of detail required to produce accurate estimates of CoM using digital models also currently remains poorly understood, with a lack of published data on extant taxa hindering any rigorous investigations into this area of potentially substantial error.

1.2.3. *CoM and evolutionary studies*

Due to the wide range of factors influenced by CoM position, it has often been used to inform conclusions about the biology of extinct taxa. CoM position represents an invaluable, indirect route to information on locomotion which is otherwise inaccessible in fossil species. Sensitivity analyses have shown that different CoM positions can have drastic impacts on predictions of various aspects of an organism's biology.

For example, CoM has been used in conjunction with an organism's interactions with the ground to help inform feasible postures for *T. rex* (Gatesy et al., 2009). As a result of the effect of CoM on posture, CoM position also affects the moment arms of muscles around the hindlimb joints, which determines the magnitude of force generation possible through a gait cycle, which in turn influences factors such as top speed (Hutchinson, 2004b). The various

impacts CoM has on the function of the musculoskeletal system combine to produce proven effects on the maximum running speed (+/- 8.9%) and stride length (+/- 26.4%) (Bates et al., 2010). This demonstrates the potential impact of whole body CoM position on a range of higher biological conclusions, which are often drawn about extinct taxa, highlighting the importance of accurate CoM estimates for fossil taxa.

Few studies have examined trends in CoM through time (with the exception of Allen et al., 2013, Bates et al., 2016). Allen et al. (2013) investigated CoM in range of archosaur species from modern crocodylians, through extinct taxa to modern birds. They found a gradual cranial CoM shift approaching crown Aves, which then reversed in the modern bird node (Figure 1.8A-C). However, that node (and the extant crocodylian node) is only represented by one species. By representing the two extant groups with one specimen each, Allen et al. (2013) likely underestimate the variability present within these groups, undermining their interpretations of the resulting evolutionary trends. Additionally, the currently limited understanding of the correlates of any given CoM position in extant species hinders conclusions regarding the locomotor capabilities of extinct taxa. It has therefore been recognised in palaeontological studies that more data linking locomotion and CoM in living species are required to further our understanding of the same features in extinct taxa (Hutchinson, 2011). The work of Allen et al. (2013) is further weakened by their use of subjectively generated body outlines for the fossil taxa studied, using a manual shape fitting method (see Section 1.2.2.2 here for summary). Bates et al. (2016) conducted a similar investigation into the changes in whole body CoM position across the sauropod radiation, using skin outlines objectively generated by a mathematical shape fitting method (see Section 1.2.2.2 here for summary). Bates et al. (2016) found a series of cranial CoM shifts coinciding with the evolution of quadrupedalism and subsequently with drastic neck elongation in the titanosauriforms (Figure 1.8D and E). Bates et al. (2016) include substantial

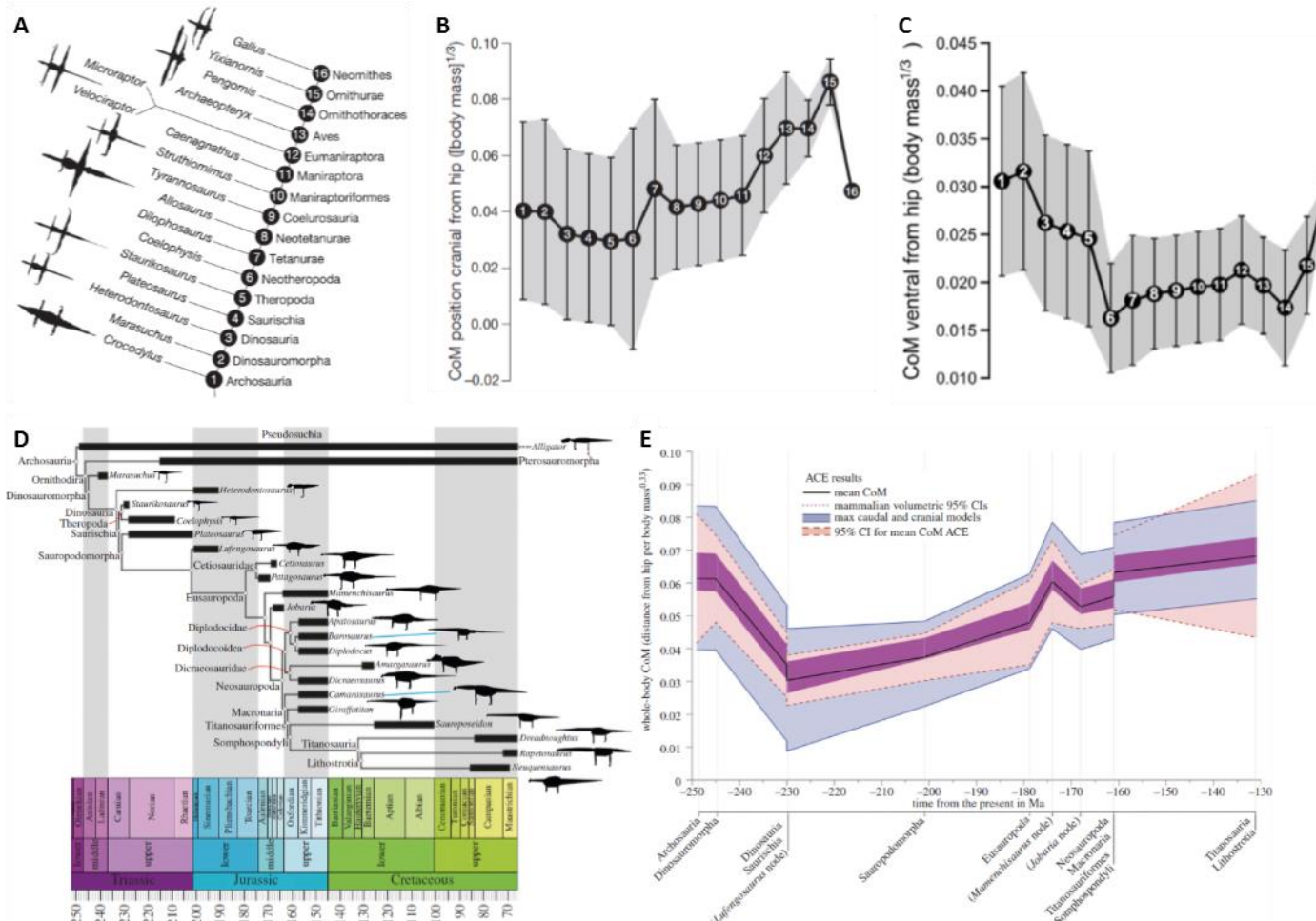


Figure 1.8: A-C: Taken from Allen et al. (2013). 16 specimens across Archosauria (A) were modelled using a manual shape fitting approach to predict “best guess” CoM positions, along with CoMs skewed maximally in the cranio-caudal and dorso-ventral directions in order to generate error margins (B & C). D &

E: Taken from Bates et al. (2016). 22 specimens covering the sauropod radiation (**D**) were modelled using a mathematical shape fitting approach to predict “best guess” CoM positions, along with CoMs skewed maximally in the cranio-caudal direction in order to generate error margins (**E**).

error margins, recognising the considerable uncertainty inherent to any predictions of soft tissue outlines in fossil species with no modern analogues, as for many dinosaurs. Though these considerable error margins do not mask all trends, it is highly likely that more subtle shifts in CoM are being obscured as a result of the limitations of current methods. The reconstructions of Bates et al. (2016) benefit from a quantitative grounding in data from extant taxa. However, there are issues with the specifics of the method applied (based on Sellers et al., 2012). Firstly, the applicability of data generated from large bodied mammals to sauropod dinosaurs is questionable. For studies seeking to investigate dinosaur fossil species, it is possible that data from extant archosaurs would be a closer fit - this is particularly true for bipedal theropods. Additionally, the relationship used by Bates et al. (2016) to generate segment masses, and therefore whole body CoM was originally designed for body mass estimation. Bates et al. (2016) assume the extent of soft tissue around the skeletal material is consistent across all body segments. This assumption is unlikely to be true and which will result in unknown effects on whole body CoM. Future work should examine the relationships between skeleton and skin volumes on a segment-by-segment basis. This would provide a better understanding of the relationships and extent of variation present in living taxa, which would help to inform more accurate CoM predictions and better constrain the associated error bars in extinct species.

Examining CoM through time and in transitional species has the potential to shed new light on our understanding of enigmatic taxa. However, current methods are hindered by limited extant datasets or subjective methods to generate CoM position. The interpretation of CoM data is further hindered by a lack of understanding of the correlates of CoM in extant taxa.

1.2.4. Systematics

Existing volumetric approaches (e.g. Henderson, 1999, Hutchinson et al., 2007, Sellers et al., 2012) are ultimately seeking information on soft tissue properties, in order to examine mass properties. This biological information is not preserved in the fossil record, and must therefore be inferred from osteological remains. Many previous studies on fossil dinosaurs have used qualitative approaches which contain inherent subjectivity (e.g. Bates et al., 2009, Henderson, 1999, Hutchinson et al., 2007), while current quantitative approaches (based on Sellers et al., 2012) are based on data from distantly related taxa. This thesis seeks to develop existing quantitative approaches, while focussing on specimens which form an ‘extant phylogenetic bracket’ (EPB) around the extinct species of interest.

An EPB approach uses data on extant, closely related taxa in order to provide insights into the likely biology of the extinct species of interest (Witmer, 1995). This thesis uses an EPB based on (1) extant birds, as the direct descendants of dinosaurs; (2) extant crocodylians (i.e. crocodiles and alligators) which belong to Pseudosuchia, the sister group of Dinosauria; and (3) extant lepidosaurs (lizards and tuatara) as an outgroup (see Figure 1.9 for a summary of these phylogenetic relationships). If a soft tissue feature with an associated osteological feature is present in extant species at both ends of the bracket, and that osteological feature is present in the extinct species of interest, then it is possible to confidently conclude that the extinct species also possessed that soft tissue feature. However, in many cases, extant crocodylians and extant birds possess disparate soft tissue morphologies. Even in these cases, an EPB can be used to constrain a range of plausible conditions for the extinct taxa, thereby informing their likely morphology and enabling higher conclusions to be drawn based on quantified error margins.

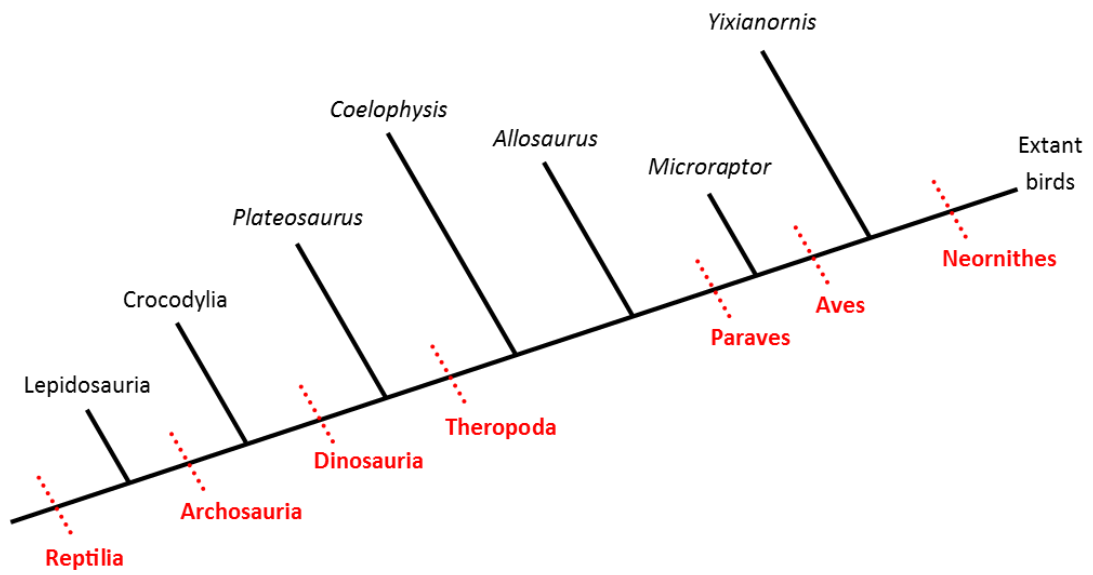


Figure 1.9: Schematic displaying the phylogenetic relationships between the three extant groups and the fossil species which are studied in this thesis.

The following chapters of this thesis use different subsets of specimens as follows:

- Chapter 2: three birds (chicken, buzzard, duck)
- Chapter 3, integument testing: 49 specimens from 17 bird, 5 crocodylian and 11 lepidosaur species (NB: these specimens are used in this dataset only, and were not available for digital modelling)
- Chapter 3, digital modelling: three birds (chicken, buzzard, duck from Chapter 2), three reptiles (lizard, crocodile, alligator) and three fossil dinosaurs (*Coelophysis*, *Microraptor*, *Yixianornis*)
- Chapter 4: 27 birds from 27 avian families, covering a range of body sizes and ecologies (see Table 4.1, Figure 4.2)

Chapter 5: 48 specimens from 27 bird, 11 crocodylian and 10 lepidosaur species (see Table 4.1, Table 5.1); with subsequent application to five fossil dinosaurs (*Plateosaurus*, *Coelophysis*, *Allosaurus*, *Microraptor*, *Yixianornis*)

1.2.5. Background summary

- CoM is a fundamentally important biomechanical parameter, which impacts factors such as posture and ultimately locomotor capabilities in terrestrial and volant behaviours.
- CoM has the potential to inform our understanding of locomotor behaviours in fossil species which cannot be observed directly. However, the links between locomotion and CoM are currently poorly understood in extant taxa.
- Numerous methods have been used to predict CoM position in physical specimens, however there have been no assessments of their absolute or relative accuracies.
- Various digital methods have recently been proposed which can be used to predict CoM position in extant and extinct specimens of interest. While offering substantial advances over physical methods, they suffer from limitations.
- Previously published studies examining the evolution of CoM are hindered by a lack of data on closely related living animals. This limits their ability to confidently predict CoM position and to interpret the resulting CoM estimates.

1.3. Aims and Objectives

The overall aim of this thesis is to quantify links between body shape and locomotor diversity during the evolution of birds. This aim will be achieved through a number of smaller objectives which address key knowledge gaps currently present in the field, as identified in Section 1.2. These objectives are:

- 1) Assess the absolute accuracies of three commonly used methods for determining centre of mass position, and their applicability to biological specimens.
- 2) Investigate the integumentary changes which occurred in bird-line archosaurs with the advent of feathers, in the context of impact on whole body centre of mass position.
- 3) Explore links between centre of mass position and locomotor behaviours across Aves.
- 4) Establish and apply a new methodology for the estimation of centre of mass position in fossil archosaurs, grounded in an extensive extant dataset.

1.4. Thesis Structure

1.4.1. Chapter 2

This chapter has been published in the Journal of Anatomy.

MACAULAY, S., HUTCHINSON, J. R. & BATES, K. T. 2017. A quantitative evaluation of physical and digital approaches to centre of mass estimation. *Journal of Anatomy*, 231, 758-775. <https://doi.org/10.1111/joa.12667>

Author contributions: SM and KTB conceived the project, provided specimens, and collected data. SM analysed and interpreted data, and drafted manuscript. All authors critically revised manuscript and approved article.

1.4.2. Chapter 3

This chapter is based on a manuscript which is currently in review at Evolution.

MACAULAY, S., BATES, K. T., BROPHY, P., ALLEN, V., HONE, D. W. E. & HUTCHINSON, J. R. (In review). Linking integument and body shape evolution in archosaurs. *Evolution*.

Author contributions: PB, VA, DWEH and JRH designed and carried out the experimental integument data collection. SM analysed experimental integument data. SM and KTB designed the computer modelling. SM carried out the computer modelling and analysed the resulting data. All authors contributed to the manuscript.

1.4.3. Chapter 4

I am currently developing this chapter for publication. The version of this chapter presented in this thesis has been completed with the following collaborators: K.T. Bates, J.R. Hutchinson and E.R. Schachner.

MACAULAY, S., SCHACHNER, E. R., HUTCHINSON, J. R. & BATES, K. T. (In preparation).

Body shape and the evolution of locomotor diversity in birds.

Collaborator contributions: SM and KTB conceived the project. SM, KTB, JRH and ERS provided specimens and collected data. SM processed, analysed and interpreted data, and wrote the chapter.

1.4.4. Chapter 5

I am currently developing this chapter for publication. The version of this chapter presented in this thesis has been completed with the following collaborators: K.T. Bates, J.R. Hutchinson and E.R. Schachner.

MACAULAY, S., SCHACHNER, E. R., HUTCHINSON, J. R. & BATES, K. T. (In preparation).

A new method for predicting mass distribution in extinct archosaurs.

Collaborator contributions: SM and KTB conceived the project. All authors provided specimens and collected data. SM processed, analysed and interpreted data, and wrote the chapter.

1.5. References

- ALEXANDER, D. E., GONG, E., MARTIN, L. D., BURNHAM, D. A. & FALK, A. R. 2010. Model tests of gliding with different hindwing configurations in the four-winged dromaeosaurid *Microraptor gui*. *Proceedings of the National Academy of Sciences of the United States of America*, 107, 2972-2976.
- ALEXANDER, R. M. 1983. *Animal Mechanics*, London, Blackwell Scientific.
- ALEXANDER, R. M. 1985. Mechanics of posture and gait of some large dinosaurs. *Zoological Journal of the Linnean Society*, 83, 1-25.
- ALEXANDER, R. M. 2006. Dinosaur biomechanics. *Proceedings of the Royal Society B: Biological Sciences*, 273, 1849-1855.
- ALLEN, V., HUTCHINSON, J. R., BATES, K. T. & LI, Z. 2013. Linking the evolution of body shape and locomotor biomechanics in bird-line archosaurs. *Nature*, 497, 104-107.
- ALLEN, V., PAXTON, H. & HUTCHINSON, J. R. 2009. Variation in center of mass estimates for extant sauropsids and its importance for reconstructing inertial properties of extinct archosaurs. *Anatomical Record*, 292, 1442-1461.
- BASU, C., FALKINGHAM, P. L. & HUTCHINSON, J. R. 2016. The extinct, giant giraffid *Sivatherium giganteum*: Skeletal reconstruction and body mass estimation. *Biology Letters*, 12.
- BATES, K. T., FALKINGHAM, P. L., BREITHAUPT, B. H., HODGETTS, D., SELLERS, W. I. & MANNING, P. L. 2009a. How big was 'Big Al'? Quantifying the effect of soft tissue and osteological unknowns on mass predictions for *Allosaurus* (Dinosauria, Theropoda). *Palaeontologia Electronica*, 12, 1-33.
- BATES, K. T., FALKINGHAM, P. L., MACAULAY, S., BRASSEY, C. & MAIDMENT, S. C. R. 2015. Downsizing a giant: re-evaluating *Dreadnoughtus* body mass. *Biology Letters*, 11, 20150215.
- BATES, K. T., MANNING, P. L., HODGETTS, D. & SELLERS, W. I. 2009b. Estimating Mass Properties of Dinosaurs Using Laser Imaging and 3-D Computer Modelling. *PLoS ONE*, 4, 1-26.
- BATES, K. T., MANNION, P. D., FALKINGHAM, P. L., BRUSATTE, S. L., HUTCHINSON, J. R., OTERO, A., SELLERS, W. I., SULLIVAN, C., STEVENS, K. A. & ALLEN, V. 2016. Temporal and phylogenetic evolution of the sauropod dinosaur body plan. *Royal Society Open Science*, 3, 150636.
- BATES, K. T., SELLERS, W. I., MANNING, P. L. & MARGETTS, L. 2010. Sensitivity analysis in evolutionary robotic simulations of bipedal dinosaur running. *Journal of Vertebrate Paleontology*, 30, 458-466.
- BRASSEY, C. A. & GARDINER, J. D. 2015. An advanced shape-fitting algorithm applied to quadrupedal mammals: improving volumetric mass estimates. *Royal Society Open Science*, 2.

- BRASSEY, C. A., HOLDAWAY, R. N., PACKHAM, A. G., ANNÉ, J., MANNING, P. L. & SELLERS, W. I. 2013. More than One Way of Being a Moa: Differences in Leg Bone Robustness Map Divergent Evolutionary Trajectories in Dinornithidae and Emeidae (Dinornithiformes). *PLoS ONE*, 8, 1-10.
- BRASSEY, C. A., MAIDMENT, S. C. R. & BARRETT, P. M. 2015. Body mass estimates of an exceptionally complete Stegosaurus (Ornithischia: Thyreophora): comparing volumetric and linear bivariate mass estimation methods. *Biology Letters*, 11, 1-5.
- BRASSEY, C. A., O'MAHONEY, T. G., CHAMBERLAIN, A. T. & SELLERS, W. I. 2018. A volumetric technique for fossil body mass estimation applied to *Australopithecus afarensis*. *Journal of Human Evolution*, 115, 47-64.
- BRASSEY, C. A., O'MAHONEY, T. G., KITCHENER, A. C., MANNING, P. L. & SELLERS, W. I. 2016. Convex-hull mass estimates of the dodo (*Raphus cucullatus*): application of a CT-based mass estimation technique. *PeerJ*, 4, e1432.
- BRASSEY, C. A. & SELLERS, W. I. 2014. Scaling of convex hull volume to body mass in modern primates, non-primate mammals and birds. *PLoS ONE*, 9, 1-12.
- BUCHNER, H. H. F., SAVELBERG, H. H. C. M., SCHAMHARDT, H. C. & BARNEVELD, A. 1997. Inertial properties of Dutch Warmblood horses. *Journal of Biomechanics*, 30, 653-658.
- CARRANO, M. T. & BIEWENER, A. A. 1999. Experimental alteration of limb posture in the chicken (*Gallus gallus*) and its bearing on the use of birds as analogs for dinosaur locomotion. *Journal of Morphology*, 240, 237-249.
- CHANDLER, R. F., CLAUSER, C. E., MCCONVILLE, J. T., REYNOLDS, H. M. & YOUNG, J. W. 1975. Investigation of Inertial Properties of Human Body Segments. *AMRL Technical Report No. 74-137, Aerospace Medical Research Laboratories, Wright-Patterson Airforce Base, OH*.
- CHATTERJEE, S. & TEMPLIN, R. J. 2007. Biplane wing planform and flight performance of the feathered dinosaur *Microraptor gui*. *Proceedings of the National Academy of Sciences of the United States of America*, 104, 1576-1580.
- CLEMENTE, C. J. 2014. The evolution of bipedal running in lizards suggests a consequential origin may be exploited in later lineages. *Evolution*, 68, 2171-2183.
- CLEMENTE, C. J., BISHOP, P. J., NEWMAN, N. & HOCKNULL, S. A. 2018. Steady bipedal locomotion with a forward situated whole-body centre of mass: the potential importance of temporally asymmetric ground reaction forces. *Journal of Zoology*, 304, 193-201.
- CROMPTON, R. H., LI, Y., ALEXANDER, R. M., WANG, W. & GUNTHER, M. M. 1996. Segment inertial properties of primates: New techniques for laboratory and field studies of locomotion. *American Journal of Physical Anthropology*, 99, 547-570.
- DEMPSTER, W. T. 1955. Space Requirements of the Seated Operator. *WADC Technical Report No. 55-159, Wright Air Development Centre, Wright-Patterson Airforce Base, OH*.

- DEMPSTER, W. T. & GAUGHRAN, G. R. L. 1967. Properties of body segments based on size and weight. *American Journal of Anatomy*, 120, 33-54.
- DYKE, G., PALMER, C., NAISH, D., GANAPATHISUBRAMANI, B., DE KAT, R. & VAN DER KINDERE, J. 2013. Aerodynamic performance of the feathered dinosaur *Microraptor* and the evolution of feathered flight. *Nature Communications*, 4, 1-9.
- FARLOW, J. O., SMITH, M. B. & ROBINSON, J. M. 1995. Body Mass, Bone "Strength Indicator" and Cursorial Potential of *Tyrannosaurus rex*. *Journal of Vertebrate Paleontology*, 15, 713-725.
- FEDAK, M. A., HEGLUND, N. C. & TAYLOR, C. R. 1982. Energetics and mechanics of terrestrial locomotion. II. Kinetic energy changes of the limbs and body as a function of speed and body size in birds and mammals. *Journal of Experimental Biology*, 97, 23-40.
- GATESY, S. M. 1990. Caudofemoral musculature and the evolution of theropod locomotion. *Paleobiology*, 16, 170-186.
- GATESY, S. M., BÄKER, M. & HUTCHINSON, J. R. 2009. Constraint-based exclusion of limb poses for reconstructing theropod dinosaur locomotion. *Journal of Vertebrate Paleontology*, 29, 535-544.
- GATESY, S. M. & BIEWENER, A. A. 1991. Bipedal locomotion: effects of speed, size and limb posture in birds and humans. *Journal of Zoology*, 224, 127-147.
- GOETZ, J. E., DERRICK, T. R., PEDERSEN, D. R., ROBINSON, D. A., CONZEMIUS, M. G., BAER, T. E. & BROWN, T. D. 2008. Hip joint contact force in the emu (*Dromaius novaehollandiae*) during normal level walking. *Journal of Biomechanics*, 41, 770-778.
- HARTMAN, F. A. 1961. *Locomotor Mechanisms of Birds*, City of Washington, Smithsonian Miscellaneous Collections.
- HENDERSON, D. M. 1999. Estimating the masses and centers of mass of extinct animals by 3-D mathematical slicing. *Paleobiology*, 25, 88-106.
- HENDERSON, D. M. 2003. Effects of stomach stones on the buoyancy and equilibrium of a floating crocodilian: A computational analysis. *Canadian Journal of Zoology*, 81, 1346-1357.
- HENDERSON, D. M. 2004. Tipsy punters: Sauropod dinosaur pneumaticity, buoyancy and aquatic habits. *Proceedings of the Royal Society B: Biological Sciences*, 271, S180-S183.
- HENDERSON, D. M. 2006. Burly gaits; centers of mass, stability, and the trackways of sauropod dinosaurs. *Journal of Vertebrate Paleontology*, 26, 907-921.
- HENDERSON, D. M. 2010. Pterosaur body mass estimates from three-dimensional mathematical slicing. *Journal of Vertebrate Paleontology*, 30, 768-785.
- HENDERSON, D. M. 2018. A buoyancy, balance and stability challenge to the hypothesis of a semi-aquatic *Spinosaurus* Stromer, 1915 (Dinosauria: Theropoda). *PeerJ*, 6, e5409.

- HENDERSON, D. M. & NICHOLLS, R. 2015. Balance and Strength—Estimating the Maximum Prey-Lifting Potential of the Large Predatory Dinosaur *Carcharodontosaurus saharicus*. *The Anatomical Record*, 298, 1367-1375.
- HENDERSON, D. M. & SNIVELY, E. 2004. Tyrannosaurus en pointe: allometry minimized rotational inertia of large carnivorous dinosaurs. *Proceedings of the Royal Society B: Biological Sciences*, 271, S57-S60.
- HUTCHINSON, J. R. 2004a. Biomechanical modeling and sensitivity analysis of bipedal running ability. I. Extant taxa. *Journal of Morphology*, 262, 421-440.
- HUTCHINSON, J. R. 2004b. Biomechanical modeling and sensitivity analysis of bipedal running ability. II. Extinct taxa. *Journal of Morphology*, 262, 441-461.
- HUTCHINSON, J. R. 2011. On the inference of function from structure using biomechanical modelling and simulation of extinct organisms. *Biology Letters*, 8, 115-118.
- HUTCHINSON, J. R., BATES, K. T., MOLNAR, J., ALLEN, V. & MAKOVICKY, P. J. 2011. A Computational Analysis of Limb and Body Dimensions in *Tyrannosaurus rex* with Implications for Locomotion, Ontogeny, and Growth. *PLoS ONE*, 6, 1-20.
- HUTCHINSON, J. R., NG-THOW-HING, V. & ANDERSON, F. C. 2007. A 3D interactive method for estimating body segmental parameters in animals: Application to the turning and running performance of *Tyrannosaurus rex*. *Journal of Theoretical Biology*, 246, 660-680.
- JONES, T. D., FARLOW, J. O., RUBEN, J. A., HENDERSON, D. M. & HILLENIUS, W. J. 2000b. Cursoriality in bipedal archosaurs. *Nature*, 406, 716.
- KARDONG, K. V. 2012. *Vertebrates: Comparative Anatomy, Function, Evolution*, New York, McGraw-Hill.
- KILBOURNE, B. M. 2013. On birds: Scale effects in the neognath hindlimb and differences in the gross morphology of wings and hindlimbs. *Biological Journal of the Linnean Society*, 110, 14-31.
- KOEHL, M. A. R., EVANGELISTA, D. & YANG, K. 2011. Using physical models to study the gliding performance of extinct animals. *Integrative And Comparative Biology*, 51, 1002-1018.
- LEPHART, S. A. 1984. Measuring the inertial properties of cadaver segments. *Journal of Biomechanics*, 17, 537-543.
- LINDHE NORBERG, U. M. 2002. Structure, form, and function of flight in engineering and the living world. *Journal of Morphology*, 252, 52-81.
- MAIDMENT, S. C. R., HENDERSON, D. M. & BARRETT, P. M. 2014. What drove reversions to quadrupedality in ornithischian dinosaurs? Testing hypotheses using centre of mass modelling. *Naturwissenschaften*, 101, 989-1001.
- MALLISON, H. 2010. The digital Plateosaurus I: body mass, mass distribution, and posture assessed using CAD and CAE on a digitally mounted complete skeleton. *Palaeontologia Electronica*, 13, 1-26.

- MALLISON, H. 2014. Osteoderm distribution has low impact on the centre of mass of stegosaurs. *Foss. Rec.*, 17, 33-39.
- MOTANI, R. 2001. Estimating body mass from silhouettes: Testing the assumption of elliptical body cross-sections. *Paleobiology*, 27, 735-750.
- MYERS, M. J. & STEUDEL, K. 1997. Morphological conservation of limb natural pendular period in the domestic dog (*Canis familiaris*): Implications for locomotor energetics. *Journal of Morphology*, 234, 183-196.
- NAUWELAERTS, S., ALLEN, W. A., LANE, J. M. & CLAYTON, H. M. 2011. Inertial properties of equine limb segments. *Journal of Anatomy*, 218, 500-509.
- ÖZKAYA, N., NORDIN, M., GOLDSHEYDER, D. & LEGER, D. 2012. Statics: Systems in Equilibrium. *Fundamentals of Biomechanics: Equilibrium, Motion, and Deformation*. New York, NY: Springer New York.
- RAYNER, J. M. V. 1988. Form and Function in Avian Flight. In: JOHNSTON, R. F. (ed.) *Current Ornithology*. Boston, MA: Springer US.
- REN, L. & HUTCHINSON, J. R. 2008. The three-dimensional locomotor dynamics of African (*Loxodonta africana*) and Asian (*Elephas maximus*) elephants reveal a smooth gait transition at moderate speed. *Journal of the Royal Society Interface*, 5, 195-211.
- RUBENSON, J. & MARSH, R. L. 2009. Mechanical efficiency of limb swing during walking and running in Guinea Fowl (*Numida meleagris*). *Journal of Applied Physiology*, 106, 1618-1630.
- SAVILE, O. 1957. Adaptive evolution in the avian wing. *Evolution*, 11, 212-224.
- SELLERS, W. I., HEPWORTH-BELL, J., BRASSEY, C. A., EGERTON, V. M., MANNING, P. L., FALKINGHAM, P. L. & BATES, K. T. 2012. Minimum convex hull mass estimations of complete mounted skeletons. *Biology Letters*, 8, 842-845.
- SELLERS, W. I., MARGETTS, L., CORIA, R. A. & MANNING, P. L. 2013. March of the titans: The locomotor capabilities of sauropod dinosaurs. *PLoS ONE*, 8, 1-21.
- SELLERS, W. I., POND, S. B., BRASSEY, C. A., MANNING, P. L. & BATES, K. T. 2017. Investigating the running abilities of *Tyrannosaurus rex* using stress-constrained multibody dynamic analysis. *PeerJ*, 5, e3420.
- SNIVELY, E., O'BRIEN, H., HENDERSON, D. M., MALLISON, H., SURRING, L. A., BURNS, M. E., HOLTZ, J. T. R., RUSSELL, A. P., WITMER, L. M., CURRIE, P. J., HARTMAN, S. A. & COTTON, J. R. 2018. Lower rotational inertia and larger leg muscles indicate more rapid turns in tyrannosaurids than in other large theropods. *PeerJ Preprints*, 6, e27021v1.
- SPRIGINGS, E. & LEACH, D. 1986. Standardised technique for determining the centre of gravity of body and limb segments of horses. *Equine Veterinary Journal*, 18, 43-49.
- SUMMERS, R. W., UNDERHILL, L. G., NICOLL, M., RAE, R. & PIERSMA, T. 1992. Seasonal, size- and age-related patterns in body-mass and composition of purple sandpipers *Calidris maritima* in Britain. *Ibis*, 134, 346-354.

- TOBALSKE, B. W. 2007. Biomechanics of bird flight. *Journal of Experimental Biology*, 210, 3135.
- THOMAS, A. L. R. & TAYLOR, G. K. 2001. Animal flight dynamics I. Stability in gliding flight. *Journal of Theoretical Biology*, 212, 399-424.
- VILENSKY, J. A. 1979. Masses, centers-of-gravity, and moments-of-inertia of the body segments of the Rhesus Monkey (*Macaca mulatta*). *American Journal of Physical Anthropology*, 50, 57-65.
- WALTER, R. M. & CARRIER, D. R. 2002. Scaling of rotational inertia in murine rodents and two species of lizard. *Journal of Experimental Biology*, 205, 2135-2141.
- WARHAM, J. 1977. Wing loadings, wing shapes, and flight capabilities of procellariiformes. *New Zealand Journal of Zoology*, 4, 73-83.
- WILLEY, J. S., BIKNEVICIUS, A. R., REILLY, S. M. & EARLS, K. D. 2004. The tale of the tail: Limb function and locomotor mechanics in *Alligator mississippiensis*. *Journal of Experimental Biology*, 207, 553-563.
- WITMER, L. M. 1995. The Extant Phylogenetic Bracket and the importance of reconstructing soft tissues in fossils. In: THOMASON, J. J. (ed.) *Functional Morphology in Vertebrate Paleontology*. Cambridge: Cambridge University Press.

CHAPTER 2 - A QUANTITATIVE EVALUATION OF PHYSICAL AND DIGITAL APPROACHES TO CENTRE OF MASS ESTIMATION

This chapter has been published in the Journal of Anatomy.

MACAULAY, S., HUTCHINSON, J. R. & BATES, K. T. 2017. A quantitative evaluation of physical and digital approaches to centre of mass estimation. *Journal of Anatomy*, 231, 758-775. <https://doi.org/10.1111/joa.12667>

Author contributions: SM and KTB conceived the project, provided specimens, and collected data. SM analysed and interpreted data, and drafted manuscript. All authors critically revised manuscript and approved article.

2.1. Abstract

Centre of mass is a fundamental anatomical and biomechanical parameter. Knowledge of centre of mass is essential to inform studies investigating locomotion and other behaviours, through its implications for segment movements, and whole body factors such as posture. Previous studies have estimated centre of mass position for a range of organisms, using various methodologies. However, few studies assess the accuracy of the methods that they employ, and often provide only brief details on their methodologies. As such no rigorous, detailed comparisons of accuracy and repeatability within and between methods currently exist. This paper therefore seeks to apply three methods common in the literature (suspension, scales and digital modelling) to three ‘calibration objects’ in the form of bricks, as well as three birds to determine centre of mass position. Application to bricks enabled conclusions to be drawn on the absolute accuracy of each method, in addition to comparing these results to assess the relative value of these methodologies. Application to birds provided insights into the logistical challenges of applying these methods to biological specimens. For bricks, it was found that, provided appropriate repeats were conducted, the scales method yielded the most accurate predictions of centre of mass (within 1.49mm), closely followed by digital modelling (within 2.39mm), with results from suspension being the most distant (within 38.5mm). Scales and digital methods both also displayed low variability between centre of mass estimates, suggesting they can accurately and consistently predict centre of mass position. The suspension method here resulted not only in high margins of error, but also substantial variability, highlighting problems with this method.

2.2. Introduction

Centre of mass (CoM) is a fundamentally important anatomical and biomechanical parameter. At the level of the whole organism, it is a key determinant of stability at rest and in motion, and is therefore crucial in determining posture and limb kinematics (Attwells et al., 2006, Carrano and Biewener, 1999, Gatesy and Biewener, 1991, Grossi et al., 2014, Loverro et al., 2015, Young et al., 2007). Knowledge of CoM and other mass properties (i.e. mass and moment of inertia) of individual body segments are also essential in determining how a whole organism can move. These mass properties are essential inputs in research seeking to quantitatively characterise the spatial translations and rotations of segments, the muscular forces required to achieve any given motion and the associated energetic costs (Kilbourne, 2013). As such, mass properties are primary input parameters in biomechanical approaches investigating locomotion using both inverse and forward dynamic assessments of movement. Through its consequences for segment movements and for the whole organism, CoM therefore has a highly significant impact on determining the locomotor capabilities of an organism, and subsequently its wider behaviours and ecological role. The impact of CoM on behaviours such as posture and locomotor capabilities has been assessed through various sensitivity analyses (Bates et al., 2010, Gatesy et al., 2009, Hobbs et al., 2014, Hutchinson, 2004b) which found CoM position to have a substantial impact on these traits, further highlighting the importance of accurate estimates of CoM. Given its fundamental importance, it is unsurprising that CoM position has been estimated in a variety of species from primates and equids to dinosaurs (e.g. Allen et al., 2009, Crompton et al., 1996, Spriggins and Leach, 1986). Indeed, CoM is of particular interest in extinct taxa where it provides a valuable indirect route to information that cannot be directly observed. For example, on the locomotor habits of long extinct species, especially those possessing disparate body forms unlike those of living animals such as dinosaurs (e.g. Alexander, 1985, Henderson, 2004, Hutchinson et al., 2007, Sellers et al., 2013).

Historically, a range of physical methods have been employed to determine CoM position for whole organisms (e.g. Alexander, 1983, Alexander, 1985, Clemente, 2014, Henderson, 2003, Henderson, 2006), as well as organisms divided into their major component segments (e.g. Andrada et al., 2013, Crompton et al., 1996, Dempster, 1955, Nyakatura et al., 2012, Sprigings and Leach, 1986) (for overview, see Nigg and Herzog, 2007, Öz kaya et al., 2012). Three primary physical methods are present in the literature, each having been applied to a range of species. Balancing approaches have been applied to whole organisms and to individual segments (e.g. Crompton et al., 1996, Dempster, 1955, Dempster and Gaughran, 1967, Goetz et al., 2008, Hutchinson, 2004a, Myers and Steudel, 1997, Vilensky, 1979). This has been done most frequently using forms of balance boards (Dempster, 1955, Vilensky, 1979), but also using knife edges (Goetz et al., 2008). Suspension techniques rely on the same physical principles, but instead involve the suspension of specimens (or body segments) from one point, where they are either allowed to hang naturally (Alexander, 1983, Alexander, 1985, Chandler et al., 1975, Dempster, 1955, Dempster and Gaughran, 1967, Fedak et al., 1982, Rubenson and Marsh, 2009), or the position of the support is moved until they come to rest in alignment with a defined axis (Nauwelaerts et al., 2011). This process is repeated from multiple suspension points, from which results are overlaid (often with the help of photography (Fedak et al., 1982)). The point of intersection of the lines of suspension then gives the CoM of the object under study. The third technique, uses a scale, or scales, over which a specimen is supported to determine the moment arm of the specimen's weight that is acting on the scale at one end of the support system. Published variants of this approach include using scales at only one end of the system (Lephart, 1984, Sprigings and Leach, 1986, Walter and Carrier, 2002, Willey et al., 2004) or scales at both ends of the system with the organism lying on a support (Clemente, 2014, Henderson, 2003, Kilbourne, 2013) or resting directly on the scales (Henderson, 2006). It has been suggested that this technique is most

effective when the CoM is only to be investigated along one axis at a time (Eshbach et al., 1990), though this is also the case for some variants of the suspension method. It should be noted that the balancing and suspension methods both work based on the same physical principles - that an object will only come to rest if it is supported through its CoM. In the case of suspension, an object left to hang freely will come to rest with its CoM in line with the string it is suspended from; i.e. the vector of its weight and the vector of tension in the string are parallel and collinear, passing through the CoM. In the case of balancing methods, a plate (and any object placed upon it) will only balance on a support if the combined CoM of the system lies directly above the support; i.e. the vector of combined weight, passing through the combined CoM of the system, passes through the support.

Very few studies investigating CoM position using physical methods, such as those described above, include any form of assessment of the accuracy of their methods. Though the physical principles behind each of the methods are sound, any physical experimentation method has the potential for error, at the very least human error, in the set-up, capture and recording of data. Assessing the accuracy of the scale based technique, Lephart (1984) found mean absolute percentage errors of 0.03% in their estimations of CoM position (37 test objects ranging from 316 to 30,426g, unknown geometries). The balance board technique employed by Sprigings and Leach (1986) resulted in a predicted CoM position within 2mm of the geometric centre of their test object (an Olympic standard weightlifting disc: 20kg, 450mm diameter). Nauwelaerts et al. (2011) assessed the accuracy of their suspension method on test objects with simple geometries, finding that accuracy was dependent on the length and radius of their objects, and overall determined their method to be within approximately 1cm of the true CoM for a number of test objects of unknown geometries. Although some attempts have been made to compare results across studies (e.g. Nigg and Herzog, 2007),

such comparisons are hindered by the often extremely limited descriptions of the methodologies used in many cases.

Recent advances in computing technology have seen digital modelling used more and more frequently as a method for calculating CoM position (e.g. Allen et al., 2013, Amit et al., 2009, Bates et al., 2009a, Bates et al., 2016, Henderson, 1999, Hutchinson et al., 2007, Maidment et al., 2014, Nyakatura et al., 2015, Park et al., 2014, Paxton et al., 2014, Peyer et al., 2015, Ren and Hutchinson, 2008). Digital models offer some advantages over physical methods including ease of data sharing and simple manipulation for sensitivity analyses and repeatability analyses, in addition to the advantages of scanning procedures such as computed tomography (CT). Models based on CT scans or similar data enable internal and external anatomy to be visualised, and used as the basis for model generation, therefore incorporating a greater amount of the anatomical data available into models. It has been suggested that the detail of digital models is constrained more by researcher time than by limits of technology (Allen et al., 2009), highlighting the extensive opportunities and challenges presented by this medium.

It is however, frequently recognised that the validity of any methodology employing digital modelling techniques should be assessed before further application, and before any higher conclusions are drawn (Hutchinson, 2011). Comparisons are often made between physical measurements of body mass and values predicted from digital volumetric models (e.g. Allen et al., 2009, Bates et al., 2015, Bates et al., 2009b, Henderson, 2006, Hutchinson et al., 2007), where in some cases the discrepancies are appreciable (for example up to 16% in extant taxa (Allen et al., 2009)). However, assessing the ability of a model to accurately predict body mass does not indicate how accurately the model is able to predict CoM. The CoM estimates produced by digital models are rarely checked (with some notable exceptions; e.g.

Henderson, 2003, Henderson, 2006, Hutchinson et al., 2007), in part due to the relative difficulty of physically measuring CoM in comparison to body mass. Considering the fundamental importance of CoM in biomechanical and functional analyses (e.g. for dinosaurs: Allen et al., 2013, Bates et al., 2010, Gatesy et al., 2009), and the ever-increasing usage of digital models, the current lack of a comprehensive assessment of the accuracy of these digital modelling techniques in their ability to predict CoM is problematic.

This study therefore aimed to assess the accuracy of three commonly used methods for estimating CoM by application to a set of objects with known geometries, as well as biological specimens. Two physical methodologies for CoM estimation and a digital volumetric approach were applied to each object. Due to the similarities between suspension and balancing methods, only one was investigated here. A version of the suspension method was selected over balancing for inclusion in this study because it did not require the fabrication of specialist equipment, and it has been more widely applied across disciplines and species, for example in studies of both extant (Chandler et al., 1975, Dempster and Gaughran, 1967, Fedak et al., 1982, Hutchinson et al., 2007, Nauwelaerts et al., 2011) and extinct (Alexander, 1985, Koehl et al., 2011) taxa. A variant of the scales method was also included. The comparison of results from these three methodologies to the geometric centres of the test objects enabled an assessment of absolute accuracy for each method. By comparison with each other, the relative accuracies of these commonly employed methods were then investigated. Application of each of these approaches to the same three biological specimens allowed absolute CoM predictions to be compared, in addition to enabling an examination of the differences in repeatability and logistical limitations between the methodologies.

2.3. Methodology

2.3.1. Specimens and background

Six specimens were studied here - three intact cadavers of birds (as specimens of biological interest), and three bricks. Bricks were selected due to their simple, known geometries, and therefore predictable CoM positions. The bricks acted as standards by which the absolute and relative accuracy of our methodologies could be assessed, and therefore aided our interpretation of the results obtained from biological specimens. The three birds studied here were a leghorn chicken (*Gallus gallus domesticus*), common buzzard (*Buteo buteo*) and mallard duck (*Anas platyrhynchos*), selected to represent a range of different avian body plans and locomotor types. The linear dimensions and masses of the six specimens studied here are presented in Table 2.1.

As it was our aim to compare results from physical and digital methodologies, it was necessary to transfer the results of physical methods to digital space. This could be achieved in a variety of ways, such as a series of still photographs, or through the creation of photogrammetric models. Such methods have their merits (namely that they are cheap, and require no specialist equipment or knowledge to operate), and would be valid solutions to this problem. Here, however we opted to use an Oqus 7 Qualisys infrared motion capture system (www.qualisys.com), as the technology offered a quicker solution than photogrammetry, a more complete record of testing than still photographs and was not adversely affected by any movement of the specimens occurring during captures (e.g. during suspension testing). Calibration of the Qualisys system was performed before each data collection session to ensure that errors in capture accuracy were suitably low, i.e. approximately 1mm (mean error across cameras, across data collections: 1.32mm). This represents an additional benefit over other potential methods, for which the error margins

Table 2.1: Data on body mass and approximate dimensions for the six specimens studied here.

Specimen	Mass (kg)	Dimensions (mm)*	Additional information
Brick1	3.13	216 x 99 x 67	
Brick2	2.37	214 x 102 x 65	
Brick3	4.26	203 x 210 x 133	
Chicken (<i>Gallus gallus domesticus</i>)	1.08	500 x 250 x 570	Leghorn chicken, male, 14 weeks
Buzzard (<i>Buteo buteo</i>)	0.69	475 x 230 x 980	Common buzzard, gender and age unknown
Duck (<i>Anas platyrhynchos</i>)	1.12	545 x 150 x 610	Mallard duck, female, age unknown

* Dimensions for bricks are listed along the axes EF x CD x AB (see Figure 2.4 for more information on brick axes), and bird dimensions are listed along the axes cranio-caudal x dorso-ventral x left-right.

may be poorly investigated, and may vary considerably between trials. The Qualisys system used here consisted of 12 cameras, positioned around a large laboratory space usually used for capturing human gait trials. The Qualisys system enabled the 3D coordinates of a series of reflective spherical markers (12.7mm diameter), to be captured and transferred to digital space. All raw data (including Qualisys and CT data captures), data at key stages of processing, and final data produced here are available online at <http://datacat.liverpool.ac.uk/310>.

For the bricks, six markers were attached, one on each face (Figure 2.1A). The faces were designated as A-F, as identification was essential for running later tests. Seven markers were attached to the birds in the following positions: cranial surface of the head, lateral surface of the torso at the junction with the neck, lateral surface of the torso at the junction with the tail, one on each wing tip (on the ventral and dorsal surfaces respectively; corresponding to the distal phalanges rather than the flight feathers) and two on the left and right distal tarsometatarsi (Figure 2.1B). Markers were affixed to the skin (e.g. distal hindlimb) or to the outer surface of the birds' feathers and secured with tape to minimise movement of markers between testing runs. In all cases, markers were placed in order to give maximal coverage of the whole object under study, including the geometric extremes.

Consistency of posture for the *ex vivo* bird specimens was crucial in preventing CoM shifts relating to postural changes, which could affect comparisons between methodologies (Allen et al., 2009). Before testing, all bird specimens were therefore thawed to enable them to be positioned in a standardised posture. The posture used here was selected to be comparable to those typically used in digital modelling studies (e.g. Allen et al., 2013), where the aim is to compare the morphology of often vastly different organisms, and is therefore unlikely to

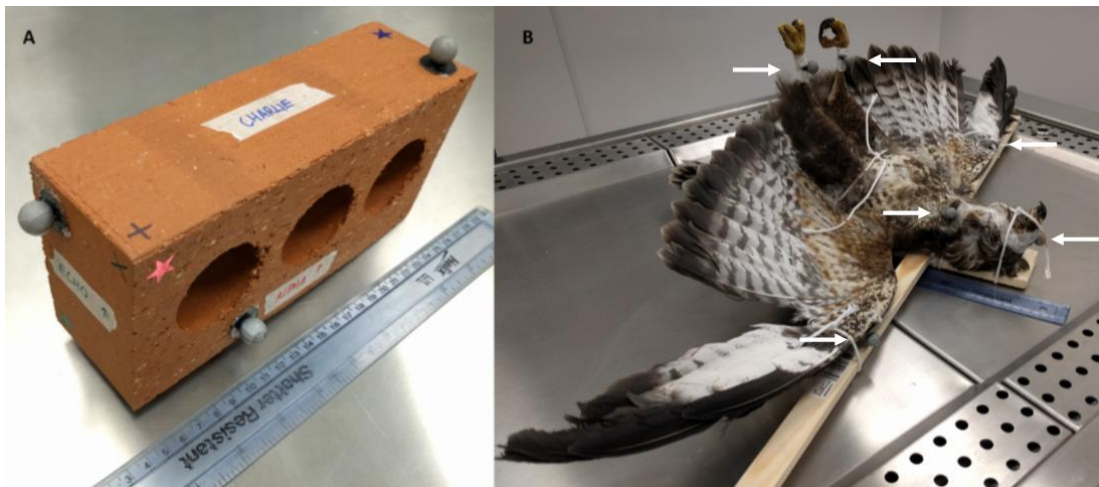


Figure 2.1: Pictures showing marker positions (silver balls indicated by white arrows) in bricks (A), and birds (B) as well as the standardised posture used for all bird specimens.

reflect a life-like position used by any given specimen. Our standardised posture was as follows: head and neck straightened cranially, forelimbs straightened laterally, hips extended and the remaining hindlimb joints straightened and allowed to freely hang ventrally (Figure 2.1B). To achieve this, specimens were tied to frames and then frozen at -20°C. It was necessary to remove the frozen specimens from these supporting frames for the duration of each testing period. Some defrosting, and therefore postural changes, inevitably occurred during this time, with the extent dependent on the nature and duration of testing. Attempts were made to minimise any changes by packing specimens with ice for transport in the case of CT scanning, and replacing the specimens onto their frames after each testing phase. The magnitudes of these postural changes were quantified from data captured during testing. Posture change was measured by computing the 3D distance between each marker and each other marker for each testing condition. Inter-marker distances were then compared across testing conditions, those with the largest summed discrepancy between tests were taken to represent the largest posture shift. Models from one of these testing conditions could then be manipulated to match the other extreme posture, thereby producing approximations of the CoM shift resulting from this change in posture. The resulting data informed the degree of caution necessary when drawing comparisons between testing methods for the bird data.

2.3.2. Physical CoM - suspension methodology

Our suspension method is based on the approaches used by Alexander (1983) and Nauwelaerts et al. (2011). Specific details of our methodology follow, and a visual overview is presented in Figure 2.2.

Specimens were suspended from a string via a loop that was tightened around each specimen. In order to estimate CoM with this method, it was also necessary to collect data on the position of the string in relation to the object under study. Two Qualisys markers were

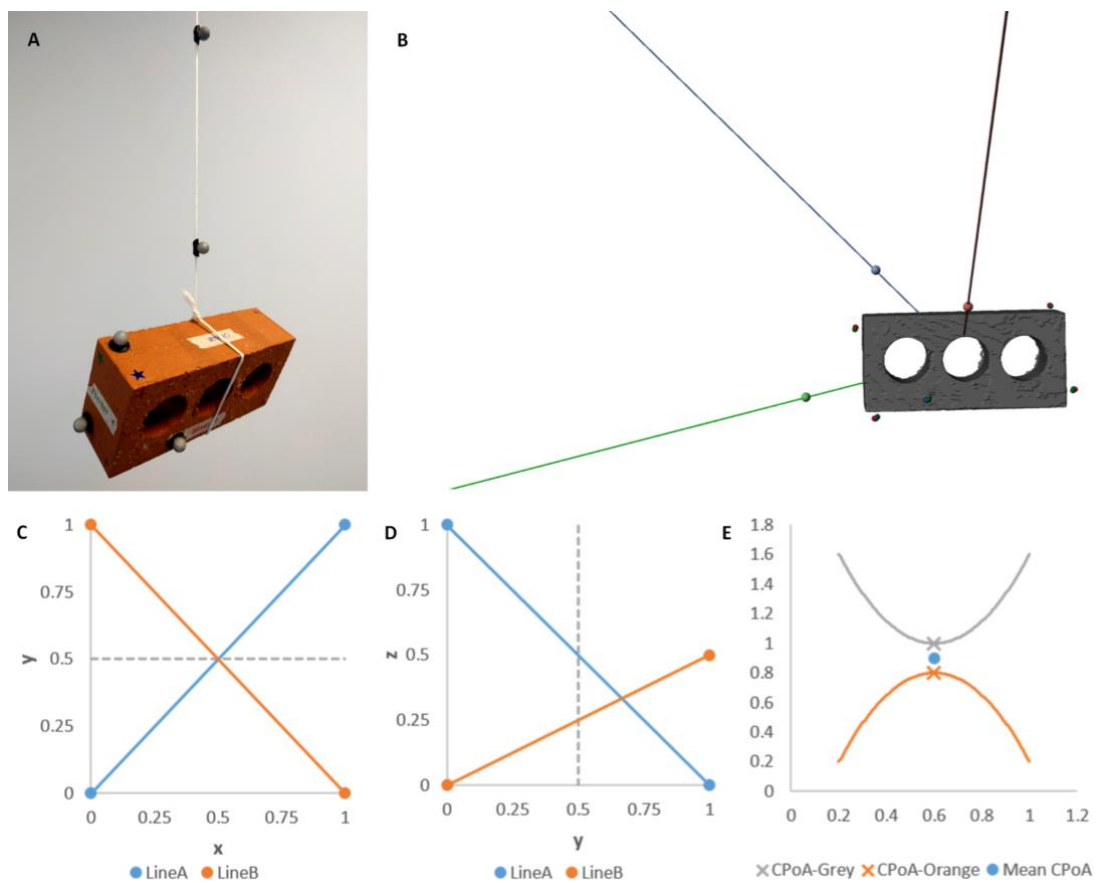


Figure 2.2: Stages of the suspension methodology performed in this study. **A:** Suspension of object for Qualisys capture, at least three different suspension positions were captured for each object. **B:** After the multiple Qualisys runs for the same specimen were matched, the specimen markers are aligned, and the various lines of suspension are now distributed around the specimen. **C & D:** Two hypothetical 3D lines plotted in two, 2D graphs. Note that in **(C)**, the lines have equal x values at y=0.5, but at y=0.5 in **(D)**, they have different z values, and therefore do not intersect in 3D space. **E:** Two hypothetical, non-intersecting curves, highlighting the point of closest approach (CPoA) on each line, and the resulting mean CPoA.

therefore placed on the string for each position, as far apart as possible (see Figure 2.2A). The system was allowed to come to rest, after which a data capture was performed for at least three seconds at 200Hz. This procedure was repeated for multiple positions for each specimen. Between each position, specimens were removed from the string loop, repositioned and reaffixed to the string. Positions were selected attempting to provide coverage of the whole object, with at least one position taken in each plane. All specimens had data collected for at least three positions. To assess the impact of the selection of suspension location and other potential sources of human error on the CoM predicted by the method, data were collected for a total of 10 positions for one brick and two bird specimens.

The 3D marker coordinate data resulting from the Qualisys data captures for each position were exported, and marker coordinates from one timeframe extracted in Matlab (www.mathworks.com). In order to determine CoM for each specimen, it was necessary to determine the point in space where the strings from each position intersected with one another in relation to the object. Coordinate sets for each object were therefore matched to one another, using the position of the markers directly on the specimens (i.e. those not on the string) as inputs. This was achieved using a global least square optimisation algorithm within the open source physics package GaitSym (www.animalsimulation.com). This algorithm matched the objects by a combination of translation and rotation in order to find the best global statistical fit (defined as the position with minimal error across all markers) between the two sets of markers. Once all the positions for a given object had been matched in digital space, the new coordinates for all markers were extracted in Matlab.

The matched coordinates for the two string markers for each position were carried forward to estimate the overall object CoM. When considered in 2D (as in previous studies; e.g.

Alexander, 1985), the point of intersection between two lines of suspension (here represented by the string) is the CoM estimated for that object. However, in 3D, two lines will very rarely intersect exactly with one another (see Figure 2.2C and D for schematic representation of this). As an alternative to a strict intersect point, the point of closest approach was calculated for each pair of lines using custom Matlab code, which is freely available online (<http://datacat.liverpool.ac.uk/310>). The mean of the two points of closest approach was taken to be the CoM predicted by those two lines (see Figure 2.2E for simplified example). This approach was repeated for each pair of lines in turn, giving a total of three predicted CoM positions where three suspensions were carried out, and 45 predicted CoMs where ten suspensions were carried out. The mean of all the predicted CoM positions for each object was then taken, giving the overall CoM predicted for that object by the suspension method (CoM_{SU}).

2.3.3. Physical CoM - scales methodology

Our scales method is based on the approach used by Clemente (2014). Specific details of our methodology follow, and a visual overview is presented in Figure 2.3.

Two identical Ohaus Scout electronic balances ($\pm 0.1\text{g}$) were placed on a flat table. The scales were aligned with one another, and with the table they were resting on. A support was placed in the centre of each scale, perpendicular to the long axis of the table (Figure 2.3A). Here, the supports were inverted triangular prisms, length 60mm. A wooden plank was then placed between the two supports so that it rested on them evenly, with care taken to align the plank with the long axis of the table (Figure 2.3A). This plank, in addition to a metre ruler perpendicular to it, had one Qualisys marker placed at the centre of each end to enable the specimen-scales system to be aligned to the digital world axes in the processing phase. The scales were positioned to give approximately 10-20mm overhang between the plank ends

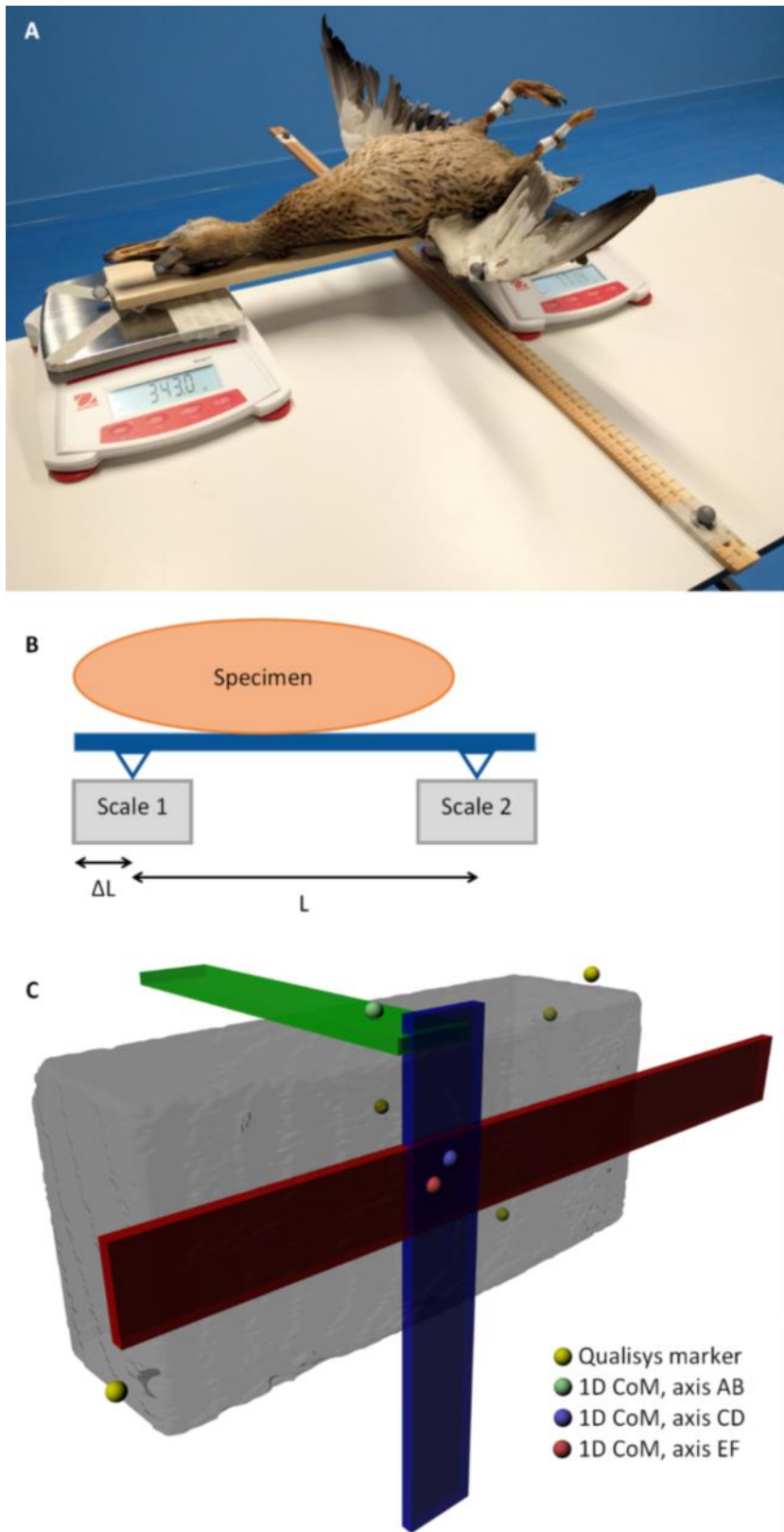


Figure 2.3: Stages of the scales methodology performed in this study. **A:** Photograph of the experimental set-up, with the duck specimen. **B:** Schematic of experimental set-up, showing

specimen resting on plank, lying on the two scales. The distance between supports (L) and distance from proximal plank edge to proximal support (ΔL) are indicated. These data combined with mass readings from the two scales enable calculations of CoM position. **C:** Rendering of Brick1, after marker data from three data captures was matched, showing the position of the three planks aligned with the three axes, and the three, 1D CoM positions plotted. These are then combined to give a 3D, final CoM prediction from the method.

and the centre of the supports (see Figure 2.3A for experimental set-up). Both scales were then tared.

The specimen under investigation was then placed onto the plank, with the proximal face of the brick, or the beak tip of the bird, in line with the proximal plank edge (see Figure 2.3A for experimental set-up). In the case of the bricks, this was repeated for each of the three axes, with a different axis aligned with the plank in each run, in order to estimate CoM position in 3D. For bird specimens, CoM was measured only along the cranio-caudal axis, resulting in 1D CoMs along that axis for all three birds. Though it is desirable to measure dorso-ventral CoM position, to achieve this for the complex geometries of the biological specimens would have required specimen specific modifications to the experimental set-up, which were deemed beyond the remit of this study. Although the cranio-caudal axis is the primary axis of interest in many studies (e.g. Allen et al., 2013, Bates et al., 2010, Clemente, 2014, Gatesy et al., 2009, Hutchinson, 2004a), this represents a limitation of this methodology when applied to biological specimens where 3D CoM positions are essential to investigate problems in a complex 3D system such as an organism.

For each run, a Qualisys capture was performed (at least three seconds, at 200Hz), in addition to recording the values from the proximal and distal scales, the distance between the two supports, and the distance from the proximal plank edge to the centre of the proximal support. The distance of the CoM, along the axis that is in line with the plank, from the proximal plank edge could then be calculated as follows:

$$CoM_{Sc} = \left(W_2 * \frac{L}{(W_1 + W_2)} \right) + \Delta L$$

Equation 2.1

Where CoM_{Sc} is the distance of the CoM from the proximal plank edge along the axis of the plank, W_1 and W_2 are the masses on the proximal and distal scales respectively, L is the distance between supports and ΔL is the distance between proximal plank edge and the point where the proximal support contacts the proximal scale (see Figure 2.3B for a schematic highlighting these values).

Runs for the same specimen were spatially aligned using GaitSym, as described in Section 2.3.2. Bird and brick data were then plotted in Maya (www.autodesk.com/maya). The specimen axes were aligned with the digital world axes using trigonometry based on the markers on the plank and ruler. Once aligned, calculated values for CoM_{Sc} could be plotted in digital space. In the case of bricks, it was necessary to plot three 1D CoMs, one for each axis investigated (see Figure 2.3C). The combination of these 1D CoMs gave a 3D CoM for each brick, which along with the 1D CoMs for birds, formed the final coordinates for CoM_{Sc} for each specimen.

Using the original methodology described here, it was noted that the predicted CoM position was consistently skewed towards the proximal scale. To address this issue, ‘reversed repeats’ were conducted for two bricks. Here, a further three data collection runs were performed, so that each brick face was aligned with the proximal plank edge for one run, giving two runs per axis. Additionally, it was noted that the construction of this experimental set-up and subsequent object placement had the potential to introduce human error into resulting predictions of CoM position. The associated error was therefore quantified using one brick, by conducting repeats where the experimental set-up was de-constructed and re-constructed between each of five trials, with full data captures performed for each individual trial.

2.3.4. Digital CoM - digital modelling

All specimens were scanned in a medical grade CT scanner at the University of Liverpool Small Animal Hospital, Leahurst (Toshiba Aquilion PRIME helical scanner, slice thickness: 1mm, 120kVp, 100mA). All scan data are freely available online (<http://datacat.liverpool.ac.uk/310>). Scan data were segmented in Avizo 7.1 (www.Avizo3D.com) using a combination of automated and manual thresholding as required to extract clean models. For bricks, the whole brick outline was extracted, along with the Qualisys markers. For birds, Qualisys markers, a solid skin outline, and all notable air cavities (defined as regions of zero density on CT scan) present in the torso, neck and head regions were extracted. The condition of the air cavities varied considerably between the bird specimens, due to differences in conditions and handling prior to freezing (Supplementary Information 2.1). All air cavities were left as they were in the original frozen specimen, meaning the conditions captured in the CT scans were equivalent to those present during the experimental work, though they are unlikely to represent the resting condition for a living bird. Previous studies have shown that any subjectivity present in the segmentation process has minimal effect on the final mass properties estimated (Allen et al., 2009). To ensure our methodology followed this finding, segmentation of the original CT data for one brick was repeated, giving a total of three models.

Extracted surfaces were edited in Geomagic Studio 10 (www.geomagic.com) to remove any excess material captured by segmentation. Mass properties (volume and CoM) for the final surfaces were calculated in FormZ (www.formz.com). In the case of bricks, this CoM was the final digital CoM, but further steps were required for avian specimens due to the inclusion of multiple components (i.e. flesh and air cavities) in the models. For birds, the masses of each component were calculated from their respective volumes by the application of a density value of 1000kgm^{-3} , with air cavities subtracted where appropriate, as in numerous previous

studies (e.g. Alexander, 1985, Allen et al., 2009, Bates et al., 2009b, Henderson, 1999, Hutchinson et al., 2007). This method is referred to as our ‘best guess’ digital CoM for birds, CoM_D . It should be noted that although this method is commonplace in recent literature, it represents a simplification of the anatomy, and one that has the potential to affect the CoM predicted by models. Though a thorough investigation of the consequences of these decisions on density modelling was beyond the scope of this study, a sensitivity analysis was conducted on this parameter to assess the impact on predicted CoM position. This was achieved by applying a range of published density data (Buchner et al., 1997, Dempster and Gaughan, 1967, Henderson, 2004, Henderson, 2006, Lovvorn and Jones, 1991, Tserveni and Yannakopoulos, 1988), derived by a variety of methods in a range of taxa, to our models (see Table 2.2 for details). Once mass properties were calculated, centres of mass for all components were combined, to give an overall CoM for the specimen according to the following equation:

$$\text{CoM}_D = \frac{\sum(\text{CoM}_f * \text{mass}_f) - \sum(\text{CoM}_a * \text{mass}_a)}{\sum \text{mass}_f - \sum \text{mass}_a}$$

Equation 2.2

Where CoM_D is the digital CoM for the whole system, CoM_f and mass_f refer to the mass properties of flesh components, and CoM_a and mass_a refer to air cavity mass properties.

2.3.5. Geometric centres

For brick specimens, by virtue of their simple geometry, symmetry and uniform density, it was assumed that the geometric centre (CoM_G) of each brick was also the true CoM position. The accuracy of each method could therefore be assessed by comparing the CoM predictions made to CoM_G . CoM_G was calculated, after aligning bricks with the digital world axes as

Table 2.2: Details of the density data used in the sensitivity analysis.

CoM abbreviation	Density data source	Taxonomic group	Density data applied (kgm ⁻³)
CoM _{D1}	Best guess (see e.g. Allen 2013)	Generic	Flesh: 1000, Air cavities: 0
CoM _{D2}	Tsirveni & Yannakopoulos 1988 - Homogeneous flesh (maximum density)	Bird	Flesh: 1069
CoM _{D3}	Lovvorn & Jones 1991 - Homogeneous flesh (minimum density)	Bird	Flesh: 536.8
CoM _{D4}	Henderson 2006	Bird/archosaur	Head and Neck: 300, Trunk: 800, Limbs: 1000
CoM _{D5}	Henderson 2004	Bird/archosaur	Head: 1000, Neck: 600, Trunk: 850, Limbs: 1050
CoM _{D6}	Dempster & Gaughran 1967	Human	Head and Neck: 1170.8, Trunk: 1013.8, Forelimbs: 1080*, Hindlimbs: 1062*
CoM _{D7}	Buchner et al. 1997	Horse	Head: 1031, Neck: 1038, Trunk: 850, Forelimbs: 1155*, Hindlimbs: 1170*

* Values calculated as an average for all segments of that limb.

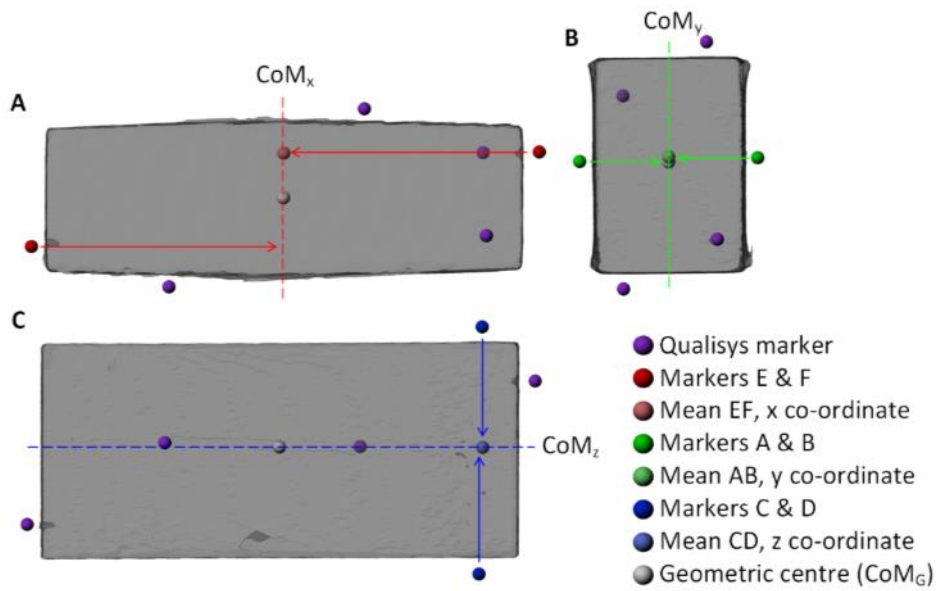


Figure 2.4: Render of Brick1 from the top (A), left side (B) and front (C) depicting the method for calculating the geometric centre (CoM_G). This was calculated by taking the mean of three pairs of Qualisys markers, one pair per axis. CoM_x , CoM_y and CoM_z then combine to give the final xyz co-ordinates for a 3D CoM_G .

described in Section 2.3.3, by taking the mean coordinates of markers on opposite faces of the brick, using a different pair for each axis of interest. Combining these 1D coordinates gave the 3D CoM_G (see Figure 2.4 for a visual overview).

To enable comparisons between methods, and with CoM_G , the marker coordinates resulting from the two physical methods were matched to those extracted from the CT data of the corresponding specimen using GaitSym, as described in Section 2.3.2. Once data from all methods were combined, models were translated so that for bricks corner ADE (i.e. the corner shared by faces A, D and E) or the right hip (for birds) were at the origin of the world coordinate system in digital space (i.e. $x=0$, $y=0$, $z=0$), for ease of interpretation of CoM values. All raw and processed data, as well as the code used to generate them, are freely available online (<http://datacat.liverpool.ac.uk/310>).

2.4. Results

2.4.1. Overview

Data on the geometric centres and CoM positions predicted by each method conducted here are visualised in Figures 2.5 and 2.6, with differences presented in Figure 2.7 and Tables 2.3 and 2.4. Further data on CoM positions are reported (Supplementary Information 2.2 and 2.3), along with data on 1D differences in CoM positions and normalised versions of CoM results (Supplementary Information 2.4 and 2.5). No statistics were performed on the data collected here; all results are therefore purely descriptive.

First, we report the results from bricks, stating the absolute and relative errors of the different methodologies in these reference objects in comparison to their known CoM positions. These results include those from the various repeatability tests. We then discuss results from bird specimens by methodology. It should be noted that, as true CoM is not

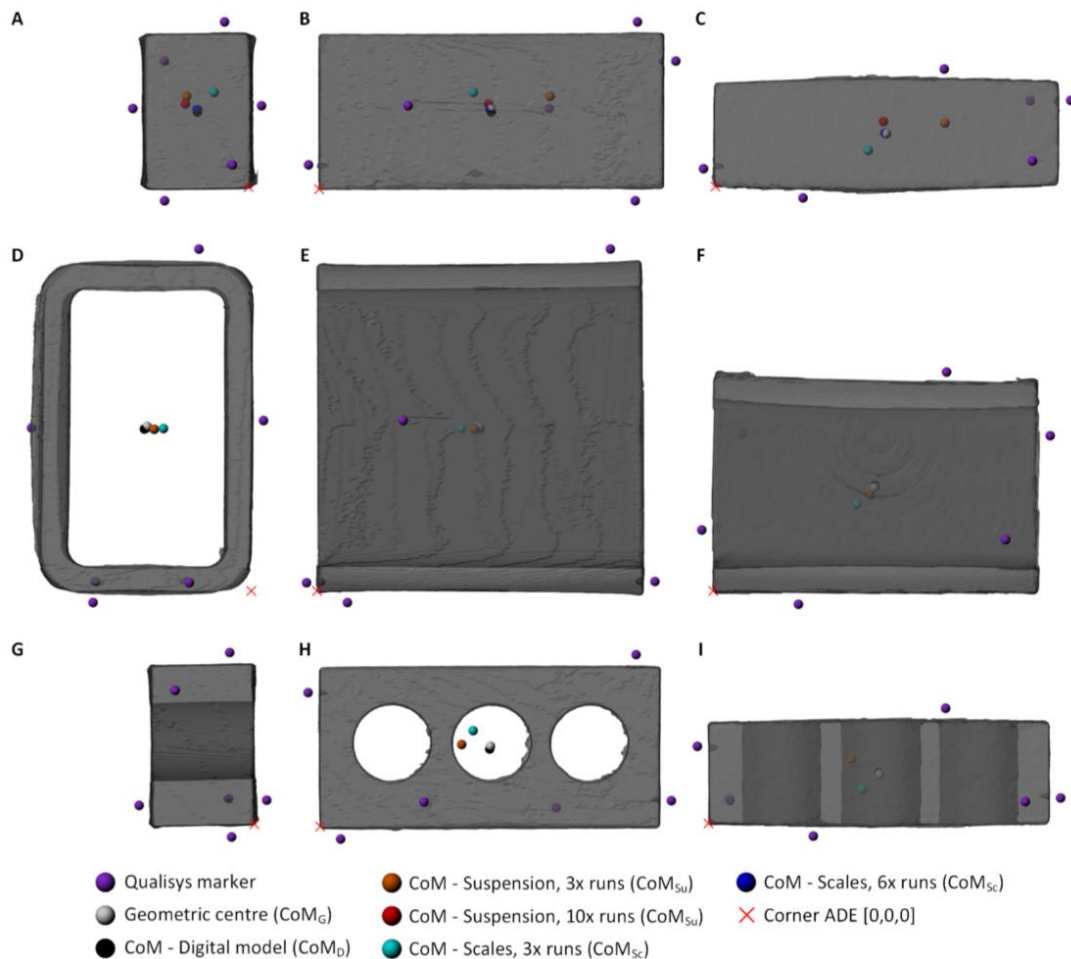


Figure 2.5: Predicted CoM positions displayed on renders of Brick1 (A-C), Brick2 (D-F) and Brick3 (G-I), shown from the left (A, D, G), front (B, E, H) and top (C, F, I). Predicted CoM positions are shown for each methodology, coloured according to the key. In cases where multiple CoM positions were available for the initial suspension and scales methods, only the CoM from the first runs are displayed here, for clarity.

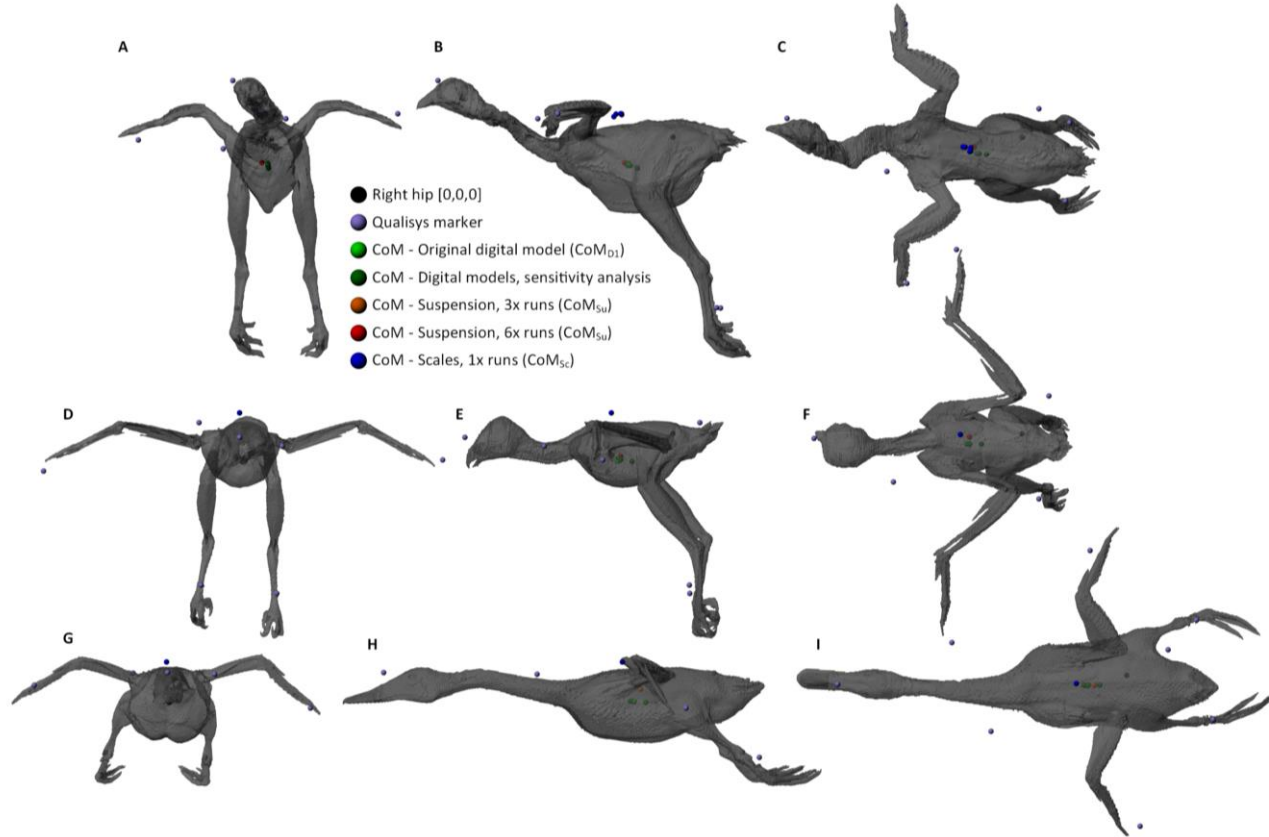


Figure 2.6: Predicted CoM positions displayed on renders of chicken (A-C), buzzard (D-F) and duck (G-I), shown in cranial view (A, D, G), left lateral view (B, E, H) and dorsal view (C, F, I). Predicted CoM positions are shown for each methodology, coloured according to the key. In the chicken and buzzard, multiple suspension CoMs are shown along with multiple scales CoMs in the chicken.

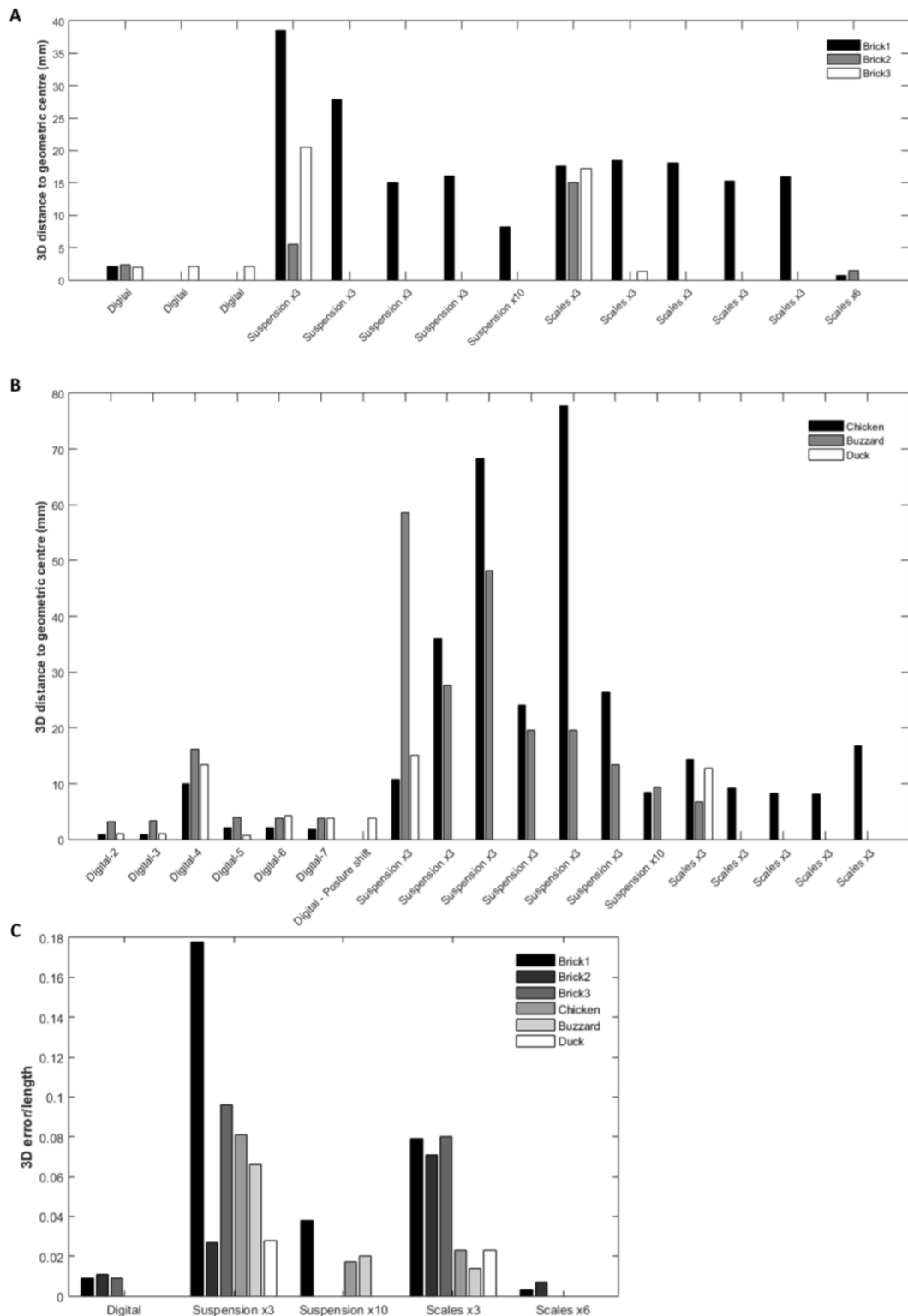


Figure 2.7: A: Graph displaying 3D distances from brick geometric centre (CoM_G) to the CoM positions predicted by the methodologies listed on the x axis. **B:** Graph displaying 3D distances from our ‘best guess’ bird digital CoM (CoM_{D1}) to the CoM positions predicted by

the methodologies listed on the x axis. (C) 3D differences between geometric centre (bricks)/best guess digital CoM (birds) and CoM predictions produced by the methods studied here, normalised by maximum side length (bricks)/cranio-caudal body length (birds).

Table 2.3: 3D distances from brick geometric centre (CoM_G) to the centres of mass predicted by the methodologies examined here for the three brick specimens.

CoM Description	3D distance to CoM_G (mm)		
	Brick1	Brick2	Brick3
Digital (CoM_D)	2.1	2.4	2.0
Digital (CoM_D)	-	-	2.1
Digital (CoM_D)	-	-	2.0
Suspension (CoM_{Su}) - 10 runs	8.2	-	-
Suspension (CoM_{Su}) - 3 runs	38.5	5.6	20.5
Suspension (CoM_{Su}) - 3 runs	27.8	-	-
Suspension (CoM_{Su}) - 3 runs	15.1	-	-
Suspension (CoM_{Su}) - 3 runs	16.0	-	-
Scales (CoM_{Sc}) - 6 runs	0.7	1.5	-
Scales (CoM_{Sc}) - 3 runs	17.6	15.0	17.2
Scales (CoM_{Sc}) - 3 runs	18.5	-	-
Scales (CoM_{Sc}) - 3 runs	18.1	-	-
Scales (CoM_{Sc}) - 3 runs	15.4	-	-
Scales (CoM_{Sc}) - 3 runs	16.0	-	-
Geometric (CoM_G) - 3 runs	2.0	0.4	-
Geometric (CoM_G) - 3 runs	0.4	-	-
Geometric (CoM_G) - 3 runs	2.2	-	-
Geometric (CoM_G) - 3 runs	0.9	-	-

Table 2.4: 3D distances from the digital centre of mass predicted by our original model ($\text{CoM}_{\text{D}1}$) to the centres of mass predicted by the methodologies examined here for the three bird specimens.

CoM Description	3D distance to $\text{CoM}_{\text{D}1}$ (mm)		
	Chicken	Buzzard	Duck
Digital - $\text{CoM}_{\text{D}2}$ - Tsvorani 1988	0.9	3.8	1.0
Digital - $\text{CoM}_{\text{D}3}$ - Lovvorn 1991	0.9	3.8	1.0
Digital - $\text{CoM}_{\text{D}4}$ - Henderson 2006	10.0	16.2	13.3
Digital - $\text{CoM}_{\text{D}4}$ - Henderson 2004	2.0	4.0	0.7
Digital - $\text{CoM}_{\text{D}6}$ - Dempster 1967	2.2	3.1	4.3
Digital - $\text{CoM}_{\text{D}7}$ - Buchner 1997	1.8	3.4	3.8
Digital - Extreme posture shift	-	-	3.8
Suspension (CoM_{Su}) - 10 runs	8.5	9.5	-
Suspension (CoM_{Su}) - 3 runs	10.7	58.5	15.0
Suspension (CoM_{Su}) - 3 runs	36.0	27.6	-
Suspension (CoM_{Su}) - 3 runs	68.3	48.1	-
Suspension (CoM_{Su}) - 3 runs	24.1	19.6	-
Suspension (CoM_{Su}) - 3 runs	77.8	19.6	-
Suspension (CoM_{Su}) - 3 runs	26.4	13.4	-
Scales (CoM_{Sc}) - 3 runs *	14.4	6.8	12.8
Scales (CoM_{Sc}) - 3 runs *	9.3	-	-
Scales (CoM_{Sc}) - 3 runs *	8.3	-	-
Scales (CoM_{Sc}) - 3 runs *	8.1	-	-
Scales (CoM_{Sc}) - 3 runs *	16.8	-	-

* Scales CoM positions in birds were only determined in one dimension, therefore the distances here are 1D only.

known for the birds, the methodologies are instead compared back to our ‘best guess’ digital CoM predictions ($\text{CoM}_{\text{D}1}$). The results reported for the avian specimens here are therefore strictly relative, suitable for comparison with one another, but do not provide a quantitative measure of the accuracy of any given method. Results from further repeatability tests are presented for these exemplar animals, which have more complex geometries and which therefore present more logistical challenges for testing than simple objects like bricks.

2.4.2. Bricks

2.4.2.1. Geometric centres

The interpretations made here are reliant on the accuracy of estimates of the geometric centres (CoM_G) of each brick. In an attempt to maximise the accuracy of CoM_G , it was calculated using data from six runs wherever possible, or in the case of Brick3, from three runs. The variability present in CoM_G predictions from repeated runs was quantified in Brick1. When comparing CoM_G values for this brick, the difference between the alternative CoM_G predictions ranged from 0.374 to 2.18mm, with a mean of 1.34mm (Table 2.3).

2.4.2.2. Suspension method

Initial predictions of CoM by suspension (CoM_{Su}) from three suspension positions were within 16, 5.6 and 20.5mm of CoM_G for Bricks 1-3 respectively (Table 2.3, Figure 2.5). In Brick1, where data from four iterations of this basic suspension method were collected to assess the effect of human inputs, distance from CoM_{Su} to CoM_G ranged from 15.1 to 38.5mm, a total range of 23.4mm (Table 2.3, Figure 2.5A-C). The error present in CoM_{Su} decreased when additional runs were performed on Brick1; for a total of ten suspension positions CoM_{Su} was then within 8.2mm of CoM_G (Table 2.3, Figure 2.5A-C). This represented a 66% improvement in the ability to predict CoM_G when ten, rather than three, positions were considered for Brick1 (Table 2.3, Figure 2.5A-C). However, it should be noted that for

Brick2, CoM_{Su} predicted from only three suspension positions was closer to CoM_G (5.6mm; Table 2.3, Figure 2.5D-F) than was CoM_{Su} for Brick1, predicted from ten suspension positions (8.2mm) (Table 2.3, Figure 2.5A-C).

2.4.2.3. *Scales method*

Initial predictions of CoM by the scales method (CoM_{Sc}) from three runs (one per axis), were within 17.6, 15 and 17.2mm of CoM_G , for Bricks 1-3 respectively (Table 2.3, Figure 2.5). The error present in CoM_{Sc} decreased substantially when additional ‘reversed repeats’ were performed (giving two runs per axis). This effect was assessed in Bricks 1 and 2, where CoM_{Sc} was then within 0.691 and 1.499mm of CoM_G respectively. Those ‘reversed repeats’ values represented 90% and 96% improvements in the ability of the scales method to predict CoM_G . Five CoM_{Sc} positions were predicted for Brick1 from repeats to assess the repeatability of this method, where the experimental set-up had been completely deconstructed and reconstructed between runs. These predicted CoMs were between 15.4mm and 18.5mm from CoM_G , a maximum variance of 3.13mm (Table 2.3).

2.4.2.4. *Digital modelling*

Predictions of CoM position by the digital methodology (CoM_{D}) were within 2.05, 2.39 and 2mm of CoM_G , for Bricks 1-3 respectively (Table 2.3, Figure 2.5). Two additional models were generated for Brick3 by repeating the segmentation of the raw CT data. For these additional repeats, CoM_{D} was within 2.05 and 2.03mm of CoM_G (Table 2.3). The three CoM_{D} values estimated were highly consistent with one another, with a range of 0.058mm.

2.4.2.5. *Overview*

Comparing the initial runs across the three bricks (i.e. three suspension positions, three scales captures [one per axis], and the initial CT segmentation), CoM_{D} was consistently

closest to CoM_G (2.05, 2.39, 2mm; Figure 2.7A). In Bricks 1 and 3, CoM_{Sc} was the next closest (17.1, 17.12mm; Figure 2.7A), followed by CoM_{Su} (24.4, 20.5mm; Figure 2.7A). In contrast, in Brick2, CoM_{Su} was closer to CoM_G than was CoM_{Sc} (5.58mm versus 15mm; Figure 2.7A). The variation present in the predicted values across bricks for these initial runs was lowest for CoM_D (0.391mm), followed by CoM_{Sc} (3.47mm) and CoM_{Su} (32.9mm). Alternatively, considering only the best performing runs for each methodology (i.e. ten suspension positions, six scales captures [two per axis], and the original CT segmentation) in Brick1, CoM_{Sc} was closest to the geometric centre (0.692mm), followed by CoM_D (2.05mm), with CoM_{Su} the most distant (8.18mm).

2.4.3. Birds

2.4.3.1. Suspension method

Initial predictions of CoM by suspension (CoM_{Su}) in birds were within 10.7, 58.5 and 15mm of CoM_{D1} , for the chicken, buzzard and duck respectively (Table 2.4, Figure 2.6). As seen in the brick data, CoM_{Su} predictions were highly variable. In the chicken and buzzard, where six repeats of the basic suspension run were conducted, predicted values of CoM_{Su} varied by 67 and 45mm respectively (Table 2.4, Figure 2.6A-F), a maximum distance of 77.8mm from CoM_{D1} . CoM_{Su} positions calculated from ten runs were closer to CoM_{D1} compared to those from three runs, for both the chicken (8.47mm versus 40.55mm; Table 2.4, Figure 2.6A-C) and the buzzard (9.46mm versus 31.1mm; Table 2.4, Figure 2.6D-F).

2.4.3.2. Scales method

Initial predictions of CoM position by the scales method (CoM_{Sc}) were within 14.4, 6.8 and 12.8mm of CoM_{D1} for the chicken, buzzard and duck respectively (Table 2.4, Figure 2.6). In the chicken, where the experimental set-up was dismantled and reassembled between repeats, the variability between CoM positions was relatively low (8.66mm; Table 2.4, Figure

2.6), considerably lower than in suspension for avian specimens (i.e. up to 67mm; Table 2.4, Figure 2.6), but greater than that seen in equivalent repeats for bricks (3.13mm; Table 2.4, Figure 2.6).

2.4.3.3. *Digital modelling*

Digital CoM predictions in biological specimens require not only a detailed representation of object geometry (as for bricks), but also the assignment of density data. Results from the sensitivity analysis conducted on this variable show that the CoM predicted using density data from Henderson (2006) ($\text{CoM}_{\text{D}4}$) was most distant from the original $\text{CoM}_{\text{D}1}$ in all three birds (10, 16 and 13mm; Table 2.4, Figure 2.6). The remainder of the CoM positions, predicted with applications of different density data (see Table 2.2 for details), were all close to one another, and to the original $\text{CoM}_{\text{D}1}$ (maximum distance of 3.58mm; Table 2.4, Figure 2.6).

2.4.3.4. *Quantifying posture change*

The effect of posture change was quantified in the bird with the most extreme posture shift between testing conditions (defined by the greatest total difference in distances between markers). Specifically, the greatest posture change occurred in the duck between the digital and suspension methodologies. The segments of the digital duck model were manipulated to match the Qualisys marker positions to their altered positions, as captured during the suspension runs. This rigid body transformation was achieved in Maya by rotating segments around appropriate joint centres, indicated by the skeletal material. This resulted in a CoM shift of 3.81mm from the original $\text{CoM}_{\text{D}1}$ (Table 2.4). This can be considered an approximation of the maximum error present in CoM positions due to posture changes between the different methodologies. As the CoM positions predicted by the different methodologies in the biological specimens studied were different from one another by more than 4mm, it can

be concluded that the differences seen between methodologies are real and not the effect of postural changes between testing runs.

2.4.3.5. *Overview*

Taking the best runs from each methodology, CoM_{Sc} was marginally closer (8.11, 6.78 and 12.8mm) to CoM_{D1} compared to CoM_{Su} (8.46, 9.46 and 15mm), in these birds (Figure 2.7B). It should be noted that the scales method used here did not include ‘reversed repeats’, which was shown to increase the accuracy of CoM predictions in the bricks (Table 2.3, Figure 2.5). The variability within the methods showed similar trends to bricks: CoM_{Su} from three runs showed relatively high variability (up to 67.1mm), CoM_{Sc} from three runs displayed relatively low variability (8.66mm) and the variability seen in digital models with the sensitivity analysis on density parameters (if outlying data from Henderson (2006) were excluded; see Section 2.5.4 below), was lower again (1.28mm).

2.5. Discussion

2.5.1. *Overview*

The CoM positions predicted by the three methodologies here varied considerably across each of the bricks (Table 2.3, Figure 2.5). This variability is indicative of differences in their ability to accurately predict CoM_{G} , which is taken to be a good measure of true CoM position ($\pm 2\text{mm}$) in these test objects. For both bricks and birds, the variability present within methods was found to differ considerably between the three approaches (Tables 2.3 and 2.4, Figures 2.5 and 2.6). This is suggestive of differences in consistency and repeatability of the different methods. Briefly, we found that the scales methodology with reversed repeats was the most accurate, as well as being highly consistent (Tables 2.3 and 2.4, Figures 2.5 and 2.6). It was very closely followed by the digital method, which also appeared accurate, and with good consistency across the repeats performed on bricks here (Table 2.3, Figure 2.5). The

suspension method was identified as the least accurate, yielding predictions that were the most distant from CoM_G , as well as displaying high variability between repeats (Tables 2.3 and 2.4, Figures 2.5 and 2.6).

We recognise that the small sample size studied here, and the associated lack of statistical testing has the potential to hinder conclusions being drawn about the differences between the methodologies investigated. However, we suggest that as the differences present between suspension and the other methods are so stark, and our experimental design identified and investigated multiple influencing factors, that these descriptive results can be used to confidently identify real differences.

A standardised posture was used here (see Section 2.3.1), which sought to replicate the standard postures commonly used in digital modelling studies (e.g. Allen et al., 2013, Bates et al., 2016, Hutchinson et al., 2007) as closely as possible in physical *ex vivo* specimens. The use of a standardised posture enables comparisons to be drawn between the morphologies of species with considerably different body plans. However, *in vivo*, drastic differences in morphology and the associated changes in CoM position are often accompanied by differences in posture which can act to mitigate these differences. Similarly, two specimens with a similar CoM in a standard posture may utilise substantially different postures, and therefore possess distinct CoMs *in vivo*. Model posture should therefore be selected based on the purpose of the study in question. For studies seeking to quantify morphology using CoM, a standard posture is appropriate.

Though previous studies (Nauwelaerts et al., 2011) found correlations between features of object geometry and the error present in CoM predictions, we found no strong evidence of such an effect in any of the methods investigated here (Supplementary Information 2.6). In

the absence of a strong correlation, and given that all our objects are approximately equal in size, we suggest that the absolute errors reported here can be interpreted with confidence.

Normalising the data by length (longest side in bricks, cranio-caudal body length in birds) did not change the overall trends seen in the data (Figure 2.7C, Supplementary Information 2.5).

The digital and scales methods, including reversed repeats, still had very low errors (less than 1.2% of body/brick length), further supporting our conclusion that these methods perform best for the specimens studied here. In the normalised data, errors relative to length were notably lower in birds than in bricks. This is a reflection of their greater lengths, and the fact that error is independent of size (Supplementary Information 2.6).

Below, we discuss results from all methodologies in more detail, highlighting their benefits and limitations. We seek to identify issues with the methods, discuss the potential causes of these problems as well as possible solutions which could improve the future use of these methodologies.

2.5.2. Suspension methodology

In the bricks, CoM_{Su} positions predicted from three runs were markedly different from CoM_{G} (3D distance: 15–38mm), indicating this method performed relatively poorly at predicting CoM. This, along with the high variability (maximum range in bricks: 23mm and birds: 67mm) in the results not only indicates that this method is a relatively poor predictor of CoM_{G} , but that there is also considerable variation in its ability to do so (Figure 2.7). This is suggestive of complex human-incurred error inherent to this methodology, with potential sources of error including the subjective selection of suspension position, and placement of string markers. A small amount of additional error was introduced here, as the string axis was defined using the raw marker centres, which were offset from the string itself (by 6.35mm,

the marker radius). However this error was in one dimension only, and the effect was consistent across runs and between specimens. While this would affect the absolute accuracy of our suspension method, the error was small in comparison to the total error detected in this method (up to 38mm), and did not affect our observation that results from the suspension methodology were highly variable. Further, the error present in this method was potentially influenced by the mass of the object under investigation. Error margins may be greater if an object of the same size as our bricks, but with a lower density, and therefore lower mass and inertia, was used as the test object. Such an effect may explain the different error margins seen in the brick and bird specimens, though we did not explicitly test this hypothesis.

For Brick1, the chicken and the buzzard, where additional suspension runs were conducted (taking the total to ten runs, rather than three), the apparent accuracy of CoM_{Su} improved compared to the best results from three runs for those objects (Figure 2.7). However, this improvement was only slight in the chicken (2.24mm) and buzzard (3.93mm). Additionally, the error in CoM_{Su} for Brick1 using ten runs was actually higher than that obtained from only three runs on Brick2 (Figure 2.7A). This further highlights problems with consistency in this methodology, regardless of the addition of further data runs. The addition of extra data captures here increases the number of unique lines of suspension (10 versus 3), and therefore increases the number of string intersect points drastically (45 versus 3). However, in the case of all the specimens studied here, these intersect points remained widely scattered (see Figure 2.8). As the final predicted CoM_{Su} is calculated as the mean of all these points, the addition of more unique lines of suspension, and therefore intersect points, should act to increase the chances of a more central overall CoM being predicted, despite the fact that the accuracy of any given run does not improve. However, this is not a predictable effect; hence results from three suspension runs may be more accurate than

those from ten runs. If enough unique suspension positions were tested, it may be possible to consistently derive highly accurate CoM positions from this methodology, but the cost in time and effort associated with performing the presumably large number of runs required might not always be desirable, particularly when other methods are available which address the issue in a more efficient, and more accurate manner.

2.5.3. Scales methodology

CoM_{Sc} positions predicted from the original three runs for each brick were a notable distance from CoM_{G} (mean 3D distance of 17mm, approximately equivalent to that in CoM_{Su}). Despite this relatively low accuracy, the variation within these predictions was low (bricks: 3.13mm, birds: 8.66mm), indicating the relatively high repeatability of this method (Figure 2.7). It was identified that there was a consistent shift of CoM towards the proximal scale; additional reversed repeats were conducted for two bricks in an attempt to counter this and to consequently improve the accuracy of this methodology. These repeats resulted in a drastic improvement in the ability of the scales method to predict CoM_{G} in bricks (within 0.69 and 1.49mm in Bricks1 and 2; see Table 2.3, Figure 2.7A). In both of those cases, the improved CoM_{Sc} was fractionally closer than CoM_{D} to the brick's geometric centre (Table 2.3, Figure 2.7A).

The short distance between CoM_{G} and CoM_{Sc} further highlights the absolute and relative accuracy of this methodology, provided that the appropriate repeats are conducted. It should be noted that in the birds studied here, only the initial runs (i.e. from the proximal end only, with no reversed repeats) were conducted. There is no reason to assume that the proximal skew observed in bricks would not also be seen in biological specimens. It is therefore safe to assume that the CoM_{Sc} positions predicted for birds are not accurate predictors of true CoM position, instead lying more cranially than the 'true' CoM position.

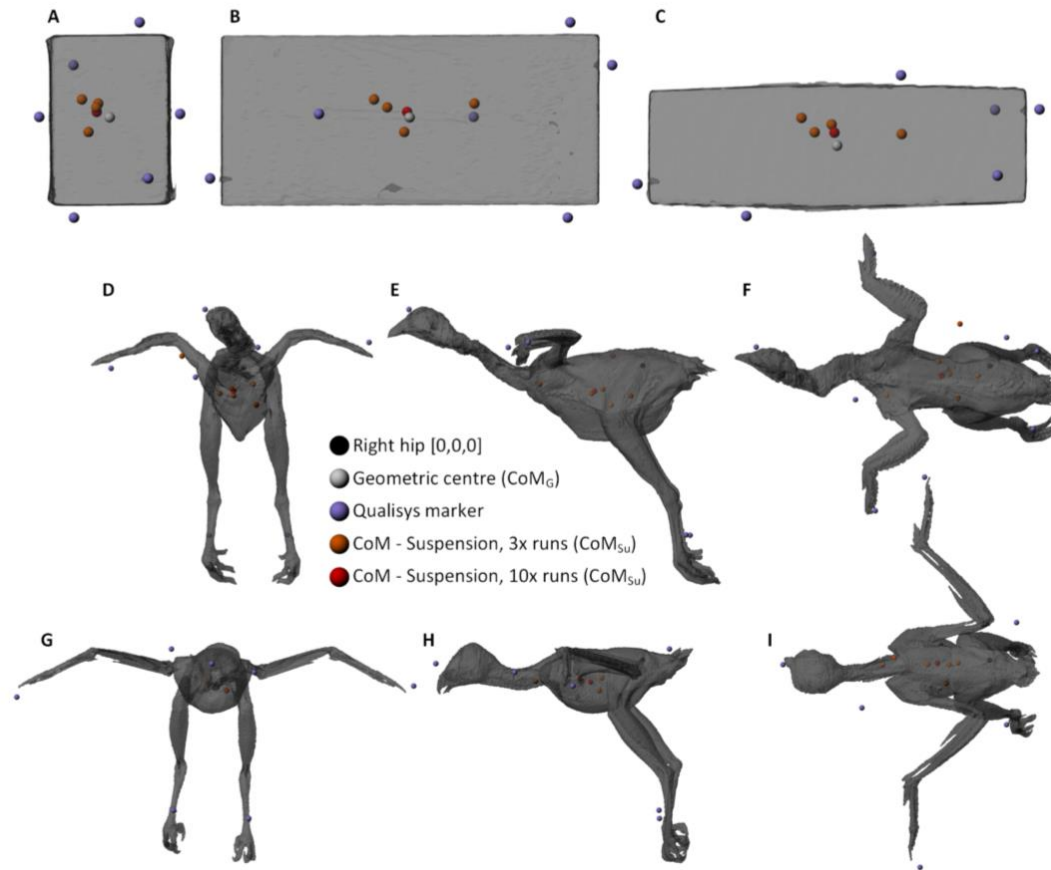


Figure 2.8: Renders of Brick1 (**A-C**), chicken (**D-F**) and buzzard (**G-I**) displaying the broad spread of centre of mass positions predicted by the suspension methodology with three repeats (orange) and ten repeats (red).

The reversed repeats, which impart such a considerable improvement in CoM_{Su} prediction ability, are rarely conducted in the literature (with the notable exception of Henderson, 2003), with the vast majority of papers conducting only the initial runs performed here (e.g. Clemente, 2014, Kilbourne, 2013, Lephart, 1984). Our results suggest that reversed repeats are fundamentally important in order for this scale-based methodology to accurately predict CoM position, and should therefore be employed wherever data on absolute CoM position are required from this method.

Investigation of the error associated with the subjective processes of de-constructing and re-constructing the scales experimental set-up between data captures found relatively small errors (bricks: 3.13mm, birds: 8.66mm; Tables 2.3 and 2.4). However, it should be noted that this margin of error, along with that identified from the calculation of geometric centre in bricks (2.18mm; Table 2.3), mean it is not possible to confidently distinguish between the accuracies of the scales and digital methods.

One key limitation of this scales methodology is the difficulty of deriving 3D CoM positions for biological specimens. Lying specimens along the plank was straightforward for the cranio-caudal dimension here, and could also be easily achieved for the medio-lateral dimension (though the almost universal assumption of bilaterally symmetry in analyses involving CoM limits the need to measure in this axis). However, determination of CoM position along the dorso-ventral axis would require specimens to be positioned with that plane in line with the plank. While possible, developing a set-up which would be capable of supporting a range of biological specimens in the precarious posture required, in a systematic and repeatable manner, was deemed to be beyond the scope of this study. Given that the scales method is accurate (to within 1.5mm) along the cranio-caudal axis, developing such a set-up is an avenue that is potentially worth exploring. This is especially relevant for biological subjects,

where the accuracy of digital CoMs are currently poorly constrained due to a scarcity of avian-specific density data; a scale-based method could therefore provide an avenue for validating digital CoM predictions in 1D or 2D. However, it should be noted that the error in the scales method (set-up error, bricks: 3.13mm, birds: 8.66mm; error in CoM_G : 2.18mm; Tables 2.3 and 2.4) overlaps the error margin for digital estimates. This is the case for the crano-caudal axis, but the error present in an estimation of CoM along the dorso-ventral axis is likely to be greater again due to the irregular shape of biological specimens. Hence overall error in CoM_{Sc} would be expected to exceed that present in a digital modelling approach when applied to biological specimens in more than one dimension. The relative merits and limitations of these techniques should be considered, along with specific aims of the study, when considering the best method to apply in future studies seeking to derive CoM estimates.

2.5.4. Digital modelling

Predictions of CoM_D in bricks were close to CoM_G (3D distance: 1.99-2.39mm; Table 2.3), indicating that the digital modelling method employed here resulted in accurate predictions of CoM position. Repeats of the segmentation protocol in bricks seeking to assess the variability introduced by that process found only minor differences (maximum difference between estimates: 0.39mm; Table 2.3). Our findings therefore agree with those of Allen et al. (2009) obtained in biological specimens, that the process of digital segmentation from CT image data is highly repeatable, providing consistently accurate representations of object geometry which facilitate the accurate determination of CoM position.

In birds however, an accurate representation of specimen geometry is only the first stage of digital model making. Biological specimens are heterogeneous, being composed of various tissue types with different densities, unlike bricks that can safely be assumed to be

homogeneous. Previously, this heterogeneity has been recognised to a degree when constructing digital models, in order to provide a more realistic representation of not only volume distribution, but also of mass distribution. There is a history of including air cavities in digital models of birds and dinosaurs (Bates et al., 2009b, Henderson, 1999, Hutchinson et al., 2007). However, to our knowledge, the consequences of incorporating these structures have not been assessed to determine if this brings predicted CoM closer to true CoM position. For other species (e.g. human, horse), more detailed mass properties are available on segment-specific densities, which could be included in digital models. To our knowledge, there are no published data on segment-specific densities for birds, and therefore the implications for CoM position of incorporating this additional heterogeneity are untested. We sought to explore the effects of this uncertainty with a sensitivity analysis here, applying our initial method, as well as five alternative sets of density data to our bird models (Table 2.2).

Results from this sensitivity analysis show that five of the six density applications tested lie close to one another (within a maximum range of 3.58mm across the three birds; Table 2.4, Figure 2.7B). It is encouraging that the majority of data points cluster together in this way, despite the use of a variety of density assignment methods, and the wide range of sources (including human and horse segment mass properties) for the density data applied. However, the CoM estimates generated using data from Henderson (2006) were markedly different from the others (10-15mm from the main group, across the three birds; Table 2.4, Figure 2.7B). The density values applied to the head and neck by Henderson (2006) seem unrealistically low (density: 300kgm^{-3} , cited as taken from Bramwell and Whitfield (1974) [although it should be noted that we were unable to reconstruct this number from the original text, so this may be erroneous]), and it is this low density which is the main contributor to the appreciably different CoM position predicted. The consistency of CoM

predictions derived here using a range of density datasets highlights the relatively small effect of density variations on CoM position, provided broadly realistic data are used.

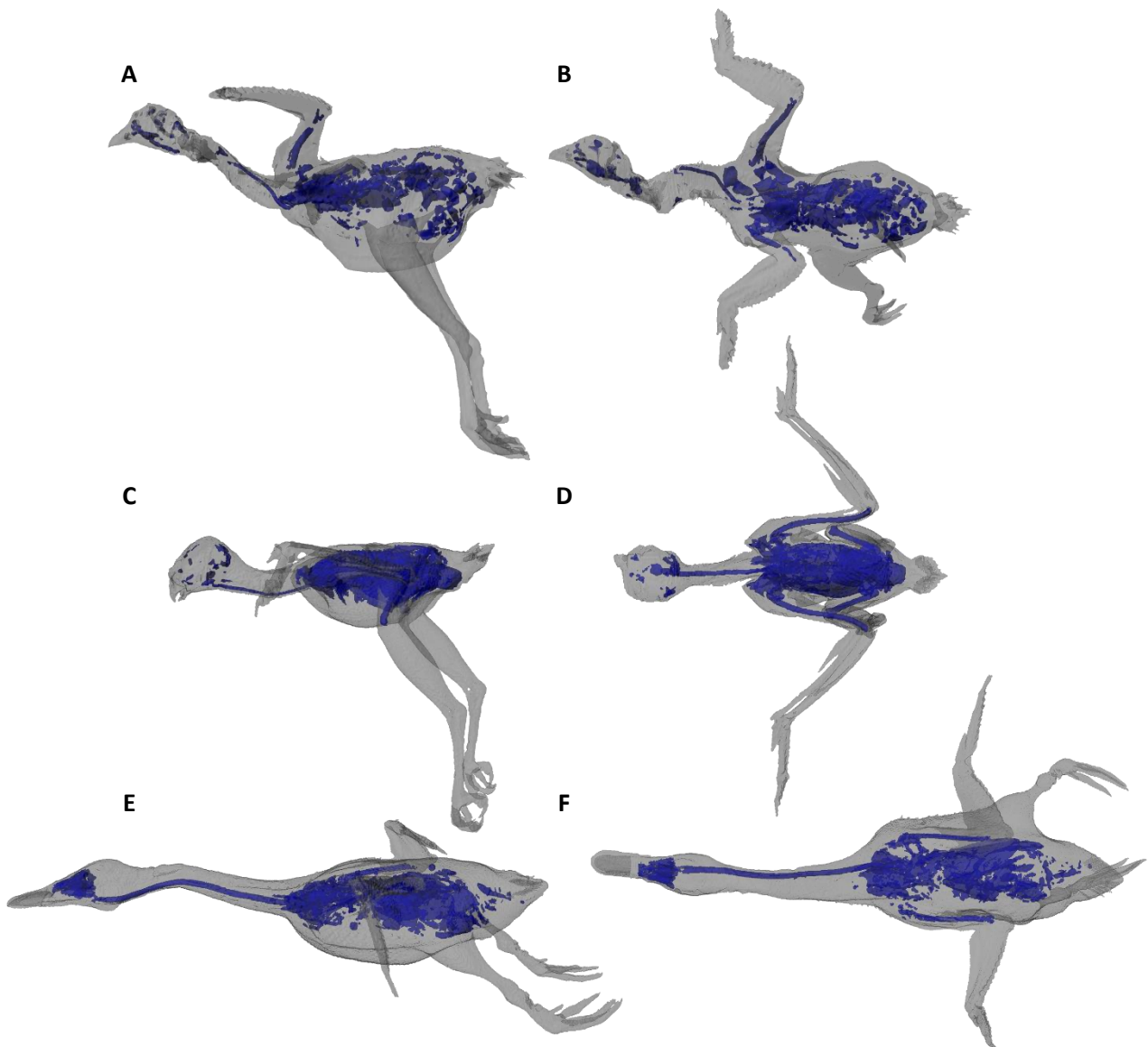
Application of different density datasets to different bird specimens resulted in different relative CoM shifts. The chicken and buzzard showed low variability, regardless of density data, with maximum CoM shifts of ~1mm (Table 2.4, Figure 2.6). The duck however displayed higher variability, with a maximum of 3.6mm between CoM_D estimates (between CoM_{D5} (Henderson, 2004) and CoM_{D6} (Dempster and Gaughran, 1967) respectively) (Table 2.4, Figure 2.6). This reflects a cranial shift in CoM_D when data from humans in Dempster and Gaughran (1967), and to a lesser extent horses in Buchner et al. (1997), are applied to the duck model. This difference is driven by differences in the neck and torso density values used by these studies. The fact that these differences appear in one bird, but not the others, potentially reflects the different relative body proportions of these birds, which result in effects of different magnitudes by specific segments on the overall CoM. Alternatively, it may be indicative of different density datasets matching the true density data for some birds more closely than others. Unfortunately, no density data by segment are available for birds, nor is there a comprehensive quantitative examination of body proportions across Aves, so it is difficult to determine if either or both of these, or indeed other factors, are influencing this trend.

2.6. Conclusion

In conclusion, the scales (with reversed repeats) and digital modelling methods were found to be highly accurate predictors of true CoM position in the test objects examined here. The scales method was marginally more accurate (1.31mm closer to CoM_G ; Table 2.3), though the error associated with calculating the geometric centres (up to 2.18mm; Table 2.3) means the relative accuracies of these two methods cannot be confidently distinguished. Both

scales and digital methods were identified as being highly consistent in their ability to predict CoM position, as well as demonstrating high levels of repeatability in experimental procedures. The suspension methodology was a generally poor predictor of CoM position, in addition to showing high variability and poor levels of repeatability (8.2-38.5mm error; Table 2.3). These accuracies were assessed in test objects, with simple geometries and mass properties, and are arguably therefore a 'best case' representation of methodological accuracy. Biological specimens introduce additional complicating factors, varying by method. For the scales method, problems arise with the repeatability of capturing the required measurements; this is the case along the crano-caudal axis, but additional complications (and most likely greater error) would arise if data for additional axes were sought. Digital methods meanwhile face problems around the inclusion of heterogeneous densities. However, the sensitivity analysis conducted here, using a broad range of density datasets, found that variations in density data had a relatively low impact on CoM position. Provided bird segment densities do not differ substantially from the data used here, it is likely that uncertainty around density data will not introduce large inaccuracies in CoM position. However, we found that density has the potential to affect birds of different body plans differently, and there are currently no avian-specific density data published to conclusively rule out density as an important influencing factor on CoM position. Future studies wishing to quantify CoM position in biological taxa should consider these factors in the light of their specific aims to determine the optimum method for CoM determination.

2.7. Supplementary Information



Supplementary Information 2.1: Renders of chicken (**A, B**), buzzard (**C, D**) and duck (**E, F**) showing the skin outlines (grey) and air cavities (blue) extracted from CT data and used in digital predictions of CoM position.

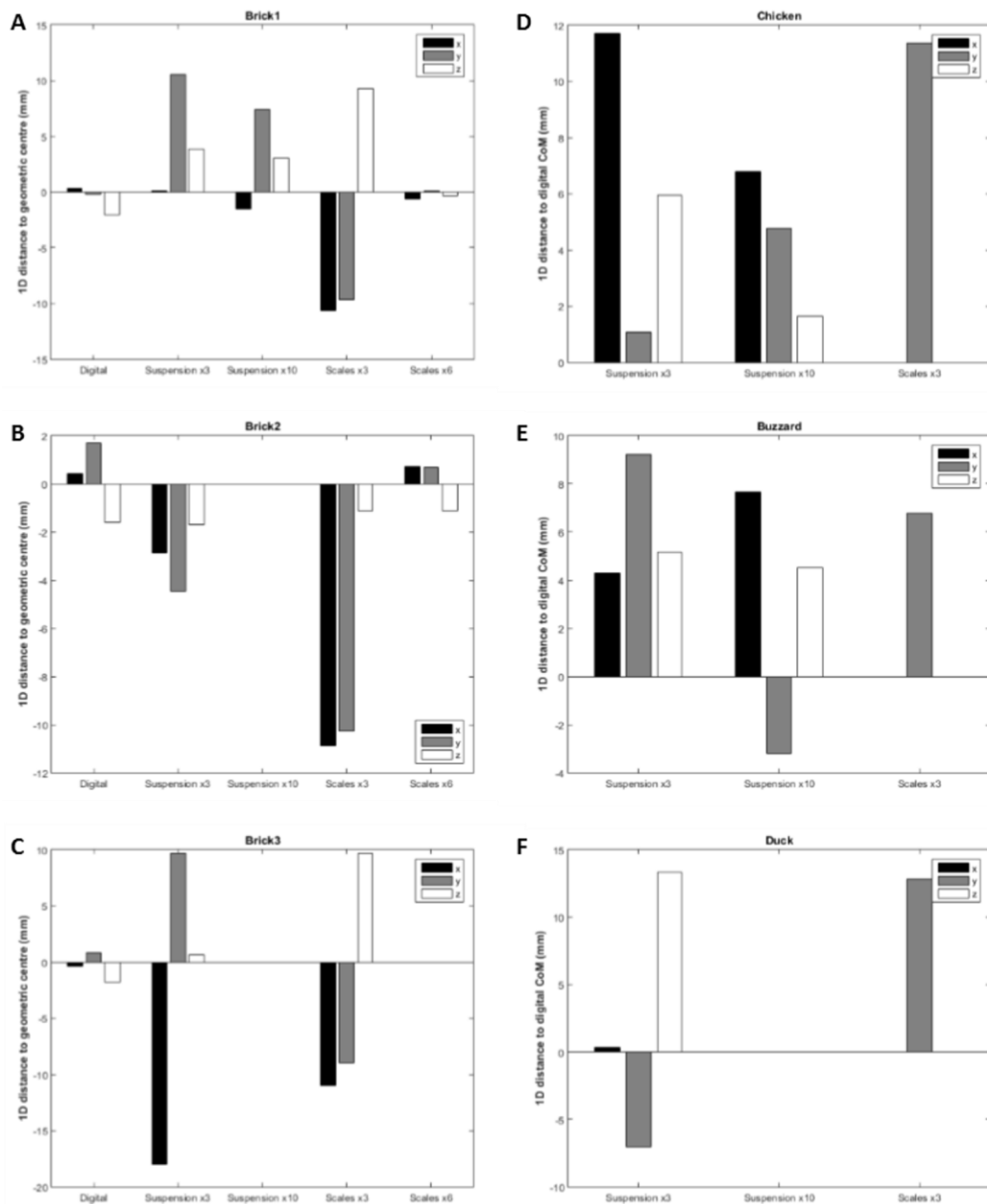
Supplementary Information 2.2: Data for centre of mass positions for three brick specimens, as predicted by the three different methodologies examined here. Where, x axis = E-F, y axis = A-B, z axis = C-D.

CoM Description	Brick1			Brick2			Brick3		
	x	y	z	x	y	z	x	y	z
Digital (CoM _D)	108.1	34.7	49.1	102.4	68.3	102.3	106.7	33.1	51.6
Digital (CoM _D)	-	-	-	-	-	-	106.8	33.1	51.5
Digital (CoM _D)	-	-	-	-	-	-	106.7	33.1	51.6
Suspension (CoM _{Su}) - 10 runs	106.3	42.3	54.2	-	-	-	-	-	-
Suspension (CoM _{Su}) - 3 runs	144.8	41.4	59.5	99.1	62.1	102.2	89.1	42.0	54.0
Suspension (CoM _{Su}) - 3 runs	87.3	50.7	61.2	-	-	-	-	-	-
Suspension (CoM _{Su}) - 3 runs	104.8	47.0	42.7	-	-	-	-	-	-
Suspension (CoM _{Su}) - 3 runs	94.9	42.5	56.7	-	-	-	-	-	-
Scales (CoM _{Sc}) - 6 runs	107.2	35.0	50.8	102.7	67.3	102.7	-	-	-
Scales (CoM _{Sc}) - 3 runs	96.4	25.5	60.8	91.1	56.3	102.7	96.1	23.3	63.1
Scales (CoM _{Sc}) - 3 runs	96.6	24.3	61.3	-	-	-	-	-	-
Scales (CoM _{Sc}) - 3 runs	96.2	25.0	60.8	-	-	-	-	-	-
Scales (CoM _{Sc}) - 3 runs	98.5	25.4	58.9	-	-	-	-	-	-
Scales (CoM _{Sc}) - 3 runs	98.2	25.8	60.2	-	-	-	-	-	-
Geometric (CoM _G) - 6 runs	107.8	34.8	51.1	102.0	66.6	103.9	-	-	-
Geometric (CoM _G) - 3 runs	108.3	34.1	49.4	102.1	67.0	103.6	107.1	32.3	53.4
Geometric (CoM _G) - 3 runs	108.1	34.9	51.0	-	-	-	-	-	-
Geometric (CoM _G) - 3 runs	108.1	34.8	49.0	-	-	-	-	-	-
Geometric (CoM _G) - 3 runs	108.2	35.1	50.4	-	-	-	-	-	-

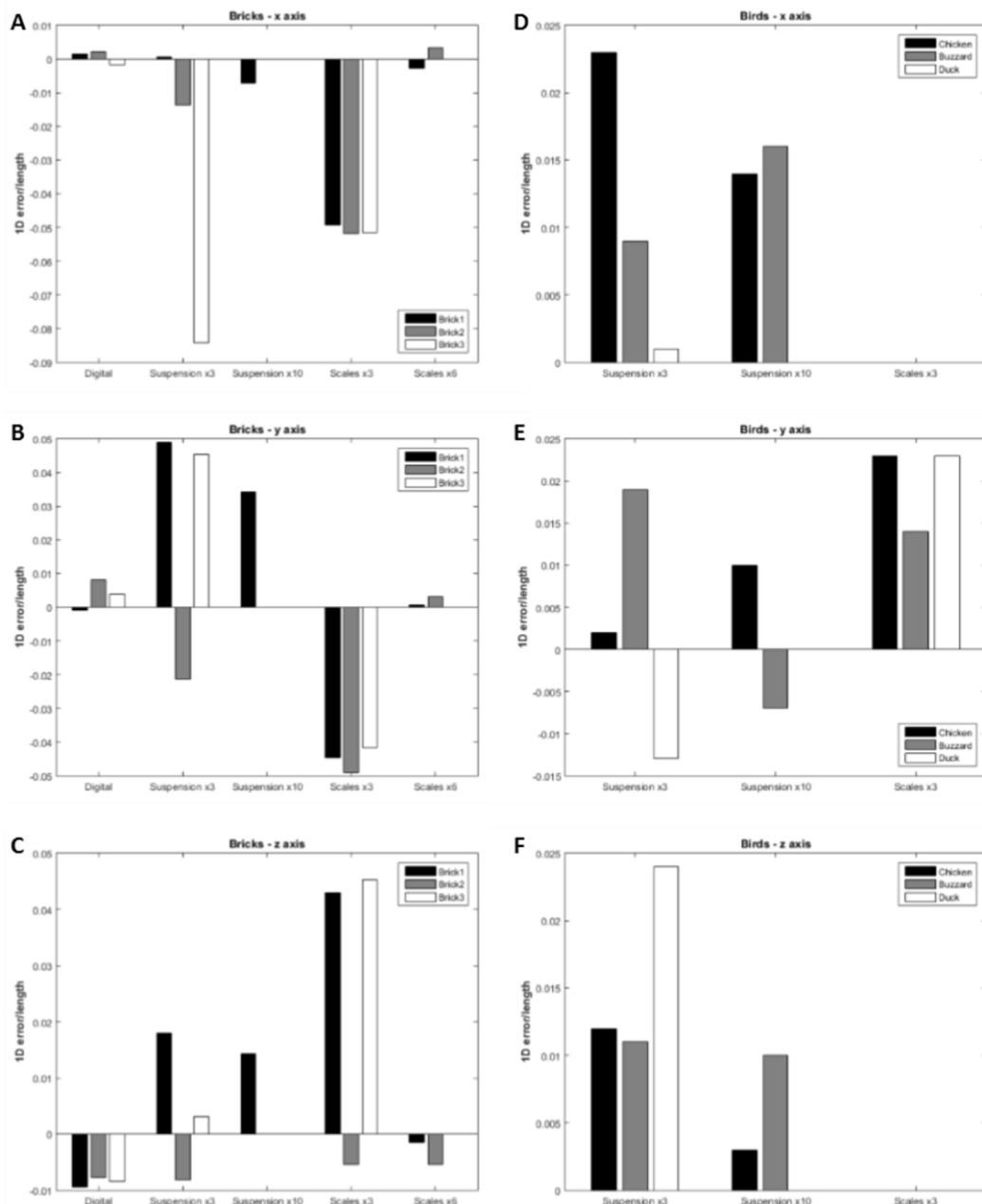
Supplementary Information 2.3: Data for centre of mass positions for three bird specimens, as predicted by the different methodologies examined here. Where, x axis = left-right, y axis = cranio-caudal, z axis = dorso-ventral.

CoM Description	Chicken			Buzzard			Duck		
	x	y	z	x	y	z	x	y	z
Digital - CoM _{b1} - Best guess	-18.1	48.4	-30.0	-11.2	61.2	-28.9	-11.1	43.1	-28.8
CoM _{b2} - Tsvetkova 1988	-18.9	39.4	-34.2	-11.4	45.0	-29.1	-10.5	29.8	-30.1
CoM _{b3} - Lovvold 1991	-18.1	46.9	-31.3	-11.6	57.7	-27.0	-10.6	42.8	-29.1
CoM _{b4} - Henderson 2006	-18.0	48.8	-29.2	-11.2	58.5	-26.2	-11.0	44.1	-28.5
CoM _{b4} - Henderson 2004	-18.0	48.8	-29.2	-11.2	58.5	-26.2	-11.0	44.1	-28.5
CoM _{b6} - Dempster 1967	-17.8	50.4	-29.1	-11.5	60.6	-25.8	-10.8	47.3	-28.7
CoM _{b7} - Buchner 1997	-17.9	49.8	-31.2	-11.7	58.1	-27.6	-10.7	46.9	-28.7
CoM _D - Extreme posture shift	-	-	-	-	-	-	-14.7	44.2	-29.4
Suspension (CoM _{su}) - 10 runs	-11.3	53.2	-28.4	-3.6	58.0	-24.3	-	-	-
CoM _{su} - 3 runs	-9.0	44.4	-26.2	-5.0	119.	-23.0	-10.8	36.1	-15.5
CoM _{su} - 3 runs	-11.2	13.3	-33.5	-2.9	35.2	-32.5	-	-	-
CoM _{su} - 3 runs	-32.8	114.	-20.6	2.4	105.	-17.4	-	-	-
CoM _{su} - 3 runs	4.5	56.7	-31.0	-5.2	45.3	-19.3	-	-	-
CoM _{su} - 3 runs	46.4	33.2	10.7	-26.0	48.4	-30.3	-	-	-
CoM _{su} - 3 runs	-36.3	35.1	-43.8	-5.1	69.0	-19.8	-	-	-
Scales (CoM _{sc}) - 3 runs *	-11.1	62.8	25.5	-0.9	68.0	23.5	-9.0	55.9	14.6
CoM _{sc} - 3 runs *	-16.0	57.7	25.9	-	-	-	-	-	-
CoM _{sc} - 3 runs *	-15.7	56.7	25.7	-	-	-	-	-	-
CoM _{sc} - 3 runs *	-11.6	56.6	24.9	-	-	-	-	-	-
CoM _{sc} - 3 runs *	-10.7	65.2	22.6	-	-	-	-	-	-

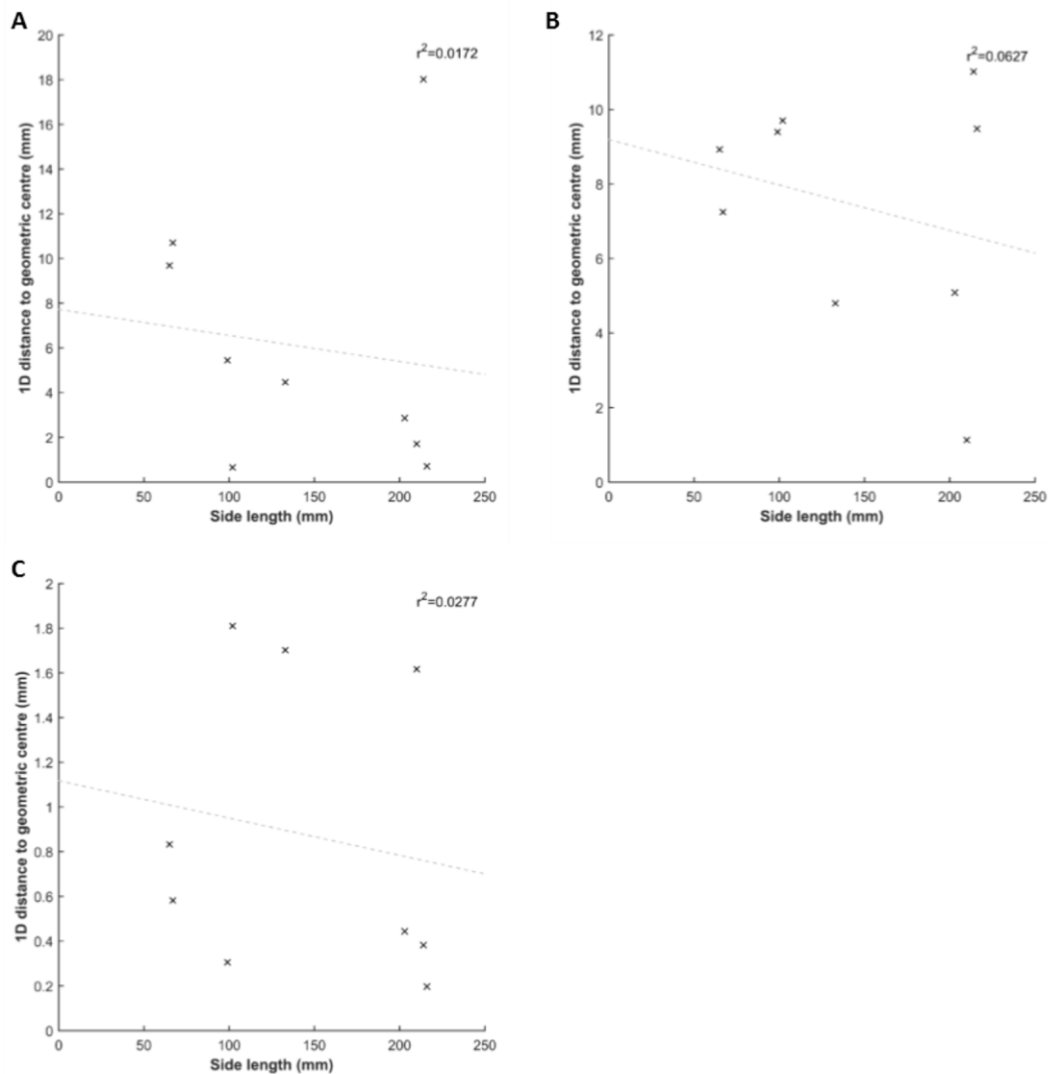
*Scales CoM positions were only determined in one dimension, along the cranio-caudal (y) axis.



Supplementary Information 2.4: Differences between geometric centre (bricks)/best guess digital CoM (birds) and CoM predictions produced by the methods studied here, presented as 1D differences for each axis. **A-C:** Data for Bricks1-3, where positive values represent shifts towards sides F (x), B (y) and C (z) of the predicted CoM position relative to the brick geometric centre. **D-F:** Data for chicken, buzzard and duck, where positive values represent right (x), cranial (y) and dorsal (z) shifts to predicted CoM position relative to the best guess digital CoM.



Supplementary Information 2.5: 1D differences between geometric centre (bricks)/best guess digital CoM (birds) and CoM predictions produced by the methods studied here, normalised by maximum side length (bricks)/cranio-caudal body length (birds). **A-C:** Data for Bricks1-3, presented by axis. **D-F:** Data for chicken, buzzard and duck, presented by axis.



Supplementary Information 2.6: Distance to geometric centre (i.e. error) plotted against side length, for three sides of three bricks of different dimensions. Least squares linear regression fitted to data, and r^2 value displayed at top right of each plot. For suspension (A), scales (B) and digital (C) methodologies.

2.1. Appendices

Appendix 2.1: An examination of potential sources of error in the suspension methods used in this thesis chapter.

Substantial, variable error was found for the suspension method used in this thesis chapter (error 8.2-38.5mm). This contradicts previously published studies which find considerably lower errors for suspension based methods (e.g. < 1cm, Nauwelaerts et al., 2011). One potential explanation for this discrepancy was the offset of the string markers from the string itself, by 6.35mm (the radius of the Qualisys markers) (see Section 2.5.2 for discussion). However, other factors have since been identified which could help explain the large error found in this version of the suspension method; these are discussed below.

Examining the method used to define the string axis

In the suspension method used in this thesis, two Qualisys markers were affixed to the string and used to define the axis of the string, with the line between them representing the line of suspension in digital space (see Figure 2.2). As identified in the main text (Section 2.5.2), the method of affixing the markers to the outside of the string was not ideal, and would result in an error of 6.35mm (the marker radius), even if all subsequent application was faultless. When applied, the string markers should be in the same plane in the x and y dimensions, with the differences in their positions explained wholly by the z dimension. However, any error in the original marker placement or due to twisting of the string has the potential to displace the string markers in the x and/or y dimensions.

Examination of the xyz co-ordinates of the string markers in the original Qualisys files (available at <http://datacat.liverpool.ac.uk/310>) shows that there was considerable displacement (> 3mm) of the two string markers in at least one of the x and y dimensions in

most runs (27/39 runs). The mean marker offset across all runs of all specimens was 3.8mm (minimum offset: 0.02mm, maximum offset: 21.0mm). 12/39 runs included a marker offset of greater than the marker radius. Though some of these offsets are considerable, and would certainly affect the accuracy of resulting CoM predictions, there is only a weak correlation between marker offset and CoM prediction error for the sample tested here.

The original offset of markers from the string would produce small errors in the resulting CoM predictions. Any additional marker displacements would produce further error when drawing a line through them and extrapolating onto the brick itself. The point of closest approach (a proxy for the intersection point, see Figure 2.2) of these incorrect lines of suspension were then used to determine the CoM of each object, which would likely compound the original error. This issue could have been avoided by drilling through the Qualisys markers and threading them onto the string itself. These issues should be noted by any future studies wishing to use a digitised version of the traditional suspension method.

Testing a purely physical suspension method

As the problems encountered with the original method were a result of the digitisation process, a test was done using a purely physical version of this method, after Nauwelaerts et al. (2011). The three bricks were suspended in a loop of string, as per the original method (see Section 2.3.2). However, rather than being allowed to come to rest, the position of the string support was shifted until the brick came to rest horizontally. This was repeated for each axis, with the point of support marked on the bricks. These support points were then compared with the geometric centres for each brick.

The results of this test showed that errors for individual dimensions were all less than 3.5mm, with a mean of 2.05mm. Assuming the maximum error for all three dimensions of a brick,

this would give a maximum 3D error of 6mm when compared to the geometric centre. This error is equivalent to those reported in the literature, and less than the error reported by Nauwelaerts et al. (2011).

I therefore conclude that although the version of the suspension method used in the original thesis contained substantial errors, suspension based methods themselves are not inherently flawed. Any future applications of a suspension based method should either stay entirely physical in nature, or if digitisation is required, care should be taken to avoid the issues outlined here.

2.2. References

- ALEXANDER, R. M. 1983. *Animal Mechanics*, London, Blackwell Scientific.
- ALEXANDER, R. M. 1985. Mechanics of posture and gait of some large dinosaurs. *Zoological Journal of the Linnean Society*, 83, 1-25.
- ALLEN, V., HUTCHINSON, J. R., BATES, K. T. & LI, Z. 2013. Linking the evolution of body shape and locomotor biomechanics in bird-line archosaurs. *Nature*, 497, 104-107.
- ALLEN, V., PAXTON, H. & HUTCHINSON, J. R. 2009. Variation in center of mass estimates for extant sauropsids and its importance for reconstructing inertial properties of extinct archosaurs. *Anatomical Record*, 292, 1442-1461.
- AMIT, T., GOMBERG, B. R., MILGRAM, J. & SHAHAR, R. 2009. Segmental inertial properties in dogs determined by magnetic resonance imaging. *Veterinary Journal*, 182, 94-99.
- ANDRADA, E., NYAKATURA, J. A., BERGMANN, F. & BLICKHAN, R. 2013. Adjustments of global and local hindlimb properties during terrestrial locomotion of the Common Quail (*Coturnix coturnix*). *Journal of Experimental Biology*, 216, 3906-3916.
- ATTWELLS, R. L., BIRRELL, S. A., HOOPER, R. H. & MANSFIELD, N. J. 2006. Influence of carrying heavy loads on soldiers' posture, movements and gait. *Ergonomics*, 49, 1527-1537.
- BATES, K. T., FALKINGHAM, P. L., BREITHAUPT, B. H., HODGETTS, D., SELLERS, W. I. & MANNING, P. L. 2009a. How big was 'Big Al'? Quantifying the effect of soft tissue and osteological unknowns on mass predictions for *Allosaurus* (Dinosauria, Theropoda). *Palaeontologia Electronica*, 12, 1-33.
- BATES, K. T., FALKINGHAM, P. L., MACAULAY, S., BRASSEY, C. & MAIDMENT, S. C. R. 2015. Downsizing a giant: re-evaluating *Dreadnoughtus* body mass. *Biology Letters*, 11, 20150215.
- BATES, K. T., MANNING, P. L., HODGETTS, D. & SELLERS, W. I. 2009b. Estimating Mass Properties of Dinosaurs Using Laser Imaging and 3-D Computer Modelling. *PLoS ONE*, 4, 1-26.
- BATES, K. T., MANNION, P. D., FALKINGHAM, P. L., BRUSATTE, S. L., HUTCHINSON, J. R., OTERO, A., SELLERS, W. I., SULLIVAN, C., STEVENS, K. A. & ALLEN, V. 2016. Temporal and phylogenetic evolution of the sauropod dinosaur body plan. *Royal Society Open Science*, 3, 150636.
- BATES, K. T., SELLERS, W. I., MANNING, P. L. & MARGETTS, L. 2010. Sensitivity analysis in evolutionary robotic simulations of bipedal dinosaur running. *Journal of Vertebrate Paleontology*, 30, 458-466.
- BRAMWELL, C. D. & WHITFIELD, G. R. 1974. Biomechanics of *Pteranodon*. *Philosophical Transactions of the Royal Society of London B: Biological Sciences*, 267, 503-581.
- BUCHNER, H. H. F., SAVELBERG, H. H. C. M., SCHAMHARDT, H. C. & BARNEVELD, A. 1997. Inertial properties of Dutch Warmblood horses. *Journal of Biomechanics*, 30, 653-658.

- CARRANO, M. T. & BIEWENER, A. A. 1999. Experimental alteration of limb posture in the chicken (*Gallus gallus*) and its bearing on the use of birds as analogs for dinosaur locomotion. *Journal of Morphology*, 240, 237-249.
- CHANDLER, R. F., CLAUSER, C. E., MCCONVILLE, J. T., REYNOLDS, H. M. & YOUNG, J. W. 1975. Investigation of Inertial Properties of Human Body Segments. *AMRL Technical Report No. 74-137, Aerospace Medical Research Laboratories, Wright-Patterson Airforce Base, OH*.
- CLEMENTE, C. J. 2014. The evolution of bipedal running in lizards suggests a consequential origin may be exploited in later lineages. *Evolution*, 68, 2171-2183.
- CROMPTON, R. H., LI, Y., ALEXANDER, R. M., WANG, W. & GUNTHER, M. M. 1996. Segment inertial properties of primates: New techniques for laboratory and field studies of locomotion. *American Journal of Physical Anthropology*, 99, 547-570.
- DEMPSTER, W. T. 1955. Space Requirements of the Seated Operator. *WADC Technical Report No. 55-159, Wright Air Development Centre, Wright-Patterson Airforce Base, OH*.
- DEMPSTER, W. T. & GAUGHRAN, G. R. L. 1967. Properties of body segments based on size and weight. *American Journal of Anatomy*, 120, 33-54.
- ESHBACH, O. W., TAPLEY, B. D. & POSTON, T. R. 1990. *Eshbach's Handbook of Engineering Fundamentals*, New York, Wiley.
- FEDAK, M. A., HEGLUND, N. C. & TAYLOR, C. R. 1982. Energetics and mechanics of terrestrial locomotion. II. Kinetic energy changes of the limbs and body as a function of speed and body size in birds and mammals. *Journal of Experimental Biology*, 97, 23-40.
- GATESY, S. M., BÄKER, M. & HUTCHINSON, J. R. 2009. Constraint-based exclusion of limb poses for reconstructing theropod dinosaur locomotion. *Journal of Vertebrate Paleontology*, 29, 535-544.
- GATESY, S. M. & BIEWENER, A. A. 1991. Bipedal locomotion: effects of speed, size and limb posture in birds and humans. *Journal of Zoology*, 224, 127-147.
- GOETZ, J. E., DERRICK, T. R., PEDERSEN, D. R., ROBINSON, D. A., CONZEMIUS, M. G., BAER, T. E. & BROWN, T. D. 2008. Hip joint contact force in the emu (*Dromaius novaehollandiae*) during normal level walking. *Journal of Biomechanics*, 41, 770-778.
- GROSSI, B., IRIARTE-DÍAZ, J., LARACH, O., CANALS, M. & VÁSQUEZ, R. A. 2014. Walking like dinosaurs: Chickens with artificial tails provide clues about non-avian theropod locomotion. *PLoS ONE*, 9.
- HENDERSON, D. M. 1999. Estimating the masses and centers of mass of extinct animals by 3-D mathematical slicing. *Paleobiology*, 25, 88-106.
- HENDERSON, D. M. 2003. Effects of stomach stones on the buoyancy and equilibrium of a floating crocodilian: A computational analysis. *Canadian Journal of Zoology*, 81, 1346-1357.

- HENDERSON, D. M. 2004. Tipsy punters: Sauropod dinosaur pneumaticity, buoyancy and aquatic habits. *Proceedings of the Royal Society B: Biological Sciences*, 271, S180-S183.
- HENDERSON, D. M. 2006. Burly gaits; centers of mass, stability, and the trackways of sauropod dinosaurs. *Journal of Vertebrate Paleontology*, 26, 907-921.
- HOBBS, S. J., RICHARDS, J. & CLAYTON, H. M. 2014. The effect of centre of mass location on sagittal plane moments around the centre of mass in trotting horses. *Journal of Biomechanics*, 47, 1278-1286.
- HUTCHINSON, J. R. 2004a. Biomechanical modeling and sensitivity analysis of bipedal running ability. I. Extant taxa. *Journal of Morphology*, 262, 421-440.
- HUTCHINSON, J. R. 2004b. Biomechanical modeling and sensitivity analysis of bipedal running ability. II. Extinct taxa. *Journal of Morphology*, 262, 441-461.
- HUTCHINSON, J. R. 2011. On the inference of function from structure using biomechanical modelling and simulation of extinct organisms. *Biology Letters*, 8, 115-118.
- HUTCHINSON, J. R., NG-THOW-HING, V. & ANDERSON, F. C. 2007. A 3D interactive method for estimating body segmental parameters in animals: Application to the turning and running performance of *Tyrannosaurus rex*. *Journal of Theoretical Biology*, 246, 660-680.
- KILBOURNE, B. M. 2013. On birds: Scale effects in the neognath hindlimb and differences in the gross morphology of wings and hindlimbs. *Biological Journal of the Linnean Society*, 110, 14-31.
- KOEHL, M. A. R., EVANGELISTA, D. & YANG, K. 2011. Using physical models to study the gliding performance of extinct animals. *Integrative And Comparative Biology*, 51, 1002-1018.
- LEPHART, S. A. 1984. Measuring the inertial properties of cadaver segments. *Journal of Biomechanics*, 17, 537-543.
- LOVERRO, K. L., BROWN, T. N., COYNE, M. E. & SCHIFFMAN, J. M. 2015. Use of body armor protection with fighting load impacts soldier performance and kinematics. *Applied Ergonomics*, 46, 168-175.
- LOVVORN, J. R. & JONES, D. R. 1991. Body mass, volume, and buoyancy of some aquatic birds, and their relation to locomotor strategies. *Canadian Journal of Zoology*, 69, 2888-2892.
- MAIDMENT, S. C. R., HENDERSON, D. M. & BARRETT, P. M. 2014. What drove reversions to quadrupedality in ornithischian dinosaurs? Testing hypotheses using centre of mass modelling. *Naturwissenschaften*, 101, 989-1001.
- MYERS, M. J. & STEUDEL, K. 1997. Morphological conservation of limb natural pendular period in the domestic dog (*Canis familiaris*): Implications for locomotor energetics. *Journal of Morphology*, 234, 183-196.

- NAUWELAERTS, S., ALLEN, W. A., LANE, J. M. & CLAYTON, H. M. 2011. Inertial properties of equine limb segments. *Journal of Anatomy*, 218, 500-509.
- NIGG, B. M. & HERZOG, W. 2007. *Biomechanics of the musculo-skeletal system*, West Sussex, John Wiley & Sons.
- NYAKATURA, J. A., ALLEN, V. R., LAUSTRÖER, J., ANDIKFAR, A., DANCZAK, M., ULLRICH, H. J., HUFENBACH, W., MARTENS, T. & FISCHER, M. S. 2015. A three-dimensional skeletal reconstruction of the stem amniote *Orobates pabsti* (Diadectidae): Analyses of body mass, centre of mass position, and joint mobility. *PLoS ONE*, 10, e0137284.
- NYAKATURA, J. A., ANDRADA, E., GRIMM, N., WEISE, H. & FISCHER, M. S. 2012. Kinematics and center of mass mechanics during terrestrial locomotion in Northern Lapwings (*Vanellus vanellus*, Charadriiformes). *Journal of Experimental Zoology Part A: Ecological Genetics and Physiology*, 317, 580-594.
- ÖZKAYA, N., NORDIN, M., GOLDSHEYDER, D. & LEGER, D. 2012. Statics: Systems in Equilibrium. *Fundamentals of Biomechanics: Equilibrium, Motion, and Deformation*. New York, NY: Springer New York.
- PARK, S. B., KIM, S. Y., HYEONG, J. H. & CHUNG, K. R. 2014. A study on the development of image analysis instrument and estimation of mass, volume and center of gravity using CT image in Korean. *Journal of Mechanical Science and Technology*, 28, 971-977.
- PAXTON, H., TICKLE, P. G., RANKIN, J. W., CODD, J. R. & HUTCHINSON, J. R. 2014. Anatomical and biomechanical traits of broiler chickens across ontogeny. Part II. Body segment inertial properties and muscle architecture of the pelvic limb. *PeerJ*, 2, e831.
- PEYER, K. E., MORRIS, M. & SELLERS, W. I. 2015. Subject-specific body segment parameter estimation using 3D photogrammetry with multiple cameras. *PeerJ*, 3, e831.
- REN, L. & HUTCHINSON, J. R. 2008. The three-dimensional locomotor dynamics of African (*Loxodonta africana*) and Asian (*Elephas maximus*) elephants reveal a smooth gait transition at moderate speed. *Journal of the Royal Society Interface*, 5, 195-211.
- RUBENSON, J. & MARSH, R. L. 2009. Mechanical efficiency of limb swing during walking and running in Guinea Fowl (*Numida meleagris*). *Journal of Applied Physiology*, 106, 1618-1630.
- SELLERS, W. I., MARGETTS, L., CORIA, R. A. & MANNING, P. L. 2013. March of the titans: The locomotor capabilities of sauropod dinosaurs. *PLoS ONE*, 8, 1-21.
- SPRIGINGS, E. & LEACH, D. 1986. Standardised technique for determining the centre of gravity of body and limb segments of horses. *Equine Veterinary Journal*, 18, 43-49.
- TSERVENI, A. S. & YANNAKOPoulos, A. L. 1988. Specific gravity, carcass fat and prediction of fatness in quail carcasses. *The Journal of Agricultural Science*, 111, 95-98.
- VILENSKY, J. A. 1979. Masses, centers-of-gravity, and moments-of-inertia of the body segments of the Rhesus Monkey (*Macaca mulatta*). *American Journal of Physical Anthropology*, 50, 57-65.

- WALTER, R. M. & CARRIER, D. R. 2002. Scaling of rotational inertia in murine rodents and two species of lizard. *Journal of Experimental Biology*, 205, 2135-2141.
- WILLEY, J. S., BIKNEVICIUS, A. R., REILLY, S. M. & EARLS, K. D. 2004. The tale of the tail: Limb function and locomotor mechanics in *Alligator mississippiensis*. *Journal of Experimental Biology*, 207, 553-563.
- YOUNG, J. W., PATEL, B. A. & STEVENS, N. J. 2007. Body mass distribution and gait mechanics in Fat-tailed Dwarf Lemurs (*Cheirogaleus medius*) and Patas Monkeys (*Erythrocebus patas*). *Journal of Human Evolution*, 53, 26-40.

CHAPTER 3 - LINKING INTEGUMENT AND BODY SHAPE EVOLUTION IN ARCHOSAURS

This chapter is based on a manuscript which is currently in review at Evolution.

MACAULAY, S., BATES, K. T., BROPHY, P., ALLEN, V., HONE, D. W. E. & HUTCHINSON,
J. R. (In review). Linking integument and body shape evolution in archosaurs.
Evolution.

Author contributions: PB, VA, DWEH and JRH designed and carried out the experimental integument data collection. SM analysed experimental integument data. SM and KTB designed the computer modelling. SM carried out the computer modelling and analysed the resulting data. All authors contributed to the manuscript.

3.1. Abstract

Body shape, locomotion and ecology are tightly correlated in living archosaurs (birds and crocodylians). Alongside changes in body shape, the ancestors of birds also evolved a feathered integument. How integument properties are adapted to locomotion in living taxa is poorly understood, and the links between integument and body shape evolution in archosaurs remains completely unstudied. Here, we present a new dataset on integument mass properties from 33 species of living archosaurs and lizards. We statistically assess the correlation between integument properties and species locomotor mode, phylogeny and body size. This demonstrates key correlations between feather mass properties and locomotor ecology in extant birds, for example flight feather length, thickness, surface area and density were all found to significantly differ between locomotor groups. This highlights adaptive links between feather properties and the degree of flight capability. Application of these mass property data to validated computational models of body shape indicates that a feathered integument impacts mass distribution as significantly as other major organs (e.g. lungs). Additionally, the presence of a feathered integument further exaggerates existing differences in the mass distribution of extant archosaurs, whereby centre of mass is distant to the hip in the caudal direction in reptiles, and in the ventral direction in birds. By applying integument to models of three extinct bird-line dinosaurs (*Coelophysis*, *Microraptor* and *Yixianornis*), we track interactions between body proportions and integument during the evolution of flight. Our models demonstrate that feather evolution in bird-line ancestors acted to shift whole body centre of mass ventrally, providing increased inherent stability which would have provided key mechanical benefits to early fliers, before the advent of complex neuromuscular control of flight behaviours.

3.2. Introduction

Living archosaurs (crocodylians and birds) have evolved disparate body shapes that reflect adaptations to different locomotor styles, and ultimately different environmental and ecological niches. Crocodylians are characterised by a long streamlined body, relatively short limbs and a large muscular tail that drives both aquatic and terrestrial locomotion (Gatesy, 1990, Reilly et al., 2005). By contrast, living birds lack this muscular tail and have evolved enlarged limbs, chest and neck regions and a reduced head (Allen et al., 2013, Gatesy, 1990, Gatesy and Dial, 1996). The body shape of living birds is intrinsically linked with two unique functional traits that underpin their exceptional ecological diversity: feather-assisted flight and the use of crouched hindlimbs in terrestrial locomotion (Gatesy and Biewener, 1991, Ostrom, 1974). Body shape shows a clear mechanistic link to both these remarkable traits: the enlarged forelimbs and reduced tail mean that the whole body centre of mass (CoM) is more cranially positioned (Allen et al., 2013, Jones et al., 2000a). This relatively cranial CoM position serves to reduce moments about the shoulder joint and therefore aids stability during flight, whilst placing the highly flexed hindlimbs beneath the CoM during bipedal behaviours (Carrano and Biewener, 1999, Gatesy and Biewener, 1991, Thomas and Taylor, 2001). Building on earlier anatomical studies (Christiansen and Bonde, 2002, Gatesy, 1990, Gatesy and Dial, 1996, Gatesy and Middleton, 1997), the development of computer modelling approaches for quantifying mass distribution in fossils has revealed that this basic avian body plan evolved in a gradual step-wise pattern in non-avian dinosaurs (Allen et al., 2013). This was reflected by an accelerated cranial shift in CoM occurring in early maniraptoran theropods with some degree of aerial capability (Allen et al., 2013).

However, at present these evolutionary changes in body shape have been considered independently of the other major morphofunctional trait of birds - feathers. This is surprising given the role that feathers play in the mechanics and energetics of locomotion in birds

(McGowan, 1979, Ostrom, 1974), and the fact that feathers make up a substantial proportion of whole body mass (with published values up to 19% (Summers et al., 1992); see Supplementary Table 3.1). Furthermore, aerodynamic assessments of both living and fossil birds are also intrinsically influenced by the contribution of the feathered integument to body mass, mass distribution and wing area, through their role in determining both the aerodynamic forces required for flight, and the magnitudes of force generation possible (Alexander et al., 2010, Chatterjee and Templin, 2007, Dyke et al., 2013, Koehl et al., 2011). However, there are currently limited quantitative data on integumentary mass properties (e.g. volume, density) reported in the literature. It is therefore unknown to what extent integumentary (including feather) mass properties are adapted to locomotion and behaviour in living birds occupying different ecological niches, and no data to quantitatively reconstruct integument evolution in extinct taxa.

Here, we combine new quantitative data on the mass properties of integument from living birds and non-avian sauropsids (Figure 3.1A) with validated computer models of body shape (Figure 3.1B) to address three novel questions about archosaur locomotor ecology and evolution. First, do integument mass properties correlate with life habits in extant birds? Second, does integument affect CoM position in extant birds, crocodylians and lizards (Figure 3.1B)? Finally, we apply our integument dataset to models of bird-line dinosaurs (Figure 3.1C), asking for the first time, what impact did the evolution of feathers have on CoM position during the early stages of flight evolution in bird-line theropods (Figure 3.1D)?

3.3. Methodology

3.3.1. Integument mass property data

For our investigation into integument mass properties, samples were taken from 49 specimens, from 33 species (17 birds, 5 crocodylians, 11 lizards). Three integument types

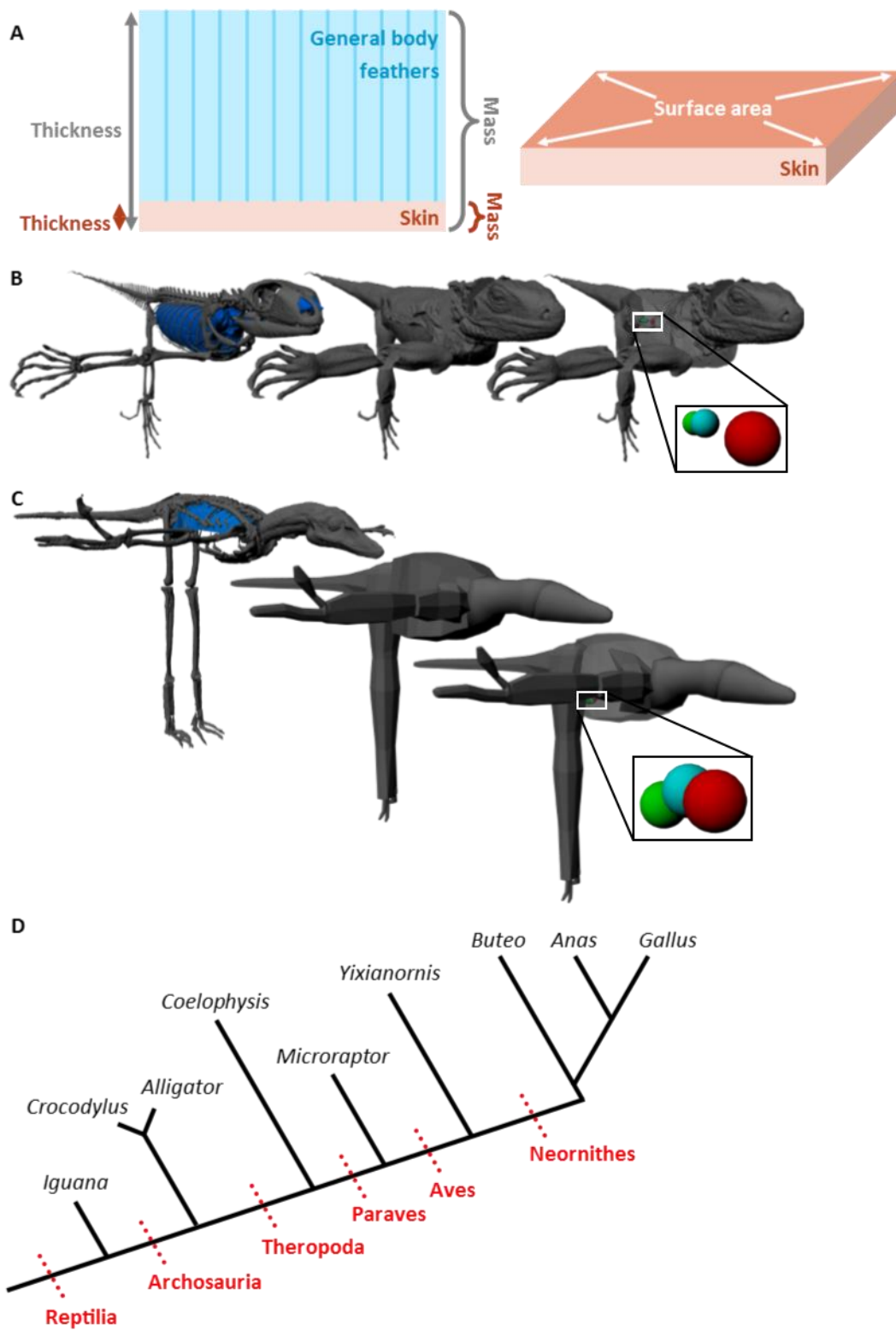


Figure 3.1: A: Diagrammatic representation of data collection protocol for integument mass properties. Mass and thickness measures were taken for the whole sample, and retaken after plucking of body feathers. Surface area calculated for remaining skin sample. B: Digital model

of iguana model in standardised posture. Shown from left to right as: skeleton with air cavities (in blue), overlying skin, and skin with centre of mass positions indicated. **C:** Digital model of *Microraptor* model in standardised posture. Shown from left to right as: skeleton with air cavities (in blue), overlying skin, and skin with centre of mass positions indicated. **D:** Schematic representing the phylogenetic relationships of the species modelled in this study (not to scale).

were identified *a priori* in the extant archosaurs studied here: scaly skin, non-flight feathers and flight feathers. Samples of each integument type were taken across a range of specimens, from numerous locations across the body attempting to capture the full extent of mass property variability within and between specimens. In 25 birds, skin samples with overlying feathers were taken from the head, neck, torso (including ventral, dorsal and lateral regions wherever possible), shoulder and both feathered and scaly areas of the hindlimb. For the flight feathers, samples were taken from 22 birds from the distal, middle, and proximal segments of the wing (to represent primary, secondary and tertiary flight feathers), along with caudal flight feathers. In nine non-avian sauropsid specimens, samples were taken from the pectoral and pelvic limbs, the dorsal, ventral and lateral surfaces of the tail and torso, the head wherever possible, and the scutes (in the case of crocodylians).

For each integument type, the following methodology was followed, with minor alterations according to the differing natures of integument under investigation. Integument samples were extracted, and any non-integumentary structures removed (e.g. subcutaneous fat, vessels, etc). Each sample was weighed ($\pm 0.01\text{g}$), a minimum of three thickness measurements were made using digital callipers ($\pm 0.1\text{-}0.01\text{mm}$), and a scale photograph taken. In samples with overlying feathers, the samples were then plucked, and the mass and thickness measurements were repeated for the skin alone. From the scale photographs, surface area was calculated for all samples in ImageJ (imagej.nih.gov/ij), along with flight feather length (from the base of the rachis proximally, to the tip of the feather distally). Integument volumes were then calculated from these surface area and thickness data. By dividing these volumes by the recorded masses integument density was calculated. Full plucks were also conducted on an additional whole 13 avian specimens (see Supplementary Table 3.1). All feathers were plucked, and total feather mass was measured ($\pm 0.01\text{g}$). Whole body mass was also recorded.

3.3.2. Statistical analysis of integument data

Data on the density and thickness (and in the case of flight feathers, surface area and length) of each integument type were examined for trends with body mass, body region, phylogeny, feather type (where applicable) and locomotor type. The regions compared here corresponded to key body segments, as represented in our computer models (see below). For investigations into differences according to phylogeny, birds were grouped by taxonomic order, and non-avian sauropsids were classified as either crocodylian or lizard. Feather type was assessed during data collection, with feathers classified as either contour, down, filoplume, mixed or semiplume. For the purposes of our analyses, specimens were identified as belonging to one of five locomotor types (after Close and Rayfield, 2012, Martin-Silverstone et al., 2015): continuous flapping flight, flap-gliding, soaring, burst-adapted flight and terrestrial. Details of the classifications of all specimens are in Supplementary Table 3.2. Statistically significant differences between groups were determined by Kruskal-Wallis or one-way ANOVA testing, for skewed and normally distributed data respectively. Where significant differences were detected (i.e. $p < 0.05$), post-hoc testing was applied, using a Mann-Whitney U test or Tukey's honestly significant difference test (according to the normality of the data's distribution). All statistical analysis was done in R (www.r-project.org).

3.3.3. Digital modelling

The models used here are those of Allen et al. (2013) and Macaulay et al. (2017) (but see Chapter 2 here) which have been previously validated and used in assessments of CoM, along with two previously unpublished models of *Iguana iguana* and *Alligator mississippiensis* (see Supplementary Table 3.3 for details of all models). These models are different specimens, which were not part of the original dataset from which integument was sampled. Briefly, skin

outlines were extracted from CT data (for extant organisms, using Avizo) following Macaulay et al. (2017), or reconstructed based on the digitised skeleton (for extinct taxa, using Maya) following Allen et al. (2013). Likewise, air cavities were modelled from CT data or reconstructed with reference to the skeletal material (Allen et al., 2013, Macaulay et al., 2017). The models were then split into segments (e.g. for forelimb: upper arm, forearm and hand), and placed into a standardised posture, with forelimbs and hindlimbs outstretched medio-laterally and dorso-ventrally respectively (Figure 3.1B) (for full methodological details, see (Allen et al., 2013, Allen et al., 2009, Macaulay et al., 2017)). In recognition of the uncertainty surrounding soft tissue reconstruction in fossil taxa, maximum and minimum versions of these models were created to represent the maximal feasible range of segment volumes (Allen et al., 2013).

Integument property data were applied to our models, informed by our statistical analyses comparing the properties of different regions across specimens (Supplementary Figure 3.1). Where statistically significant differences were found between regions for a given property, it was applied heterogeneously across the model. If no significant differences were identified, an average value (mean/median according to the normality of the data's distribution) was applied. Of the four integument types, across their nine properties, seven were heterogeneous across models, and two (general body feather density and bird skin thickness) were homogeneous (see Supplementary Table 3.4). These differences between integument in other regions are presented in Supplementary Figure 3.1; summary of data applied to models in Supplementary Table 3.5.

In order to calculate a mass for the integument overlying each segment, it was necessary to determine an integument volume, to which our derived density values could be applied. The area of the integument-bearing surface only (i.e. excluding the artificial surfaces which lay

inside joints between segments) was determined for each segment using FormZ (www.formz.com). This area, multiplied by the appropriate thickness value from our dataset, produced an estimation of integument volume for each segment. This protocol assumed, for each segment, that integument CoM was equal to the CoM of the skin outline; i.e. the flesh component of our model segments. This assumes that the integument outline followed the contours of the skin outline, that integument thickness was constant within each segment, and that regions not bearing integument would have a small effect on integument CoM for each segment. Although not strictly biologically accurate, these assumptions allowed simple, consistent application of integument to models, and are unlikely to appreciably impact whole body CoM position (see sensitivity analysis on flight feather CoM position outlined below, and see Supplementary Text 3.1 for details).

Representations of the flight feathers were included, given that they constitute a substantial proportion of the feather mass for birds (published values of up to 26%, DesRochers et al., 2010) and should exert a relatively large effect on whole body CoM due to their distal positioning on the forelimb. However, wing shape is highly variable, even within extant taxa (Wang and Clarke, 2015), making a rigorous reconstruction of flight feathers surfaces challenging. This is especially true for fossil taxa, which have been suggested to possess traits, including tetrapteryx flight (Xu et al., 2003) and unusual wing compositions (Longrich et al., 2012), which have no modern homologue. We therefore included only a simplistic representation of the flight surfaces. A sensitivity analysis was conducted to assess the impact of subjective modelling decisions regarding the geometries and mass properties of the flight surfaces. Flight feathers were considered separately for each segment of the wing and the tail (plus shank and metatarsal for *Microraptor* model (Xu et al., 2003)). The thickness and lengths of these flight surfaces were dictated by our integument dataset. Combined with specimen-specific segment lengths taken from the models, and our integument density data,

a mass for each flight surface was calculated. Determination of a CoM position for each flight surface required more subjective decisions. CoM position was dictated by the geometry of the flight surfaces, which are variable even between extant species, and can be varied *in vivo* under neuromuscular control. We assessed the difference made to overall CoM position with a range of flight surface geometries and orientations, all grounded in the empirical data collected here. We compared these results with those obtained if it was assumed that flight surface CoM was equal to the CoM of the flesh component of each segment (as was done for the general body feathers). Our sensitivity analysis showed only small differences between these model variants (< 1.5mm, see Supplementary Text 3.1). We therefore proceeded with the simplest solution: assuming that all components of a segment share the same CoM, the CoM of the flesh component.

Mass data were calculated for flesh components using a density of 1000kgm⁻³; and zero density for air cavities. Centre of mass was then determined for these components from the closed skin outlines and air cavities using FormZ. The centres of mass for all components were summed to give segment, and subsequently whole organism, CoM, according to the following equation:

$$CoM_W = \frac{\Sigma(CoM_s * mass_s) - \Sigma(CoM_a * mass_a)}{\Sigma(mass_s) - \Sigma(mass_a)}$$

Equation 3.1

Where CoM_W is the centre of mass of the whole organism (or simply ‘CoM’ in the remainder of this study), CoM_s and mass_s refer to segment mass properties (i.e. flesh and integument components) and CoM_a and mass_a refer to air cavity mass properties.

3.4. Results

3.4.1. Do integument mass properties correlate with ecology and locomotion in archosaurs?

Here, we present key results from our investigations of integumentary mass properties.

These only represent a selection of the 42 analyses conducted.

Flight feather density, length and thickness were all found to vary significantly between the different locomotor and phylogenetic groups studied here (Figure 3.2A-C). Notably, with increasing flight ability (from purely terrestrial, through burst-adapted flight, to other fully aerial flight behaviours), flight feather density decreased (Figure 3.2A), while feather length and thickness both increased (Figure 3.2B and C). Additionally, flight feather surface area was found to correlate with locomotor type (Figure 3.2D). The surface areas of the individual flight feathers of weaker fliers (i.e. terrestrial and burst-adapted) were low; birds favouring soaring and gliding behaviours had high surface areas; while those using continuous flapping represented an intermediate group (Figure 3.2A). Further significant differences were found between the different types of flight feather (i.e. primary, secondary, tertiary and caudal). Each feather type was significantly distinct in length, primary feathers were significantly thicker than all others, and primary and caudal feathers were more dense (Supplementary Figure 3.1C-E).

Examination of the mass property data for scaly integument highlighted significant differences in the density and thickness of scaly skin from lizards, crocodylians and birds (Figure 3.3A). Different feather types (i.e. contour, filoplume, semiplume) also displayed significant differences in their density and thickness (Figure 3.3B and C). General body feathers showed insignificant variance in density across phylogenetic and locomotor groups. However, their thickness varied significantly between the wholly terrestrial ratites and the

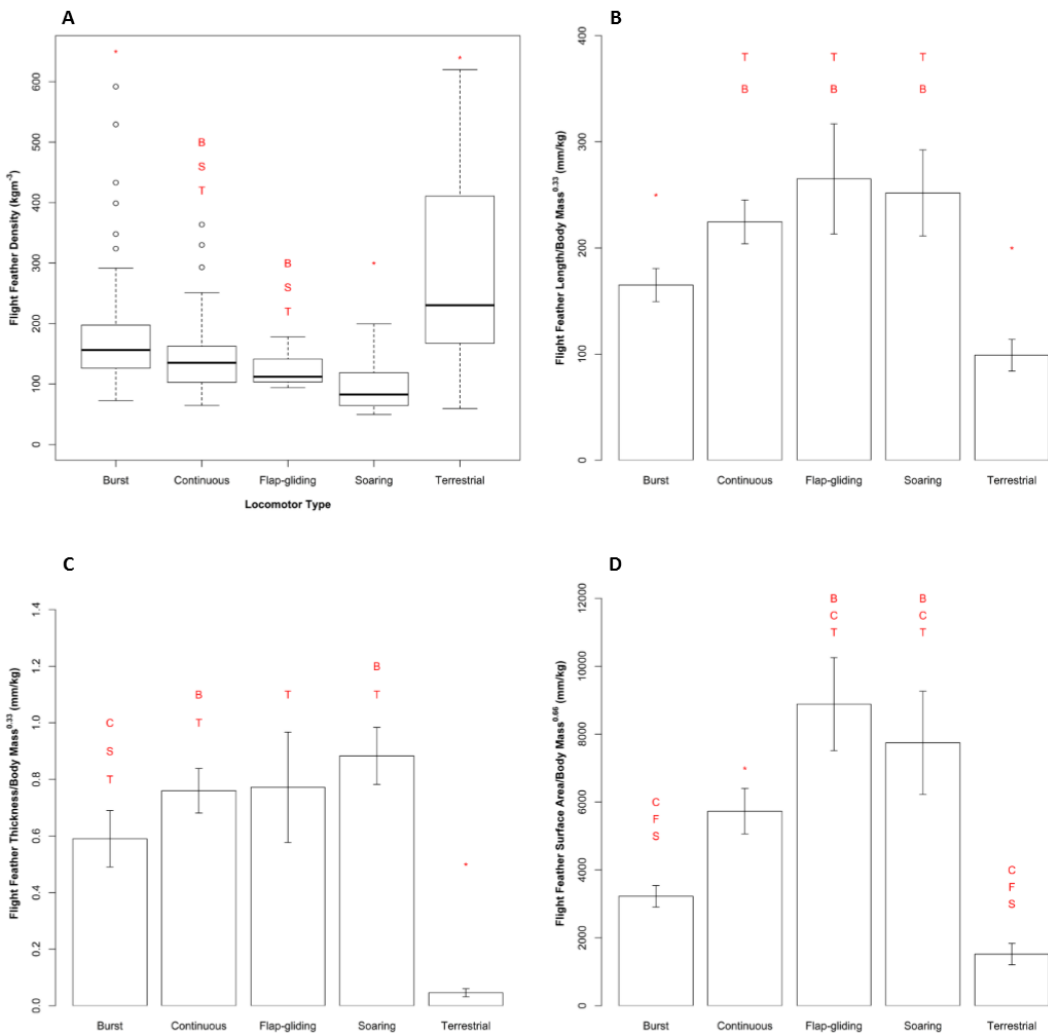


Figure 3.2: Flight feather properties (A: density, B: length, C: thickness, D: surface area) showing differences between birds of different locomotor types. Significant differences were determined and are indicated by text over each bar (where * indicates significant difference to all other groups, and letters indicate significant differences to another group - B: Burst-adapted flight, C: Continuous flapping, F: Flap-gliding, S: Soaring, T: Terrestrial). N = 140 flight feathers from 22 specimens.

For box and whisker plots (A): black line represents median value, box represents interquartile range, the whiskers mark the maximum and minimum values within 1.5 interquartile ranges of the box extremes and any values outside this range are displayed as points.

*For bar charts (**B-D**): the mean value is plotted, with 95% confidence limits displayed as error bars.*

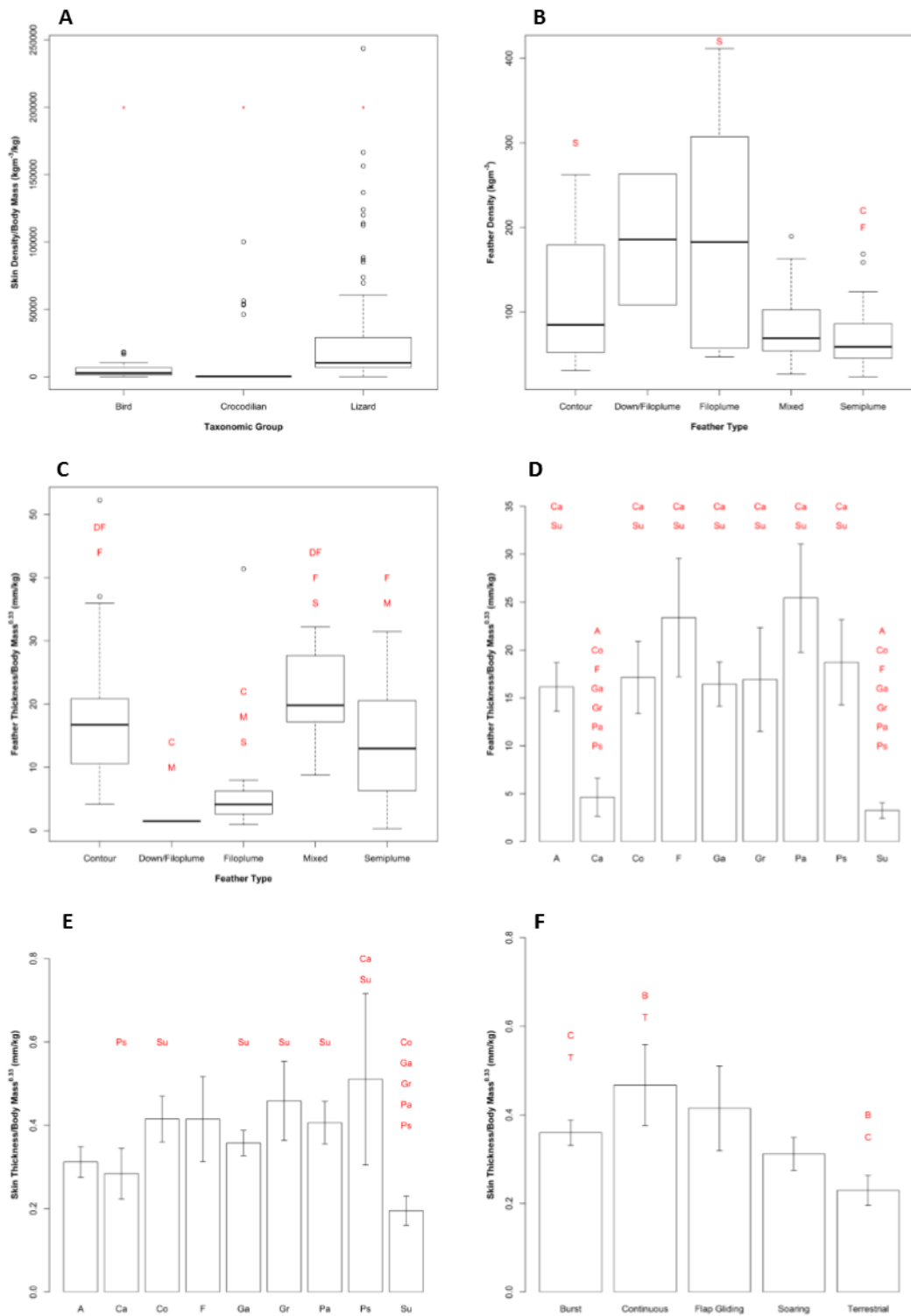


Figure 3.3: Integument properties (**A**: scaly skin density, **B**: feather density, **C & D**: feather thickness, **E & F**: skin thickness) showing differences between different taxonomic groups (**A**, **D**, **E**), different feather types (**B**, **C**) and different locomotor types (**F**). Significant differences

were determined and are indicated by text over each bar (where * indicates significant difference to all other groups, and letters indicate significant differences to another group).

Abbreviations for taxonomic groups in **D & E** - A: Accipitriformes, Ca: Casuariiformes, Co: Columbiformes, F: Falconiformes, Ga: Galliformes, Gr: Gruiformes, Pa: Passeriformes, Ps: Psittaciformes, Su: Struthioniformes. N = 152 scaly skin samples from 22 specimens; 155 feathered skin samples from 27 specimens.

*For box and whisker plots (**A-C**): black line represents median value, box represents interquartile range, the whiskers mark the maximum and minimum values within 1.5 interquartile ranges of the box extremes and any values outside this range are displayed as points.*

*For bar charts (**D-F**): the mean value is plotted, with 95% confidence limits displayed as error bars.*

other birds included in this study (i.e. Neognathae), all of which are capable of flight (Figure 3.3D). Similarly, the thickness of the skin underlying these feathers varied significantly between phylogenetic and locomotor groups (Figure 3.3E and F), whereas skin density did not. These differences were more complex than those seen in feather thickness, with differences present between neognath groups (Figure 3.3E), and several locomotor types (Figure 3.3F).

There were also numerous significant differences detected in the mass properties of integument between different regions (Supplementary Figure 3.1). These differences impacted model construction, and are outlined in Section 3.3.3.

3.4.2. How does integument impact mass distribution in extant archosaurs?

Results from digital models, normalised by body mass, are outlined here (Figure 3.4). Models displaying raw CoM positions are shown in Figure 3.5, and graphically presented in Supplementary Figure 3.2.

First, we outline the differences between our various model iterations, comparing CoM position from models with flesh, flesh with air cavities, and the latter model with integument added (Figure 3.4A). Extant birds and non-avian sauropsids were affected differently by the addition of both air cavities and integument, relative to the ‘flesh-only’ models. In non-avian sauropsids, CoM was strongly shifted in the caudal direction, while birds displayed a notable ventral shift (Figure 3.4A). For two of the three bird specimens (chicken and duck), adding integument had a markedly greater effect on CoM position than adding air cavities (225 and 346% greater shifts respectively). The two birds where this was the case did have poorly inflated air cavities; however, a sensitivity analysis showed that even drastic increases in air cavity volume (+ 300%) or extreme shifts in air cavity CoM position (+ 30mm) did not negate

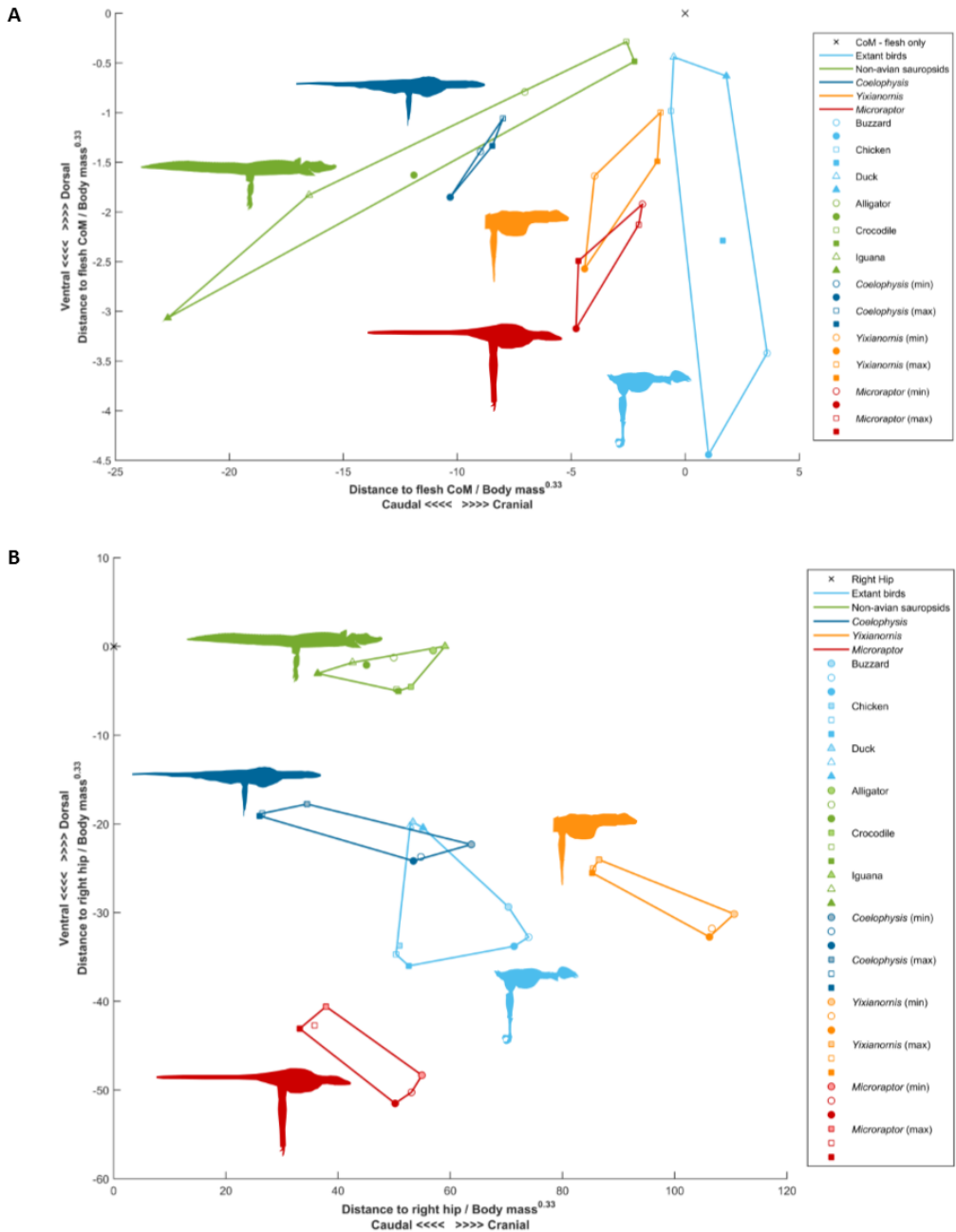


Figure 3.4: CoM positions for all models, normalised by body mass^{0.33}, with convex hulls around specimens from the same groups. Displayed **A**: relative to flesh CoM (displayed as 'x', set to 0 0 0 in x y z coordinates for all models) and **B**: relative to right hip (displayed as 'x', at 0 0 0 in xyz coordinates for all models). Different colours represent different taxa as per the legend. Lightly shaded icons: flesh only models; hollow icons: flesh and air cavities; filled icons: flesh, air cavities and integument.

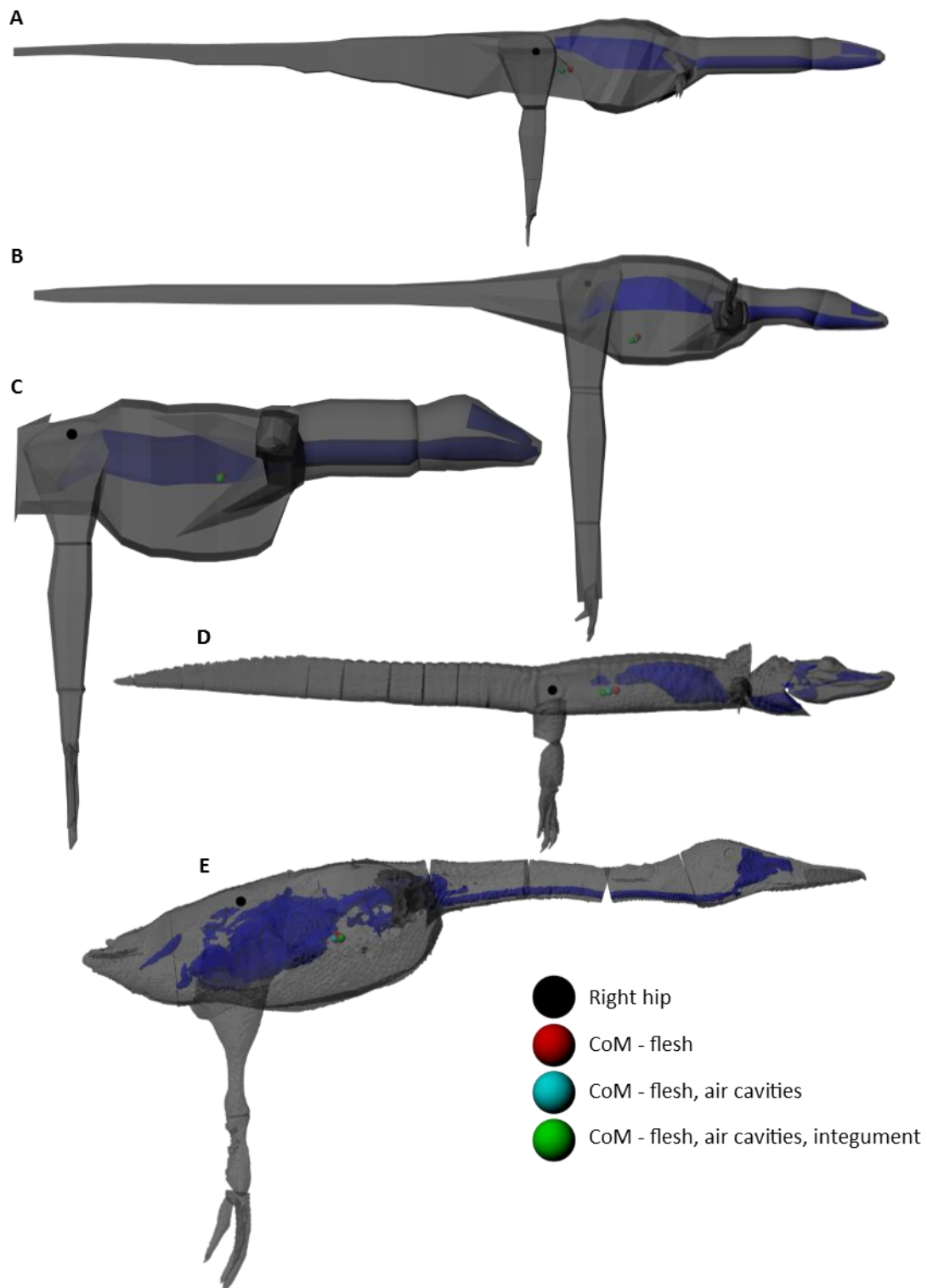


Figure 3.5: Digital models showing skin outlines (grey) and air cavities (blue) for *Coelophysis* (maximum model) (A), *Microraptor* (maximum model) (B), *Yixianornis* (maximum model) (C), alligator (D) and duck (E). Centre of mass positions indicated by coloured spheres, see key for detail. Models are not to scale.

this effect (see Supplementary Text 3.2). In the three non-avian sauropsid taxa, the effect of adding integument was markedly less than adding air cavities (16–70%).

The CoM positions of these specimens, showing the effects of adding different components, were also plotted relative to the right hip (Figure 3.4B). As above, the different groups mapped differently. However, here the extant groups were separated in the dorso-ventral rather than the cranio-caudal direction. Extant non-avian sauropsids displayed low variance in the dorso-ventral plane, with their CoM positions grouping around the level of the hip; there was much greater variability in the cranio-caudal direction (Figure 3.4B). Addition of both air cavities and integument resulted in a more caudal CoM position, with the most drastic shift seen in the iguana (Figure 3.4B). The addition of air cavities and integument to extant bird models resulted in a ventral shift of CoM position relative to the hip. The degree of shift varied across the three species from very little in the duck to a moderate shift in the buzzard (approximately 50% of the shift seen in the iguana). Substantial variation can be seen in CoM position, both in the dorso-ventral and cranio-caudal directions when observed relative to hip position for the three bird specimens. The three extant birds studied here exhibited distinct CoM positions, with some as similar to the fossil taxa as they were to the other extant birds, even when considering the extensive range of possible body forms tested here for fossil taxa.

3.4.3. How did feather evolution impact CoM position during theropod evolution?

When plotted relative to the ‘flesh-only’ models, the fossil species studied here showed intermediate responses of CoM to integument, relative to the extant taxa (Figure 3.4A). These responses were consistent with their phylogenetic position and body shape. The Triassic theropod *Coelophysis* demonstrated a more plesiomorphic response, similar to the

extant non-avian sauropsids, with a moderate caudal CoM shift. Meanwhile, the Cretaceous taxa *Microraptor* (a heavily feathered non-bird) and *Yixianornis* (a bird, close to crown group Aves) both showed more derived responses, with the CoM shifted ventrally, similar to the extant birds (Figure 3.4A).

When plotted relative to the right hip (Figure 3.4A), the three fossil taxa modelled here had CoMs fairly distinct from the other specimens. The CoM of *Cœlophysis* had some overlap with the extant bird group (closest to the duck), and was distinct from the extant non-avian sauropsid species in the dorso-ventral dimension. *Microraptor* and *Yixianornis* had CoMs both somewhat similar to one extreme of the bird group (the chicken and buzzard respectively), with similar distances between these species to those evident between the different extant bird species.

3.5. Discussion

3.5.1. Ecological and functional adaptations in integumentary structures

Our examination of the physical properties of flight feathers here revealed numerous statistically significant differences between birds that favour different locomotor behaviours (Figure 3.2A-D). In particular, we identified several parameters with strong correlations to flight capability that represent mechanical and aerodynamic adaptations for flight (Figure 3.2A-D). Comparisons of flight feather length and surface area showed strong trends to greater individual feather dimensions with increasing flight ability (Figure 3.2B and D). This matches evidence that flight feather length and whole wing surface area generally increase with increasing flight ability, especially for gliding and soaring behaviours (Lindhe Norberg, 2002, Wang et al., 2011). Flight feather thickness also increased with increasing flight ability (Figure 3.2C). This morphological change would increase the structural stability of feathers, making them more able to resist bending moments during flight (Nudds and Dyke, 2010).

A further structural change to flight feathers in birds with greater flight abilities was indicated by a decrease in density from terrestrial birds to soaring and gliding birds (Figure 3.2A). These lower density feathers would serve to slightly reduce the mass of the whole bird, and perhaps more importantly the mass of the distal wing segment during flight, perhaps resulting in increased efficiency. Our results also revealed that different types of flight feathers had different densities (Supplementary Figure 3.1C). Flight feathers were split into two groups, with primary and caudal feathers possessing higher densities, while secondary and tertiary feathers were less dense (Supplementary Figure 3.1C). We suggest this is a reflection of the different functional demands placed on these feathers, also evident in their different morphologies.

The significantly greater thickness of primary flight feathers is a further indication of the different morphology of feathers with more rigorous functional requirements (Supplementary Figure 3.1D), reflecting the thicker rachis required to resist greater bending moments nearer the wing tip (Nudds and Dyke, 2010). Similarly, the differences detected in the density and thickness of the different general body feather types (i.e. contour, filoplume, semiplume etc) are logical reflections of their different functions and match the visible morphological differences (Figure 3.3B and C). General body feathers did not vary in density, but did vary in thickness, across locomotor and phylogenetic groups (Figure 3.3D). However, these properties were both constant within Neognathae. This consistency hints that these physical properties are dictated by another function of feathers, for example thermoregulation, which would likely exert a greater selection pressure than locomotion on these generalised feathers.

Overall, our analysis reveals how flight capabilities and ecology are correlated with simple geometrical measurements taken from flight feathers. These correlations indicate the potential to inform conclusions on the locomotor behaviours of extinct taxa, with simple geometry serving as predictors of relative flight capability in fossils with feather preservation. Our models and data can also contribute to more complex aerodynamics simulations in extant and extinct taxa. However, herein we used our dataset to examine the evolution of integument and body shape in archosaurs (Figure 3.1D).

3.5.2. Functional consequences of the evolution of body shape and integument

Our models (Figure 3.5) are the first to explicitly incorporate empirical integumentary data into mathematical assessments of body shape in archosaurs, in order to use CoM position to investigate the impact of feather evolution on the evolution of flight in theropod dinosaurs. This was made possible by our experimental dataset, which enabled inclusion of heterogeneous integumentary surfaces to our models where appropriate. This allows us to address the role of integument in body shape evolution in detail (Figure 3.4).

Examination of fossil taxa can provide unprecedented insights into transitional morphologies. They provide important insights into the functional ecology of these transitional species, which are unlike anything alive today. By gradual application of components to each of our models, our methodology and results simulated the changes associated with the evolution of a feathered integument, while keeping all other aspects of the model constant. Comparing our ‘flesh-only’ CoM data to our complete CoM estimates (including air cavities and integument), it is evident that extant birds and non-avian sauropsids were affected differently by the addition of integument to models (Figure 3.4A). This effect was related to their different body plans, as well as their different integumentary coverings. In particular, the Triassic theropod *Coelophysis* displays a plesiomorphic response

to the addition of integument; more like the extant non-avian sauropsids studied here; whereas the feathered maniraptorans *Microraptor* and *Yixianornis* display more ‘bird-like’ responses (Figure 3.4A). In the case of *Coelophysis* and *Microraptor* in particular, these fossil species possess transitional body plans between those of ancestral Sauropsida and Aves. The result that they group with the modern non-avian sauropsids and birds respectively, indicates that it was specifically the integument type (scaly versus feathered) that strongly influenced these different effects on CoM (Figure 3.4). This effect was further confirmed by application of a purely scaly integument to *Microraptor* (see Supplementary Text 3.3). In two of the three bird species, the effect of adding integument was greater than that of adding air cavities (Figure 3.4). In contrast, in all three extant non-avian sauropsids, the effect of air cavities was greater than integument (Figure 3.4). Air cavity volumes were no larger in these non-avian sauropsids relative to body mass than in the bird specimens, again suggesting that it was integumentary differences driving this disparity in the effects of air cavities and integument on CoM position (Figure 3.4A). Feathers have varied properties across the body as well as varied distributions, both of which would contribute to a more substantial impact on whole body CoM (Figure 3.4A).

Absolute CoM positions provide insights into the functional ecology of organisms (Alexander, 1985, Allen et al., 2013, Gatesy and Biewener, 1991, Henderson, 2004, Maidment et al., 2014, Sellers et al., 2017, Henderson, 2018) (Figure 3.4B). A cranial shift of CoM position in bird-line archosaurs occurred alongside the evolution of aerial capabilities (Allen et al., 2013). A more craniad CoM, combined with modified wing positions (together determining centre of lift and the forces acting about it) contributes to the improved stability of birds in gliding and flapping flight behaviours (Taylor and Thomas, 2002, Thomas and Taylor, 2001). Alongside the evolution of flight, a novel feathered integument was also evolving, facilitating the development of increasingly aerial behaviours (Dial, 2003, Ostrom, 1974, Padian and

Chiappe, 1998). Our results show that increased feathering also changed the CoM of maniraptoran theropods, producing a marked CoM shift in the ventral direction as evident in all five feathered specimens studied here (Figure 3.4B). This too is a benefit for stable flight - a more ventral CoM relative to the centre of lift produced by the wings provides passive 'pendulum' stability to the system by resisting pitch (about the left-right axis) and roll (about the crano-caudal axis) (Thomas and Taylor, 2001). The stability conferred by having a more ventral CoM is likely a key factor in the overwhelming success of birds in aerial environments, enabling them to develop a huge range of flight morphologies, unlike other extant flying vertebrates (Thomas and Taylor, 2001).

There are some similarities in our results when comparing absolute CoMs relative to 'flesh-only' models (Figure 3.4A), and assessing CoMs relative to the right hip joint (Figure 3.4B). These similarities are evident in the extant taxa: non-avian sauropsids vary mostly in crano-caudal CoM position, as reflects their body plan. Birds again show substantial CoM variability in the dorso-ventral plane across the species studied here. This CoM variability is likely indicative of the more diverse morphologies (in particular different body segment proportions) of the bird specimens in comparison to non-avian sauropsids. In plots of CoM positions relative to the hip joint (Figure 3.4B), *Coelophysis* showed an overlap with the bird group. Though *Coelophysis* was chosen as a representative early dinosaur species, its body plan was more derived than in other non-avian sauropsids due to the elongate hindlimbs, but it lacked the more derived, enlarged forelimbs typical of extant avians. Examination of first mass moment data for the various components of this model indicate that it was the long hindlimbs of *Coelophysis* that drove this ventral CoM shift, exerting a much greater influence (at least double) on whole body CoM relative to body mass than in extant non-avian sauropsids (Supplementary Text 3.4). *Microraptor* and *Yixianornis* were both distinct from the extant bird group (Figure 3.4B), reflecting differences in their morphology - neither

had mass properties equivalent to our extant bird subjects. Though our extant bird sample is a decent representation of the ancestral avian body plan, it is possible that incorporation of a larger sample of living birds (e.g. tinamous, other Galloanseres and Neoaves) would result in overlap with the fossil taxa. The large ventral shift in the CoM of *Microraptor* was driven by the elongate hindlimbs, exerting a much greater (almost four times) influence relative to body mass than in *Yixianornis* (Supplementary Text 3.4).

It should be noted that the alligator specimen used here was a young juvenile (body mass: 0.6kg). Previous studies have found significant differences in whole body CoM between adult and juvenile crocodiles (Allen et al., 2009). Though no research has been published in this area, it would be expected that alligators would show similar differences across their ontogenetic development. Addition of a wider ontogenetic range of alligators and crocodiles to this dataset would therefore be likely to expand the envelope of CoM positions established here for reptiles, as would the addition of a wider range of bird species (Figure 3.4). These additions would be of great benefit to future work seeking to interpret the CoM positions of fossil archosaurs in order to predict their locomotor capabilities.

3.6. Conclusion

We conclude that the magnitude of the effects of adding integument, along with the variable effects across specimens, even within Aves, indicates that integument should be incorporated into future volumetric models seeking to precisely determine CoM position in feathered archosaurs. The effects of integument were often at least as great as adding air cavities, which have long been included as standard in volumetric modelling approaches (e.g. Alexander, 1985, Bates et al., 2009b, Henderson, 1999, Hutchinson et al., 2007). Furthermore, our comparison of integumentary effects on CoM in archosaurs with different body plans (Figure 3.4) reveals important biomechanical consequences with clear links to

evolutionary changes in locomotor function and ecology. Thus, we infer that the evolution of integument amplified changes in CoM positions between birds and earlier sauropsids (Allen et al., 2013). The evolution of the highly specialised feathered integument in bird-line archosaurs, through its effect on mass distribution alone, also served to confer important mechanical advantages and therefore functional benefits, aiding the evolution of flight and contributing to the success of birds in their occupation of aerial ecological niches.

3.7. Supplementary Information

Supplementary Text 3.1: Details of the sensitivity analysis on the effect of flight feather geometry on CoM position.

Flight feathers make up approximately 20% of total feather mass in extant birds (DesRochers et al., 2010, Summers et al., 1992). This, along with their position, at large distances from the whole body CoM, mean they are likely to exert a substantial effect on whole body CoM position. To explicitly include flight feathers in our models, data was required on their mass, and CoM position. Mass was calculated for each series of flight feathers (primary, secondary, tertiary and caudal) directly from our dataset on feather mass properties. However, determination of a suitable CoM position was more subjective. We therefore sought to investigate the effect of different flight feather CoM positions on whole body CoM position to determine the most effective method for inclusion in our final models.

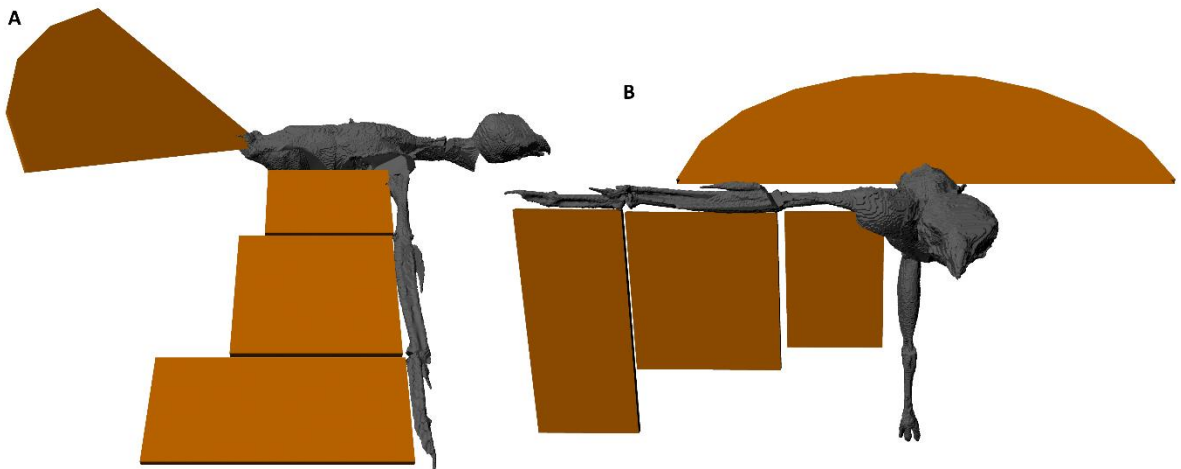
In this sensitivity analysis, for the three extant bird specimens, we considered the following scenarios:

- **SA0** - flight feather CoM is equal to the ‘flesh’ CoM for the corresponding segment (e.g. primary feather CoM = hand flesh CoM)
- **SA1** - ventrally directed wing flights, wide tail feathers
- **SA2** - ventrally directed wing flights, narrow tail feathers
- **SA3** - caudally directed wing flights, wide tail feathers
- **SA4** - caudally directed wing flights, narrow tail feathers

In SA1-4, the three wing flight surfaces were represented by cuboids, one per wing segment (see Supplementary Text 3.1.1). Flight surface length was calculated as an average from our integument dataset, width from model specific segment length, and thickness set to 5mm (thickness did not affect CoM position, it only assisted with visualising and positioning of the

flight surfaces). Wing flight surfaces were directed either ventrally (in accordance with the orientation of the rest of the wing), or caudally (to represent the *in vivo* condition). The flight feather surface of the tail was a semicircle (wide variant) or quarter circle (narrow variant) to assess the impact of the kind of variation seen *in vivo*. In both cases, the circle radius was set to the average caudal feather length from our dataset (see Supplementary Text 3.1.1).

In all birds, the differences between whole body CoM positions calculated from each iteration of the sensitivity analysis were small when compared to the original model (SA0). Maximum differences were 1.5mm, 0.9mm and 0.9mm for the buzzard, chicken and duck specimens respectively (see Supplementary Text 3.2). These differences are small, and the process of modelling flight surfaces is inherently subjective. In contrast, SA0 (which produces similar CoM estimates) assumes that flight feather CoM is equal to flesh CoM for the same segment. This approach is objective and repeatable, and therefore we proceeded to use the SA0 models.



Supplementary Text 3.1.1: Rendering of buzzard model showing caudally (**A**) and ventrally orientated (**B**) wing flight surfaces, and narrow (**A**) and wide (**B**) tail flight surfaces as included in sensitivity analysis.

Supplementary Text 3.1.2: Data from 5 iterations of bird models examining the effects of changing flight feather CoM position. CoMs presented in two dimensions, cranio-caudal and dorso-ventral respectively. Air cavity shift (mm) calculated as the distance between the 2D flesh CoM and flesh-air cavities CoM. Integument shift (mm) calculated as the distance between the 2D flesh-air cavities CoM and the flesh-air cavities-integument CoM. Distance to SA0 (mm) is 2D distance to the flesh-air cavities-integument CoM of SA0.

Buzzard	SA0	SA1	SA2	SA3	SA4
Flesh CoM	62.8	62.8	62.8	62.8	62.8
	-26.2	-26.2	-26.2	-26.2	-26.2
Flesh-air cavities CoM	66.0	66.0	66.0	66.0	66.0
	-29.3	-29.3	-29.3	-29.3	-29.3
Flesh-air cavities-integument CoM	63.7	63.3	63.2	62.5	62.3
	-30.2	-30.9	-30.8	-30.0	-29.9
Air cavity shift	4.43	-	-	-	-
Integument shift	2.47	-	-	-	-
Distance to SA0	-	0.82	0.87	1.30	1.49
Chicken	SA0	SA1	SA2	SA3	SA4
Flesh CoM	51.0	51.0	51.0	51.0	51.0
	-33.7	-33.7	-33.7	-33.7	-33.7
Flesh-air cavities CoM	50.3	50.3	50.3	50.3	50.3
	-34.7	-34.7	-34.7	-34.7	-34.7
Flesh-air cavities-integument CoM	52.6	51.9	51.8	51.9	51.7
	-36.0	-36.0	-36.0	-36.0	-36.0
Air cavity shift	1.16	-	-	-	-
Integument shift	2.62	-	-	-	-
Distance to SA0	-	0.71	0.82	0.75	0.87
Duck	SA0	SA1	SA2	SA3	SA4
Flesh CoM	57.0	57.0	57.0	57.0	57.0
	-21.1	-21.1	-21.1	-21.1	-21.1
Flesh-air cavities CoM	56.4	56.4	56.4	56.4	56.4
	-21.6	-21.6	-21.6	-21.6	-21.6
Flesh-air cavities-integument CoM	58.9	58.2	58.1	58.1	58.0
	-21.8	-21.9	-21.9	-21.8	-21.9
Air cavity shift	0.71	-	-	-	-
Integument shift	2.47	-	-	-	-
Distance to SA0	-	0.70	0.82	0.74	0.86

Supplementary Text 3.2: Details of the sensitivity analysis on the impact of bird air cavity volume on CoM.

In two of our bird specimens (chicken and duck), CoM position was affected more by the addition of integument than the addition of air cavities. The air cavities in these two birds were deflated due to conditions between collection and CT scanning. We sought to determine if our observation (that a feathered integument had a greater effect on CoM position than air cavities in these specimens) was real, or an artefact resulting from the deflated air cavities.

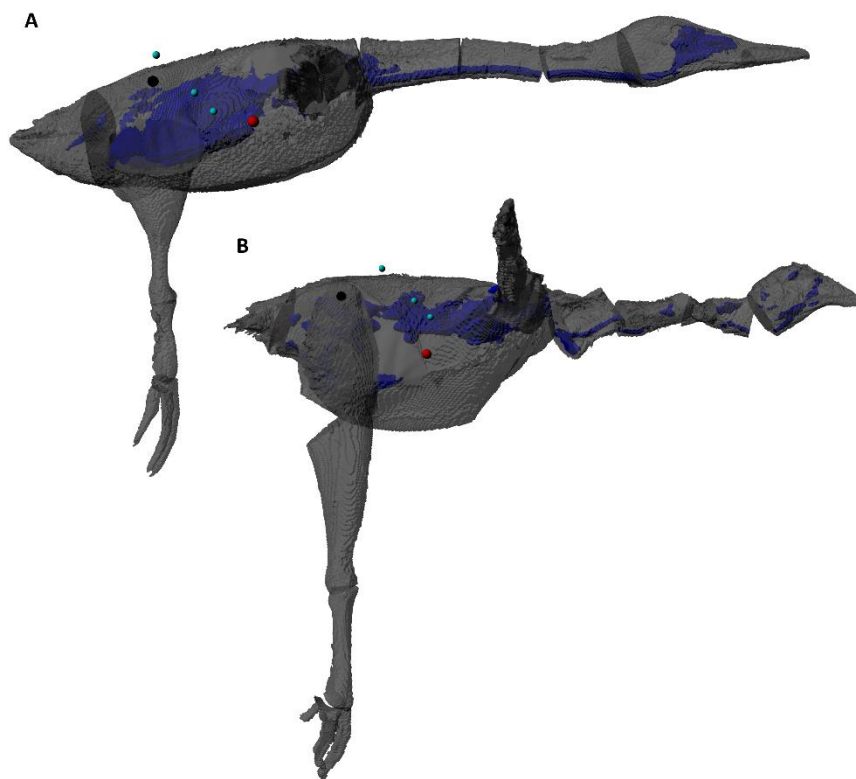
For both specimens, we examined seven versions of the models, including the originals. These model iterations included changes to air cavity volume (and therefore mass) and CoM position, in order to reflect a more life-like condition. Model iterations in the sensitivity analysis were as follows:

- **SA0** - original model
- **SA1** - torso air cavity volume increased by 150%
- **SA2** - torso air cavity volume increased by 200%
- **SA3** - torso air cavity volume increased by 300%
- **SA4** - torso air cavity CoM moved dorso-caudally 10mm
- **SA5** - torso air cavity CoM moved dorso-caudally 30mm
- **SA6** - torso air cavity volume increased by 200% & CoM moved dorso-caudally 30mm

Air cavity volume was increased in both specimens to a maximum of 300%, at which point air cavity volume represents 15% of torso volume, as expected for birds (Henderson, 2010).

Air cavity CoM was moved incrementally dorso-caudally. A 30mm dorso-caudal shift is a drastic shift, in both specimens this puts the CoM just outside the torso flesh outline (see Supplementary Text 3.2.1).

For the duck, all model iterations maintained the observed trend - integument had a greater impact on CoM position than air cavities (see Supplementary Text 3.2.2). For the chicken, 6 out of 7 model iterations (with the exception of SA3) maintained the observed trend - integument had a greater impact on CoM position than air cavities (see Supplementary Text 3.2.3). For the majority of the extreme scenarios covered by our sensitivity analysis, the observed trend is maintained. We therefore conclude that our observation of a greater impact of integument than air cavities on CoM is true, not an artefact of air cavity deflation.



Supplementary Text 3.2.1: Renderings of duck (A) and chicken (B) models. Showing skin outline (grey), air cavities (blue), right hip (black sphere), flesh CoM (red sphere), and three versions of CoM position of the torso air cavity (light blue spheres).

Supplementary Text 3.2.2: Data from 9 iterations of duck model examining the effects of changing air cavity properties. CoMs presented in two dimensions, cranio-caudal and dorso-

ventral respectively. Air cavity shift (mm) calculated as the distance between the 2D flesh CoM and flesh-air cavities CoM. Integument shift (mm) calculated as the distance between the 2D flesh-air cavities CoM and the flesh-air cavities-integument CoM. Greater shifts are highlighted in red.

	SA0	SA1	SA2	SA3	SA4	SA5	SA6
Flesh CoM	57.0	57.0	57.0	57.0	57.0	57.0	57.0
	-21.1	-21.1	-21.1	-21.1	-21.1	-21.1	-21.1
Flesh-air cavities CoM	56.4	56.8	57.3	58.2	56.0	55.3	54.9
	-21.6	-21.7	-21.8	-22.1	-21.2	-20.5	-19.5
Flesh-air cavities-integument CoM	58.9	59.3	59.7	60.5	58.6	57.9	57.7
	-21.8	-21.9	-22.0	-22.2	-21.5	-20.9	-20.1
Air cavity shift	0.71	0.59	0.76	1.53	0.92	1.80	2.65
Integument shift	2.47	2.44	2.40	2.32	2.55	2.69	2.88

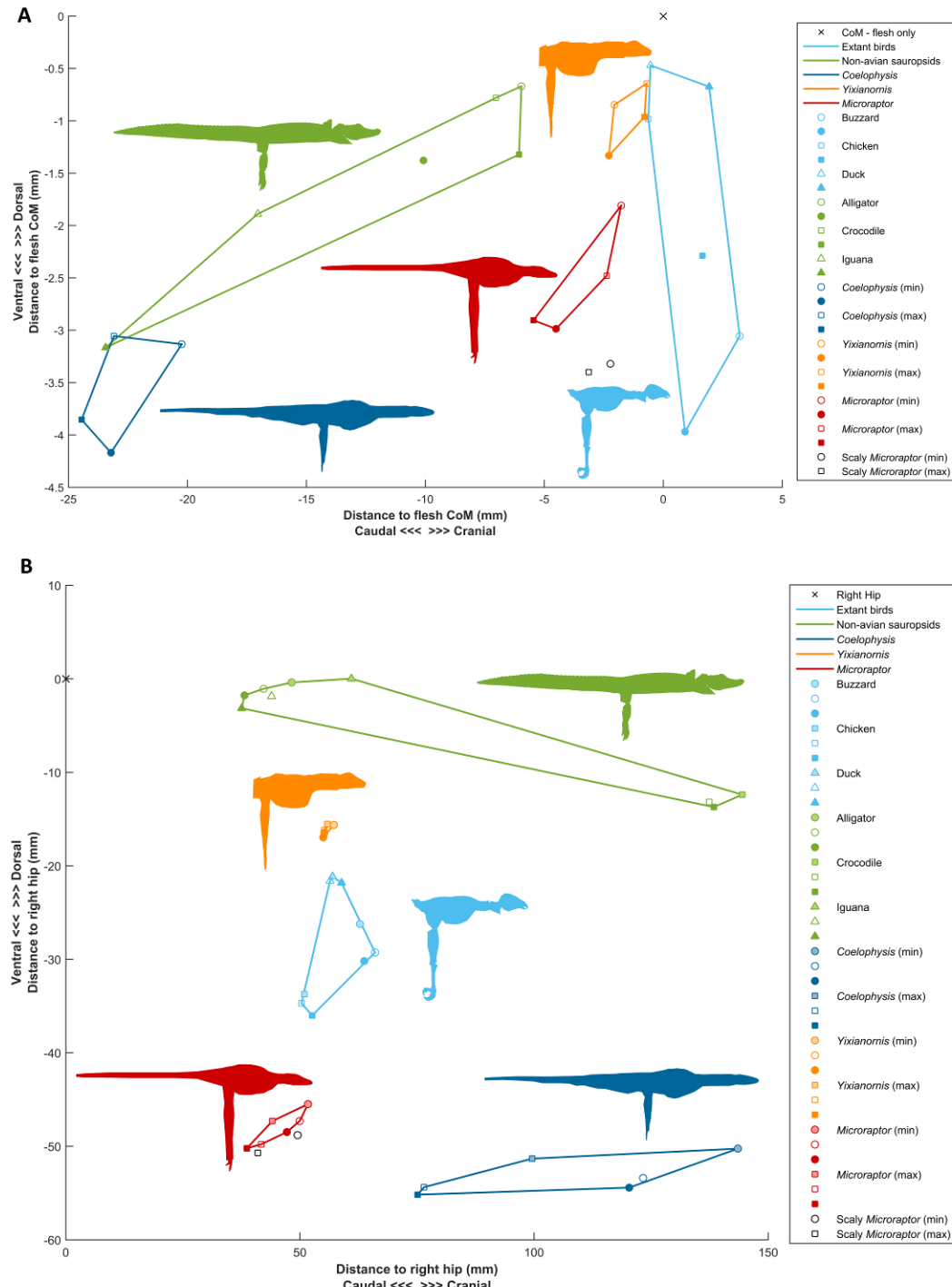
Supplementary Text 3.2.3: Data from 9 iterations of chicken model examining the effects of changing air cavity properties. CoMs presented in two dimensions, cranio-caudal and dorso-ventral respectively. Air cavity shift (mm) calculated as the distance between the 2D flesh CoM and flesh-air cavities CoM. Integument shift (mm) calculated as the distance between the 2D flesh-air cavities CoM and the flesh-air cavities-integument CoM. Greater shifts are highlighted in red.

	SA0	SA1	SA2	SA3	SA4	SA5	SA7
Flesh CoM	51.0	51.0	51.0	51.0	51.0	51.0	51.0
	-33.7	-33.7	-33.7	-33.7	-33.7	-33.7	-33.7
Flesh-air cavities CoM	50.3	50.3	50.2	50.1	50.0	49.2	48.0
	34.7	-35.1	-35.6	-36.6	-34.3	-33.6	-33.3
Flesh-air cavities-integument CoM	52.6	52.6	52.6	52.6	52.3	51.7	50.8
	-36.0	-36.4	-36.8	-37.6	-35.7	-35.1	-35.0
Air cavity shift	1.16	1.57	2.01	2.95	1.17	1.71	3.00
Integument shift	2.62	2.63	2.64	2.66	2.72	2.91	3.24

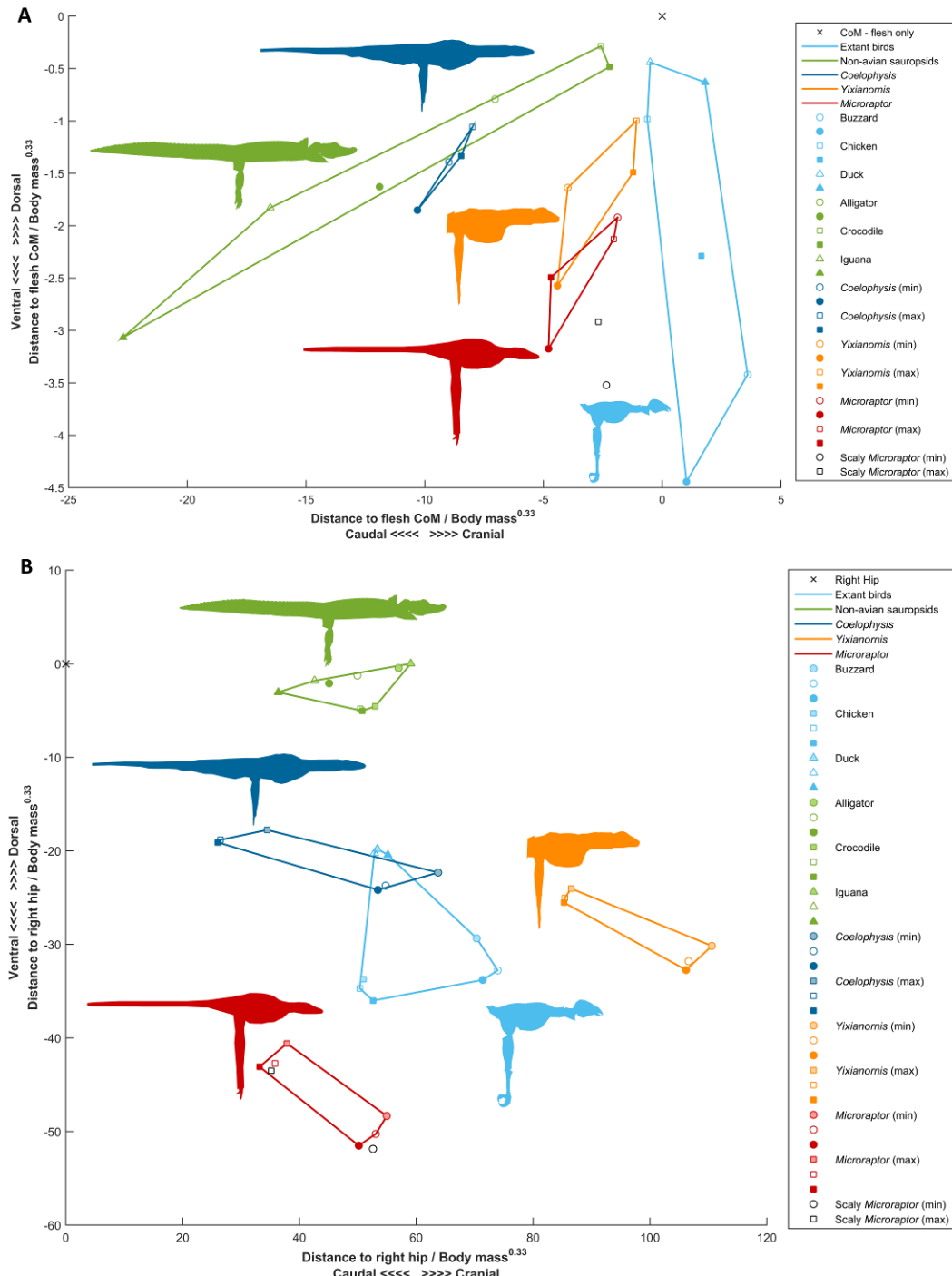
Supplementary Text 3.3: Comparison of feathered and scaly *Microraptor* models.

We sought to investigate the difference in the observed magnitudes of CoM shifts between feathered and scaly integument types, particularly in the fossil species *Coelophysis* and *Microraptor* which possess broadly similar body plans. This was achieved by application of a purely scaly integument to our *Microraptor* models, with the same thickness and density data as applied to the non-avian sauropsid and *Coelophysis* models.

For the minimum *Microraptor* model, the addition of scaly integument resulted in a small CoM shift from the ‘flesh + air cavities’ model (absolute 2D distance: 1.57mm), 53% of the shift produced by the addition of a fully feathered integument (2.98mm) (see Supplementary Text 3.3.1). The maximum *Microraptor* model displayed a greater difference in CoM position produced by scaly versus feathered models, with a scaly integument having only 38% of the effect on CoM (1.19mm vs 3.11mm) (see Supplementary Text 3.3.1). These results confirmed our observation that it is feathered integument specifically, that results in large CoM shifts.



Supplementary Text 3.3.1: Raw CoM positions for all models, with convex hulls around specimen from the same groups. Displayed **A**: relative to flesh CoM (displayed as 'x', set to 0 0 0 in xyz coordinates for all models) and **B**: relative to right hip (displayed as 'x', at 0 0 0 in xyz coordinates). Different colours represent different taxa as per the legend. Lightly shaded icons: flesh only models; hollow icons: flesh + air cavities; filled icons: flesh + air cavities + integument.



Supplementary Text 3.3.2: CoM positions for all models, normalised by body mass^{0.33}, with convex hulls around specimens from the same groups. Displayed **A**: relative to flesh CoM (displayed as 'x', set to 0 0 0 in xyz coordinates for all models) and **B**: relative to right hip (displayed as 'x', at 0 0 0 in xyz coordinates). Different colours represent different taxa as per the legend. Lightly shaded icons: flesh only models; hollow icons: flesh and air cavities; filled icons: flesh, air cavities and integument.

Supplementary Text 3.4: Summary of first mass moment data for nine models.

In order to investigate which segments were driving CoM differences between our specimens, first mass moments (FMMs) were calculated for each segment, including all component parts (i.e. flesh, integument, air cavities).

FMM was calculated for each segment according to the following equation:

$$FMM = (CoM_W - CoM_S) * mass_S$$

Equation 3.2

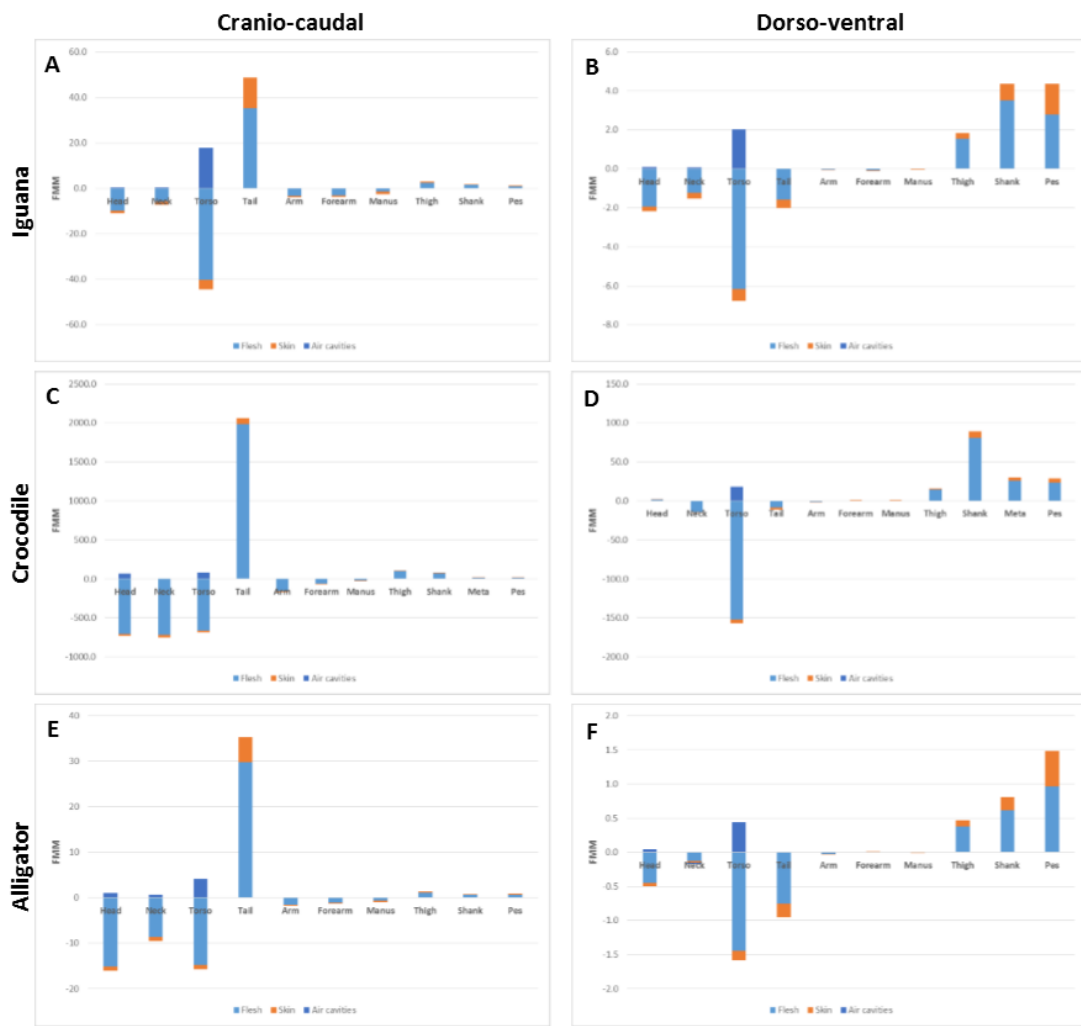
Where CoM_W is the centre of mass of the whole organism and CoM_S and $mass_S$ refer to segment mass properties. FMMs were calculated in the cranio-caudal and dorso-ventral dimensions, using the y and z components of the CoM respectively. Where necessary, the resulting FMMs were summed to produce one value for the necks and tails which were represented by numerous sections in the models. Additionally, FMMs for the limbs were doubled, to account for the missing contralateral limb pair. This raw FMM data is presented at Supplementary Text 3.4.1 - 3.4.3. When drawing comparisons between specimens, summed FMM data were normalised by specimen body mass, as predicted by our models.

FMMs for extant, non-avian sauropsid models (see Supplementary Text 3.4.1) were high for the axial components, in both cranio-caudal and dorso-ventral directions. A large caudally directed FMM for the tail was particularly evident in the crocodile and alligator, reflecting their muscular tails relative to the iguana. Hindlimb FMMs were relatively large in ventral direction, due to their orientation in models. The influence of integument and air cavity

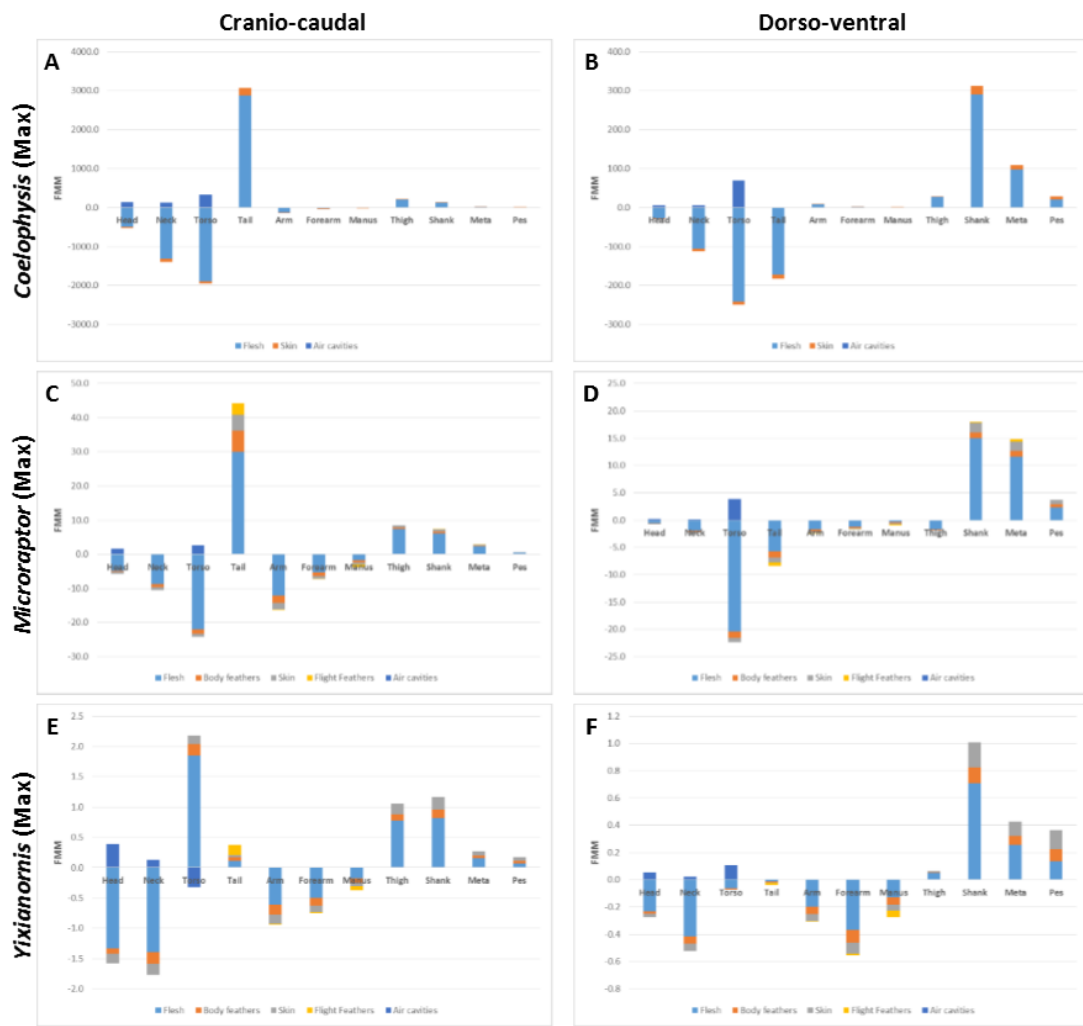
components on FMMs were generally small, but varied across specimens, and across segments within specimens.

FMMs for extinct fossil taxa studied here show variation across specimens, reflecting the substantial morphological differences between the three species (see Supplementary Text 3.4.2). The FMMs for the tails of *Coelophysis* and *Microraptor* were large in the caudal direction, similar to those of the extant crocodylians, reflecting their similar morphology (Supplementary Text 3.4.2). Relative to whole body mass, FMMs for the hindlimbs of *Coelophysis* were high in comparison to the extant non-avian sauropsids. This difference was driven by both a greater limb mass, and a slightly greater limb length relative to body mass. The FMMs of the forelimbs transition from a more plesiomorphic condition to a more derived, ‘bird-like’ condition in *Microraptor* in the cranio-caudal direction and *Yixianornis* in the dorso-ventral direction (Supplementary Text 3.4.2). The hindlimb of *Microraptor* was found to drive the ventral CoM seen in that taxa, with a much greater hindlimb FMM present compared to *Yixianornis* as a result of a substantially larger limb mass and longer length relative to body mass in *Microraptor*.

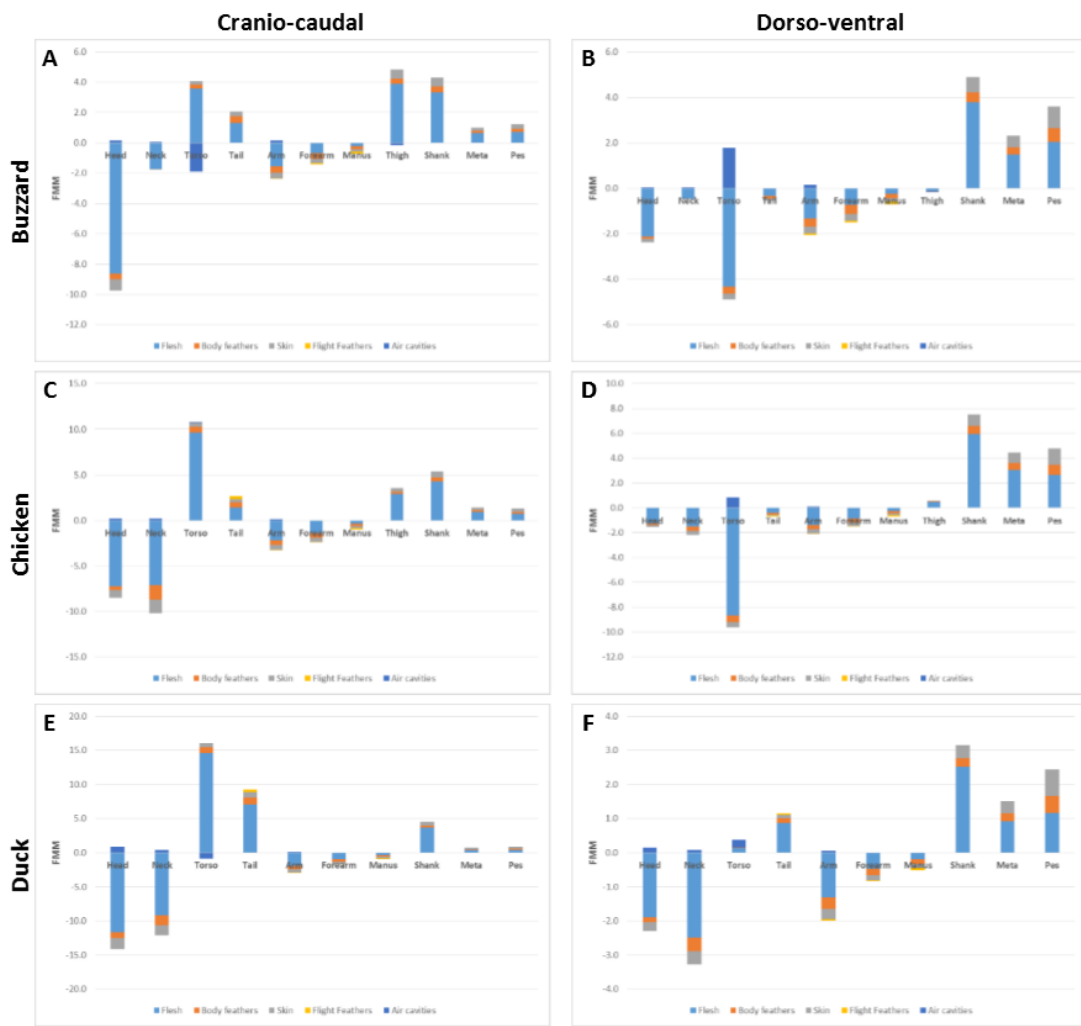
FMMs for extant birds (see Supplementary Text 3.4.3) vary across the three species studied, reflecting their different morphologies and their different whole body CoM positions. For example, despite a relatively short neck in the buzzard, the head has high FMM values in relation to the other axial segments. The influence of forelimb varied most in dorso-ventral plane, whereas hindlimb showed higher variance in cranio-caudal direction.



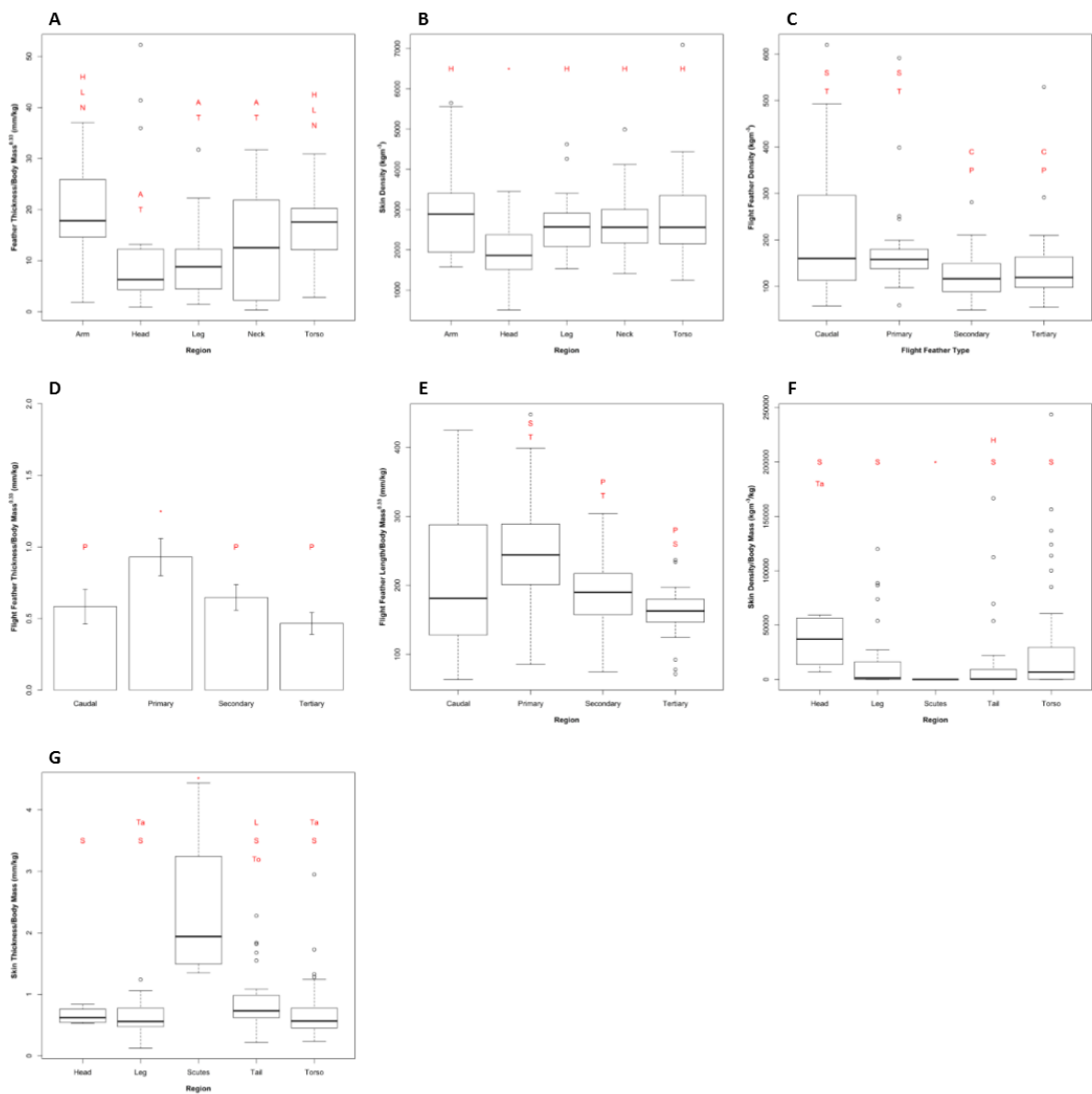
Supplementary Text 3.4.1: Graphs displaying first mass moment (FMM) data for the three extant non-avian sauropsid models (**A & B**: iguana, **C & D**: crocodile, **E & F**: alligator) in the crano-caudal (**A, C, E**) and dorso-ventral (**B, D, F**) directions. Contributions by different segment components are indicated by different colour portions of each bar, as per the figure legend.



Supplementary Text 3.4.2: Graphs displaying first mass moment (FMM) data for the maximum variants of three fossil models (**A & B: Coelophysis**, **C & D: Microraptor**, **E & F: Yixianornis**) in the cranio-caudal (**A, C, E**) and dorso-ventral (**B, D, F**) directions. Contributions by different segment components are indicated by different colour portions of each bar, as per the figure legend.



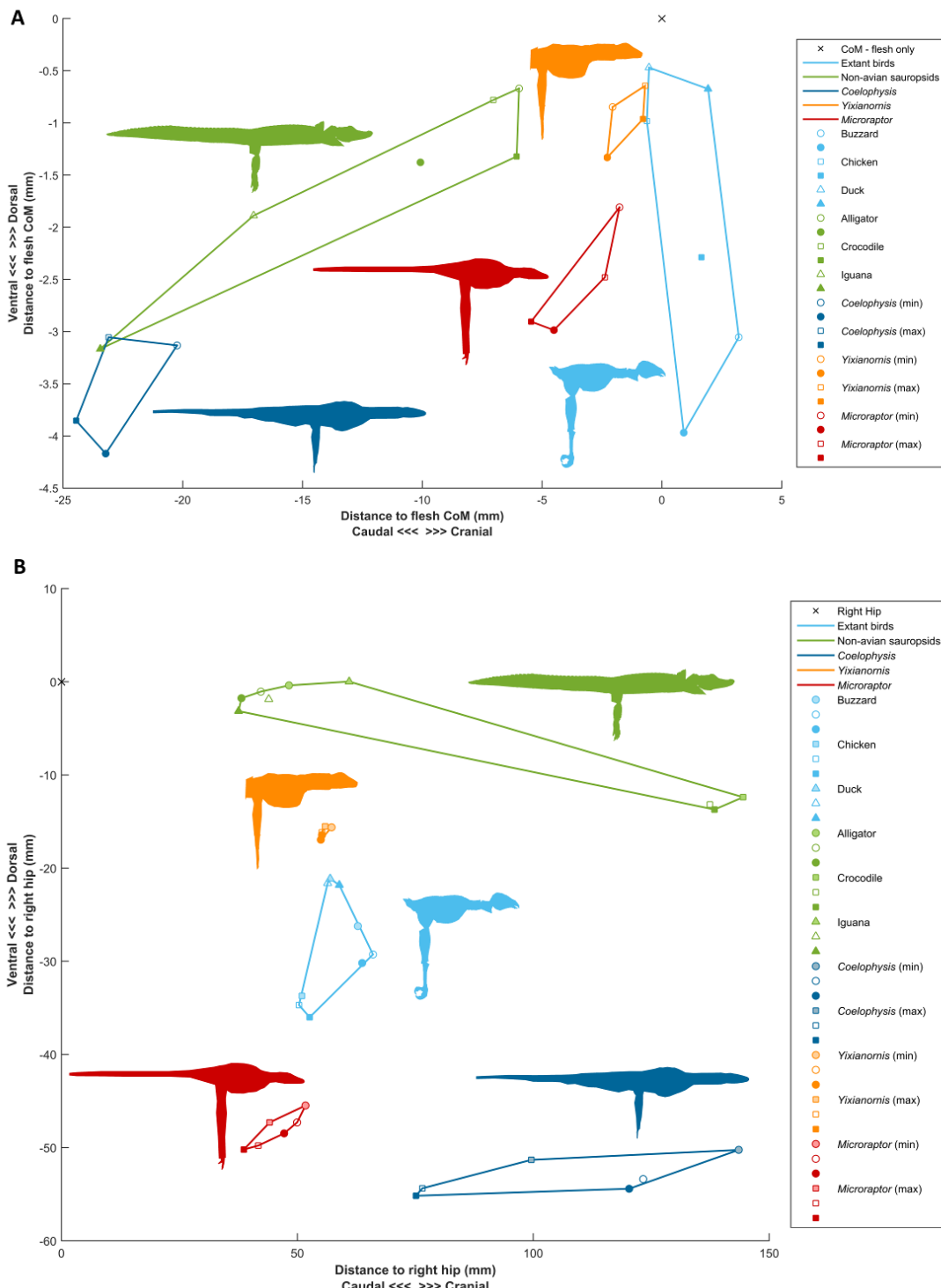
Supplementary Text 3.4.3: Graphs displaying first mass moment (FMM) data for three extant bird specimens (**A & B**: buzzard, **C & D**: chicken, **E & F**: duck) in the cranio-caudal (**A, C, E**) and dorso-ventral (**B, D, F**) directions. Contributions by different segment components are indicated by different colour portions of each bar, as per the figure legend.



Supplementary Figure 3.1: Graphs showing statistically significant differences between regions for each integument type modelled heterogeneously. **A:** general body feather thickness, **B:** bird skin density, **C:** flight feather density, **D:** flight feather thickness, **E:** flight feather length, **F:** scaly skin density, **G:** scaly skin thickness. Significant differences are indicated by text over each bar (where * indicates significant difference to all other groups, and letters indicate significant differences to another region - A: Arm, H: Head, L: Leg, N: Neck, S: Scutes, Ta: Tail, T/To: Torso; or differences to another flight feather type - C: Caudal, P: Primary, S: Secondary; T: Tertiary). N = 155 feathered skin samples from 27 specimens; 140 flight feathers from 22 specimens; 152 scaly skin samples from 22 specimens.

*For box and whisker plots (**A-C, E-G**): black line represents median value, box represents interquartile range, the whiskers mark the maximum and minimum values within 1.5 interquartile ranges of the box extremes and any values outside this range are displayed as points.*

*For bar charts (**D**): the mean value is plotted, with 95% confidence limits displayed as error bars.*



Supplementary Figure 3.2: Raw CoM positions for all models, with convex hulls around specimen from the same groups. Displayed **A**: relative to flesh CoM (displayed as 'x', set to 0 0 0 in xyz coordinates for all models) and **B**: relative to right hip (displayed as 'x', at 0 0 0 in xyz coordinates for all models). Different colours represent different taxa as per the legend. Lightly shaded icons: flesh only models; hollow icons: flesh and air cavities; filled icons: flesh, air cavities and integument.

Supplementary Table 3.1: Data on feather mass as proportion of whole body mass in birds, adapted from (Brassey and Sellers, 2014). Values presented from the literature, and from specimens sampled here.

Order	Species	Common name	Feather mass (% body mass)	Source	Notes
STRUTHIONIFORMES	<i>Struthio camelus</i>	Ostrich	1.5%	Brand, 2010	Total body feathers
	<i>Struthio camelus</i>	Ostrich	1.7%	Brand, 2010	Total body feathers
	<i>Struthio camelus</i>	Ostrich	1.9%	Morris, 1995	Feather mass
RHEIFORMES	<i>Rhea americana</i>	Greater rhea	1.5%	Sales, 1997	Feather mass
	<i>Rhea pennata</i>	Lesser rhea	1.8%	Sales, 1997	Feather mass
CASUARIIFORMES	<i>Dromaius novaehollandiae</i>	Emu	1.7%	Sales, 1999	Feather mass
	<i>Dromaius novaehollandiae</i>	Emu	1.1%	Naveena, 2013	Feather mass
	<i>Apteryx sp.</i>	Kiwi	4.7%	Reid, 1975	Total feather mass
APTERYGIFORMES	<i>Apteryx sp.</i>	Kiwi	6.8%	Reid, 1975	Total feather mass
	<i>Aythya fuligula</i>	Tufted duck	4.8%	Daan, 1990	Dry total feather mass
	<i>Anas platyrhynchos</i>	Mallard duck	6.4%	Daan, 1990	Dry total feather mass
	<i>Anas platyrhynchos</i>	Mallard duck	6.1%	Hopps, 2002	Total feather mass
	<i>Anas platyrhynchos</i>	Mallard duck	6.0%	Hopps, 2002	Total feather mass
	<i>Anas platyrhynchos domesticus</i>	Miniature Silver Appleyard Duck	7.1%	This study	Total feather mass
	<i>Branta bernicla</i>	Brant goose	8.0%	Daan, 1990	Dry total feather mass
	<i>Branta bernicla</i>	Brant Goose	12.7%	This study	Total feather mass

Order	Species	Common name	Feather mass (% body mass)	Source	Notes
	<i>Aix sponsa</i>	Wood duck	5.4%	Hopps, 2002	Total feather mass
	<i>Aix sponsa</i>	Wood duck	5.2%	Hopps, 2002	Total feather mass
	<i>Anas strepera</i>	Gadwall	6.5%	Hopps, 2002	Total feather mass
	<i>Anas strepera</i>	Gadwall	6.5%	Hopps, 2002	Total feather mass
	<i>Anas americana</i>	American wigeon	5.5%	Hopps, 2002	Total feather mass
	<i>Anas americana</i>	American wigeon	5.9%	Hopps, 2002	Total feather mass
	<i>Anas discors</i>	Blue-winged teal	5.8%	Hopps, 2002	Total feather mass
	<i>Anas discors</i>	Blue-winged teal	5.7%	Hopps, 2002	Total feather mass
	<i>Anas carolinensis</i>	Green-winged teal	6.9%	Hopps, 2002	Total feather mass
	<i>Anas carolinensis</i>	Green-winged teal	5.1%	Hopps, 2002	Total feather mass
	<i>Aythya americana</i>	Redhead	5.5%	Hopps, 2002	Total feather mass
	<i>Aythya americana</i>	Redhead	5.0%	Hopps, 2002	Total feather mass
	<i>Aythya collaris</i>	Ring-necked duck	5.4%	Hopps, 2002	Total feather mass
	<i>Aythya collaris</i>	Ring-necked duck	4.7%	Hopps, 2002	Total feather mass
	<i>Aythya affinis</i>	Lesser scaup	4.5%	Hopps, 2002	Total feather mass
	<i>Aythya affinis</i>	Lesser scaup	4.2%	Hopps, 2002	Total feather mass
	<i>Lophodytes cucullatus</i>	Hooded merganser	5.2%	Hopps, 2002	Total feather mass
	<i>Lophodytes cucullatus</i>	Hooded merganser	5.0%	Hopps, 2002	Total feather mass
	<i>Cygnus columbianus</i>	Whistling Swan	10.1%	Ammann, 1937	Contour feather mass
GALLIFORMES	<i>Meleagris gallopavo</i>	Wild turkey	5.6%	Schorger, 1996	Total feather mass
	<i>Gallus gallus domesticus</i>	Broiler chicken	6.0%	Leeson, 2007	Total feather mass
	<i>Gallus gallus domesticus</i>	Broiler chicken	5.8%	Leeson, 2007	Total feather mass
	<i>Gallus gallus domesticus</i>	Athens Canadian Random Bred Chicken	8.7%	Collins, 2014	
	<i>Gallus gallus domesticus</i>	Cobb 500 Broiler chicken	3.5%	Collins, 2014	

Order	Species	Common name	Feather mass (% body mass)	Source	Notes
COLUMBIIFORMES	<i>Coturnix coturnix</i>	Common quail	4.7%	Daan, 1990	Dry total feather mass
	<i>Callipepla californica</i>	California Quail	4.3%	This study	Total feather mass
	<i>Rollulus rouloul</i>	Crested Partridge	11.3%	This study	Total feather mass
APODIFORMES	<i>Streptopelia decaocto</i>	Eurasian collared dove	9.6%	Daan, 1990	Dry total feather mass
	<i>Streptopelia risoria</i>	Barbary Dove	10.0%	This study	Total feather mass
	<i>Zenaida macroura</i>	Mourning dove	7.7%	Wetmore, 1936	Contour feather mass
APODIFORMES	<i>Archilochus colubris</i>	Ruby-throated hummingbird	7.1%	Wetmore, 1936	Contour feather mass
CAPRIMULGIFORMES	<i>Chordeiles minor</i>	Eastern nighthawk	8.1%	Wetmore, 1936	Contour feather mass
	<i>Chordeiles minor</i>	Eastern nighthawk	8.4%	Wetmore, 1936	Contour feather mass
GRUIFORMES	<i>Gallinula chloropus sandvicensis</i>	Hawaiian moorhen	3.6%	DesRochers, 2010	Total feather mass
	<i>Gallinula chloropus sandvicensis</i>	Hawaiian moorhen	3.8%	DesRochers, 2010	Total feather mass
	<i>Fulica atra</i>	Eurasian coot	7.1%	Daan, 1990	Dry total feather mass
CHARADRIIFORMES	<i>Arenaria interpres</i>	Ruddy turnstone	7.4%	Daan, 1990	Dry total feather mass
	<i>Pluvialis apricarius</i>	Golden plover	4.7%	Daan, 1990	Dry total feather mass
	<i>Limosa lapponica</i>	Bar-tailed godwit	4.5%	Daan, 1990	Dry total feather mass
	<i>Larus ridibundus</i>	Black-headed gull	10.1%	Daan, 1990	Dry total feather mass
	<i>Haematopus ostralegus</i>	Eurasian oystercatcher	8.8%	Daan, 1990	Dry total feather mass
	<i>Larus argentatus</i>	European herring gull	1.1%	Daan, 1990	Dry total feather mass
	<i>Calidris maritima</i>	Purple sandpiper	18.9%	Summers, 1992	Contour & flight feather mass

Order	Species	Common name	Feather mass (% body mass)	Source	Notes
ACCIPITRIFORMES	<i>Haliaeetus leucocephalus</i>	Bald eagle	16.6%	Brodkorb, 1955	Contour feather mass
	<i>Buteo buteo</i>	Buzzard			Total feather mass
CORACIIFORMES	<i>Unknown</i>	Kingfisher	34.9% *	This study	Total feather mass
FALCONIFORMES	<i>Falco tinnunculus</i>	Common kestral	10.4%	Daan, 1990	Dry total feather mass
PSITTACIFORMES	<i>Melopsittacus undulatus</i>	Budgerigar	10.0%	Wolf, 2003	Total feather mass
	<i>Agapornis sp.</i>	Lovebird	7.4%	Wolf, 2003	Total feather mass
	<i>Eclectus roratus</i>	Eclectus Parrot	11.2%	This study	Total feather mass
	<i>Psittacus erithacus</i>	African Grey	9.2%	This study	Total feather mass
	<i>Ara ararauna</i>	Blue and Yellow Macaw	10.2%	This study	Total feather mass
PASSERIFORMES	<i>Tyrannus tyrannus</i>	Eastern kingbird	7.5%	Wetmore, 1936	Contour feather mass
	<i>Myiarchus crinitus</i>	Northern crested flycatcher	7.4%	Wetmore, 1936	Contour feather mass
	<i>Empidonax virescens</i>	Acadian flycatcher	8.8%	Wetmore, 1936	Contour feather mass
	<i>Contopus virens</i>	Eastern wood pewee	7.5%	Wetmore, 1936	Contour feather mass
	<i>Stelgidopteryx sp.</i>	Rough-winged swallow	5.8%	Wetmore, 1936	Contour feather mass
	<i>Hirundo rustica</i>	Barn swallow	8.0%	Wetmore, 1936	Contour feather mass
	<i>Cyanocitta cristata</i>	Northern blue jay	7.0%	Wetmore, 1936	Contour feather mass
	<i>Pica pica</i>	Eurasian magpie	8.5%	Daan, 1990	Dry total feather mass
	<i>Pica pica</i>	Magpie	9.2%	This study	Total feather mass
	<i>Corvus monedula</i>	Western jackdaw	9.1%	Daan, 1990	Dry total feather mass

Order	Species	Common name	Feather mass (% body mass)	Source	Notes
	<i>Corvus corone</i>	Carriion crow	7.6%	Daan, 1990	Dry total feather mass
	<i>Poecile carolinensis</i>	Carolina chickadee	5.5%	Wetmore, 1936	Contour feather mass
	<i>Poecile carolinensis</i>	Carolina chickadee	8.0%	Wetmore, 1936	Contour feather mass
	<i>Poecile carolinensis</i>	Carolina chickadee	7.2%	Wetmore, 1936	Contour feather mass
	<i>Parus major</i>	Great tit	9.7%	Daan, 1990	Dry total feather mass
	<i>Poecile gambeli</i>	Mountain chickadee	2.5%	Cooper, 2002	Contour feather mass
	<i>Poecile gambeli</i>	Mountain chickadee	5.3%	Cooper, 2002	Contour feather mass
	<i>Baeolophus ridgwayi</i>	Juniper titmouse	2.7%	Cooper, 2002	Contour feather mass
	<i>Baeolophus ridgwayi</i>	Juniper titmouse	4.0%	Cooper, 2002	Contour feather mass
	<i>Certhia americana</i>	Brown creeper	7.1%	Wetmore, 1936	Contour feather mass
	<i>Certhia americana</i>	Brown creeper	7.1%	Wetmore, 1936	Contour feather mass
	<i>Troglodytes aedon</i>	Eastern house wren	4.5%	Wetmore, 1936	Contour feather mass
	<i>Troglodytes aedon</i>	Eastern house wren	6.1%	Wetmore, 1936	Contour feather mass
	<i>Thryothorus ludovicianus</i>	Carolina wren	3.3%	Wetmore, 1936	Contour feather mass
	<i>Cistothorus palustris</i>	Long-billed marsh wren	4.4%	Wetmore, 1936	Contour feather mass
	<i>Mimus polyglottos</i>	Eastern Mockingbird	7.0%	Wetmore, 1936	Contour feather mass
	<i>Dumetella carolinensis</i>	Catbird	6.5%	Wetmore, 1936	Contour feather mass
	<i>Toxostoma rufum</i>	Brown thrasher	4.6%	Wetmore, 1936	Contour feather mass
	<i>Hylocichla mustelina</i>	Wood thrush	5.3%	Wetmore, 1936	Contour feather mass
	<i>Catharus guttatus</i>	Eastern hermit thrush	7.7%	Wetmore, 1936	Contour feather mass
	<i>Catharus guttatus</i>	Eastern hermit thrush	7.3%	Wetmore, 1936	Contour feather mass
	<i>Catharus guttatus</i>	Eastern hermit thrush	7.2%	Wetmore, 1936	Contour feather mass
	<i>Turdus merula</i>	Common blackbird	9.3%	Daan, 1990	Dry total feather mass
	<i>Regulus satrapa</i>	Eastern golden-crowned kinglet	12.1%	Wetmore, 1936	Contour feather mass
	<i>Regulus satrapa</i>	Eastern golden-crowned kinglet	10.9%	Wetmore, 1936	Contour feather mass

Order	Species	Common name	Feather mass (% body mass)	Source	Notes
	<i>Regulus satrapa</i>	Eastern golden-crowned kinglet	10.2%	Wetmore, 1936	Contour feather mass
	<i>Regulus calendula</i>	Eastern ruby-crowned kinglet	7.8%	Wetmore, 1936	Contour feather mass
	<i>Regulus calendula</i>	Eastern ruby-crowned kinglet	10.9%	Wetmore, 1936	Contour feather mass
	<i>Regulus calendula</i>	Eastern ruby-crowned kinglet	8.1%	Wetmore, 1936	Contour feather mass
	<i>Lanius ludovicianus</i>	Migrant shrike	6.1%	Wetmore, 1936	Contour feather mass
	<i>Vireo griseus</i>	White-eyed vireo	2.5%	Wetmore, 1936	Contour feather mass
	<i>Vireo griseus</i>	White-eyed vireo	4.1%	Wetmore, 1936	Contour feather mass
	<i>Vireo griseus</i>	White-eyed vireo	6.8%	Wetmore, 1936	Contour feather mass
	<i>Vireo griseus</i>	White-eyed vireo	7.3%	Wetmore, 1936	Contour feather mass
	<i>Vireo flavifrons</i>	Yellow-throated vireo	6.0%	Wetmore, 1936	Contour feather mass
	<i>Vireo olivaceus</i>	Red-eyed vireo	5.6%	Wetmore, 1936	Contour feather mass
	<i>Vireo olivaceus</i>	Red-eyed vireo	4.4%	Wetmore, 1936	Contour feather mass
	<i>Vireo olivaceus</i>	Red-eyed vireo	5.1%	Wetmore, 1936	Contour feather mass
	<i>Mniotilla varia</i>	Black and white warbler	4.4%	Wetmore, 1936	Contour feather mass
	<i>Oreothlypis peregrina</i>	Tennessee warbler	6.5%	Wetmore, 1936	Contour feather mass
	<i>Setophaga pityayumi</i>	Southern parula warbler	5.2%	Wetmore, 1936	Contour feather mass
	<i>Setophaga magnolia</i>	Magnolia warbler	2.1%	Wetmore, 1936	Contour feather mass
	<i>Setophaga magnolia</i>	Magnolia warbler	5.1%	Wetmore, 1936	Contour feather mass
	<i>Setophaga magnolia</i>	Magnolia warbler	6.7%	Wetmore, 1936	Contour feather mass
	<i>Setophaga caerulescens</i>	Black-throated blue warbler	5.6%	Wetmore, 1936	Contour feather mass
	<i>Setophaga caerulescens</i>	Black-throated blue warbler	6.1%	Wetmore, 1936	Contour feather mass
	<i>Setophaga virens</i>	Black-throated green warbler	6.5%	Wetmore, 1936	Contour feather mass
	<i>Setophaga fusca</i>	Blackburnian warbler	4.5%	Wetmore, 1936	Contour feather mass
	<i>Setophaga pensylvanica</i>	Chestnut-sided warbler	5.4%	Wetmore, 1936	Contour feather mass
	<i>Setophaga pensylvanica</i>	Chestnut-sided warbler	6.1%	Wetmore, 1936	Contour feather mass
	<i>Setophaga castanea</i>	Bay-breasted warbler	5.0%	Wetmore, 1936	Contour feather mass

Order	Species	Common name	Feather mass (% body mass)	Source	Notes
	<i>Setophaga castanea</i>	Black-poll warbler	6.8%	Wetmore, 1936	Contour feather mass
	<i>Setophaga pinus</i>	Northern pine warbler	7.9%	Wetmore, 1936	Contour feather mass
	<i>Seiurus aurocapilla</i>	Oven-bird	6.9%	Wetmore, 1936	Contour feather mass
	<i>Parkesia motacilla</i>	Louisiana water-thrush	5.1%	Wetmore, 1936	Contour feather mass
	<i>Geothlypis formosa</i>	Kentucky warbler	4.9%	Wetmore, 1936	Contour feather mass
	<i>Oporornis agilis</i>	Connecticut warbler	7.6%	Wetmore, 1936	Contour feather mass
	<i>Geothlypis trichas brachidactyla</i>	Northern yellowthroat	6.8%	Wetmore, 1936	Contour feather mass
	<i>Geothlypis trichas brachidactyla</i>	Northern yellowthroat	7.0%	Wetmore, 1936	Contour feather mass
	<i>Geothlypis trichas brachidactyla</i>	Northern yellowthroat	4.3%	Wetmore, 1936	Contour feather mass
	<i>Geothlypis trichas brachidactyla</i>	Northern yellowthroat	5.9%	Wetmore, 1936	Contour feather mass
	<i>Geothlypis trichas trichas</i>	Maryland yellowthroat	7.3%	Wetmore, 1936	Contour feather mass
	<i>Geothlypis trichas trichas</i>	Maryland yellowthroat	7.5%	Wetmore, 1936	Contour feather mass
	<i>Icteria virens</i>	Yellow-breasted chat	6.1%	Wetmore, 1936	Contour feather mass
	<i>Icteria virens</i>	Yellow-breasted chat	5.8%	Wetmore, 1936	Contour feather mass
	<i>Cardellina canadensis</i>	Canada warbler	7.4%	Wetmore, 1936	Contour feather mass
	<i>Cardellina canadensis</i>	Canada warbler	6.5%	Wetmore, 1936	Contour feather mass
	<i>Passer domesticus</i>	House sparrow	5.3%	Wetmore, 1936	Contour feather mass
	<i>Passer domesticus</i>	House sparrow	8.6%	Daan, 1990	Dry total feather mass
	<i>Agelaius phoeniceus</i>	Eastern red-wing	5.2%	Wetmore, 1936	Contour feather mass
	<i>Icterus spurius</i>	Orchard oriole	6.3%	Wetmore, 1936	Contour feather mass
	<i>Quiscalus quiscula</i>	Purple grackle	7.1%	Wetmore, 1936	Contour feather mass

Order	Species	Common name	Feather mass (% body mass)	Source	Notes
	<i>Molothrus ater</i>	Eastern cowbird	4.6%	Wetmore, 1936	Contour feather mass
	<i>Xanthocephalus xanthocephalus</i>	Yellow-headed Blackbird	8.8%	Ammann, 1937	Contour feather mass
	<i>Piranga olivacea</i>	Scarlet tanager	6.2%	Wetmore, 1936	Contour feather mass
	<i>Pheucticus ludovicianus</i>	Rose-breasted grosbeak	3.5%	Wetmore, 1936	Contour feather mass
	<i>Passerina cyanea</i>	Indigo bunting	5.9%	Wetmore, 1936	Contour feather mass
	<i>Passerina cyanea</i>	Indigo bunting	5.2%	Wetmore, 1936	Contour feather mass
	<i>Carduelis tristis</i>	Eastern goldfinch	6.0%	Wetmore, 1936	Contour feather mass
	<i>Spinus cucullata</i>	Red Siskin	8.8%	This study	Total feather mass
	<i>Unknown</i>	Canary	15.3%	This study	Total feather mass
	<i>Serinus canaria domestica</i>	Canary	13.9%	Wolf, 2003	Total feather mass
	<i>Pipilo erythrorththalmus</i>	Red-eyed towhee	7.4%	Wetmore, 1936	Contour feather mass
	<i>Passerculus sandwichensis</i>	Eastern Savannah sparrow	7.3%	Wetmore, 1936	Contour feather mass
	<i>Ammodramus savannarum</i>	Eastern Grasshopper sparrow	5.0%	Wetmore, 1936	Contour feather mass
	<i>Ammodramus savannarum</i>	Eastern Grasshopper sparrow	7.3%	Wetmore, 1936	Contour feather mass
	<i>Ammodramus savannarum</i>	Eastern Grasshopper sparrow	4.3%	Wetmore, 1936	Contour feather mass
	<i>Ammodramus henslowii</i>	Henslow's sparrow	6.2%	Wetmore, 1936	Contour feather mass
	<i>Ammodramus sp.</i>	Sharp-tailed sparrow	5.4%	Wetmore, 1936	Contour feather mass
	<i>Ammodramus maritimus</i>	Northern seaside sparrow	6.1%	Wetmore, 1936	Contour feather mass
	<i>Ammodramus maritimus</i>	Northern seaside sparrow	6.1%	Wetmore, 1936	Contour feather mass

Order	Species	Common name	Feather mass (% body mass)	Source	Notes
	<i>Pooecetes gramineus</i>	Vesper sparrow	5.6%	Wetmore, 1936	Contour feather mass
	<i>Pooecetes gramineus</i>	Vesper sparrow	4.9%	Wetmore, 1936	Contour feather mass
	<i>Spizella passerina</i>	Chipping sparrow	4.3%	Wetmore, 1936	Contour feather mass
	<i>Spizella passerina</i>	Chipping sparrow	6.3%	Wetmore, 1936	Contour feather mass
	<i>Spizella passerina</i>	Chipping sparrow	7.1%	Wetmore, 1936	Contour feather mass
	<i>Spizella passerina</i>	Chipping sparrow	4.6%	Wetmore, 1936	Contour feather mass
	<i>Spizella pusilla</i>	Field sparrow	8.3%	Wetmore, 1936	Contour feather mass
	<i>Spizella pusilla</i>	Field sparrow	5.2%	Wetmore, 1936	Contour feather mass
	<i>Zonotrichia albicollis</i>	White-throated sparrow	7.4%	Wetmore, 1936	Contour feather mass
	<i>Zonotrichia albicollis</i>	White-throated sparrow	6.1%	Wetmore, 1936	Contour feather mass
	<i>Melospiza melodia</i>	Song sparrow	5.3%	Wetmore, 1936	Contour feather mass
	<i>Junco hyemalis</i>	Dark-eyed junco	3.4%	Swanson, 1991	Dry total feather mass
	<i>Junco hyemalis</i>	Dark-eyed junco	4.1%	Swanson, 1991	Dry total feather mass
	<i>Poephila guttata</i>	Zebra finch	5.6%	Daan, 1990	Dry total feather mass
	<i>Lonchura striata</i>	White-rumped munia	3.8%	Daan, 1990	Dry total feather mass
	<i>Erithacus rubecula</i>	European robin	9.0%	Daan, 1990	Dry total feather mass
	<i>Saxicola torquata rubicula</i>	European stonechat	6.4%	Klaassen, 1995	Feather mass
	<i>Saxicola torquata axillaris</i>	East African stonechat	7.2%	Klaassen, 1995	Feather mass
	<i>Malurus cyaneus</i>	Superb fairy-wren	2.6%	Lill, 2006	Dry contour mass
	<i>Malurus cyaneus</i>	Superb fairy-wren	4.0%	Lill, 2006	Dry contour mass

* The value obtained by this study suggesting that 34.9% of the body mass of a kingfisher seems unreasonably high. It has been included here for completeness only, and is not believed to be biologically realistic.

Supplementary Table 3.2: Details on the phylogenetic and locomotor classifications applied to each species of bird in our integument mass property dataset.

Species	Common Name	Order	Locomotor group
<i>Numida meleagris</i>	Guineafowl	Galliformes	Burst adapted flight ^a
<i>Coturnix coturnix</i>	Quail	Galliformes	Burst adapted flight ^a
<i>Rollulus rouloul</i>	Crested Partridge	Galliformes	Burst adapted flight*
<i>Columba livia</i>	Pigeon	Columbiformes	Continuous flapping ^b
<i>Gallicolumba luzonica</i>	Bleeding Heart Pigeon	Columbiformes	Burst adapted flight*
<i>Gallinula chloropus</i>	Moorhen	Gruiformes	Continuous flapping ^a
<i>Milvus milvus</i>	Red Tailed Kite	Accipitriformes	Soaring ^c
<i>Buteo buteo</i>	Buzzard	Accipitriformes	Soaring ^c
<i>Strix aluco</i>	Tawny Owl	Strigiformes	Flap gliding ^a
<i>Falco peregrinus</i>	Peregrine Falcon	Falconiformes	Flap gliding ^b
<i>Psittacus erithacus</i>	African Grey Parrot	Psittaciformes	Continuous flapping ^a
<i>Ara ararauna</i>	Blue & Yellow Macaw	Psittaciformes	Continuous flapping ^a
<i>Cacatua moluccensis</i>	Cockatoo	Psittaciformes	Continuous flapping ^a
<i>Pica pica</i>	Magpie	Passeriformes	Continuous flapping ^b

* Locomotor style determined from online videos, or from data on similar species.

^a Locomotor style determined from Close & Rayfield (2012).

^b Locomotor style determined from Martin-Silverstone et al. (2015).

^c Locomotor style determined from Bruderer et al. (2010).

Supplementary Table 3.3: Details of all models included in this study. Measured body mass (kg) measured with scales for extant specimens, estimated body mass (kg) and 2D CoM position (mm) presented in the cranio-caudal, dorso-ventral dimensions) are as predicted by the final model (containing flesh, air cavities and integument). CoMs are expressed relative to the right hip at 0 0 0. Positive values indicate the cranial and dorsal directions respectively.

Model	Species	Measured body	Estimated body	CoM position
		mass	mass	
Iguana	<i>Iguana iguana</i>	1.102	0.99	38, -3
Crocodile	<i>Crocodylus johnstoni</i>	20.19	21.87	138, -14
Alligator	<i>Alligator mississippiensis</i>	0.60	0.65	38.2, -1.8
Coelophysis (Max)	<i>Coelophysis bauri</i>	-	25.04	75, -55
Coelophysis (Min)		-	13.90	120, -54
Microraptor (Max)	<i>Microraptor gui</i>	-	1.85	39, -50
Microraptor (Min)		-	1.16	47, -48
Yixianornis (Max)	<i>Yixianornis grabaui</i>	-	0.34	55, -16
Yixianornis (Min)		-	0.22	55, -17
Buzzard	<i>Buteo buteo</i>	0.69	0.68	64, -30
Chicken	<i>Gallus gallus domesticus</i>	1.08	1.13	-53, -36
Duck	<i>Anas platyrhynchos</i>	1.12	1.25	59, -22

Supplementary Table 3.4: Summary of integument properties applied to models.

Integument	Property	Homogeneous	Heterogeneous
General body feathers	Density	X	
	Thickness		X
Bird skin	Density		X
	Thickness	X	
Flight feathers	Density		X
	Thickness		X
	Length		X
Scaly skin	Density		X
	Thickness		X

Supplementary Table 3.5: Integument mass property data as applied to models, density (kgm^{-3}), thickness (mm), length (mm).

Integument	Property	Locations					
		All regions	Arm	Head	Leg	Neck	Torso & Tail
General body feathers	Density	65.3					
	Thickness		15.6	4.7	7.6	12.8	15.9
Bird skin	All regions		Arm	Head	Leg	Neck	Torso & Tail
	Density		2888.4	1998.9	2570.2	2703.5	2559.8
Flight feathers	Thickness	0.3					
	Primary		Secondary	Tertiary	Caudal		
Scaly skin	Density	158.1	116.6	119.4	160.2		
	Thickness	0.7	0.5	0.4	0.5		
	Length	184.6	127.5	108.3	185.9		
	Head		Limbs	Neck & Torso	Tail		
	Density	1242.0	1571.9	1671.8	1295.2		
	Thickness	0.6	0.7	0.8	1.0		

3.8. References

- ALEXANDER, D. E., GONG, E., MARTIN, L. D., BURNHAM, D. A. & FALK, A. R. 2010. Model tests of gliding with different hindwing configurations in the four-winged dromaeosaurid *Microraptor gui*. *Proceedings of the National Academy of Sciences of the United States of America*, 107, 2972-2976.
- ALEXANDER, R. M. 1985. Mechanics of posture and gait of some large dinosaurs. *Zoological Journal of the Linnean Society*, 83, 1-25.
- ALLEN, V., HUTCHINSON, J. R., BATES, K. T. & LI, Z. 2013. Linking the evolution of body shape and locomotor biomechanics in bird-line archosaurs. *Nature*, 497, 104-107.
- ALLEN, V., PAXTON, H. & HUTCHINSON, J. R. 2009. Variation in center of mass estimates for extant sauropsids and its importance for reconstructing inertial properties of extinct archosaurs. *Anatomical Record*, 292, 1442-1461.
- AMMANN, G. A. 1937. Number of Contour Feathers of *Cygnus* and *Xanthocephalus*. *The Auk*, 54, 201-2.
- BATES, K. T., MANNING, P. L., HODGETTS, D. & SELLERS, W. I. 2009. Estimating Mass Properties of Dinosaurs Using Laser Imaging and 3-D Computer Modelling. *PLoS ONE*, 4, 1-26.
- BRAND, T. S., JORDAAN, J. W., BHIYA, C. S. & AUCAMP, B. B. 2010. Effect of slaughter age and sex on the production output of South African Black ostriches. *British Poultry Science*, 51, 510-514.
- BRASSEY, C. A. & SELLERS, W. I. 2014. Scaling of convex hull volume to body mass in modern primates, non-primate mammals and birds. *PLoS ONE*, 9, 1-12.
- BRODKORB, P. 1955. Number of feathers and weights of various systems in a bald eagle. *The Wilson Bulletin*, 67, 142.
- BRUDERER, B., PETER, D., BOLDT, A. & LIECHTI, F. 2010. Wing-beat characteristics of birds recorded with tracking radar and cine camera. *Ibis*, 152, 272-291.
- CARRANO, M. T. & BIEWENER, A. A. 1999. Experimental alteration of limb posture in the chicken (*Gallus gallus*) and its bearing on the use of birds as analogs for dinosaur locomotion. *Journal of Morphology*, 240, 237-249.
- CHATTERJEE, S. & TEMPLIN, R. J. 2007. Biplane wing planform and flight performance of the feathered dinosaur *Microraptor gui*. *Proceedings of the National Academy of Sciences of the United States of America*, 104, 1576-1580.
- CHRISTIANSEN, P. & BONDE, N. 2002. Limb proportions and avian terrestrial locomotion. *Journal fur Ornithologie*, 143, 356-371.
- CLOSE, R. A. & RAYFIELD, E. J. 2012. Functional morphometric analysis of the furcula in Mesozoic birds. *PLoS ONE*, 7, e36664.

- COLLINS, K. E., KIEPPER, B. H., RITZ, C. W., MCLENDON, B. L. & WILSON, J. L. 2014. Growth, livability, feed consumption, and carcass composition of the Athens Canadian Random Bred 1955 meat-type chicken versus the 2012 high-yielding Cobb 500 broiler. *Poultry Science*, 93, 2953-2962.
- COOPER, S. 2002. Seasonal metabolic acclimatization in mountain chickadees and juniper titmice. *Physiological and Biochemical Zoology: Ecological and Evolutionary Approaches*, 75, 386-395.
- DAAN, S., MASMAN, D. & GROENEWOLD, A. 1990. Avian basal metabolic rates: their association with body composition and energy expenditure in nature. *American Journal of Physiology: Regulatory, Integrative & Comparative Physiology*, 28, R333.
- DESROCHERS, D. W., SILBERNAGLE, M. D., NADIG, A. & REED, J. M. 2010. Body size, growth, and feather mass of the endangered Hawaiian moorhen (*Gallinula chloropus sandvicensis*). *Pacific Science*, 64, 327-333.
- DIAL, K. P. 2003. Wing-assisted incline running and the evolution of flight. *Science*, 299, 402-404.
- DYKE, G., PALMER, C., NAISH, D., GANAPATHISUBRAMANI, B., DE KAT, R. & VAN DER KINDERE, J. 2013. Aerodynamic performance of the feathered dinosaur *Microraptor* and the evolution of feathered flight. *Nature Communications*, 4, 1-9.
- GATESY, S. M. 1990. Caudofemoral musculature and the evolution of theropod locomotion. *Paleobiology*, 16, 170-186.
- GATESY, S. M. & BIEWENER, A. A. 1991. Bipedal locomotion: effects of speed, size and limb posture in birds and humans. *Journal of Zoology*, 224, 127-147.
- GATESY, S. M. & DIAL, K. P. 1996. Locomotor modules and the evolution of avian flight. *Evolution*, 50, 331-340.
- GATESY, S. M. & MIDDLETON, K. M. 1997. Bipedalism, flight, and the evolution of theropod locomotor diversity. *Journal of Vertebrate Paleontology*, 17, 308-329.
- HENDERSON, D. M. 1999. Estimating the masses and centers of mass of extinct animals by 3-D mathematical slicing. *Paleobiology*, 25, 88-106.
- HENDERSON, D. M. 2004. Tipsy punters: Sauropod dinosaur pneumaticity, buoyancy and aquatic habits. *Proceedings of the Royal Society B: Biological Sciences*, 271, S180-S183.
- HENDERSON, D. M. 2018. A buoyancy, balance and stability challenge to the hypothesis of a semi-aquatic Spinosaurus Stromer, 1915 (Dinosauria: Theropoda). *PeerJ*, 6, e5409.
- HOPPS, E. C. 2002. Information on waterfowl feather characteristics. *Transactions of the Illinois State Academy of Science*, 95, 229-237.

- HUTCHINSON, J. R., NG-THOW-HING, V. & ANDERSON, F. C. 2007. A 3D interactive method for estimating body segmental parameters in animals: Application to the turning and running performance of *Tyrannosaurus rex*. *Journal of Theoretical Biology*, 246, 660-680.
- JONES, T. D., FARLOW, J. O., RUBEN, J. A., HENDERSON, D. M. & HILLENius, W. J. 2000. Cursoriality in bipedal archosaurs. *Nature*, 406, 716-718.
- KLAASSEN, M. 1995. Moult and basal metabolic costs in males of two subspecies of stonechats: the European *Saxicola torquata rubicula* and the East African *S. t. axillaris*. *Oecologia*, 104, 424-432.
- KOEHL, M. A. R., EVANGELISTA, D. & YANG, K. 2011. Using physical models to study the gliding performance of extinct animals. *Integrative And Comparative Biology*, 51, 1002-1018.
- LEESON, S. & WALSH, T. 2007. Feathering in commercial poultry I. Feather growth and composition. *World's Poultry Science Journal*, 60, 42-51.
- LILL, A., BOX, J. & BALDWIN, J. 2006. Do metabolism and contour plumage insulation vary in response to seasonal energy bottlenecks in superb fairy-wrens? *Australian Journal of Zoology*, 54, 23-30.
- LINDHE NORBERG, U. M. 2002. Structure, form, and function of flight in engineering and the living world. *Journal of Morphology*, 252, 52-81.
- LONGRICH, N. R., VINther, J., MENG, Q., LI, Q. & RUSSELL, A. P. 2012. Primitive wing feather arrangement in *Archaeopteryx lithographica* and *Anchiornis huxleyi*. *Current Biology*, 22, 2262-2267.
- MACAULAY, S., HUTCHINSON, J. R. & BATES, K. T. 2017. A quantitative evaluation of physical and digital approaches to centre of mass estimation. *Journal of Anatomy*, 231, 758-775.
- MAIDMENT, S. C. R., HENDERSON, D. M. & BARRETT, P. M. 2014. What drove reversions to quadrupedality in ornithischian dinosaurs? Testing hypotheses using centre of mass modelling. *Naturwissenschaften*, 101, 989-1001.
- MARTIN-SILVERSTONE, E., VINCZE, O., MCCANN, R., JONSSON, C. H. W., PALMER, C., KAISER, G. & DYKE, G. 2015. Exploring the relationship between skeletal mass and total body mass in birds. *PLoS ONE*, 10, e0141794.
- MCGOWAN, C. 1979. Selection Pressure for High Body Temperatures: Implications for Dinosaurs. *Paleobiology*, 5, 285-295.
- MORRIS, C. A., HARRIS, S. D., MAY, S. G., JACKSON, T. C., HALE, D. S., MILLER, R. K., KEETON, J. T., ACUFF, G. R., LUCIA, L. M. & SAVELL, J. W. 1995. Ostrich slaughter and fabrication: 1. Slaughter yields of carcasses and effects of electrical stimulation on post-mortem pH. *Poultry science*, 74, 1683-1687.

- NAVEENA, B. M., SEN, A. R., MUTHUKUMAR, M., GIRISH, P. S., PRAVEEN KUMAR, Y. & KIRAN, M. 2013. Carcass characteristics, composition, physico-chemical, microbial and sensory quality of emu meat. *British Poultry Science*, 54, 329-336.
- NUDDS, R. L. & DYKE, G. J. 2010. Narrow primary feather rachises in *Confuciusornis* and *Archaeopteryx* suggest poor flight ability. *Science*, 328, 887-889.
- OSTROM, J. H. 1974. *Archaeopteryx* and the origin of flight. *Quarterly Review of Biology*, 49, 27-47.
- PADIAN, K. & CHIAPPE, L. M. 1998. The origin and early evolution of birds. *Biological Reviews of the Cambridge Philosophical Society*, 73, 1-42.
- REID, B. & WILLIAMS, G. R. 1975. The Kiwi. In: KUSCHEL, G. (ed.) *Biogeography and Ecology in New Zealand*. Dordrecht: Springer Netherlands.
- REILLY, S. M., WILLEY, J. S., BIKNEVICIUS, A. R. & BLOB, R. W. 2005. Hindlimb function in the alligator: Integrating movements, motor patterns, ground reaction forces and bone strain of terrestrial locomotion. *Journal of Experimental Biology*, 208, 993-1009.
- SALES, J., HORBAÑCZUK, J., DINGLE, J., COLEMAN, R. & SENSIK, S. 1999. Carcase characteristics of emus (*Dromaius novaehollandiae*). *British Poultry Science*, 40, 145-147.
- SALES, J., NAVARRO, J. L., BELLIS, L., MANERO, A., LIZURUME, M. & MARTELLA, M. B. 1997. Carcase and component yields of rheas. *British Poultry Science*, 38, 378-380.
- SCHORGER, A. W. 1966. *The Wild Turkey. Its History and Domestication.*, Norman, University of Oklahoma Press.
- SELLERS, W. I., POND, S. B., BRASSEY, C. A., MANNING, P. L. & BATES, K. T. 2017. Investigating the running abilities of *Tyrannosaurus rex* using stress-constrained multibody dynamic analysis. *PeerJ*, 5, e3420.
- SUMMERS, R. W., UNDERHILL, L. G., NICOLL, M., RAE, R. & PIERSMA, T. 1992. Seasonal, size- and age-related patterns in body-mass and composition of purple sandpipers *Calidris maritima* in Britain. *Ibis*, 134, 346-354.
- SWANSON, D. L. 1991. Seasonal adjustments in metabolism and insulation in the dark-eyed junco. *Condor*, 538-545.
- TAYLOR, G. K. & THOMAS, A. L. R. 2002. Animal flight dynamics II. Longitudinal stability in flapping flight. *Journal of Theoretical Biology*, 214, 351-370.
- THOMAS, A. L. R. & TAYLOR, G. K. 2001. Animal flight dynamics I. Stability in gliding flight. *Journal of Theoretical Biology*, 212, 399-424.
- WANG, X. & CLARKE, J. A. 2015. The evolution of avian wing shape and previously unrecognized trends in covert feathering. *Proceedings of the Royal Society B: Biological Sciences*, 282.

- WANG, X., NUDDS, R. L. & DYKE, G. J. 2011. The primary feather lengths of early birds with respect to avian wing shape evolution. *Journal of Evolutionary Biology*, 24, 1226-1231.
- WETMORE, A. 1936. The number of contour feathers in passeriform and related birds. *The Auk*, 53, 159-169.
- WOLF, P., RABEHL, N. & KAMPHUES, J. 2003. Investigations on feathering, feather growth and potential influences of nutrient supply on feathers' regrowth in small pet birds (canaries, budgerigars and lovebirds). *Journal of Animal Physiology and Animal Nutrition*, 87, 134-141.
- XU, X., ZHOU, Z., WANG, X., KUANG, X., ZHANG, F. & DU, X. 2003. Four-winged dinosaurs from China. *Nature*, 421, 335-340.

CHAPTER 4 - BODY SHAPE AND THE EVOLUTION OF LOCOMOTOR DIVERSITY IN BIRDS

I am currently developing this chapter for publication. The version of this chapter presented in this thesis has been completed with the following collaborators: K.T. Bates, J.R. Hutchinson and E.R. Schachner.

MACAULAY, S., SCHACHNER, E. R., HUTCHINSON, J. R. & BATES, K. T. (In preparation).

Body shape and the evolution of locomotor diversity in birds.

Collaborator contributions: SM and KTB conceived the project. SM, KTB, JRH and ERS provided specimens and collected data. SM processed, analysed and interpreted data, and wrote the chapter.

4.1. Abstract

Birds are one of the most taxonomically and ecologically diverse groups of vertebrates in modern ecosystems. This diversity places a broad range of mechanical demands on the avian locomotor system. It is hypothesised here that these varied demands are reflected by gross morphological adaptations in body shape, which would be detectable through differences in whole body centre of mass position. While previous work has suggested that the evolution of avian flight was intrinsically linked to changes in mass distribution, no study has investigated links between whole body centre of mass and different locomotor ecologies in living birds. Here, I test the hypothesis that whole body centre of mass position will be strongly correlated with locomotor type in birds. I analyse a range of validated computer models of body proportions from species covering 27 avian families and a range of body sizes and locomotor modes. This reveals insignificant differences between whole body centre of mass position for birds using different locomotor strategies. Volant species, with locomotor behaviours dominated by the forelimbs, have more dorsally positioned centres of mass than their terrestrial counterparts, placing the centre of mass closer to the axis of the wings enabling more agile flight behaviours. These differences are determined to be driven mainly by differences in hindlimb morphologies in volant versus terrestrial birds. Significant variability was detected within the locomotor groups identified here, reflecting the considerable variability present within Aves.

4.2. Introduction

Aves is one of the most speciose vertebrate groups, containing almost 10,000 species (Jetz et al., 2012). Birds have diversified to fill a huge range of niches in ecosystems on every continent, from aquatic penguins and obligate terrestrial ostriches to arboreal turacos and almost entirely volant hummingbirds. This diversity is also evident in the huge size range of living birds spanning several orders of magnitude from the Bee Hummingbird at 2g to the Ostrich at >150kg (Blackburn and Gaston, 1994).

The evolutionary success of birds has been driven by their ability to adapt their morphology to satisfy the wide range of requirements necessary to occupy such a broad variety of niches (Kardong, 2012). Avian morphology is rooted in their initial diversification from theropod dinosaurs, when the ancestors of modern birds became one of only three tetrapod clades to develop powered flight (Kardong, 2012). This transition to aerial locomotion required a host of adaptations, including: the development of powerful flight muscles and forelimbs (Gatesy and Dial, 1996); the reduction of the tail (Gatesy, 1990); the evolution of a feathered integument (Ostrom, 1974); and the development of the head and neck complex (Kambic et al., 2017). For example, avian forelimbs have diversified from the ancestral condition in their osteology and myology, with further differences instigated by flight feathers. These specialisations have resulted in the broad range of wing shapes seen in modern birds, which are specialised for different types of locomotion (Rayner, 1988, Savile, 1957). The evolution of the head and neck complex was driven by the need for the head to be used as a surrogate hand for object manipulation, since the hyper-specialised forelimbs are no longer useful for that purpose (Krings et al., 2017). Further musculoskeletal specialisations in the hindlimbs (e.g. for high speed terrestrial locomotion, high degrees of arboreality, prey capture etc) and in the torso (e.g. expanded sternum to accommodate flight musculature) also indicate the evolutionary flexibility of avian musculoskeletal anatomy.

These key morphological changes occurring in the avian lineage combined to drastically alter centre of mass (CoM) position. A cranial shift in CoM occurs across the archosaur phylogeny towards crown Aves, largely due to the enlargement of the pectoral limb (Allen et al., 2013). Concurrently, birds shifted to a highly flexed hindlimb posture in order to facilitate bipedal, terrestrial locomotion (Gatesy, 1990, Gatesy and Dial, 1996). CoM is a key biomechanical parameter, which effectively summarises the whole body shape (i.e. mass distribution) of an organism. The morphology and body shape of birds has been heavily influenced by locomotor demands through evolutionary time. For example, this influence is evident from the variable investment in the muscular system across the body which has been identified in birds using forelimb versus hindlimb dominated locomotion (Heers and Dial, 2015). Given the changes in body shape observed during theropod evolution (Allen et al., 2013, Gatesy, 1990, Gatesy and Dial, 1996), and the disparity observed in muscle proportions in living birds (Heers and Dial, 2015), I therefore hypothesise that CoM will correlate closely with specific locomotor habits in modern birds.

The links between CoM and locomotion have been indirectly investigated in birds for their bipedal, terrestrial locomotion (e.g. Andrada et al., 2013, Gatesy, 1999, Nyakatura et al., 2012, Smith et al., 2010, Verstappen et al., 2000), but investigations directly exploring these links across a range of species are rare (e.g. Allen et al., 2013). Studies investigating associations between CoM and flight are even rarer (Henderson, 2010, Thomas and Taylor, 2001). Previous studies using volumetric modelling techniques have looked at small samples of birds, with insufficient numbers to draw any conclusive assessments about links between CoM and locomotor behaviours (Allen et al., 2013, Allen et al., 2009, Henderson, 2010, Macaulay et al., 2017). A knowledge of the links between CoM and locomotion in birds would facilitate a greater understanding, not only for living birds, but also for an appreciation of

these same behaviours in extinct species, including transitional avian fossils and pterosaurs. CoM has been used previously to quantify body shape changes in fossil taxa on the evolutionary pathway to birds (Allen et al., 2013). However, the current lack of quantified links between locomotor behaviours and CoM in living species limits the ability to draw any nuanced conclusions from CoM positions predicted for extinct taxa. Additionally, Allen et al. (2013) included only one extant bird species in their investigation, focussing primarily on a broad range of fossil taxa. This limited modern sample (consisting of a single junglefowl specimen) yielded an unexpected reversal in CoM position: having gradually shifted in a cranial direction along the bird lineage, CoM position seemingly undergoes a substantial, counter-intuitive caudal shift in the final node for modern birds (Figure 3 of Allen et al. (2013)). This study seeks to explore CoM position across Aves to place this finding in a wider context.

In this study, digital volumetric models are created for 27 species from 27 avian families, covering a range of body sizes (4g - 13kg) spanning five orders of magnitude and numerous locomotor types. These models are used to examine the following hypotheses:

- (1) CoM position will differ between birds using different locomotor modes, and will vary considerably across crown-group Aves.
- (2) The differences in whole body CoM positions between terrestrial and volant locomotor groups will be driven by differences in limb morphologies.
- (3) Species reliant on uncommon specialist behaviours (e.g. diving, extensive arboreality) will display highly adapted morphologies, which will be reflected in unique CoM positions.
- (4) The simplifications in the modelling process will not significantly influence the ability of models to accurately predict mass properties. Specifically, does (a) skin

closing technique or (b) selection and application of body density data affect the accuracy of predictions of CoM?

4.3. Methodology

4.3.1. Digital modelling: calculating body segment mass properties and whole body CoM

This study utilised computed tomography (CT) scans of 27 specimens from 27 different avian families (see Table 4.1 for details). Specimens were a mixture of captive and wild animals. Specimens, or whole body scans, were obtained from a variety of sources, including Twycross Zoo, The World Museum Liverpool, Emma Schachner, Bill Sellers and Charlotte Brassey. No specimens were killed for the purpose of this study. All specimens were scanned in medical grade CT scanners, at a variety of locations. Body masses were measured for each cadaver, with the exception of the hummingbird and ostrich. Various methods for body mass estimation (Brassey et al., 2013, Campione et al., 2014, Field et al., 2013) were used to generate estimates of whole body mass for these two specimens. Comparison of the results from these different methods (Brassey et al., 2013, Campione et al., 2014, Field et al., 2013) with published values for the species in question informed the selection of the most suitable value (see Supplementary Information 4.1).

The scan data were segmented using Avizo 7.1 (www.Avizo3D.com), in order to generate models of the skeletal material and a whole body skin outline. The resulting surface models were processed in Geomagic Studio 10 (www.geomagic.com). Any unwanted material was removed, and the skeletal and skin models of each specimen were split into segments (i.e. head, neck, torso, tail, upper arm, forearm, manus, thigh, shank, tarsometatarsus, toes). Wherever possible, skin segments were closed using tools within Geomagic. However, to

Table 4.1: Details on the 27 specimens modelled here, including measured whole body mass (kg) and locomotor category.

#	Common name	Species name	Order	Body mass	Locomotor category
1	Common ostrich	<i>Struthio camelus</i>	Struthiformes	12.3*	Terrestrial
2	Darwin's rhea	<i>Rhea pennata</i>	Rheiformes	7.85	Terrestrial
3	Andean tinamou	<i>Nothoprocta pentlandii</i>	Tinamiformes	0.417	Terrestrial
4	Emu	<i>Dromaius novaehollandiae</i>	Casuariiformes	13.15	Terrestrial
5	Mallard	<i>Anas platyrhynchos</i>	Anseriformes	1.12	Volant
6	Leghorn chicken	<i>Gallus gallus domesticus</i>	Galliformes	1.08	Terrestrial
7	Clark's grebe	<i>Aechmophorus clarkii</i>	Podicipediformes	1.257	Diving
8	Chilean flamingo	<i>Phoenicopterus chilensis</i>	Phoenicopteriformes	2.55	Volant
9	Wood pigeon	<i>Columba palumbus</i>	Columbiformes	0.56	Volant
10	Anna's hummingbird	<i>Calypte anna</i>	Apodiformes	0.005*	Volant
11	Violet turaco	<i>Musophaga violacea</i>	Musophagiformes	0.29	Terrestrial
12	Red-legged seriema	<i>Cariama cristata</i>	Gruiformes	2.165	Terrestrial
13	Black-throated diver	<i>Gavia arctica</i>	Gaviiformes	1.83	Diving
14	Humboldt penguin	<i>Spheniscus humboldti</i>	Sphenisciformes	4.01	Diving
15	Sooty shearwater	<i>Puffinus griseus</i>	Procellariiformes	0.505	Diving
16	Scarlet ibis	<i>Eudocimus ruber</i>	Ciconiiformes	0.6	Volant
17	Brown pelican	<i>Pelecanus occidentalis</i>	Pelicaniformes	2.81	Diving
18	Brandt's cormorant	<i>Phalacrocorax penicillatus</i>	Suliformes	1.18	Diving
19	Western gull	<i>Larus occidentalis</i>	Charadriiformes	0.987	Volant
20	Common buzzard	<i>Buteo buteo</i>	Accipitriformes	0.69	Volant
21	Turkey vulture	<i>Cathartes aura</i>	Cathartiformes	1.893	Volant

#	Common name	Species name	Order	Body mass	Locomotor category
22	Great horned owl	<i>Bubo virginianus</i>	Strigiformes	1.268	Volant
23	Common kingfisher	<i>Alcedo atthis</i>	Coraciiformes	0.0304	Diving
24	Great spotted woodpecker	<i>Dendrocopos major</i>	Piciformes	0.106	Volant
25	Merlin	<i>Falco columbarius</i>	Falconiformes	0.129	Volant
26	Orange-winged parrot	<i>Amazona amazonica</i>	Psittaciformes	0.375	Volant
27	Blackbird	<i>Turdus merula</i>	Passeriformes	0.092	Volant

* indicates species for which body mass was estimated, rather than measured directly.

achieve watertight shells for some skin segments, it was necessary to ‘wrap’ them in Materialise 3-matic (www.materialise.com/en/software/3-matic) or in extreme cases, produce alpha shapes or convex hulls using custom Matlab code (www.mathworks.com/products/matlab) (see Section 4.4.3.1 here for an assessment of the consequences of these alternatives, addressing hypothesis 4a). Closed skin segments were exported for each segment, along with the associated skeletal material.

The skeleton and skin objects for each segment were then imported into Maya (www.autodesk.co.uk/products/maya/overview). Here, joint centres were defined with reference to the skeletal material. Each specimen was then placed in a ‘standard posture’ (see Figure 4.1) so that the proximal and distal joint centres were aligned in the appropriate plane, to within 1°. The torso was orientated so that the hip joints were aligned in the sagittal and transverse planes, and the right hip and right glenohumeral joint were aligned in the dorsal plane. For all remaining segments, flexion-extension and abduction-adduction rotations were corrected so that: the head and neck were extended cranially, the forelimbs were outstretched laterally and the hindlimbs were extended ventrally. Additionally, long axis rotation (LAR) was corrected for all forelimb segments (placing the humeral crest, radius, and alula dorsally), hindlimb segments (with the exception of the digits), the head, and (if significant LAR was observed) the neck. This standard posture is not a biologically realistic representation of *in vivo* postures for any species studied here. However, this standardisation enables comparisons to be drawn between the body plans of species with drastically different morphologies (Allen et al., 2013, Bates et al., 2016, Hutchinson et al., 2011, Hutchinson et al., 2007). If necessary, the limbs were mirrored in the sagittal plane (defined as the midpoint between the two hip joints) so that each model had right fore- and hindlimbs. The closed skin outlines, now oriented in the standard posture, were then exported.

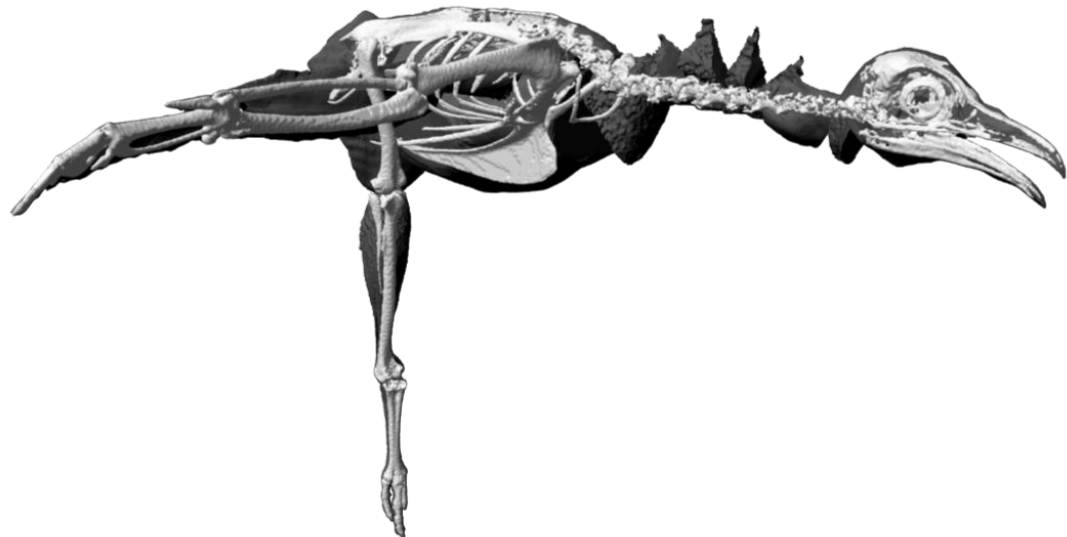


Figure 4.1: Tinamou model shown in the standardised posture used in this study, shown as skeletal material and associated skin outlines.

Segment CoMs and volumes were calculated using FormZ (www.formz.com). Segment masses were determined by multiplying segments' volumes by an appropriate value for density. Selection of a density value for volumetric models is therefore a key step, but has proven somewhat controversial, with many different values being selected throughout the literature. Generally, homogeneous density data is applied to models with air cavities accounted for separately (e.g. Allen et al., 2009, Bates et al., 2016, Macaulay et al., 2017), though some studies do represent density heterogeneously across all body segments (e.g. Henderson, 2004, Henderson, 2006). However, the current lack of whole body and segment specific density data for birds makes selection of appropriate values difficult. Here, I seek to address this issue, by applying the following to the bird models: (1) a homogeneous density of 1000kgm^{-3} and (2) segment specific density data derived here from five extant taxa of a range of locomotor, phylogenetic and ecological groups. This sensitivity analysis provides a range of plausible CoM values and enables a preliminary assessment of the impact density assignment has on whole body CoM position, testing hypothesis 4b.

It is common in volumetric studies to additionally segment the air cavities (from the torso only, or throughout the body) (e.g. Henderson, 1999, Hutchinson et al., 2007). In this way, the presence of these zero density regions can be explicitly accounted for in estimations of segment mass and CoM. However, in the scans of the specimens used here, the degree of air cavity preservation was highly variable. Additionally, the anatomy of air cavities varies substantially across Aves (Duncker, 1971, Maina, 2017), making accurate reconstructions of air cavity mass properties for each bird a significant challenge. Any attempt to include air cavities would therefore have incorporated an additional source of error, the effect of which would have been difficult to quantify. It was therefore decided that the most efficient way to standardise the models, in order to draw meaningful comparisons, was to avoid the explicit inclusion of any air cavities in models here. This study therefore models all body

segments as solid, ‘flesh only’ components. The presence of the weight-reducing air cavities is instead reflected by the lower density values which are applied to the relevant segments. Previous analyses (Allen et al., 2009, Macaulay et al., 2017) (but see Chapter 2, Section 2.4.3.3) have shown that different density values result in small differences in absolute CoM predictions, which are also small relative to the differences in CoM position observed between specimens.

Having defined segment mass properties, segment CoMs were combined to give a value for whole body CoM using following equation:

$$CoM_W = \frac{\Sigma(CoM_s * mass_s)}{\Sigma(mass_s)}$$

Equation 4.1

Where CoM_W is the centre of mass of the whole organism (or simply ‘CoM’ in the remainder of this study) and CoM_s and $mass_s$ refer to segment properties.

4.3.2. Density data

To address hypothesis 4b, I sought to produce new experimental measures of bird whole body and segment density. For this purpose, five whole specimens were used (see Table 4.2 for details), representing a range of avian orders, body plans and locomotor specialisations. These specimens were dissected into the following segments: head and neck; torso; forelimb (x2); and hindlimb (x2). The neck was split from the torso immediately cranial to the furcula. Each forelimb segment included the whole humerus, as well as the entirety of the deltoid muscle. The distal portions of the extrinsic forelimb muscles (e.g. pectoralis) were included, where they were contained within the upper arm. Both hindlimb segments included the

Table 4.2: Details on the five bird specimens for which segment specific densities were derived.

Common name	Species name	Order	Body mass (kg)
Mallard	<i>Anas platyrhynchos</i>	Anseriformes	1.36
Leghorn chicken	<i>Gallus gallus domesticus</i>	Galliformes	1.65
Wood pigeon	<i>Columba palumbus</i>	Columbiformes	0.58
Kestral	<i>Falco tinnunculus</i>	Falconiformes	0.126
Long tailed tit	<i>Aegithalos caudatus</i>	Passeriformes	0.007

whole femur, and all extrinsic hindlimb muscles (including all muscles attaching to the hip, and the caudofemoralis).

For each segment, mass was recorded using an Adam electronic balance ($\pm 0.01\text{g}$). These segments were then frozen and CT scanned, segmented in Avizo 7.1 to extract skin outlines and wrapped to produce closed outlines in Materialise 3-matic. Segment volume was determined in FormZ. Segment densities were calculated by dividing segment mass by segment volume.

Finally, as part of the modelling workflow, it was also possible to estimate whole body density for each specimen modelled here (27 birds). This whole body density was calculated from whole model volume (aka skin volume) and whole body mass physically measured in cadavers.

4.3.3. Statistical analyses

Specimens were grouped by main locomotor type (see Table 4.1 for details). Birds were deemed to be terrestrial if they primarily use their hindlimbs for locomotion. This group includes flightless ratites, as well as burst flyers (tinamou, chicken, seriema), and the predominately arboreal turaco. Birds that frequently utilise diving behaviours with complete submersion were classified as ‘divers’. Though it should be noted that all of these birds also engage in flying behaviours, with the exception of the flightless penguin. The remaining birds use flight as their primary locomotor style. Differences between the CoMs (normalised by whole body mass^{0.33}) of birds in these different locomotor groups were assessed using ANOVA, and Tukey’s post-hoc test where necessary, in R Studio (www.rstudio.com).

CoM position and locomotor mode are both linked to phylogeny. The trends observed for raw CoM data are therefore potentially influenced by phylogenetic signals. To get a true representation of differences in body plan, the interrelated nature of the data was accounted for. A phylogenetic tree for the 27 species used here was downloaded from BirdTree.org, using the Hackett backbone, based on Jetz et al. (2012) (see Figure 4.2). The tree, along with data on CoM positions and specimen locomotor categories were imported into R Studio. Differences between groups were then assessed using phylogenetic generalized least squares (PGLS) to account for phylogenetic relationships within the dataset.

To address hypothesis 2, correlations between various segment mass properties and whole body CoM were assessed. The segment mass properties investigated here were: segment mass, segment CoM and segment first mass moments (FMMs). FMMs were calculated for the cranio-caudal and dorso-ventral directions by the following equation:

$$FMM = (CoM_{whole\ body} - CoM_{segment}) * mass_{segment}$$

Equation 4.2

A Spearman's rank test was then performed in R Studio, to assess the relative influence of these various mass properties on whole body CoM.

4.4. Results

4.4.1. *CoM position across Aves*

4.4.1.1. *Does CoM correlate with locomotor style?*

The terrestrial group generally displayed more caudal CoM positions relative to the volant group (Figure 4.3). However, marked variation was present between specimens. The turaco lay within, and the tinamou slightly outside, the volant group (Figure 4.3). Meanwhile, the

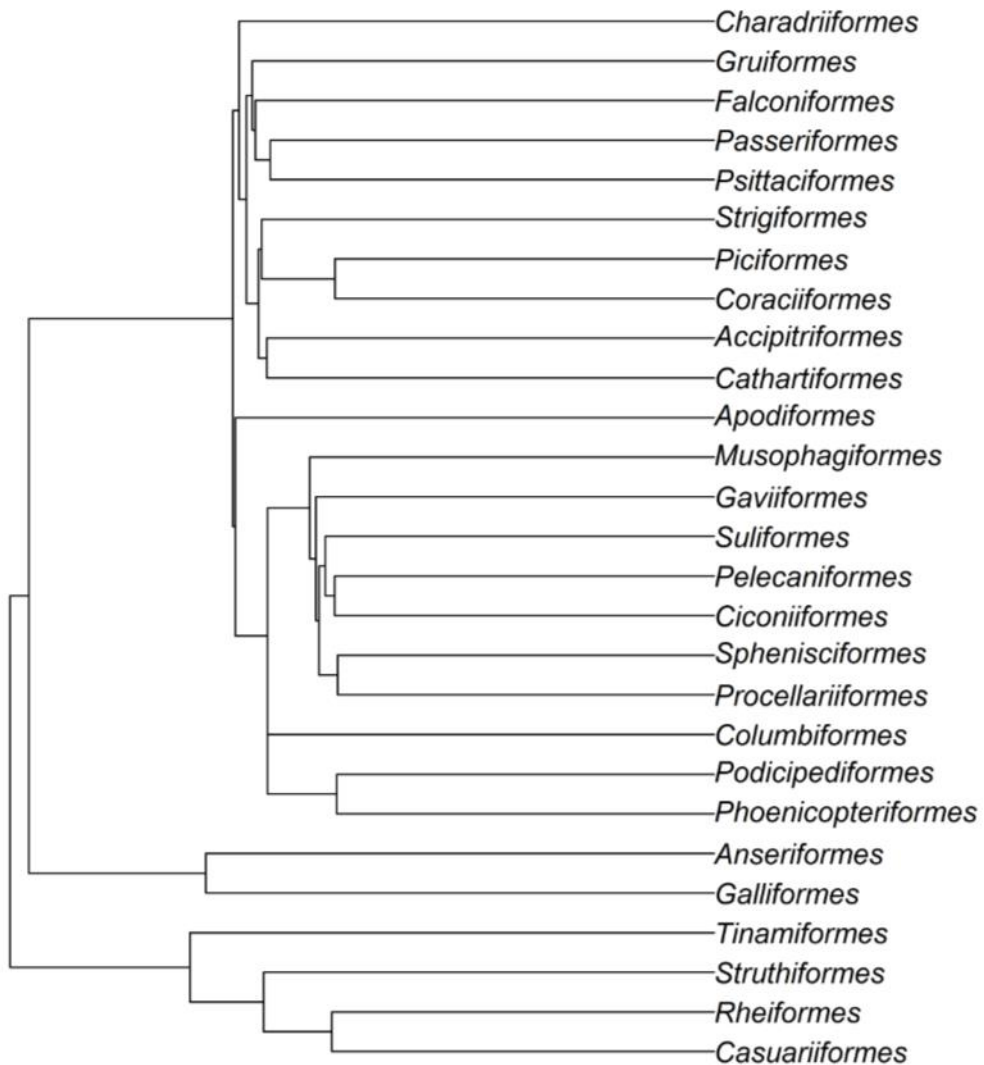


Figure 4.2: Phylogeny representing the 27 specimens used in this study, labelled with the names of their respective Orders. Based on Jetz et al. (2012).

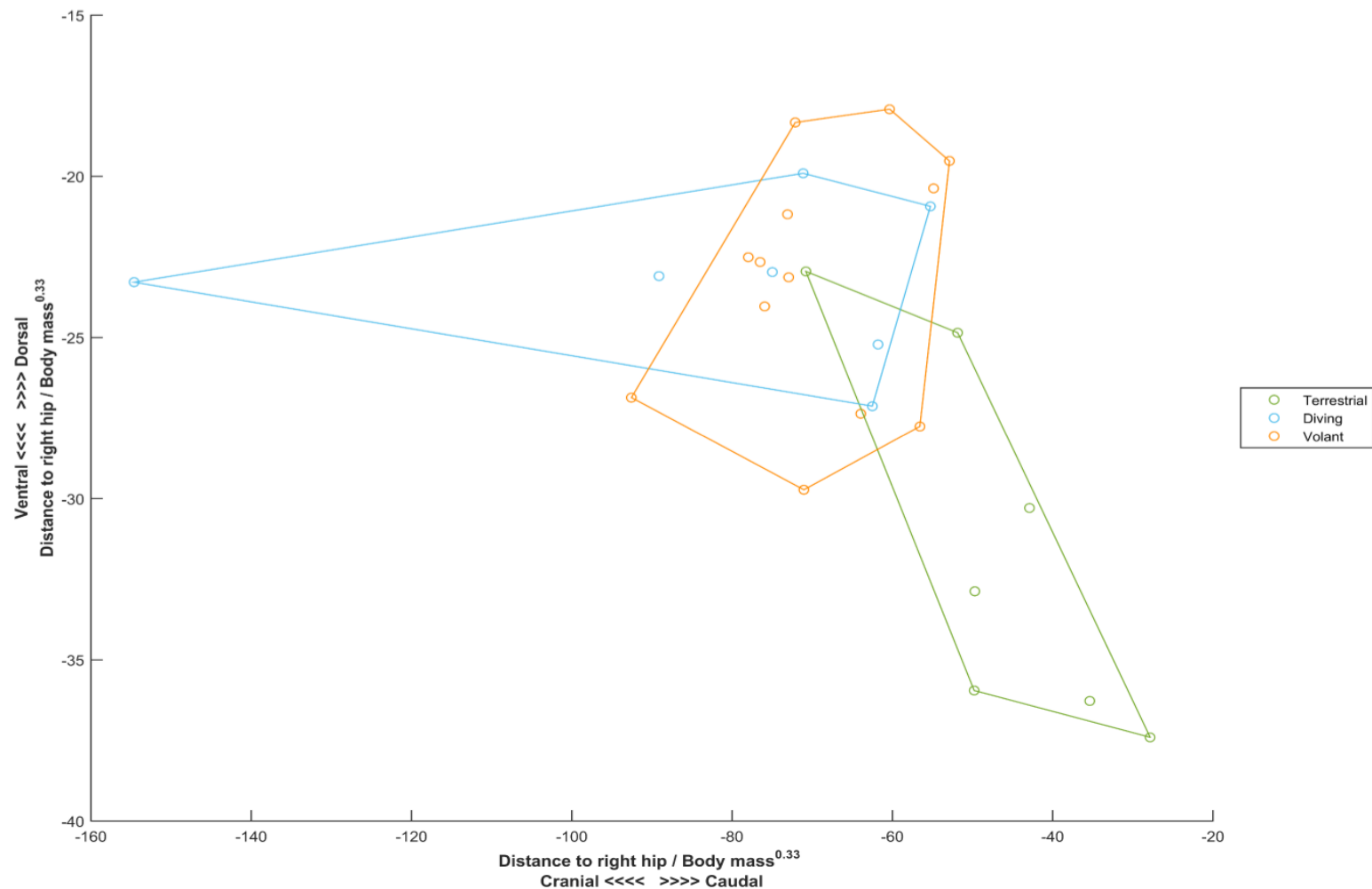


Figure 4.3: Size corrected centre of mass data for 27 bird species, grouped by locomotor type. Centre of mass position is expressed relative to the right hip (at 0, 0).

large bodied ratites, chicken and seriema had CoM positions which were markedly more caudal and more ventral (Figure 4.3). There was substantial overlap between the diving and volant birds along the cranio-caudal and dorso-ventral axes (Figure 4.3). The pelican was an extreme outlier in the cranio-caudal dimension, and the kingfisher also lay outside of the volant group. The volant birds showed substantial variation in CoM position. But generally, the volant group had a more cranial, more dorsal whole body CoM relative to the terrestrial specimens (Figure 4.3).

The differences between groups were not found to be significant in the cranio-caudal direction (ANOVA, p value = 0.294). But groups were statistically distinct in the dorso-ventral direction (ANCOVA, p value = 0.016) and post-hoc testing revealed the volant and terrestrial groups were significantly different (Tukey test, p value = 0.012). However, after correcting for phylogeny, these differences in the dorso-ventral direction were no longer statistically significant (PGLS, p value > 0.07).

4.4.1.2. *What drives differences in whole body CoM position?*

Though the differences detected between locomotor groups were not significant at $p = 0.05$, here I explore the causes of the observed differences. Examination of only the first mass moment (FMM) data for each segment, across the 27 specimens reveals the markedly different influences different segments have on CoM position (Figures 4.4 and 4.5), and the variability in segment influence present across Aves. The torso segment FMM exerted the greatest influence in the cranio-caudal direction (15 out of 27 birds, $X^2 = 28$, $p < 0.05$), followed by the head (14 out of 27 birds, $X^2 = 15$, $p < 0.05$). In the dorso-ventral direction, the hindlimb was overwhelmingly the main driver (24 out of 27 birds, $X^2 = 81$, $p < 0.05$), followed by the torso and forelimb (12 out of 27 and 11 out of 27 birds respectively, $X^2 = 14$, $p < 0.05$).

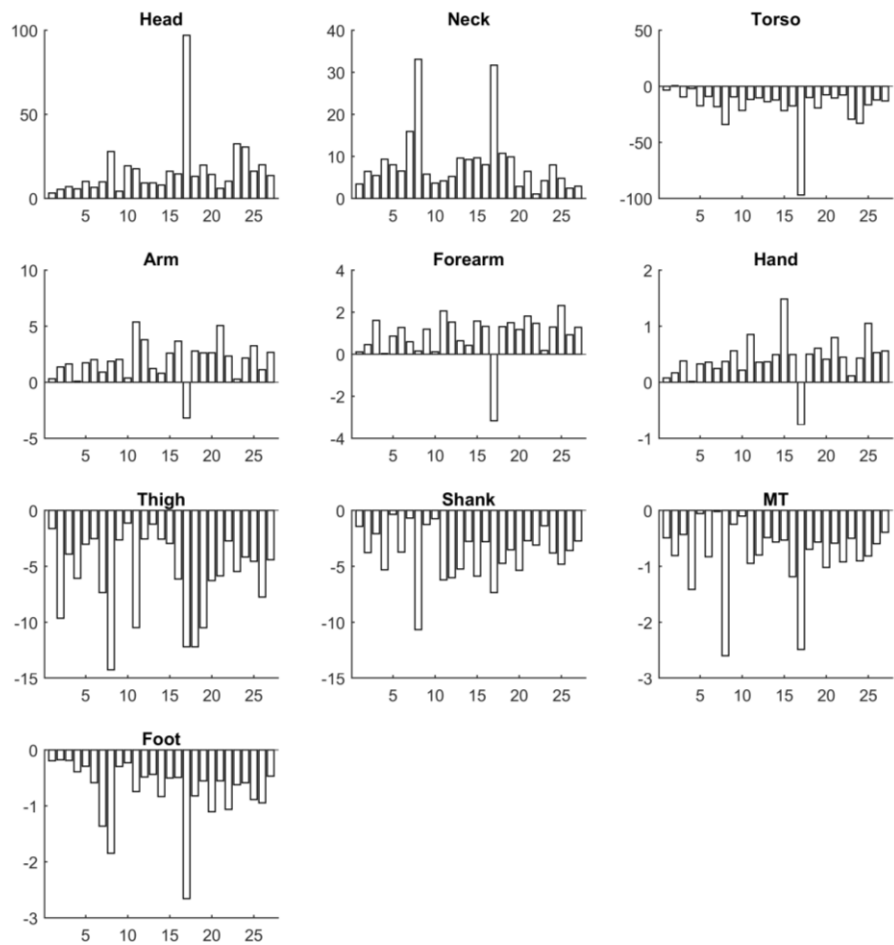


Figure 4.4: First mass moment data in the crano-caudal direction plotted on the y-axis for each of the 27 specimens on the x-axis (see Table 4.1 for specimen numbers), for each body segment. A positive FMM indicates a cranial pull, negative FMM indicates a caudal pull.

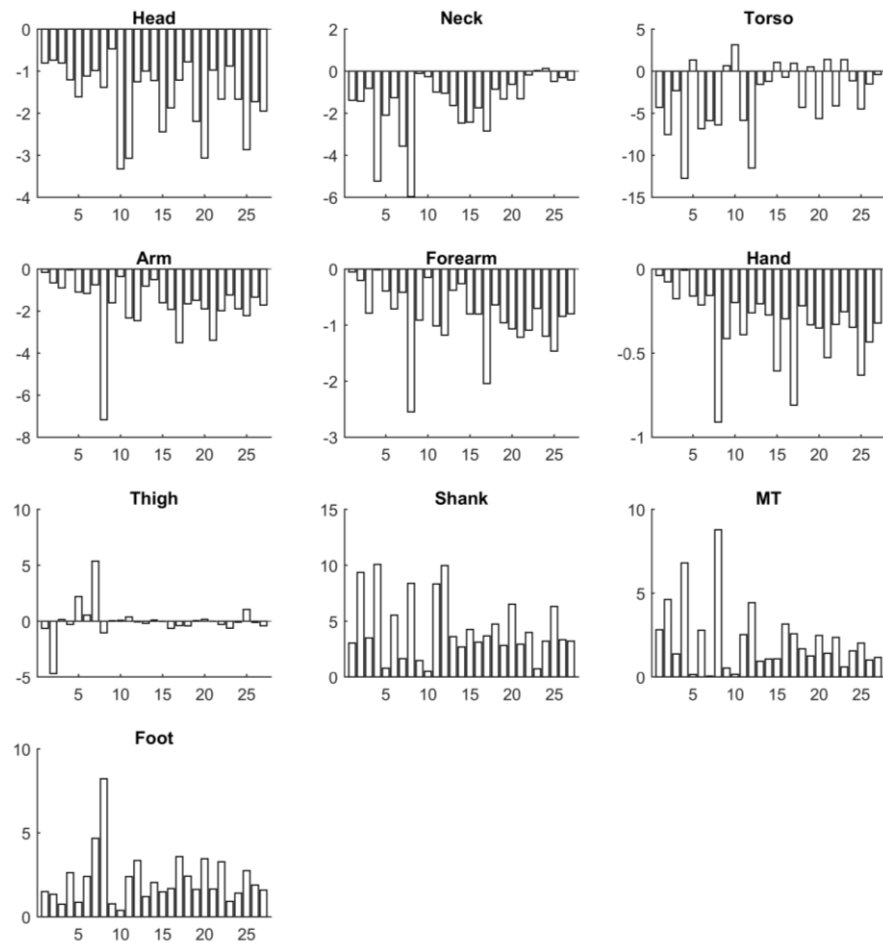


Figure 4.5: First mass moment data in the dorso-ventral direction plotted on the y-axis for each of the 27 specimens on the x-axis (see Table 4.1 for specimen numbers), for each body segment. A positive FMM indicates a ventral pull, negative FMM indicates a dorsal pull.

Table 4.3: Table showing the results of Spearman's rank test, assessing the correlations of various segment mass properties with whole body centre of mass in the dorso-ventral direction. ρ^2 indicates the percentage of CoM variation which is accounted for by a given variable. Significant results (at $p < 0.05$) are highlighted in red.

		Spearman's ρ	$\rho^2(\%)$	p value
Segment mass (kg)	Head	0.297	8.8	0.133
	Neck	0.410	16.8	0.035
	Torso	-0.110	1.2	0.584
	Forelimb	0.287	8.2	0.147
	Hindlimb	-0.502	25.2	0.008
Segment centre of mass (mm)	Head	0.077	0.6	0.702
	Neck	-0.068	0.5	0.736
	Torso	0.094	0.9	0.640
	Forelimb	0.274	7.5	0.167
	Hindlimb	0.557	31.0	0.003
Segment first mass moment (kgm)	Head	-0.187	3.5	0.348
	Neck	0.075	0.6	0.709
	Torso	0.767	58.8	0.00001
	Forelimb	-0.125	1.6	0.534
	Hindlimb	-0.624	38.9	0.001
Whole body mass (kg)		-0.328	10.8	0.095

Table 4.4: Table showing the results of Spearman's rank test, assessing the correlations of various segment mass properties with whole body centre of mass in the cranio-caudal direction. ρ^2 indicates the percentage of CoM variation which is accounted for by a given variable. Significant results (at $p < 0.05$) are highlighted in red.

		Spearman's ρ	ρ^2 (%)	p value
Segment mass (kg)	Head	-0.844	71.2	0.000002
	Neck	-0.315	9.9	0.110
	Torso	-0.104	1.1	0.605
	Forelimb	-0.655	42.9	0.0003
	Hindlimb	0.082	0.7	0.682
Segment centre of mass (mm)	Head	0.030	0.1	0.883
	Neck	0.258	6.7	0.193
	Torso	0.652	42.5	0.0003
	Forelimb	0.200	4.0	0.315
	Hindlimb	-0.206	4.2	0.302
Segment first mass moment (kgm)	Head	-0.927	86.0	0.000001
	Neck	-0.211	4.4	0.290
	Torso	0.821	67.4	0.000002
	Forelimb	-0.092	0.8	0.649
	Hindlimb	0.395	15.6	0.042
Whole body mass (kg)		0.449	20.1	0.020

When a range of specimen mass properties were assessed for correlation with CoM position, the majority (9 out of 12) of the statistically significant associations were strong (Spearman's ρ below -0.5 or above 0.5) (see Tables 4.3 and 4.4). The strongest associations to whole body dorso-ventral CoM position were shown by torso and hindlimb FMM (Spearman's ρ values: 0.767 and -0.624 respectively), and also for hindlimb mass (Spearman's ρ = -0.502) and CoM (Spearman's ρ = 0.557). Specimen mass properties showed a greater number of strong associations with whole body crano-caudal CoM position. Particularly strong associations were found for head mass, head FMM and torso FMM (Spearman's ρ values: -0.844, -0.927 and 0.821 respectively), but also for forelimb mass (Spearman's ρ = -0.655) and torso CoM (Spearman's ρ = 0.652).

4.4.1.3. *Does CoM correlate with body mass?*

Based on the raw data, CoM position shows a strong ventral shift with increasing body size (Spearman's ρ = -0.93; $p < 0.0005$; 87% of variance explained by body mass), which is maintained even after removing the large-bodied, terrestrial ratites from the dataset (see Figure 4.6). Trends in crano-caudal CoM position are similar (Spearman's ρ = -0.88; $p < 0.0005$; 77% of variance explained by body mass), but the six largest specimens show substantial variation (see Figure 4.6). Excluding the pelican, which has an extremely cranial CoM, whole body CoM position for the remaining specimens levels off approximately 100mm cranial to hip.

Normalising data by body mass to remove absolute differences in CoM position suggests that larger body masses are weakly associated with more caudal (Spearman's ρ = 0.45; $p = 0.01$; 20% of variance explained by body mass), and more ventral (Spearman's ρ = -0.33; $p = 0.09$; 10% of variance explained by body mass) CoM positions (Figure 4.7). The dorso-ventral trend

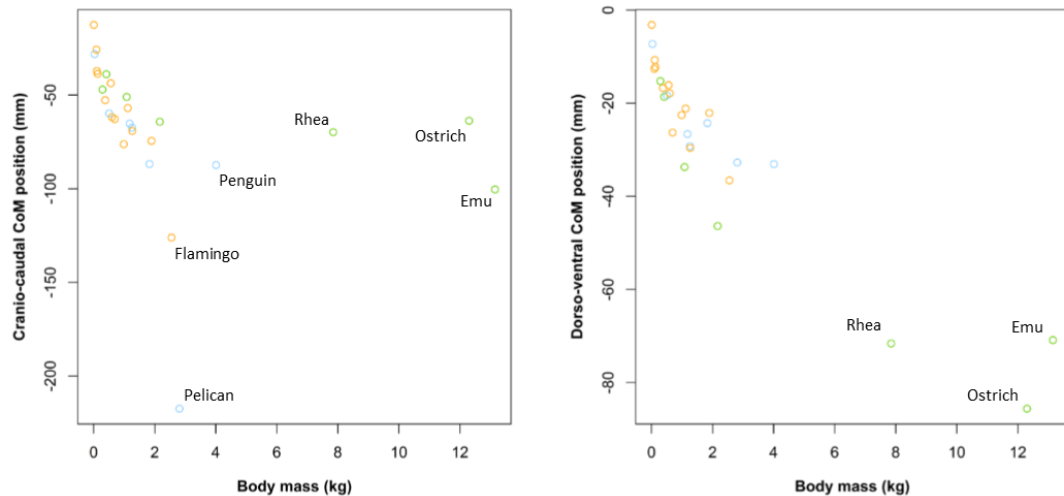


Figure 4.6: Whole body mass plotted against raw data on cranio-caudal (left), and dorso-ventral (right) centre of mass position. Negative values indicate shifts in a cranial and ventral direction respectively. Data points are colour coded according to locomotor categories: terrestrial (green), diving (blue) and volant (orange). Data points of interest are labelled with specimen names.

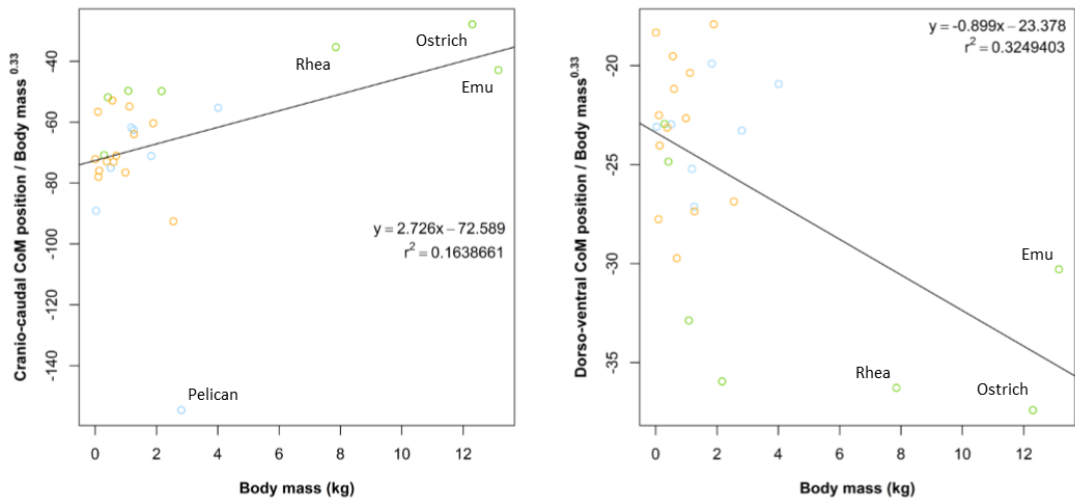


Figure 4.7: Whole body mass plotted against size normalised data on cranio-caudal (left), and dorso-ventral (right) centre of mass position. Negative values indicate shifts in a cranial and ventral direction respectively. Trendlines are for the whole dataset. Data points are colour coded according to locomotor categories: terrestrial (green), diving (blue) and volant (orange). Data points of interest are labelled with specimen names.

is driven mainly by the three large ratites, but the crano-caudal trend holds well across Aves, with the exception of the pelican (Figure 4.7).

4.4.2. Avian body density

4.4.2.1. Segment specific density data

The whole body and segment specific density values determined here are generally similar across birds (Figure 4.8, Supplementary Information 4.2). Whole body density ranged from $922 - 1114\text{kgm}^{-3}$ for the five species studied here, while the range of segment densities was greater at $733 - 1730 \text{ kgm}^{-3}$. Within specimens, segment density varied, to large degrees in some cases (e.g. kestrel $\pm 864\text{kgm}^3$, and chicken $\pm 750\text{kgm}^3$). The kestrel had the lowest whole body density, which was driven by the exceptionally low density of the torso (733kgm^{-3}). The long tailed tit had the highest body density (1114kgm^{-3}), slightly more dense than the chicken, duck and pigeon specimens.

4.4.2.2. Whole body density in 25 bird species

Whole body density was calculated for all specimens with a known body mass (i.e. excluding the ostrich and hummingbird), using body mass measured from cadavers and model skin volume. Measured density varied widely from 531kgm^{-3} (brown pelican) to 1336kgm^{-3} (black throated diver) (Table 4.5).

4.4.3. Assessing modelling approaches

4.4.3.1. Segment closing technique - validity assessment

In order to address hypothesis 4a, three different approaches were used here to generated ‘closed’ skin segments for estimation of CoM position. The effect of these different closing methods was assessed on the buzzard specimen. Three CoM estimates were generated using: (1) segments closed in Geomagic or wrapped in 3-matic, (2) alpha shapes wrapped

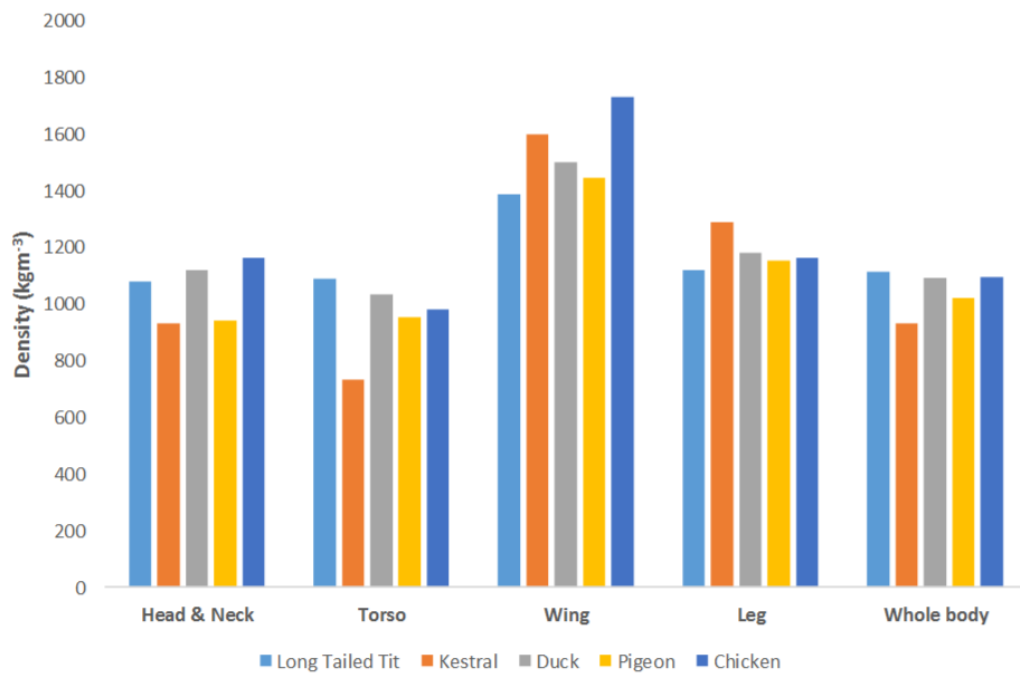


Figure 4.8: Segment specific and whole body density data measured from the cadavers of five specimens.

Table 4.5: Table showing the body density (kgm^{-3}) values calculated by dividing measured body mass by model skin volume.

#	Common name	Body density
1	Common ostrich	NA *
2	Darwin's rhea	822
3	Andean tinamou	1061
4	Emu	763
5	Mallard	1037
6	Leghorn chicken	1139
7	Clark's grebe	904
8	Chilean flamingo	613
9	Wood pigeon	1099
10	Anna's hummingbird	NA *
11	Violet turaco	843
12	Red-legged seriema	852
13	Black-throated diver	1336
14	Humboldt penguin	1004
15	Sooty shearwater	694
16	Scarlet ibis	926
17	Brown pelican	531
18	Brandt's cormorant	746
19	Western gull	781
20	Common buzzard	1129
21	Turkey vulture	877
22	Great horned owl	1325
23	Common kingfisher	951
24	Great spotted woodpecker	825
25	Merlin	802
26	Orange-winged parrot	906
27	Blackbird	982

* indicates specimens for which body mass was estimated, and for which body density was therefore not calculated.

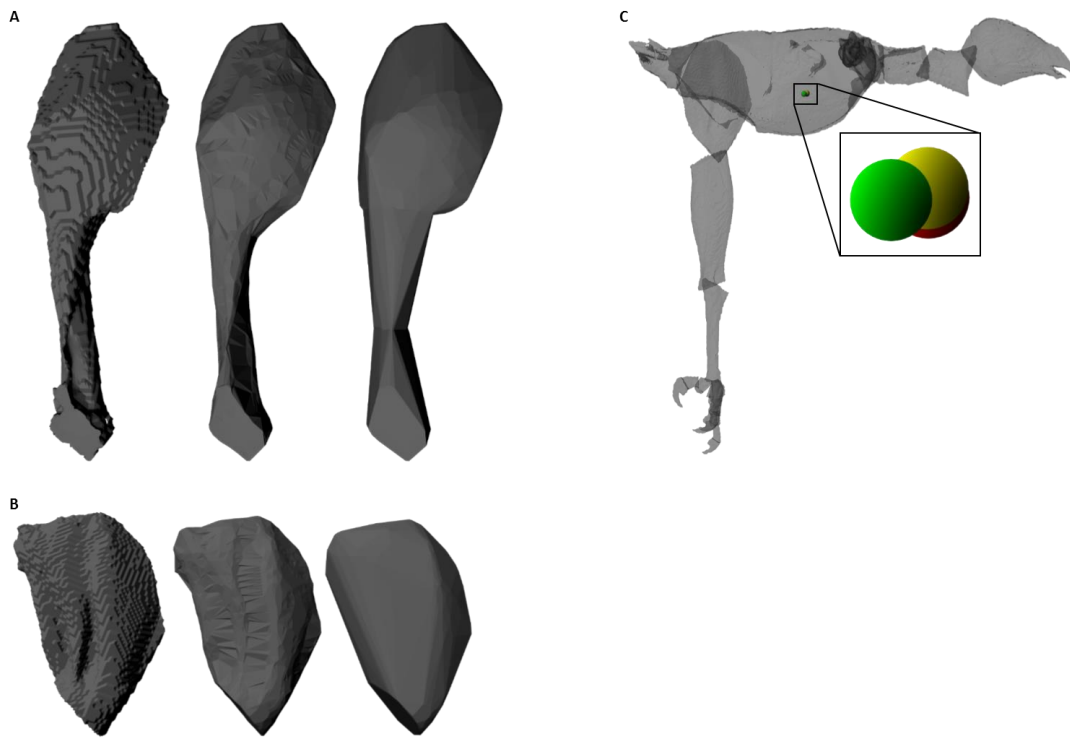


Figure 4.9: **A & B:** Example skin segments closed in Geomagic (left), using an alpha shape (centre) and using convex hulling (right). The segments shown are the upper arm (**A**) and thigh (**B**) of a buzzard. **C:** Three alternative whole body CoM predictions produced by applying the three alternative methods for closure to all body segments of a buzzard (red: closed segments, yellow: alpha-shaped segments, green: hulled segments).

Table 4.6: Table showing segment volumes (mm^3), segment CoMs (mm) and whole-body CoM estimates (mm) when all body segments are closed using three alternative methods (Geomagic, alpha shapes and convex hulls). Where +x is right, +y is dorsal, +z is caudal. See Figure 4.9 for visualisation of these differences.

		Head*	Neck1	Neck2	Torso	Tail*	Arm*	Forearm*	Hand*	Thigh	Shank*	MT*	Toes	Whole body
Closed	Volume	63792.2	11338.3	9538.4	305045.	13730.1	22802.9	11907.8	3777.0	29947.4	25582.8	4868.5	5048.0	507379.3
	CoM	-16	-11	-12	-10	-13	40	153	249	2	1	0	-1	5
		3	-9	-7	-16	-5	-1	1	2	-28	-104	-182	-235	-26
Alpha shape	Volume	66878.2	12502.3	11315.0	331078.	16896.4	25629.9	15373.4	5346.0	33795.1	27138.7	5377.3	5334.0	556665.2
	CoM	-16	-11	-12	-10	-13	43	156	250	2	1	0	-1	7
		3	-9	-6	-16	-4	-1	2	3	-29	-105	-182	-236	-26
Convex hull	Volume	71839.8	16529.9	13360.0	373342.	21417.6	30015.5	20991.1	7131.98	41609.2	30299.2	6585.8	7018.6	640141.7
	CoM	-17	-11	-12	-10	-13	44	162	253	2	1	0	-1	10
		2	-8	-6	-16	-4	-1	2	3	-29	-107	-184	-236	-26
		-200	-162	-129	-51	32	-97	-94	-96	3	1	1	4	-61

Segments marked with * were split into multiple component parts to generate convex hulls.

around each segment and (3) convex hulls for each segment (Figure 4.9, Table 4.6). To generate alpha shapes, an alpha value had to be selected for each segment. When convex hulling segments with more complex geometries, they were split into several component parts to ensure a close-fitting hull (e.g. Figure 4.9A).

All body segments of the buzzard specimen were closed using each of these methods in order to generate three whole body CoMs. These CoM positions represented extreme situations, as in the models used in the main study the majority of segments were closed in Geomagic. In the main study, segments were only alpha-shaped if they could not be closed, and failing that convex hulls were used. Very small differences were detected between the three CoM values calculated using these alternative methods. Slight differences in segment volumes and CoM positions combined to produce differences in whole body CoM position of less than 1.86mm for the buzzard (Figure 4.9C, Table 4.6).

I therefore conclude that the effects of using different closing methods is minimal, and has no significant adverse effects for the purpose of this study. The very small differences detected between estimated whole body CoMs suggests any of these methods are appropriate for estimating CoM position. The time investment relative to the reward of generating clean, closed skin outlines should be considered for future works seeking to generate CoM estimates, when an alpha shape or convex hull-based approach is virtually equivalent in accuracy.

4.4.3.2. Comparing mass property estimates from heterogeneous and homogeneous models

Addressing hypothesis 4b, the CoM positions predicted by the alternative applications of density data (Section 4.3.2), are generally very similar to one another (see Figure 4.10). The

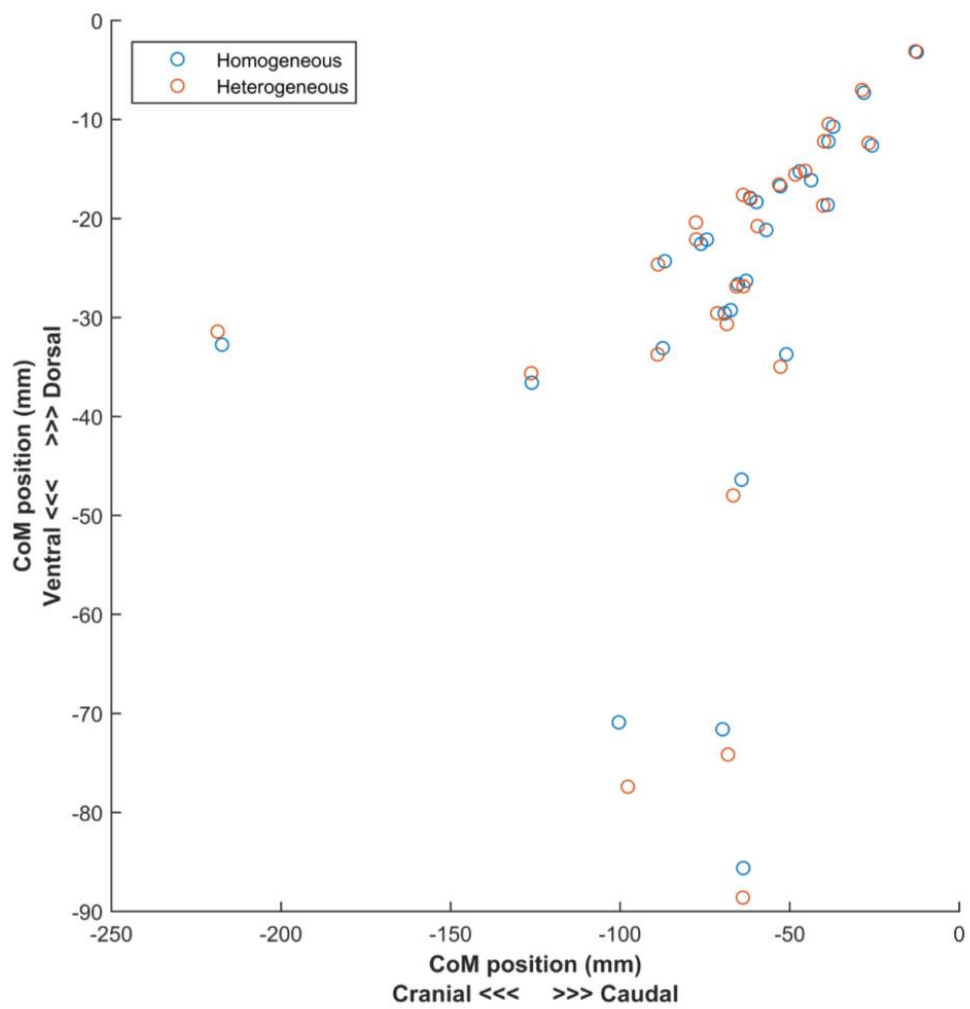


Figure 4.10: Raw centre of mass position plotted relative to the right hip (at 0, 0) for homogeneous and heterogeneous version of models (see key).

median difference across all 27 bird models was 1.80mm (range: 0.377 - 7.04mm). 21 of 27 bird models displayed lower error than that observed in the sensitivity analysis of Chapter 2 (Section 2.4.3.3), which tested a range of density data used in previously published studies. The raw, 2D differences between model versions are positively associated with body mass (Spearman's $\rho = 0.681$, $p < 0.005$); as would be expected, larger bodied specimens have absolutely larger differences (Figure 4.10). However, all differences represent only a small fraction of the whole body CoM in the dorso-ventral (2 - 16%, mean: 8%) and cranio-caudal (1 - 7%, median: 3%) directions. I therefore conclude that density assignment has only a marginal effect on whole body CoM position.

When used to estimate body mass, both model variants displayed larger errors (median: 18% of measured body mass). This error was highly variable - from 0.4% for the homogeneous penguin model, to 103% for the heterogeneous pelican model (see specimen 17 in Figure 4.11). While most models showed less than 50% error (25 out of 27 specimens), only 8 out of 27 models showed less than 10% error in their BM predictions (Figure 4.11). The homogeneous models more closely predicted measured body mass in 19 out of 27 specimens, and showed a lower average error than their heterogeneous counterparts (17% versus 21% of measured body mass). This study proceeded using data from homogeneous models in all subsequent analyses.

4.5. Discussion

4.5.1. Does whole body CoM position differ between forelimb and hindlimb dominated species?

The demands on the musculoskeletal system vary considerably across Aves, according to the wide range of locomotor habits displayed by species within the group. Previous studies have elucidated links between locomotion and muscular anatomy, reflected by different levels of

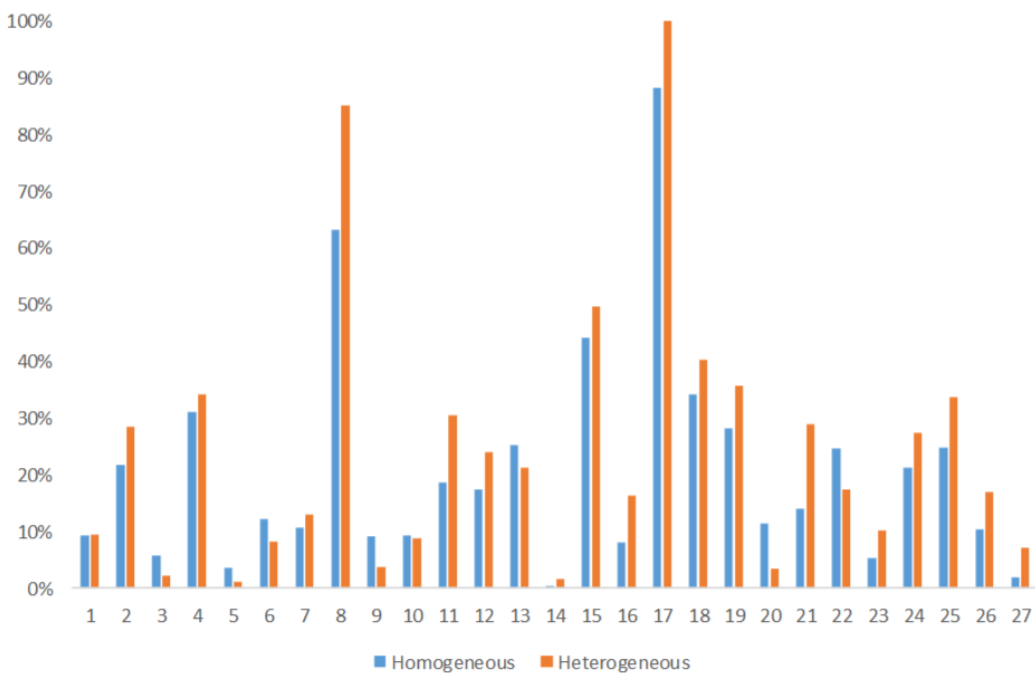


Figure 4.11: Difference between measured body mass, and predicted body mass, displayed as a percentage of measured body mass. All differences shown as positive changes, in enable easier comparison of error magnitudes. Shown for the following specimens - 1: common ostrich*, 2: Darwin's rhea, 3: Andean tinamou, 4: emu, 5: mallard, 6: leghorn chicken, 7: Clark's grebe, 8: Chilean flamingo, 9: wood pigeon, 10: Anna's hummingbird*, 11: violet turaco, 12: red-legged seriema, 13: black-throated diver, 14: Humboldt penguin, 15: sooty shearwater, 16: scarlet ibis, 17: brown pelican, 18: Brandt's cormorant, 19: western gull, 20: buzzard, 21: turkey vulture, 22: great horned owl, 23: common kingfisher, 24: great spotted woodpecker, 25: merlin, 26: orange-winged parrot, 27: blackbird.

* indicates species for which body mass was estimated, rather than measured directly.

relative investment in the hindlimb versus the forelimb musculature according to locomotor specialisations (Heers and Dial, 2015). This study seeks to examine links between morphology and locomotor style at the level of the whole organism, using CoM as a proxy for body plan. Contrary to hypothesis 1, no statistically significant differences were found in CoM position between birds of different locomotor types (Figure 4.3). Though prior to phylogenetic correction, terrestrial (hindlimb dominated) birds were found to have a more ventral CoM compared to those which are volant (forelimb dominated). The lack of statistical significance after phylogenetic correction is potentially a result of the ratite dominated terrestrial group, whose similarity to one another may be driven by their close phylogenetic relationships, rather than a convergence on morphologies suited to terrestriality. Additionally, though 27 specimens represents a large sample size for a volumetric study (e.g. previous studies on birds include a limited number of species: two in Allen et al. (2013) and six in Henderson (2010)), it is a relatively small sample size to capture the variation present across the whole of Aves. Future work should seek to include a larger number of species, and mature adult ratite specimens to better capture the variability, and any trends, present within Aves. The spread of data points observed in both the volant and terrestrial categories indicates that substantial variability is present within Aves, and within locomotor sub-categories (Figure 4.3). This reflects the fact that body plan is influenced by more than just locomotor mode, with other factors such as life history, habitat and foraging technique also influencing morphology. In Figure 4.3, the ventral-most data point in the terrestrial group is the turaco, which results in an overlap with the volant group. The arboreal turaco and the terrestrial tinamou do not group with the other terrestrial species studied here. By observation, both species superficially display a more conservative body plan, closer to that of the volant birds than the forms specialised for bipedal, terrestrial locomotion.

Based on the findings of Heers and Dial (2015), it would be expected that differences in hindlimb and forelimb morphologies, as indicated by their mass properties, would be the main drivers of the differences observed between the volant and terrestrial groups here (hypothesis 2). The results partially confirm this, highlighting the mass properties of the hindlimb as highly significant influences on dorso-ventral CoM position ($p < 0.008$ for segment mass, CoM and FMM) (Table 4.3). Forelimb mass and CoM are also correlated with a more dorsal CoM position, though not significantly ($p = 0.147$ and 0.167 respectively). This suggests that it is primarily differences in the hindlimb morphology which drive differences in whole body CoM.

The assessment of a range of mass properties to determine links with CoM position revealed numerous significant correlations. Most of these statistically significant correlations were strong (Spearman's ρ below -0.5 or above 0.5). It is encouraging that these are robust trends, even when sampling across a broad range of avian taxa. Many of these associations are stronger than those detected by Allen et al. (2013), perhaps a result of greater sample size, or more consistent differences between taxa in a more closely related group.

Previous work examining CoM position focuses almost exclusively on the cranio-caudal component (e.g. Allen et al., 2013, Bates et al., 2012, Bates et al., 2016, Hutchinson et al., 2011). This may be adequate for terrestrial species, where the cranio-caudal component is the major determinant of hindlimb posture along with terrestrial locomotor capabilities. However, for volant birds, the dorso-ventral component of CoM matters much more than for purely terrestrial organisms. Data generated here suggest that the dorso-ventral component of CoM is a better, though non-significant in this study, indicator of differences between locomotor categories (Figure 4.3; and Chapter 3, Section 3.4.2). For terrestrial species, a more ventral CoM confers greater stability for bipedal locomotion on the ground.

For volant birds, a more dorsal CoM, positioned closer to the axis of rotation about the wings, enabling greater manoeuvrability (Thomas and Taylor, 2001). However, a more ventral CoM provides greater passive stability in flight (Thomas and Taylor, 2001). These conflicting benefits for dorso-ventral positioning of CoM could explain the variation present within the volant locomotion category. For example, less acrobatic fliers such as burst adapted species could benefit from a more ventral CoM, without suffering the negative consequences. Whole body morphology could be adapted to particular flight styles, in a similar way that wing morphology varies according to the required function, (e.g. by the way of aspect ratios (Rayner, 1988, Savile, 1957)). However, it is difficult to elucidate more detailed correlations such as these from this dataset. More specimens from the specialist categories would be required to investigate any potential links. Future work could explore potential correlations with quantitative measures of locomotor ability, such as wing aspect ratio and wing loading, in order to elucidate links between CoM and locomotor ability in birds.

It should be noted that the three large bodied ratite species studied here were represented by sub-adult specimens (ostrich: 12.3kg, rhea: 7.85kg, emu: 13.15kg). To my knowledge, there has been no work directly investigating CoM position through ontogeny in ratites, though significant CoM shifts through ontogeny have been reported in other avian species (e.g. Allen et al., 2009). Additionally, the musculature of ratites has been suggested to undergo non-isometric growth rates in ratites (e.g. Picasso, 2015), further suggesting that CoM differences are likely to be present between juveniles and adults. The use of these juvenile ratites represents a limitation of the data comprising the terrestrial group in this study. In order to produce a more complete picture of the body types which occur in birds using ground dwelling behaviours, both juvenile and adult body types should be included in future analyses of this type.

4.5.2. Do birds specialised for novel behaviours possess unique CoM positions?

The third hypothesis of this study was that birds with behaviours specialised for unique environments would display specialised morphologies, which would in turn be reflected by unique CoM positions. However, no significant differences were found between the CoM positions of diving birds and volant birds. The diving birds were however consistently clustered at the ventral edge of the volant group, suggesting greater investment in the hindlimb musculoskeletal anatomy likely linked to the increased hindlimb use (for propulsion in water) compared to an average flying bird. Although the limbs of these diving species are adapted for subaqueous locomotion, in most cases they are also used for flight and bipedal locomotion on land, as for other bird species, likely imposing significant constraints on changes to morphology.

The pelican falls as an extreme outlier, due to the large head and long neck relative to body size (Figure 4.3). These extreme morphologies place whole body CoM in front of the wings, when in the standardised posture. Clearly, posture is hugely important in determining CoM position. *In vivo*, the posture for all birds would be markedly different from the standard posture used here. Alterations to posture would enable organisms to compensate for seemingly oversized body parts by repositioning them closer to the CoM. This is demonstrated by the pelican, which flies with a high degree of neck curvature, with the head folded back against the torso.

In the birds sampled here, the variability present within the volant group does not seem to be linked to specific flight styles (e.g. soaring versus gliding versus flapping flight), alternative pressures on hindlimbs (e.g. raptors, dabblers), or body mass (see Section 4.4.1.3). However, a greater number of species in each of these sub-categories would be required in order to confidently detect any such trends which may be present.

4.5.3. Does density assignment affect the ability of models to predict mass properties?

The density data determined here from physical measurements of five bird specimens (whole body density: 922 - 1114kgm⁻³) (Figure 4.8, Supplementary Table 4.2) lie well within the published range of whole body density values obtained using traditional physical methods (537 - 1069kgm⁻³) (Lovvorn and Jones, 1991, Tserveni and Yannakopoulos, 1988). Previous studies have shown that the process of digital segmentation to obtain body volumes has a high degree of accuracy and precision (Allen et al., 2009, Macaulay et al., 2017). Digital determination of object volume offers numerous benefits over traditional submersion based methods, including ease of data sharing. Here, only five specimens were physically tested (i.e. volume measured digitally for individual segments, mass measured on a lab balance). These specimens covered a range of avian groups, but such a small sample size cannot cover the full extent of variation present in body size and locomotor specialisations which are present across Aves, which likely explains the differences between this and the published range. The density values obtained from the more coarse models constructed from whole body scans (531 - 1336kgm⁻³) (Table 4.5), show a wider range than the published values for birds. Literature values obtained using submersion have produced low density values for aquatic, diving birds (e.g. 784kgm⁻³ for a double-crested cormorant, Lovvorn and Jones 1991), which raises questions about how these birds achieve and maintain submersion. The wide range of values obtained here, showing variation between closely related families with similar life histories suggest that these data may contain a degree of inaccuracy. This is likely in part due to issues with creating closed segments for volume determination. Though closing technique does not significantly impact CoM position, it also impacts segment volume and may exert a substantial effect on density estimation (Figure 4.9, Table 4.6). Future work seeking to determine density data for birds should test a large sample size, covering a range

of species of different sizes and locomotor adaptations using a range of physical and digital methods to assess the accuracy and precision of these methods.

Due to uncertainty around density data in birds, different approaches to modelling segment densities in bird models were explored. This revealed that density affects the estimation of different mass properties to varying extents. Previous work (Chapter 2, Section 2.4.3.3) has found that application of a wide range of density data has little effect on whole body CoM position, for three bird species. The current study applied homogeneous density to models, along with heterogeneous data derived for a range of taxa here (Figure 4.8). The findings of this study support the previous conclusion, with close agreement between homogeneous and heterogeneous models in predicted CoM position across 27 avian species with varying body sizes and morphologies (Figure 4.10). Earlier sensitivity analyses (see Chapter 2, Section 2.3.4) used a broad range of density data for their heterogeneous application, reflecting the wide range of values previously used in the literature (see Chapter 2, Table 2.2), due to the lack of published bird segment specific density data. The new bird specific segment density data generated here (Figure 4.8) has refined the error related to density further (less than 7mm error for all birds studied here, Figure 4.10).

Use of a homogeneous density essentially gives a centre of volume, rather than a true CoM for a given specimen. This is beneficial in studies such as this looking to assess differences in body plan, as it is standardised across all specimens. However, it does not provide a truly accurate representation of relative mass distribution or CoM across Aves. Any study aiming for a highly accurate representation of bird CoM using volumetric models (e.g. submillimetre accuracy) would require specimen specific density assessments, in addition to known postures and generation of air cavities for each individual. By generating specimen specific air cavities, any differences in pneumatisation between juveniles and adults could be

explicitly accounted for. The current method described here applies same generic density data to both juvenile (ostrich, rhea and emu) and adult specimens. This is unlikely to be a truly realistic representation of the individual specimens, though there is no published research on the changes to air cavities and associated CoM changes through ontogeny in ratites. The time demands which accompany generation of individual air cavities should be weighed against the small increases in accuracy likely to be gained. For the majority of studies interested in CoM position in birds, it can be concluded that the effect of density is negligible (Figure 4.10). Any selection of feasible density values have been demonstrated to provide answers in close agreement to each other, and to the true CoM position (see Chapter 2, Section 2.4.3.3). This has positive implications for studies predicting CoM in fossil taxa, where it can also be assumed that density assignment has minimal impact on CoM results, allowing more significant issues to be the primary focus such as improving skin outlines (i.e. segment volume estimates) for extinct specimens.

While density has a small effect (average: 1.80mm) on model CoM position, it was found to exert a much greater effect on predictions of whole body mass (average: 18% measured body mass). The poor ability of heterogeneous and homogeneous models to predict body mass suggests that bird density varies considerably across Aves; beyond the generic value of 1000kgm^{-3} , and beyond the variability captured for the five species studied here (922 - 1114kgm^{-3}). This is also indicated by the substantial variation in the ‘apparent density’ values (531 - 1136kgm^{-3}). This source of error merits further investigation, but was not deemed necessary for this study focussing on CoM position. Volumetric models are not generally used to estimate body mass for whole specimens of living taxa, given the ease of measuring body mass physically. However, the poor performance of avian models here suggests that caution should be taken when using volumetric models to predict body mass in extinct taxa.

4.6. Conclusion

Contrary to my hypotheses, this study found no statistically significant differences in whole body CoM position between birds using different primary locomotor strategies. However, non-significant differences indicated that volant taxa had more dorsally positioned CoMs than their terrestrial counterparts, a trend driven by hindlimb morphology. A more dorsal CoM would be placed closer to the axis of rotation about the wings in flight, enabling greater manoeuvrability. This study identified considerable variability within the locomotor categories investigated here, reflecting the substantial variation in CoM position which is present across Aves. This large range of CoM positions suggests that studies should avoid using one bird species as a proxy for the CoM position of all birds (e.g. Allen et al., 2013). Further work should seek to examine CoM position in a greater number of avian taxa, in order to better represent the wide range of body plans and locomotor styles present across Aves.

4.7. Supplementary Information

Supplementary Information 4.1: Generating suitable values for whole body mass for hummingbird and ostrich specimens.

Here, I used the methods of Brassey and Sellers (2014), Campione et al. (2014) and Field et al. (2013) to generate whole body mass estimates for two specimens where measured body masses were not available.

For the hummingbird, the resulting estimates of body mass were all substantially different from expected values (at 14g, 1.9g and 20g respectively). This is likely due to the extreme robustness of hummingbird humerus and pectoral girdle, combined with its extremely small body size (smaller than any specimens tested by Brassey and Sellers (2014) or Campione et al. (2014)). By taking the volume of our model and applying a density of 1000kgm^{-3} (a value widely used in volumetric modelling approaches (e.g. Allen et al., 2009, Bates et al., 2009b, Hutchinson et al., 2007)), a mass estimate of 5g is derived, which is within the reported range of body masses for this species (Kim et al., 2014, Powers and Nagy, 1988). This was carried forward as the ‘measured’ body mass for this specimen. Estimates for the ostrich specimen fared better (Campione: 13.8kg, Brassey: 12.3kg). Due to the benefits of their volumetric approach, and the ratite-based nature of their relationship, the value derived from Brassey and Sellers (2014) was carried forward here.

Supplementary Information 4.2: Table showing segment specific density values (kgm^{-3})

obtained from physical experiments on five bird cadavers.

	Head & Neck	Torso	Forelimbs	Hindlimbs	Whole body
Long Tailed Tit	1078	1088	1385	1120	1114
Kestral	931	733	1597	1288	931
Duck	1120	1032	1500	1180	1092
Pigeon	940	952	1446	1153	1022
Chicken	1163	980	1730	1162	1095

4.8. References

- ALLEN, V., HUTCHINSON, J. R., BATES, K. T. & LI, Z. 2013. Linking the evolution of body shape and locomotor biomechanics in bird-line archosaurs. *Nature*, 497, 104-107.
- ALLEN, V., PAXTON, H. & HUTCHINSON, J. R. 2009. Variation in center of mass estimates for extant sauropsids and its importance for reconstructing inertial properties of extinct archosaurs. *Anatomical Record*, 292, 1442-1461.
- ANDRADA, E., NYAKATURA, J. A., BERGMANN, F. & BLICKHAN, R. 2013. Adjustments of global and local hindlimb properties during terrestrial locomotion of the Common Quail (*Coturnix coturnix*). *Journal of Experimental Biology*, 216, 3906-3916.
- BATES, K. T., BENSON, R. B. J. & FALKINGHAM, P. L. 2012. A computational analysis of locomotor anatomy and body mass evolution in Allosauroidea (Dinosauria: Theropoda). *Paleobiology*, 38, 486-507.
- BATES, K. T., MANNING, P. L., HODGETTS, D. & SELLERS, W. I. 2009b. Estimating Mass Properties of Dinosaurs Using Laser Imaging and 3-D Computer Modelling. *PLoS ONE*, 4, 1-26.
- BATES, K. T., MANNION, P. D., FALKINGHAM, P. L., BRUSATTE, S. L., HUTCHINSON, J. R., OTERO, A., SELLERS, W. I., SULLIVAN, C., STEVENS, K. A. & ALLEN, V. 2016. Temporal and phylogenetic evolution of the sauropod dinosaur body plan. *Royal Society Open Science*, 3, 150636.
- BLACKBURN, T. M. & GASTON, K. J. 1994. The Distribution of Body Sizes of the World's Bird Species. *Oikos*, 70, 127-130.
- BRASSEY, C. A., HOLDWAY, R. N., PACKHAM, A. G., ANNÉ, J., MANNING, P. L. & SELLERS, W. I. 2013. More than One Way of Being a Moa: Differences in Leg Bone Robustness Map Divergent Evolutionary Trajectories in Dinornithidae and Emeidae (Dinornithiformes). *PLoS ONE*, 8, 1-10.
- BRASSEY, C. A. & SELLERS, W. I. 2014. Scaling of convex hull volume to body mass in modern primates, non-primate mammals and birds. *PLoS ONE*, 9, 1-12.
- CAMPIONE, N. E., EVANS, D. C., BROWN, C. M. & CARRANO, M. T. 2014. Body mass estimation in non-avian bipeds using a theoretical conversion to quadruped stylopodial proportions. *Methods in Ecology & Evolution*, 5, 913-923.
- DUNCKER, H. R. 1971. The lung air sac system of birds. A contribution to the functional anatomy of the respiratory apparatus. *Advances in Anatomy, Embryology and Cell Biology*, 45, 7-171.
- FIELD, D. J., LYNNER, C., BROWN, C. & DARROCH, S. A. F. 2013. Skeletal correlates for body mass estimation in modern and fossil flying birds. *Plos One*, 8, e82000-e82000.
- GATESY, S. M. 1990. Caudofemoral musculature and the evolution of theropod locomotion. *Paleobiology*, 16, 170-186.
- GATESY, S. M. 1999. Guineafowl hind limb function. II: Electromyographic analysis and motor pattern evolution. *Journal of Morphology*, 240, 127-142.

- GATESY, S. M. & DIAL, K. P. 1996. Locomotor modules and the evolution of avian flight. *Evolution*, 50, 331-340.
- HEERS, A. M. & DIAL, K. P. 2015. Wings versus legs in the avian bauplan: Development and evolution of alternative locomotor strategies. *Evolution*, 69, 305-320.
- HENDERSON, D. M. 1999. Estimating the masses and centers of mass of extinct animals by 3-D mathematical slicing. *Paleobiology*, 25, 88-106.
- HENDERSON, D. M. 2004. Tipsy punters: Sauropod dinosaur pneumaticity, buoyancy and aquatic habits. *Proceedings of the Royal Society B: Biological Sciences*, 271, S180-S183.
- HENDERSON, D. M. 2006. Burly gaits; centers of mass, stability, and the trackways of sauropod dinosaurs. *Journal of Vertebrate Paleontology*, 26, 907-921.
- HENDERSON, D. M. 2010. Pterosaur body mass estimates from three-dimensional mathematical slicing. *Journal of Vertebrate Paleontology*, 30, 768-785.
- HUTCHINSON, J. R., BATES, K. T., MOLNAR, J., ALLEN, V. & MAKOVICKY, P. J. 2011. A Computational Analysis of Limb and Body Dimensions in *Tyrannosaurus rex* with Implications for Locomotion, Ontogeny, and Growth. *PLoS ONE*, 6, 1-20.
- HUTCHINSON, J. R., NG-THOW-HING, V. & ANDERSON, F. C. 2007. A 3D interactive method for estimating body segmental parameters in animals: Application to the turning and running performance of *Tyrannosaurus rex*. *Journal of Theoretical Biology*, 246, 660-680.
- JETZ, W., THOMAS, G. H., JOY, J. B., HARTMANN, K. & MOOERS, A. O. 2012. The global diversity of birds in space and time. *Nature*, 491, 444-448.
- KAMBIC, R. E., BIEWENER, A. A. & PIERCE, S. E. 2017. Experimental determination of three-dimensional cervical joint mobility in the avian neck. *Frontiers in Zoology*, 14.
- KARDONG, K. V. 2012. *Vertebrates: Comparative Anatomy, Function, Evolution*, New York, McGraw-Hill.
- KIM, E. J., WOLF, M., ORTEGA-JIMENEZ, V. M., CHENG, S. H. & DUDLEY, R. 2014. Hovering performance of Anna's hummingbirds (*Calypte anna*) in ground effect. *Journal of The Royal Society Interface*, 11, 20140505.
- KRINGS, M., NYAKATURA, J. A., BOUMANS, M. L. L. M., FISCHER, M. S. & WAGNER, H. 2017. Barn owls maximize head rotations by a combination of yawing and rolling in functionally diverse regions of the neck. *Journal of Anatomy*, 231, 12-22.
- LEPHART, S. A. 1984. Measuring the inertial properties of cadaver segments. *Journal of Biomechanics*, 17, 537-543.
- MACAULAY, S., HUTCHINSON, J. R. & BATES, K. T. 2017. A quantitative evaluation of physical and digital approaches to centre of mass estimation. *Journal of Anatomy*, 231, 758-775.

- MAINA, J. N. 2017. Functional Design of the Mature Avian Respiratory System. In: MAINA, J. N. (ed.) *The Biology of the Avian Respiratory System: Evolution, Development, Structure and Function*. Cham: Springer International Publishing.
- NYAKATURA, J. A., ANDRADA, E., GRIMM, N., WEISE, H. & FISCHER, M. S. 2012. Kinematics and center of mass mechanics during terrestrial locomotion in Northern Lapwings (*Vanellus vanellus*, Charadriiformes). *Journal of Experimental Zoology Part A: Ecological Genetics and Physiology*, 317, 580-594.
- OSTROM, J. H. 1974. *Archaeopteryx* and the origin of flight. *Quarterly Review of Biology*, 49, 27-47.
- PICASSO, M. B. J. 2015. Ontogenetic Scaling of the Hindlimb Muscles of the Greater Rhea (*Rhea americana*). *Anatomia, Histologia, Embryologia*, 44, 452-459.
- POWERS, D. R. & NAGY, K. A. 1988. Field metabolic rate and food consumption by free-living Anna's hummingbirds (*Calypte anna*). *Physiological Zoology*, 61, 500-506.
- RAYNER, J. M. V. 1988. Form and Function in Avian Flight. In: JOHNSTON, R. F. (ed.) *Current Ornithology*. Boston, MA: Springer US.
- SAVILE, O. 1957. Adaptive evolution in the avian wing. *Evolution*, 11, 212-224.
- SMITH, N. C., JESPERS, K. J. & WILSON, A. M. 2010. Ontogenetic scaling of locomotor kinetics and kinematics of the ostrich (*Struthio camelus*). *Journal of Experimental Biology*, 213, 1347-1355.
- THOMAS, A. L. R. & TAYLOR, G. K. 2001. Animal flight dynamics I. Stability in gliding flight. *Journal of Theoretical Biology*, 212, 399-424.
- TSERVENI, A. S. & YANNAKOPOULOS, A. L. 1988. Specific gravity, carcass fat and prediction of fatness in quail carcasses. *The Journal of Agricultural Science*, 111, 95-98.
- VERSTAPPEN, M., AERTS, P. & VAN DAMME, R. 2000. Terrestrial locomotion in the black-billed magpie: Kinematic analysis of walking, running and out-of-phase hopping. *Journal of Experimental Biology*, 203, 2159-2170.

CHAPTER 5 - A NEW METHOD FOR PREDICTING MASS DISTRIBUTION IN EXTINCT ARCHOSAURS

I am currently developing this chapter for publication. The version of this chapter presented in this thesis has been completed with the following collaborators: K.T. Bates, J.R. Hutchinson and E.R. Schachner.

MACAULAY, S., SCHACHNER, E. R., HUTCHINSON, J. R. & BATES, K. T. (In preparation).

A new method for predicting mass distribution in extinct archosaurs.

Collaborator contributions: SM and KTB conceived the project. All authors provided specimens and collected data. SM processed, analysed and interpreted data, and wrote the chapter.

5.1. Abstract

Knowledge of mass distribution can provide key insights into various aspects of an organism's biology, and is of particular interest when a species cannot be observed directly, as is the case for fossil taxa. Mass distribution, summarised by centre of mass, is a key input for biomechanical investigations, such as those into locomotor capabilities. Numerous methods have been proposed to estimate the centre of mass of fossil taxa. Here, I develop a quantitative computational method, grounded in an unprecedented dataset from extant animals, in order to estimate whole body centre of mass in fossil taxa. The relationship between skeletal and skin volume is established in extant taxa on a segment-by-segment basis. This enables quantitative predictions of soft tissue volumes and subsequently whole body centre of mass in fossil archosaurs, with error margins informed by the variability present within closely related taxa. The results here indicate there is substantial variability in the volume of soft tissue present for a given skeletal volume between the two extant archosaur groups, which has not been recognised in previous volumetric modelling approaches. Full acknowledgment of this uncertainty leads to substantial error margins around the centre of mass positions estimated for fossil species. These quantitative error margins, grounded in data from living taxa, suggest that extreme caution should be taken when using existing methods to calculate centres of mass, from which conclusions are drawn about the biology of extinct taxa.

5.2. Introduction

Centre of mass (CoM) is a fundamentally important biomechanical parameter. It plays a role in determining organism posture, balance and locomotor abilities (e.g. Bates et al., 2010, Farlow et al., 1995, Gatesy et al., 2009, Henderson and Snively, 2004, Hutchinson et al., 2007), which in turn can provide information about species interactions and ecosystem dynamics (e.g. Henderson, 2018, Snively et al., 2018, Sellers et al., 2017). These basic functional and ecological traits can be directly observed in living taxa, but this is not the case for long extinct fossil species with no living analogue, as is the case for many dinosaurs (Gatesy, 1990, Gatesy and Dial, 1996, Hutchinson and Allen, 2009). CoM, and mass properties more widely, therefore provide a valuable, indirect route to ‘higher-level’ biological and ecological information about extinct animals.

As such, many efforts have been made to estimate mass properties for dinosaurs over the last century in order to make inferences about the biology of these enigmatic fossils (e.g. Alexander, 1983, Allen et al., 2013, Anderson et al., 1985, Bates et al., 2009b, Brassey et al., 2015, Gregory, 1905, Henderson, 1999, Hutchinson et al., 2007, Maidment et al., 2014, Mallison, 2010, Paul, 1997, Sellers et al., 2017). However, the majority of studies focus solely on whole body mass, which provides relatively broad information in comparison to CoM. Data on an organism’s CoM is essential for more in-depth studies of functional morphology and biomechanical performance because of its role in determining body segment motion. Despite this central importance, studies that attempt to determine the CoM of fossil taxa are still relatively rare (with several notable exceptions, discussed below). This is in part due to the complexity of estimating CoM in comparison to whole body mass. Additionally, CoM estimation poses more challenges when applied to fossil material, as it requires largely complete specimens for example.

Historically, studies estimated CoM by constructing physical scale models of dinosaur species and then used various physical experimentation techniques (Alexander, 1985, Colbert, 1962, Farlow et al., 1995, Gregory, 1905). For example, Alexander (1985) used suspension to determine CoM position and gradual submersion to determine the volume of sequential ‘slices’ of the organism which then informed estimates of mass distribution. However, the construction of scale models involves inherent uncertainty on the amount and distribution of soft tissue. It is also possible these physical methods have substantial error margins (see examination of the suspension methodology in Chapter 2 of this thesis). These errors, along with any inaccuracies present in the initial model construction will then be magnified once the results from models are scaled up to full size (Farlow et al., 1995).

As digital technologies improved, computational methods were developed in an attempt to provide more accurate, repeatable and objective estimates of CoM in fossil taxa. The work of Henderson (1999) represents the first major step towards this, and this mathematical slicing method has since been developed further (e.g. Henderson, 2010, Henderson, 2018, Maidment et al., 2014). Henderson’s method takes images of the fully articulated fossil of interest in dorsal and lateral views. A skin outline is then constructed around the 2D images of the skeletal material and these reconstructions are extrapolated into 3D. Those 3D models are divided into numerous thin, cylindrical sections running along the cranio-caudal axis of the animal. Density values can be set for each cylinder specifically as required, and any areas of zero-density (such as lungs) can be explicitly incorporated in the model. From these density data and segment volumes, segment masses, and subsequently whole body CoM, can be calculated. This method has been validated on a selection of large mammals (Henderson, 1999, Henderson, 2006), crocodylians (Henderson, 2003) and birds (Henderson, 2010), and was found to be in good agreement with the expected CoM positions. However, to date there have been no attempts to quantify the error present in models of extant taxa

using this method. Though this would not directly indicate the error present in reconstructions of fossil skin outlines, it would give a quantitative indicator of the minimum error present. Studies using this method are therefore yet to include quantitative error margins for CoM position in extinct taxa, despite the considerable uncertainty inherent to digital modelling of fossil species. Unlike studies using physical modelling, this method is capable of basing reconstructions directly on the skeletal material, this is ideally achieved through 2D photographs (e.g. Maidment et al., 2014); or more frequently it is based on artist's reconstructions of the soft tissue outline (e.g. Henderson, 1999, Henderson and Nicholls, 2015). The mathematical slicing method benefits from the ability to modify models relatively easily in comparison to methods using physical models. However, by using only two 2D snapshots to represent the entire skeleton, much of the biological data available to inform a reconstruction is lost.

Later studies have improved on this by basing their reconstructions on 3D representations of the whole skeleton. This can be achieved using, for example, manual digitisation (Hutchinson et al., 2007), laser surface scanning (Allen et al., 2013) or computed tomography (Mallison, 2010). Once digitised, skin outlines can then be applied directly around the whole skeleton. The initial suite of manual shape fitting studies (e.g. Allen et al., 2013, Bates et al., 2009b, Hutchinson et al., 2007, Mallison, 2010) manually fitted a series of shapes along the cranio-caudal axis to the digitised skeletal material. These shapes are then joined and expanded to generate skin outlines based on qualitative knowledge of muscular anatomy in extant archosaurs, and muscle scars present on the fossil material. Though these studies are likely to benefit from the inclusion of a fully 3D digital models of the skeleton, they include the same inherent uncertainty as previous studies when reconstructing a skin outline. The validity of these methods has been tested by application to extant, yielding good results (e.g. Allen et al., 2009, Bates et al., 2009b, Hutchinson et al., 2007). However, the ability to

accurately reconstruct the skin outline of a living species does not reflect the accuracy of a qualitative reconstruction of the skin outline for a long extinct species (Bates et al., 2009b).

Many of these previous studies have recognised this subjectivity and uncertainty by conducting extensive sensitivity analyses on their models to generate models with CoMs maximally skewed in the cranio-caudal and dorso-ventral directions, using segment volumes which are qualitatively deemed to be reasonably realistic (e.g. Allen et al., 2013, Bates et al., 2009b, Hutchinson et al., 2011).

More recently, quantitative techniques using mathematical shape fitting have been developed. These studies seek to improve digital volumetric approaches by enabling quantitative estimations of mass properties in extinct taxa, based directly on body proportion data from extant taxa (Brassey and Gardiner, 2015, Sellers et al., 2012).

Specifically, these methods generate body volumes based on the skeletal-to-skin volume ratio in extant vertebrates and the use of mathematically (rather than manually) generated body volumes. Automated derivation of volumes improves intra- and inter-investigator repeatability, and subjectivity is significantly reduced by using data from living animals to define the minimum and maximum body volumes. But so far, these methods have mostly been applied to generate predictions for whole body mass (e.g. Basu et al., 2016, Bates et al., 2015, Brassey and Gardiner, 2015, Brassey et al., 2015, Brassey et al., 2016, Brassey and Sellers, 2014, Sellers et al., 2012), (with the exception of Bates et al., 2016, Sellers et al., 2013, Sellers et al., 2017). Additionally, these relationships have only been established at the whole body level, and only for specific groups, none of which are ideal for application to CoM estimation in extinct dinosaurs (e.g. mammals (Sellers et al., 2012), ratites (Brassey et al., 2013), primates (Brassey and Sellers, 2014) and pigeons (Brassey et al., 2016)). These methods take skeletal material (whole or split into segments), and use automated processes to wrap a shape around the object (see Chapter 1, Section 1.2.2.2 for detailed overview).

When generating their predictive equations, the majority of published studies have used specimens for which there are no recorded body masses (with the exception of Brassey et al., 2016). This represents a substantial limitation, as body mass is instead calculated from skeletal measurements, and then bone geometry is used to predict body mass, making the whole process somewhat self-reinforcing. These previously published studies have also generated relationships between whole skeleton volume and whole body mass. These relationships have then been applied to specimens giving a homogeneous skeleton-to-skin expansion across the whole body. However, it can be readily observed in living taxa that different body segments vary hugely in the amount of soft tissue present around the skeletal material. This may not impact substantially on estimates of whole body mass, but means that this approach is unlikely to be accurate when generating masses for individual segments. Their ability to accurately estimate whole body CoM is therefore limited.

Therefore, despite the host of advances detailed above, current studies predicting CoM in fossil archosaurs are limited by a lack of detailed knowledge on the relationships between skeletal volume and skin volume in extant taxa. Soft tissue outlines can be subjectively constructed for fossil species in order to generate segment masses and CoMs, but in the absence of quantitative data from extant taxa, these studies are accompanied by considerable and subjectively defined error margins (e.g. Allen et al., 2013, Bates et al., 2016, Hutchinson et al., 2011). Quantitative approaches offer solutions to this issue; however, they are currently of limited use for estimating segment masses and therefore accurate whole body CoM values. Work studying the relationship between skeleton and skin volumes on a segment-by-segment basis in closely related extant taxa has the potential to provide a quantitative grounding for improved estimates of CoM position in extinct archosaurs, which would also benefit from statistically generated error margins.

This study therefore aims to:

- (1) Establish segment-specific relationships between skeletal volume and skin volume in extant archosaurs (birds and crocodylians) and an associated outgroup (lepidosaurs).
- (2) Apply the derived relationships to a selection of fossil taxa from across Dinosauria in order to produce new whole body CoM estimates.

5.3. Methodology

5.3.1. *Determining ratio of skeletal volume to skin volume in extant taxa*

This study used computed tomography (CT) data for 48 specimens, representing 27 bird, 11 crocodylian and 10 lepidosaur species (for details see: Table 4.1 (birds), and Table 5.1 (reptiles)). All specimens were scanned in medical grade CT scanners, at a variety of locations.

All CT data was processed in Avizo 7.1 (www.Avizo3D.com), to extract a complete skeleton in addition to a skin outline. These exports were cleaned up as required, and then split in Geomagic Studio 10 (www.geomagic.com). The skin outlines were split into the following functional segments: head, neck, torso, tail, upper arm, forearm, manus, thigh, shank, tarsometatarsus (for birds) or sole (for crocodylians and lepidosaurs) and toes. Skin segments were closed in Geomagic, or wrapped in Materialise 3-matic (www.materialise.com/en/software/3-matic) to achieve a watertight shell. In order to close some skin segments in extreme cases, it was necessary to generate an alpha shape or convex hull around them using custom Matlab code (www.mathworks.com/products/matlab). For all specimens, the skeletal material was split into the same main segments. In segments containing multiple bones, skeletal material was split further where necessary to achieve tight fitting hulls (e.g. separating pedal phalanges, separating the cranium and mandible

Table 5.1: Details on the reptile specimens used in extant dataset here, including measured whole body mass (kg) where available. For details on the bird specimens used in this study, see Table 4.1.

	Family	Common name	Species name	Body mass
Crocodylians	Alligatoridae	American alligator	<i>Alligator mississippiensis</i>	4.54
		American alligator	<i>Alligator mississippiensis</i>	0.604
	Crocodylidae	Black caiman	<i>Melanosuchus niger</i>	90
		Spectacled caiman	<i>Caiman crocodilus</i>	2.174
		Nile crocodile	<i>Crocodilus niloticus</i>	3.2
		Nile crocodile	<i>Crocodilus niloticus</i>	1.259
		Nile crocodile	<i>Crocodilus niloticus</i>	15.6
		Nile crocodile	<i>Crocodilus niloticus</i>	10.1
		Dwarf crocodile	<i>Osteolaemus tetraspis</i>	7.7
	Agamidae	Morelet's crocodile	<i>Crocodilus moreleti</i>	14.6
		Freshwater crocodile	<i>Crocodilus johnstoni</i>	20.19
Lepidosaurs	Agamidae	Agama	<i>Agama sp.</i>	
		Hydrosaurus	<i>Hydrosaurus sp.</i>	
		Central bearded dragon	<i>Pogona vitticeps</i>	0.49
	Chamaeleonidae	Chameleon	<i>Chamaeleo sp.</i>	
	Corytophanidae	Basilisk	<i>Basiliscus sp.</i>	
	Helodermatidae	Heloderma	<i>Heloderma sp.</i>	
	Iguanidae	Green iguana	<i>Iguana iguana</i>	1.102
	Varanidae	Savannah monitor	<i>Varanus exanthematicus</i>	0.68
		Komodo dragon	<i>Varanus komodoensis</i>	64
	Sphenodontidae	Tuatara	<i>Sphenodon punctatus</i>	

where the jaws were open, separating neck vertebrae at points of extreme curvature). The convex hull of each skeletal element was then calculated in Matlab.

The relationship between skeletal hull volume and closed skin volume was then determined for each body segment in turn using ‘ggplot’ in R (www.r-project.org). For each segment, three main relationships were derived using the following data subsets - (1) bird data only, (2) crocodylian and lepidosaur data (referred to as ‘reptile’ dataset) and (3) data from all specimens. ANCOVA tests were performed to determine the statistical similarity of the ‘bird’ and ‘reptile’ datasets. A further ANCOVA test, with subsequent Tukey post-hoc test, was performed to assess differences between the ‘bird’, ‘crocodylian’ and ‘lepidosaur’ datasets.

5.3.2. Application to extinct taxa

Convex hulls were then applied to the skeletal material of five fossil taxa from Allen et al. (2013) - *Plateosaurus*, *Coelophysis*, *Allosaurus*, *Microraptor* and *Yixianornis*. Currently, Allen et al. (2013) is one of the only studies to conduct a rigorous, systematic investigation of CoM evolution. By applying this new methodology to taxa from their study, it is possible to view this new method in the context of the latest in studies investigating CoM evolution. The specific taxa were selected based on their relative completeness and in order to cover a range of body plans and sizes.

The skeletal material for each fossil was put into a standardised pose (as per Chapters 3 and 4 here), with forelimbs outstretched laterally, legs extended ventrally, and the head and neck fully extended cranially (see Chapter 4, Figure 4.1). In some cases, the skeletal material was not sufficiently complete for immediate use. For example, the medial side of some bones were missing due to the nature of the original data capture by laser scanning. Due to the nature of convex hulling, the process has a high resistance to these effects with minimal

intervention (Bates et al., 2015). Where necessary, polygons were added in Maya, to mimic the geometric extremes of bones which were missing.

The skeletal material was then split into segments, using the same process described for the extant taxa in Section 5.3.1, and each segment was convex hulled. The skeletal convex hull volumes generated were then inputted into the segment specific equations derived in Section 5.3.1 to give predicted skin volumes. In order to apply the relationships derived here to fossil species, it was necessary to decide which scaling equation to use for each segment (bird, reptile or all species). Where no difference was detected between the bird and reptile groups, the ‘all species’ relationship was applied to that segment. In order to generate a “best guess” CoM, the remaining segments were classified as either bird- or reptile-like according to their morphology in each fossil species (see Supplementary Information 5.1). The neck was deemed to be reptile-like if it was relatively short but muscular (e.g. *Allosaurus*), compared to the elongate avian condition. A bird-type torso segment was defined by a carinate keel, while bird-type forelimbs were defined as possessing wing-like traits. Hindlimb type was defined based on the presence of a sprawling (reptile-like) or upright (bird-like) limb posture (Supplementary Information 5.1). The assignment of segment type introduces some subjectivity into model construction. The vast majority of fossil archosaurs are unlikely to be wholly comparable to either modern reptiles or to modern birds, being more likely to possess a mix of ‘bird-’ and ‘reptile-type’ body segments, if not possessing unique segment expansion factors. In an attempt to acknowledge this uncertainty, maximally cranial and caudal whole body CoM estimates were generated around the “best guess” CoM. Application of a density value to the estimated skin volumes then gave values for segment masses.

To generate a whole body CoM estimate, it is also necessary to assign each body segment a CoM position. To avoid subjective estimates of segment flesh contours to generate CoM coordinates, previous studies (e.g. Bates et al., 2016) have assumed that the CoM positions for fleshed out segments are equal to the corresponding CoMs for the hull of the skeletal material in that segment. However, a convex hull of the skeletal material of any given segment will have a different geometry to the soft tissue outline, which will result in different CoM positions for the two shapes. Here, I explore the consequences of this assumption for estimation of whole body CoM. This is achieved by comparing skeletal hull CoM to the known skin CoM for each body segment in four extant specimens (rhea, buzzard, alligator and iguana), selected to represent four different body plans.

Finally, using segment CoM coordinates derived from skeletal convex hulls, whole body CoM was then calculated according to the following equation:

$$CoM_W = \frac{\Sigma(CoM_s * mass_s)}{\Sigma(mass_s)}$$

Equation 5.1

Where CoM_W is the centre of mass of the whole organism (or simply ‘CoM’ in the remainder of this study) and CoM_s and $mass_s$ refer to segment mass properties.

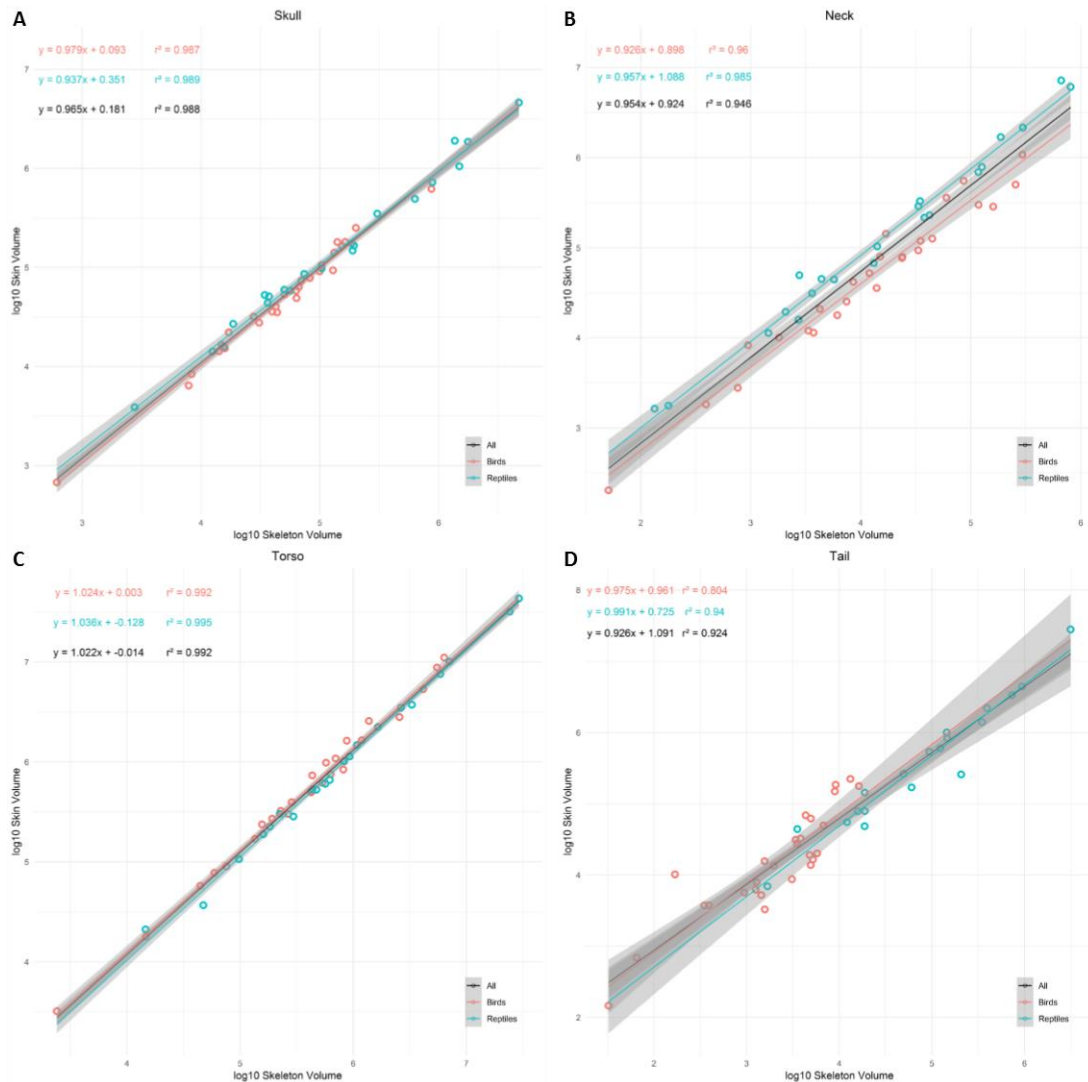


Figure 5.1 (i): Plots showing the relationship between skeletal hull volume and skin volume for individual body segments. **A:** head, **B:** neck, **C:** torso, **D:** tail, **E:** arm, **F:** forearm, **G:** hand, **H:** thigh, **I:** shank, **J:** tarsometatarsal/metatarsals, **K:** toes.

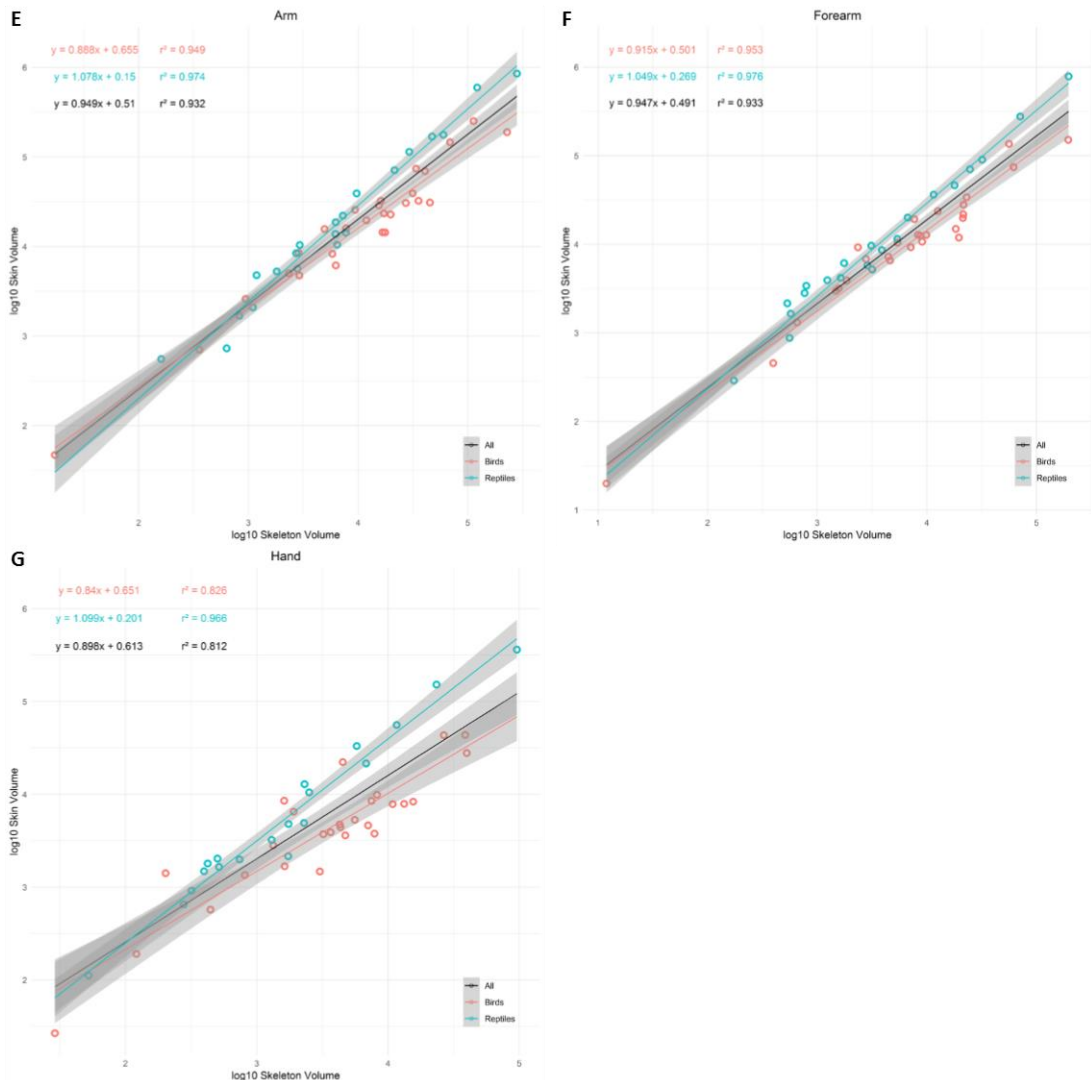


Figure 5.1 (ii): Plots showing the relationship between skeletal hull volume and skin volume for individual body segments. **A:** head, **B:** neck, **C:** torso, **D:** tail, **E:** arm, **F:** forearm, **G:** hand, **H:** thigh, **I:** shank, **J:** tarsometatarsal/metatarsals, **K:** toes.

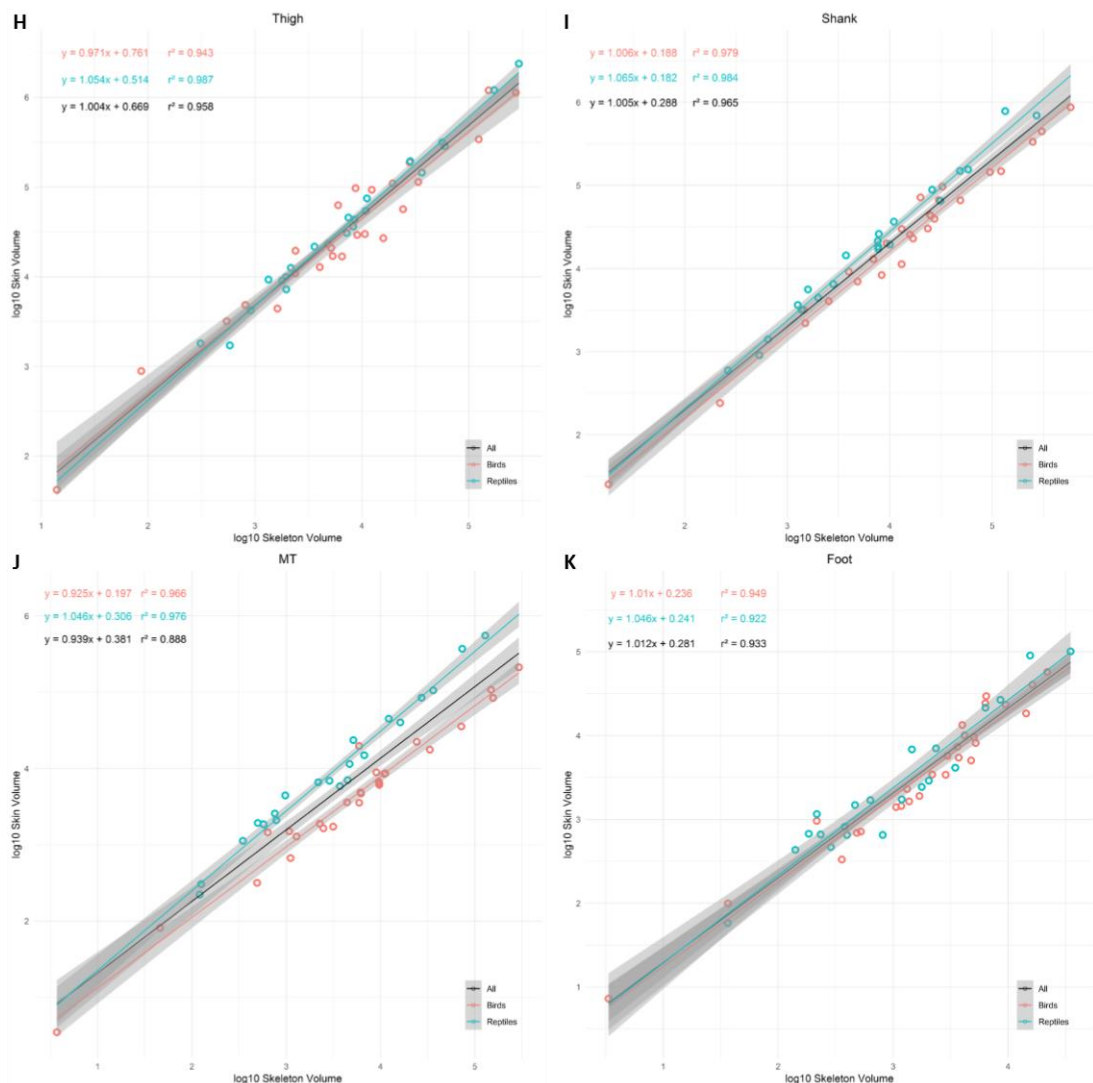


Figure 5.1 (iii): Plots showing the relationship between skeletal hull volume and skin volume for individual body segments. **A:** head, **B:** neck, **C:** torso, **D:** tail, **E:** arm, **F:** forearm, **G:** hand, **H:** thigh, **I:** shank, **J:** tarsometatarsal/metatarsals, **K:** toes.

5.4. Results

5.4.1. Establishing relationships between skeletal volume and skin volume in extant taxa

Plots showing the relationship between skeletal hull volume and skin volume are presented in Figure 5.1. The residuals for the majority of datasets used in preliminary plots of the raw data were non-normal (40 out of 55) according to Shapiro-Wilks tests. The data were therefore log10 transformed resulting in normal distribution of 52 out of 55 datasets before final plots were produced (Figure 5.1). These are the plots used to derive the final predictive relationships applied in the extinct taxa (see below). Using the whole dataset, the majority of segments were found to have statistically distinct skeletal to skin ratios (30 out of 55 comparisons of segment pairs were significantly different at $p < 0.01$, see Supplementary Information 5.2). For each segment, relationships were then established for three groups initially: ‘birds’, ‘reptiles’ and ‘all specimens’. These relationships all displayed high r^2 values (> 0.812) (Figure 5.1), indicating a close fit of the data to the trend lines. Values for mean square error (MSE) ranged from 0.001-0.105 for all trend lines reported here, which equates to mean percentage prediction errors (MPPE) of 0.44-8.65%.

For seven of the eleven segments identified here, significant differences were detected between the ‘bird’ and the ‘reptile’ relationships (ANCOVA test, p values < 0.004) (see Supplementary Information 5.3 for complete table of results). For the remaining four segments (head, tail, thigh and toes), no statistically significant differences were detected between the ‘bird’ and ‘reptile’ groups. These relationships, and their respective significances were used to inform the construction of the “best-guess” models of extinct taxa (for details, see Supplementary Information 5.1).

Additional plots, showing the relationships for the bird group as well as for the two groups comprising ‘reptiles’ (crocodylians and lepidosaurs) are shown in Supplementary Information 5.4. Further statistical tests were conducted to assess differences present between these data subsets (see Supplementary Information 5.5 for complete table of results). This analysis identifies differences which were undetected when comparing the ‘bird’ and ‘reptile’ lines. For example in the skull segment, the lepidosaur line was significantly different to that of the birds and crocodylians (Supplementary Information 5.4 and 5.5). Other previously detected differences within segments are elaborated. In several segments, slopes for the ‘bird’ relationships are significantly different to those for the crocodylians and lepidosaurs (neck, forearm, hand and metatarsal) (Supplementary Information 5.4 and 5.5). For the torso and arm segments, lepidosaurs and crocodylians displayed unique relationships (Supplementary Information 5.4 and 5.5), suggesting that the ‘reptile’ group represented here is not universally homogeneous despite general similarities in their overall body plans.

5.4.2. Method validation - predicting CoM in extinct taxa using convex hulling

5.4.2.1. Segment CoM positions

Here, I explore the accuracy of using skeletal convex hull CoM as a proxy for skin CoM. Differences in segment CoM, and whole body CoM were determined for four extant specimens (rhea, buzzard, alligator and iguana), representing four different body plans (Figure 5.2).

Absolute differences in segment CoM values ranged between 0-49mm across all specimens, or 0-20mm excluding the large bodied rhea (see Supplementary Information 5.6A for summary). The reptiles were minimally affected, with a maximum error of 6.6mm for the tail segment in the alligator (Supplementary Information 5.6A). Certain segments of the birds

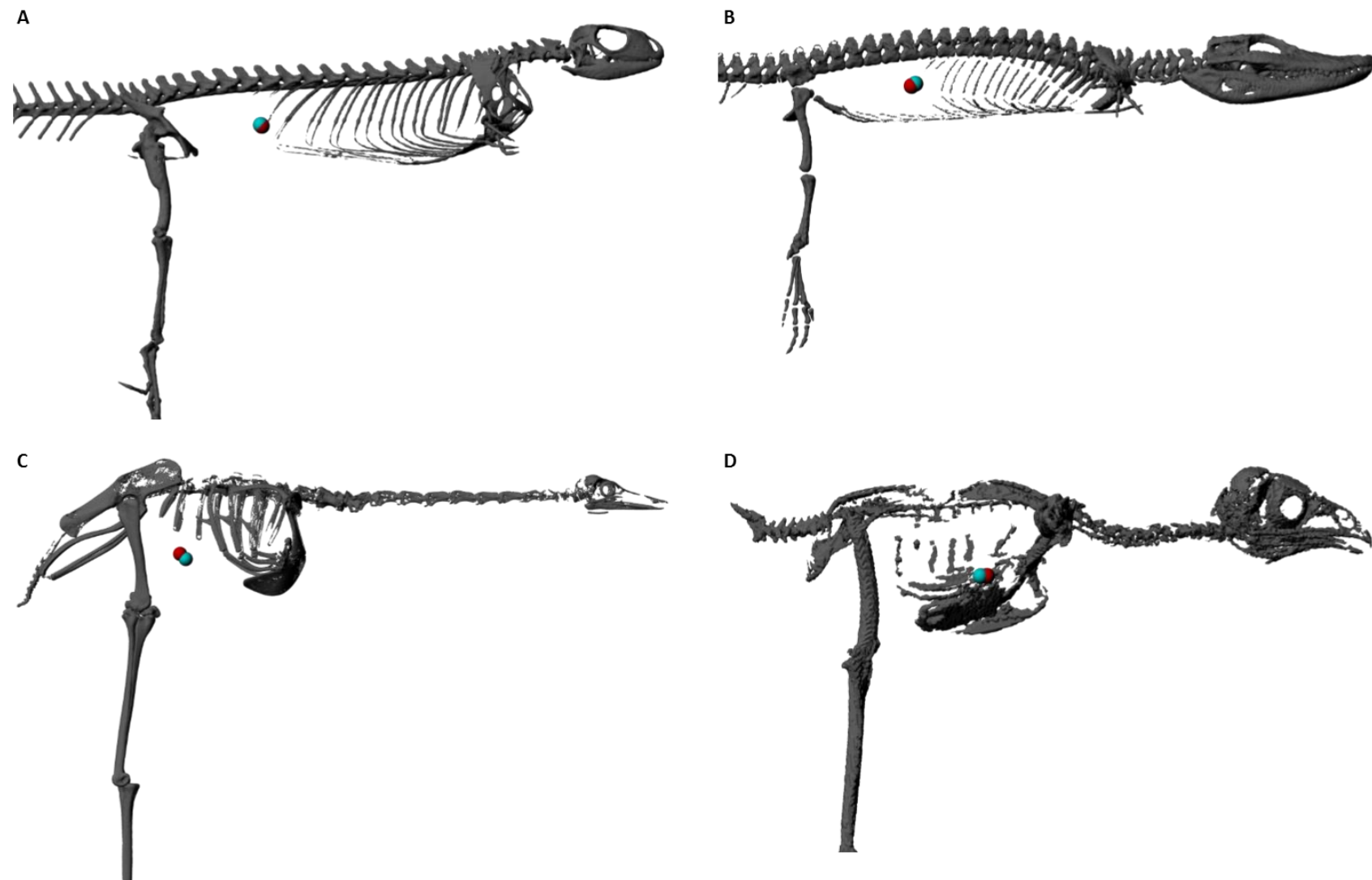


Figure 5.2: Differences between whole body CoMs derived from skeletal segment CoMs (blue spheres) and skin segment CoMs (red spheres), shown in the

context of each specimen (**A**: iguana, **B**: alligator, **C**: rhea, **D**: buzzard).

were more affected, mostly the tapered limb segments (e.g. buzzard upper arm, error = 20mm; see Supplementary Information 5.6A).

Two whole body CoM positions were then generated. Both used the same skin mass (calculated from known closed skin volume and a density of 1000kgm⁻³), and either skeletal hull CoMs or closed skin CoMs for each segment. The 3D distances between the two alternative whole body CoMs ranged between 0.849-10.8mm (see Supplementary Information 5.6B for summary). In each case, these distances were small in comparison to body size (see Figure 5.2), supporting the use of this assumption for fossil material.

5.4.2.2. *CoM estimates versus Allen et al. (2013)*

Comparing our best guess CoM values to those predicted by the models of Allen et al. (2013) reveals notable differences in CoM position (Figure 5.3). The new CoM positions derived here are notably more caudal than those of Allen et al. (2013) in all specimens with the exception of *Yixianornis* (Figure 5.3). The error margins also differ between this study and Allen et al. (2013). The maximum cranio-caudal spread of CoM positions derived from the models of Allen et al. (2013) (white spheres, Figure 5.3) are greater than those observed in methods for extant taxa (Chapter 4). The error contained within the predictive equations derived here is small, and acknowledging these differences results in small shifts in whole body CoM position (grey spheres, Figure 5.3). However, once the uncertainty around segment ‘type’ assignment is recognised, the errors for this new method increase substantially (black spheres, Figure 5.3).

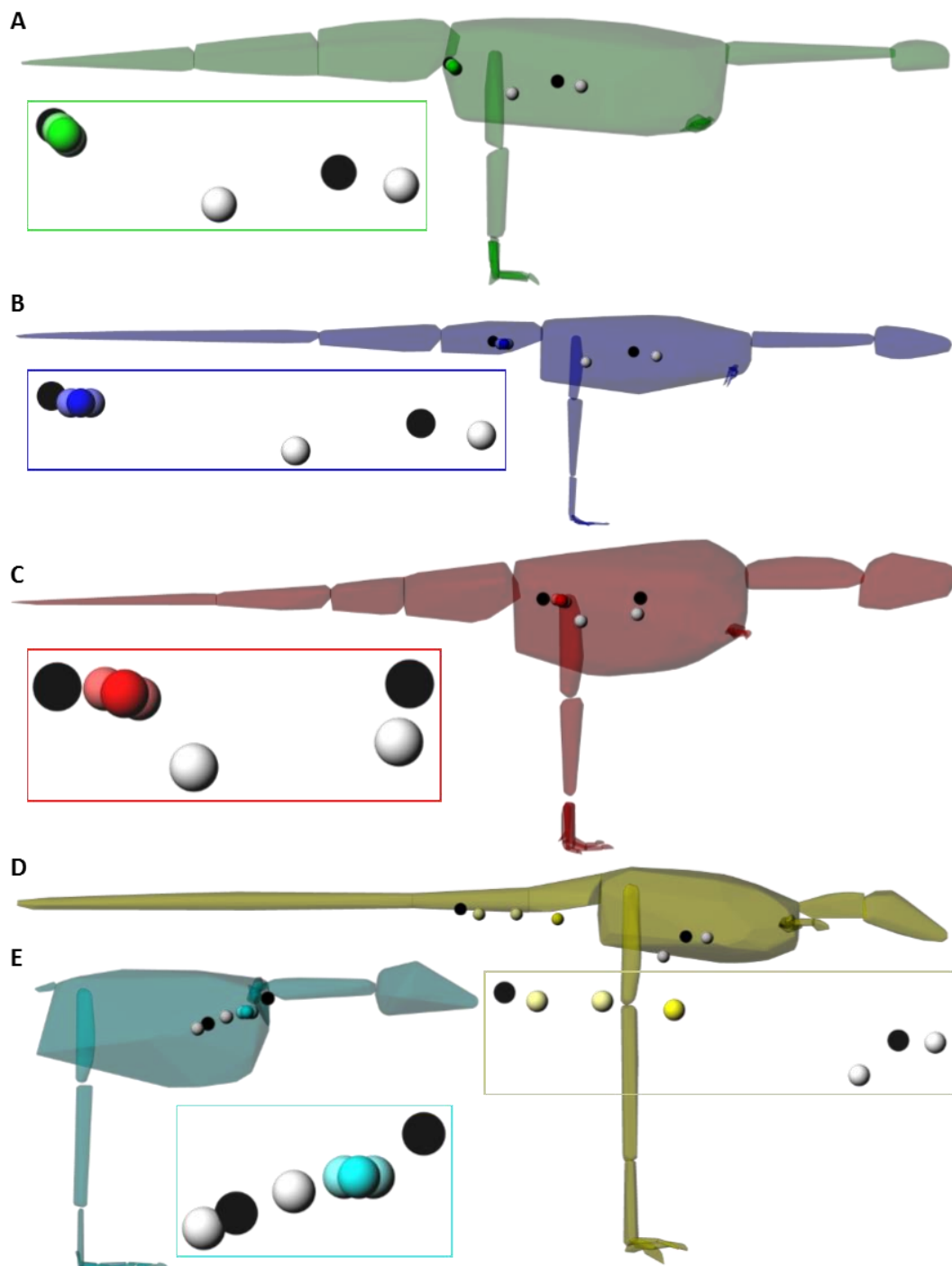


Figure 5.3: Renders in lateral view of the skeletal convex hulls of five fossils species studied here. Showing whole body CoM positions estimated using: best guess models (coloured spheres), error from predictive equations (lighter coloured spheres), maximum cranio-caudal spread (black spheres) and maximum crano-caudal spread from models of Allen et al. (2013) (white spheres) to estimate segment volumes. **A: Plateosaurus**, **B: Coelophysoid**, **C: Allosaurus**, **D: Microraptor**, **E: Yixianornis**.

5.5. Discussion

5.5.1. Segment specific relationships between skeletal volume and skin volume

In this study, segment specific relationships were generated to determine the expansion factor required to convert skeletal hull volume to skin volume. Relationships for different segments were found to vary in 30 out of 55 comparisons of segment pairs in the ‘all species’ analysis (Supplementary Information 5.2), reflecting the different amount of soft tissue present around the skeletal material in different body segments. The required conversions were also found to differ significantly across ‘bird’ and ‘reptile’ data subsets within seven of the eleven body segments identified here (Figure 5.1, Supplementary Information 5.3). Some of the differences between corresponding segments (e.g. forelimb segments) in birds and reptiles are expected, given the drastically different locomotor behaviours of bipedal birds and sprawled, quadrupedal reptiles. The head and toe segments were found to have a statistically similar ratio of skeletal volume to skin volume for the ‘bird’ and the ‘reptile’ groups (though the ANCOVA p values of 0.023 and 0.06 are very low) (Supplementary Information 5.3). This statistical similarity could be attributed to the fact that these segments consistently have minimal soft tissue around the skeletal material, which is the case for all specimens studied here. Perhaps more interesting are the thigh and tail segments which, despite drastically different appearances in birds compared to the reptile group, have statistically similar relationships (Supplementary Information 5.3). However, the p values from the ANCOVA tests are still low (0.206 and 0.174 for thigh and tail respectively), indicating a fairly low degree of similarity between groups (Supplementary Information 5.3). These similarities could reflect the fact that, despite the externally different morphologies of tails and thigh skin segments, the same volume could be present with a different distribution. For example in the thigh of a bird, the mass is concentrated at the proximal end of the segment, while mass distribution is more even across the length of a thigh of a crocodylian. This would affect the CoM of the skin segment, but not the expansion factor required to

convert skeletal volume to skin volume. The observed similarities could also be driven by variation present within data subsets, a factor likely to be particularly relevant for the bird specimens (e.g. tail relationship in birds has relatively high degree of scatter, $r^2 = 0.804$). These unexpected similarities could also be partly a result of the convex hulling process. Convex hull volume is not an accurate value for true bone volume, and the shape differences between bird and reptile femurs, for example, will result in different amounts of ‘empty’ volume within the convex hulls, which could influence relationships. This is a potential avenue for future exploration; do any segment relationships improve if an alternative method (e.g. alpha shapes) was used to generate more refined models of skeletal volume?

The majority of the trend lines generated from the data subsets here had mean percentage prediction error values of lower than 5% (48 out of 55). These low values are encouraging for application of these relationships to fossil taxa, indicating that they are able to predict skin volume within a narrow margin of the true value. Even the maximum MPPE here (8.65%) is less than for the relationships of (Brassey and Sellers, 2014) when predicting whole body mass using convex hulls (11-20%), and much lower than for predictive models using single bones to estimate whole body mass (e.g. 25-71% (Campione and Evans, 2012), 25% (Campione, 2017) and 13-128% (Field et al., 2013)). Additionally, the relationships here which had greater than 5% error were small segments which would have minimal effects on whole body CoM position (e.g. bird manus, reptile pedal phalanges).

5.5.2. Method validation - predicting CoM in extinct taxa using extant-based convex hulling

5.5.2.1. Using convex hull CoMs as segment CoM positions

Clearly, the skeletal hull for any given segment is not the same shape as the corresponding skin outline, and therefore will not have the same CoM. I sought to investigate the magnitude

of these differences in a segment context, and to examine what effect they have on whole body CoM position.

Differences between convex hull and skin CoM for segments were as high as 49mm (for the neck segment of the rhea) (Supplementary Information 5.6). Discounting the large bodied rhea, which displays absolutely larger errors by virtue of its larger size, the buzzard displayed larger errors than the two similarly sized reptiles studied (maximum error: 20 versus 6.6mm) (Supplementary Information 5.6). The errors present in the proximal limb segments of the two birds are a reflection of the highly tapered form of the skin volumes, a consequence of the concentration of muscular tissues at the proximal ends of limbs for energy conservation (Kardong, 2012). The resulting errors present in the forelimbs of birds (e.g. 20mm for the buzzard upper arm) predominantly affect the medio-lateral dimension due to the orientation of the forelimb in the standard posture of the models (Supplementary Information 5.6). These errors will not affect the final CoM value, as bilateral symmetry is assumed for all specimens, by placing the CoM in the midline medio-laterally. However, the errors resulting from tapered hindlimb segments mainly result in a more ventral segment CoMs, but also impact the cranio-caudal dimension in the case of the buzzard (Supplementary Information 5.6). For studies which require highly accurate values for individual segment CoMs, this approach may therefore not be suitable for certain body segments.

Despite differences of up to 49mm between skeletal hull CoM and skin CoM at a segment level (Supplementary Information 5.6), when segment CoMs are summed to give a whole body CoM estimate, the final differences are small relative to body size (Figure 5.2). The maximum error detected for whole body CoM was 11mm for the rhea, weighing over 7kg, followed by the buzzard at 3mm error, for a small bird weighing 0.69kg (Supplementary Information 5.6).

5.5.2.2. *Selection of segment ‘types’ for extinct taxa*

Birds and crocodylians represent the closest living relatives of extinct dinosaurs. However, these organisms represent specialised morphologies in their own right, with considerable variation in the ratio of skeletal to skin volume present even within those groups (Figure 5.1).

The extinct dinosaurs also show tremendous variability in body plan, locomotor specialisations and body size, as demonstrated by the relatively limited range of fossil taxa modelled here (Figure 5.3). For these reasons, it is not possible to confidently assume that extinct dinosaurs should be modelled as either completely bird- or reptile-like.

However, assigning segment ‘type’ is required in order to use methods which ground dinosaurs in data from extant animals, in an attempt to reduce the subjectivity present in many existing volumetric methods. Such decisions on segment ‘type’ introduce uncertainty, and subjectivity into this new method. The resulting error was identified as being substantial, regardless of the body plan or size of the fossil species (Figure 5.3). It is possible that some, if not all of these fossil species were comprised of segments which had unique ratio of skeleton to soft tissue, beyond those captured here, which would result in further error.

5.5.2.3. *Comparisons to existing work and future steps*

This study successfully quantified the segment-specific relationships between skeletal and skin volume in a range of extant birds, crocodylians and lepidosaurs. This formed the basis for application of this new methodology to estimate segment skin volumes, and subsequently whole body CoM, in five fossil taxa (Figure 5.3).

The whole body CoM positions estimated by the new method are notably different from the CoMs estimated by the models of Allen et al. (2013), and the maximum error margins here

are substantially larger than in this previous study (Figure 5.3). For the four long tailed taxa, the new CoM positions are more caudal, to varying degrees. This is particularly extreme in the cases of *Coelophysis* and *Microraptor*, where the “best guess” CoM position lies within the tail segment along the cranio-caudal axis. This is in large part due to the large ‘all species’ expansion factor for the tail segment. Meanwhile, the CoM position for the *Yixianornis* (a bird, close to crown Aves) lies just caudal to the shoulder joint, and cranial to the maximally cranial CoM of Allen et al. (2013). Though unexpected, this position is not unprecedented – some modern birds were found to possess CoMs in similarly close proximity to the shoulder joint along the cranio-caudal axis too (e.g. hummingbird, kingfisher) (see Chapter 4).

However, the error for the new method is entirely grounded in data from extant, closely related taxa. That this error is larger than for the subjective modelling approach of Allen et al. (2013) speaks to the substantial, previously underappreciated, biological variability present even between these closely related taxa. This casts significant doubt over use of a relationship based on mammalian taxa (Sellers et al., 2012), to extinct dinosaurs (e.g. Bates et al., 2016, Sellers et al., 2013). Additionally, the results suggest that segments possess unique skeletal-to-skin expansion factors (Supplementary Information 5.2), indicating segments should be modelled heterogeneously in order to derive more biologically realistic whole body CoM positions, unlike previous studies (e.g. Bates et al., 2016, Sellers et al., 2013). Before application of this method to a range of fossil archosaurs in order to draw meaningful conclusions on their biology, the dataset behind this methodology should be expanded. The dataset here represents a significant increase over the sample sizes used to generate previous relationships (e.g. 14 mammals in (Sellers et al., 2012), nine birds in (Brassey and Sellers, 2014) and 20 pigeons in (Brassey et al., 2016)). However, 48 specimens is a small number of samples to fully represent the range of body morphologies and sizes

present within archosaurs and lepidosaurs. The addition of more large bodied specimens should be a particular focus, including fully grown ratites.

It should be noted that this dataset includes juvenile ratites and crocodylians. It is likely that the ratio of skeletal volume to soft tissue volume, which is the foundation of this study, varies across ontogeny. Studies in birds have found muscle mass scales with positive allometry with age (e.g. Picasso, 2015, Rose et al., 2016). Though a study of crocodylian musculature (Allen et al., 2010) found an isometric relationship across a range of body sizes, it is possible that changes to osteology would change the convex hull volume around the skeletal material, and therefore alter the soft tissue to bone ratio. Certainly, for the ratite specimens, adult specimens should ideally be used in order to match the growth state of the other specimens, and the fossils which are the subjects of the resulting investigation. If these limitations are acknowledged and suitably addressed, the inclusion of juveniles has the potential to provide benefits. For example, it would increase the size range it is possible to study (particularly in case of crocodylians). Additionally, it could also shed light on the juvenile state and therefore enable more quantitative investigations into likely mass properties, and subsequently behaviours, of juvenile fossil specimens.

5.6. Conclusion

This study successfully established the relationship between skeletal and skin volume in individual body segments across a range of extant archosaurs and lepidosaurs. Skeletal to skin expansion factors were found to differ significantly across different body segments, highlighting the need for heterogeneous expansions in studies wishing to estimate whole body CoM position. This new method offers several benefits over previously published techniques, including quantified error margins and objective generation of skin outlines. However, due to uncertainty in segment ‘type’ (bird or reptile like) assignment in fossil taxa,

the maximum potential error in CoM position was found to be substantial. This considerable error margin suggests that CoM positions predicted for fossil species by current qualitative methods should be interpreted with caution.

5.7. Supplementary Information

Supplementary Information 5.1: Table indicating the segment exponents ('bird', 'reptile' or 'all species') applied to the segments of each fossil specimen in order to derive the "best-guess" whole body CoM positions.

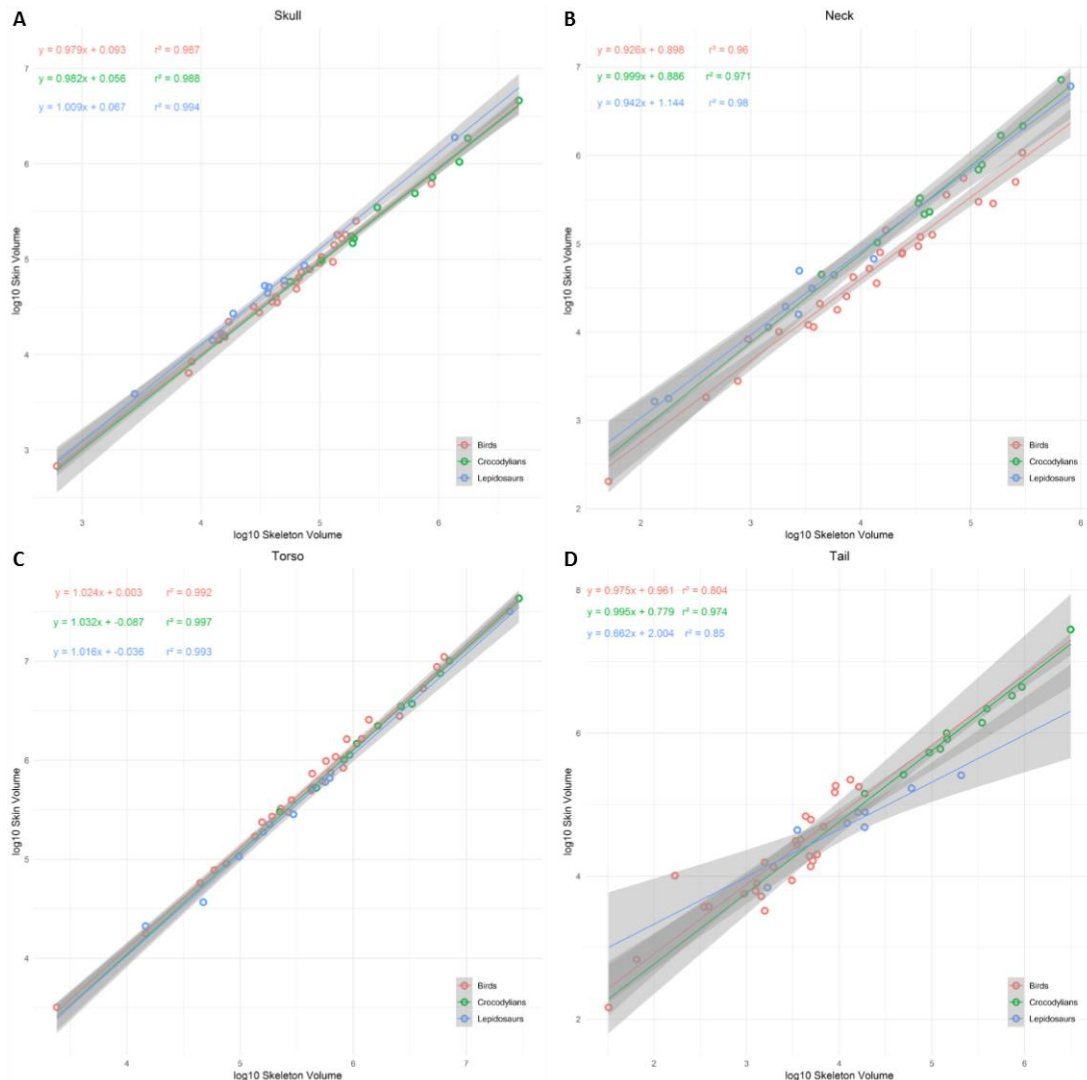
	Head	Neck	Torso	Tail	Arm	Forearm	Hand	Thigh	Shank	MT	Foot
Plateosaurus	All species	Bird	Reptile	All species	Reptile	Reptile	Reptile	All species	Bird	Bird	All species
Coelophysis	All species	Bird	Reptile	All species	Reptile	Reptile	Reptile	All species	Bird	Bird	All species
Allosaurus	All species	Reptile	Reptile	All species	Reptile	Reptile	Reptile	All species	Bird	Bird	All species
Microraptor	All species	Bird	Reptile	All species	Bird	Bird	Bird	All species	Bird	Bird	All species
Yixianornis	All species	Bird	Bird	All species	Bird	Bird	Bird	All species	Bird	Bird	All species

Supplementary Information 5.2: Results of post-hoc Tukey test to explore differences in relationships for different body segments across all specimens. A significant result indicates a significant difference in the relationships between the groups specified. Significant results (at $p < 0.01$) are highlighted in red.

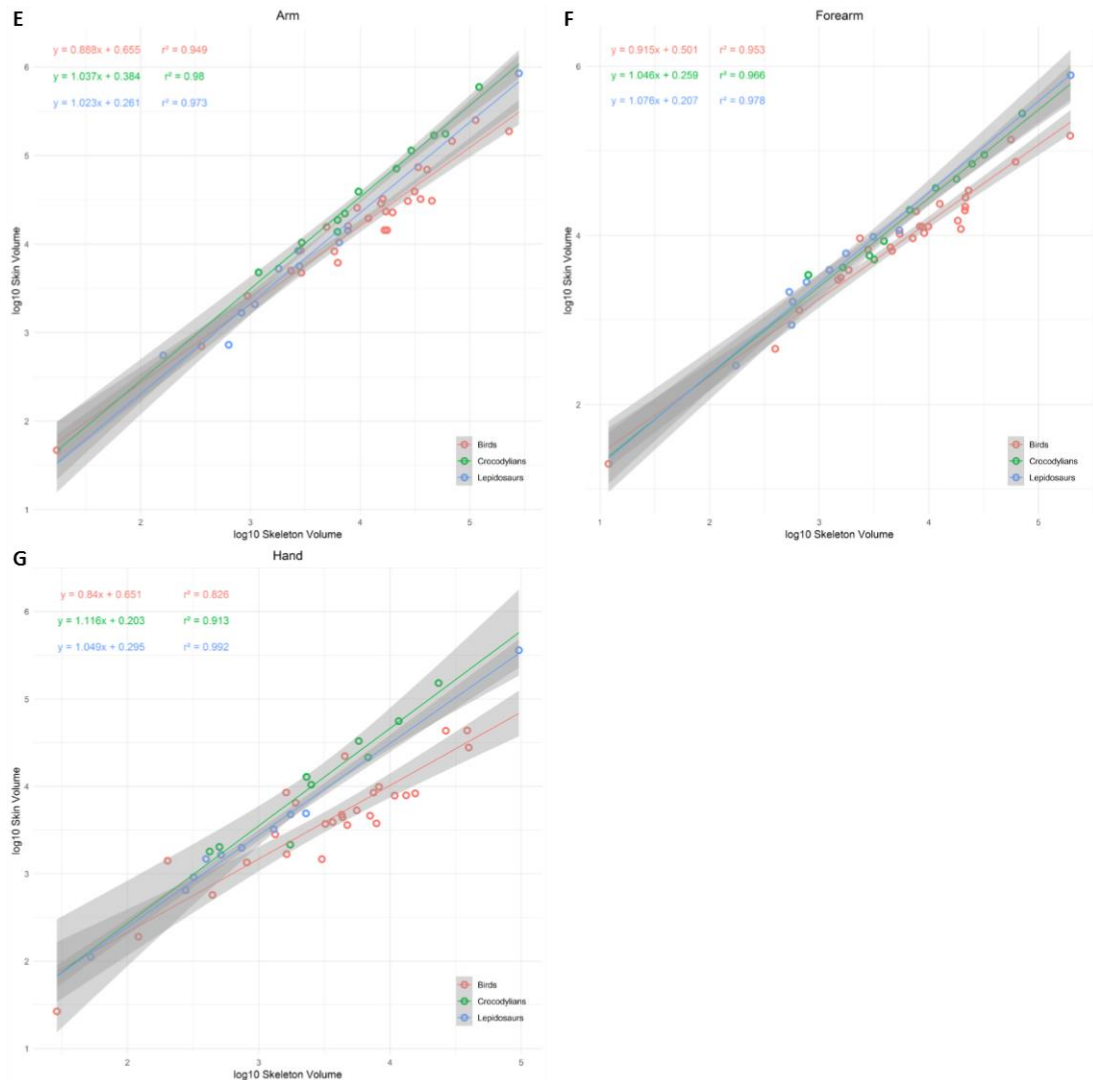
	Neck	Torso	Tail	Arm	Forearm	Hand	Thigh	Shank	MT	Toes
Skull	<0.001	0.023	<0.001	<0.001	<0.001	0.023	<0.001	<0.001	0.920	0.001
Neck		<0.001	0.988	<0.001	<0.001	<0.001	0.921	<0.001	<0.001	<0.001
Torso			<0.001	0.812	0.992	1.000	<0.001	0.779	0.663	0.999
Tail				<0.001	<0.001	<0.001	0.246	<0.001	<0.001	<0.001
Arm					1.000	0.844	<0.001	1.000	0.010	0.998
Forearm						0.995	<0.001	1.000	0.084	1.000
Hand							<0.001	0.813	0.649	1.000
Thigh								<0.001	<0.001	<0.001
Shank									0.008	0.996
MT										0.164

Supplementary Information 5.3: Results of ANCOVA test on lines in Figure 5.1, where a significant result indicates a significant difference in the relationship between the ‘bird’ and ‘reptile’ groups. Significant results (at $p < 0.01$) are highlighted in red.

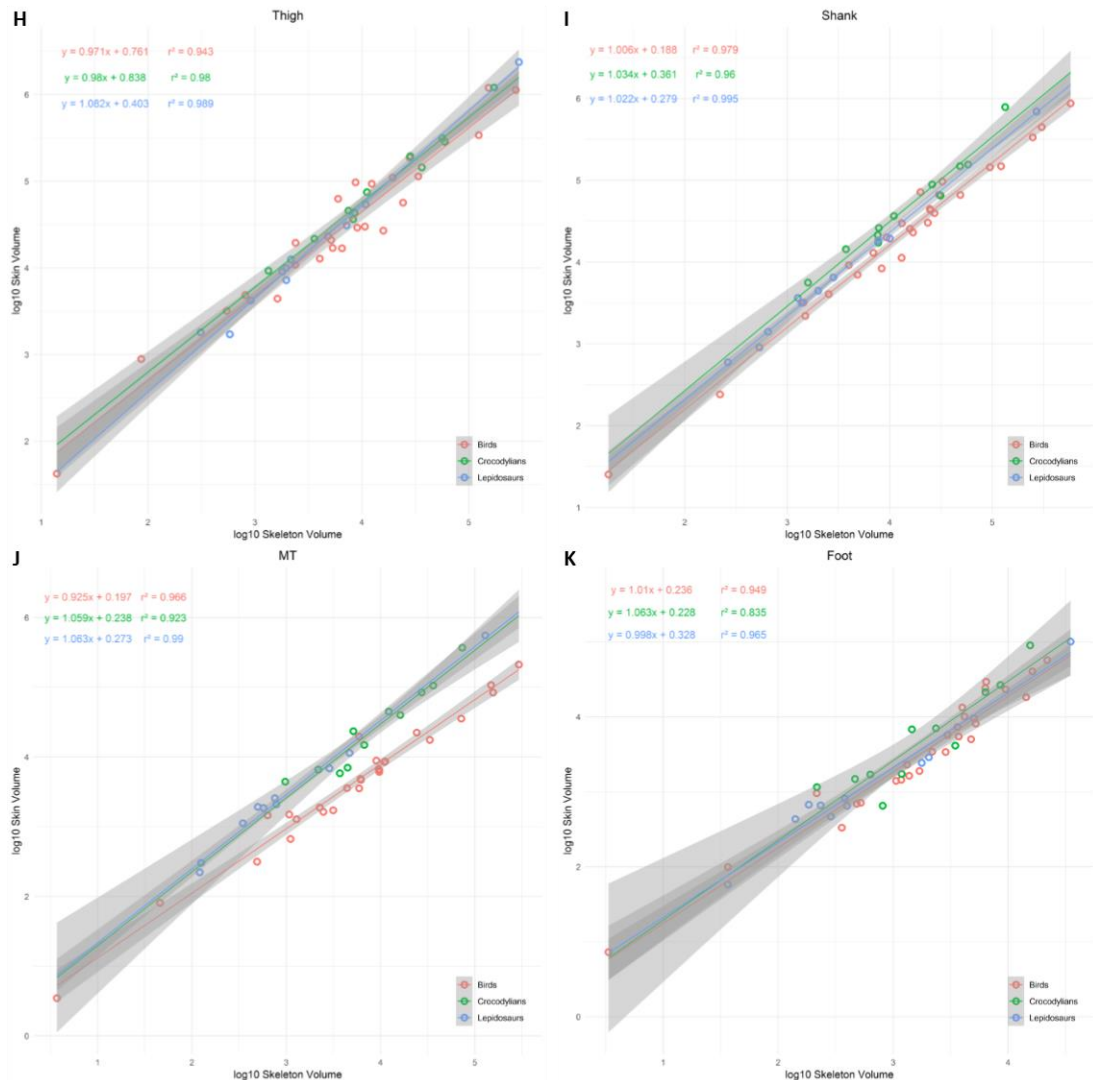
	F value	p value
Skull	5.488	0.024
Neck	51.896	<0.001
Torso	9.478	0.004
Tail	1.909	0.174
Arm	19.550	<0.001
Forearm	30.189	<0.001
Hand	26.629	<0.001
Thigh	1.649	0.206
Shank	35.030	<0.001
MT	112.336	<0.001
Toes	3.562	0.066



Supplementary Information 5.4 (i): Plots showing the relationship between skeletal hull volume and skin volume for individual body segments. Relationships are shown with specimens split into birds, crocodylians and lepidosaurs. **A:** head, **B:** neck, **C:** torso, **D:** tail, **E:** arm, **F:** forearm, **G:** hand, **H:** thigh, **I:** shank, **J:** tarsometatarsal/metatarsals, **K:** toes.



Supplementary Information 5.4 (ii): Plots showing the relationship between skeletal hull volume and skin volume for individual body segments. Relationships are shown with specimens split into birds, crocodylians and lepidosaurs. **A:** head, **B:** neck, **C:** torso, **D:** tail, **E:** arm, **F:** forearm, **G:** hand, **H:** thigh, **I:** shank, **J:** tarsometatarsal/metatarsals, **K:** toes.



Supplementary Information 5.4 (iii): Plots showing the relationship between skeletal hull volume and skin volume for individual body segments. Relationships are shown with specimens split into birds, crocodylians and lepidosaurs. **A:** head, **B:** neck, **C:** torso, **D:** tail, **E:** arm, **F:** forearm, **G:** hand, **H:** thigh, **I:** shank, **J:** tarsometatarsal/metatarsals, **K:** toes.

Supplementary Information 5.5: Results of ANCOVA, and post-hoc Tukey test on lines in Supplementary Information 5.4, where a significant result indicates a significant difference in the relationships between the groups specified (B: birds, C: crocodylians, L: lepidosaurs). Significant results (at $p < 0.01$) are highlighted in red.

	F value	ANCOVA p value	Tukey p value B v C	Tukey p value B v L	Tukey p value L v C
Skull	11.8257	0.0001	0.988	0.0002	0.001
Neck	25.4686	<0.0001	<0.0001	<0.0001	0.9988
Torso	5.8572	0.0056	0.2639	0.0046	0.2789
Tail	2.4301	0.1003	0.9605	0.1143	0.13
Arm	16.94	<0.0001	<0.0001	0.1923	0.006
Forearm	14.7606	<0.0001	0.0001	0.0006	0.9637
Hand	15.2188	<0.0001	<0.0001	0.0098	0.1665
Thigh	1.1643	0.322	0.3033	0.8556	0.7161
Shank	22.5459	<0.0001	<0.0001	0.0073	0.028
MT	55.4071	<0.0001	<0.0001	<0.0001	0.6838
Toes	2.3758	0.1048	0.0872	0.7248	0.5018

Supplementary Information 5.6: **A:** Differences between skeletal hull CoM and skin CoM for four specimens. **B:** Whole body CoMs derived from skeletal segment CoMs and skin segment CoMs, with 3D distances between the two estimates. Where +x is right, +y is dorsal and +z is caudal. All measurements in mm.

A		Head	Neck	Torso	Tail	Arm	Forearm	Hand	Thigh	Shank	MT	Toes
Iguana	x	0.0	2.0	0.0	-0.1	-5.0	-1.0	2.2	0.0	-1.0	0.7	1.0
	y	1.0	6.0	0.0	2.8	0.0	-1.0	-0.2	-4.0	5.0	-0.6	-0.7
	z	-1.0	1.0	2.0	-1.9	-1.0	1.0	0.5	-3.0	-2.0	-0.4	-0.5
Alligator	x	0.4	0.0	-1.0	-0.1	-2.0	2.0	-0.2	-1.0	-2.0	-0.7	-1.1
	y	1.5	6.0	0.0	1.6	-1.0	0.0	0.5	1.0	1.0	1.9	-0.2
	z	-0.5	0.0	0.0	-6.6	-1.0	1.0	1.1	-2.0	-1.0	-0.7	-1.4
Rhea	x	-0.8	-0.2	0.0	-1.0	26.0	9.0	5.0	7.0	-2.0	0.0	0.1
	y	0.3	0.3	7.0	2.0	-1.0	1.0	2.0	-35.0	-25.0	3.0	0.6
	z	-2.4	48.9	-17.0	12.0	-5.0	-2.0	-1.0	0.0	3.0	-3.0	-0.6
Buzzard	x	0.0	-2.4	-2.0	-3.0	20.0	13.0	3.0	1.0	-1.0	-1.0	0.0
	y	-1.0	2.3	2.0	2.0	1.0	0.0	1.0	-6.0	-6.0	-6.0	0.4
	z	-2.0	0.4	7.0	2.0	3.0	-1.0	0.0	-4.0	-1.0	0.0	0.0

B		Skeletal CoM	Skin CoM	3D distance
Iguana	x	-0.5	-0.5	
	y	0.6	0.0	0.849
	z	-60.4	-61	
Alligator	x	-12.7	-12.2	
	y	0.6	-0.4	2.035
	z	-50.2	-48.5	
Rhea	x	6.4	4.4	
	y	-78.7	-71.6	10.808
	z	-77.7	-69.8	
Buzzard	x	5.3	4.4	
	y	-26.3	-26.2	3.134
	z	-59.8	-62.8	

5.8. Appendices

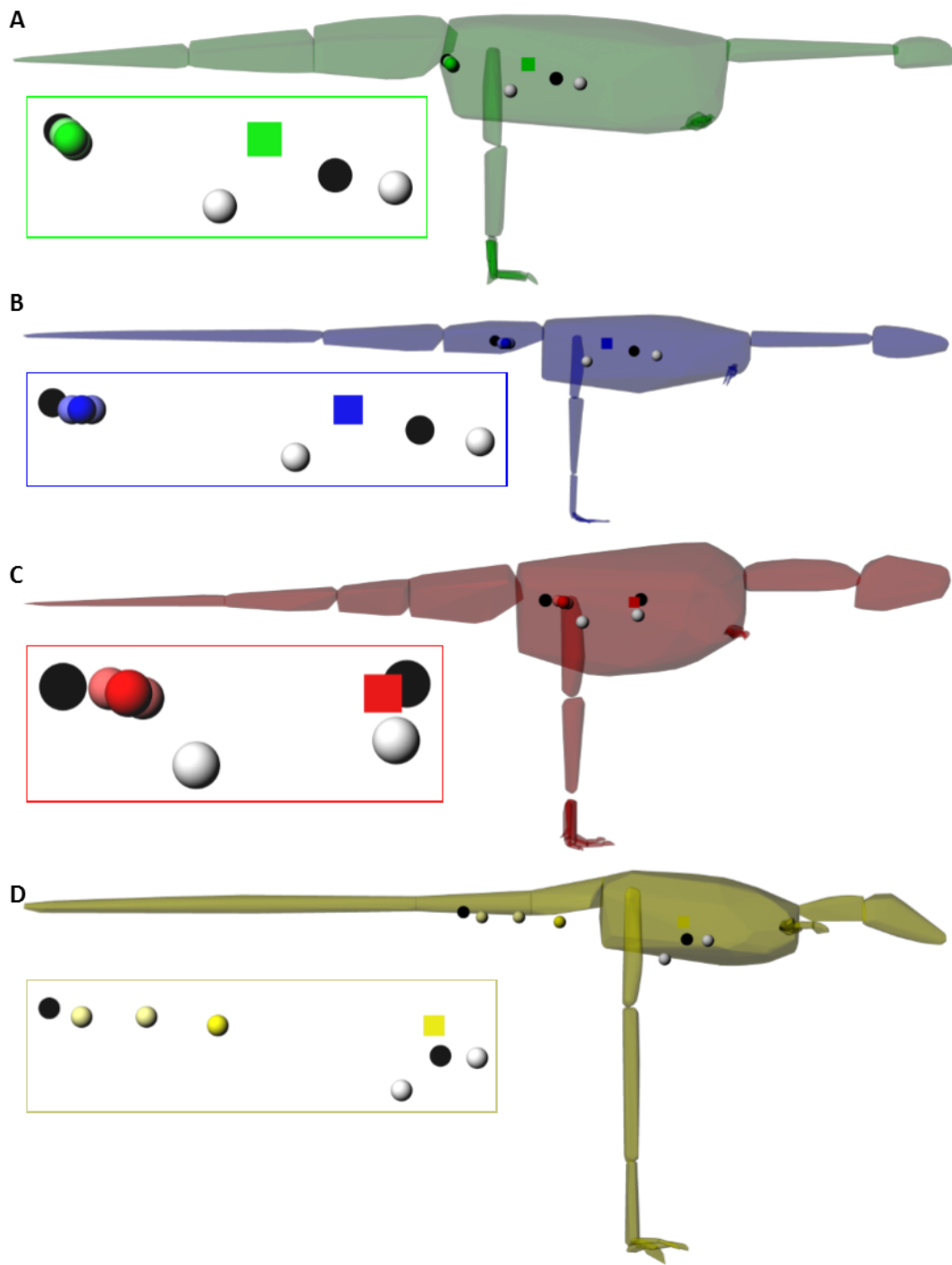
Appendix 5.1: Examining the results of an alternative application of the expansion equations for the tail segment.

For the original generation of a “best guess” model (as presented in the main body of Chapter 5 here), the ‘all species’ exponent was applied to the tail segments of all fossil species in order to derive a volume estimate. This ‘all species’ exponent was selected as there were no significant differences detected between the expansion factors for birds compared to the group containing crocodylians and lepidosaurs. However, when used to determine whole body CoM for fossil species with large tails (i.e. all fossils studied here with the exception of *Yixianornis*), a very caudal CoM was predicted (see coloured spheres in Appendix 5.1.1). The resulting “best guess” CoMs lie outside the error margins defined by Allen et al. (2013), and caudal to the hip joint in all cases. This was determined to be primarily due to an unrealistically high tail volume.

Therefore, the application of scaling exponent to tail segments was re-examined. It was found that the expansion produced by the bird only equation was large, and it was this which was skewing the “best guess” CoMs. Birds possess only a short pygostyle, which has limited external muscular control; unlike the reptiles which possess long tails, with extensive musculature in the form of the caudofemoralis. Therefore, the skin outline of the tail segments had drastically different compositions for the bird versus the ‘reptile’ group. Because of these fundamental differences in morphology, application of the ‘all species’ exponent was deemed appropriate for only *Yixianornis*, which possesses a pygostyle much like modern birds. For the other, long-tailed fossils, an alternative “best guess” CoM was generated using the ‘reptile’ relationship for the tail segment.

The new “best guess” CoMs all lie within the error margins of Allen et al. (2013) (see coloured cubes in Appendix 5.1.1). These new estimates are also now biologically feasible; the CoMs are more cranially positioned, which would enable the hindfoot to be placed below the CoM during locomotion.

In conclusion, by constraining the assignment of segment type for the tail using biological information as well as statistical methods, more biologically feasible CoM estimates are produced for the four long tailed fossils here. Though this would shrink the overall error margins for the new method presented in Chapter 5, it does not alter the conclusions presented in Section 5.6.



Appendix 5.1.1: Renders in lateral view of the skeletal convex hulls of fossils species studied here. Showing whole body CoM positions derived using: best guess models using 'all species' exponent for tail (coloured spheres), best guess models using 'reptile' exponent for tail (coloured cubes), error from predictive equations (grey spheres), maximum cranio-caudal spread (black spheres) and maximum cranio-caudal spread from models of Allen et al. (2013)

(white spheres) to estimate segment volumes. **A:** *Plateosaurus*, **B:** *Coelophysis*, **C:** *Allosaurus*,

D: *Microraptor*.

5.9. References

- ALEXANDER, R. M. 1983. *Animal Mechanics*, London, Blackwell Scientific.
- ALEXANDER, R. M. 1985. Mechanics of posture and gait of some large dinosaurs. *Zoological Journal of the Linnean Society*, 83, 1-25.
- ALLEN, V., ELSEY, R. M., JONES, N., WRIGHT, J. & HUTCHINSON, J. R. 2010. Functional specialization and ontogenetic scaling of limb anatomy in *Alligator mississippiensis*. *Journal of Anatomy*, 216, 423-445.
- ALLEN, V., HUTCHINSON, J. R., BATES, K. T. & LI, Z. 2013. Linking the evolution of body shape and locomotor biomechanics in bird-line archosaurs. *Nature*, 497, 104-107.
- ALLEN, V., PAXTON, H. & HUTCHINSON, J. R. 2009. Variation in center of mass estimates for extant sauropsids and its importance for reconstructing inertial properties of extinct archosaurs. *Anatomical Record*, 292, 1442-1461.
- ANDERSON, J. F., HALL-MARTIN, A. & RUSSELL, D. A. 1985. Long-bone circumference and weight in mammals, birds and dinosaurs. *Journal of Zoology*, 207, 53-61.
- BASU, C., FALKINGHAM, P. L. & HUTCHINSON, J. R. 2016. The extinct, giant giraffid *Sivatherium giganteum*: Skeletal reconstruction and body mass estimation. *Biology Letters*, 12.
- BATES, K. T., FALKINGHAM, P. L., MACAULAY, S., BRASSEY, C. & MAIDMENT, S. C. R. 2015. Downsizing a giant: re-evaluating *Dreadnoughtus* body mass. *Biology Letters*, 11, 20150215.
- BATES, K. T., MANNING, P. L., HODGETTS, D. & SELLERS, W. I. 2009. Estimating Mass Properties of Dinosaurs Using Laser Imaging and 3-D Computer Modelling. *PLoS ONE*, 4, 1-26.
- BATES, K. T., MANNION, P. D., FALKINGHAM, P. L., BRUSATTE, S. L., HUTCHINSON, J. R., OTERO, A., SELLERS, W. I., SULLIVAN, C., STEVENS, K. A. & ALLEN, V. 2016. Temporal and phylogenetic evolution of the sauropod dinosaur body plan. *Royal Society Open Science*, 3, 150636.
- BATES, K. T., SELLERS, W. I., MANNING, P. L. & MARGETTS, L. 2010. Sensitivity analysis in evolutionary robotic simulations of bipedal dinosaur running. *Journal of Vertebrate Paleontology*, 30, 458-466.
- BRASSEY, C. A. & GARDINER, J. D. 2015. An advanced shape-fitting algorithm applied to quadrupedal mammals: improving volumetric mass estimates. *Royal Society Open Science*, 2.
- BRASSEY, C. A., HOLDAWAY, R. N., PACKHAM, A. G., ANNÉ, J., MANNING, P. L. & SELLERS, W. I. 2013. More than One Way of Being a Moa: Differences in Leg Bone Robustness Map Divergent Evolutionary Trajectories in Dinornithidae and Emeidae (Dinornithiformes). *PLoS ONE*, 8, 1-10.

- BRASSEY, C. A., MAIDMENT, S. C. R. & BARRETT, P. M. 2015. Body mass estimates of an exceptionally complete Stegosaurus (Ornithischia: Thyreophora): comparing volumetric and linear bivariate mass estimation methods. *Biology Letters*, 11, 1-5.
- BRASSEY, C. A., O'MAHONEY, T. G., KITCHENER, A. C., MANNING, P. L. & SELLERS, W. I. 2016. Convex-hull mass estimates of the dodo (*Raphus cucullatus*): application of a CT-based mass estimation technique. *PeerJ*, 4, e1432.
- BRASSEY, C. A. & SELLERS, W. I. 2014. Scaling of convex hull volume to body mass in modern primates, non-primate mammals and birds. *PLoS ONE*, 9, 1-12.
- CAMPIONE, N. E. 2017. Extrapolating body masses in large terrestrial vertebrates NICOLÁS E. CAMPIONE EXTRAPOLATING BODY MASSES. *Paleobiology*, 43, 693-699.
- CAMPIONE, N. E. & EVANS, D. C. 2012. A universal scaling relationship between body mass and proximal limb bone dimensions in quadrupedal terrestrial tetrapods. *BMC Biology*, 10, 1-22.
- COLBERT, E. H. 1962. The Weights of Dinosaurs. *American Museum Novitates*, 2076, 1-16.
- FARLOW, J. O., SMITH, M. B. & ROBINSON, J. M. 1995. Body Mass, Bone "Strength Indicator" and Cursorial Potential of *Tyrannosaurus rex*. *Journal of Vertebrate Paleontology*, 15, 713-725.
- FIELD, D. J., LYNNER, C., BROWN, C. & DARROCH, S. A. F. 2013. Skeletal correlates for body mass estimation in modern and fossil flying birds. *Plos One*, 8, e82000-e82000.
- GATESY, S. M. 1990. Caudofemoral musculature and the evolution of theropod locomotion. *Paleobiology*, 16, 170-186.
- GATESY, S. M., BÄKER, M. & HUTCHINSON, J. R. 2009. Constraint-based exclusion of limb poses for reconstructing theropod dinosaur locomotion. *Journal of Vertebrate Paleontology*, 29, 535-544.
- GATESY, S. M. & DIAL, K. P. 1996. Locomotor modules and the evolution of avian flight. *Evolution*, 50, 331-340.
- GREGORY, W. K. 1905. The Weight of the Brontosaurus. *Science*, 22, 572.
- HENDERSON, D. M. 1999. Estimating the masses and centers of mass of extinct animals by 3-D mathematical slicing. *Paleobiology*, 25, 88-106.
- HENDERSON, D. M. 2003. Effects of stomach stones on the buoyancy and equilibrium of a floating crocodilian: A computational analysis. *Canadian Journal of Zoology*, 81, 1346-1357.
- HENDERSON, D. M. 2006. Burly gaits; centers of mass, stability, and the trackways of sauropod dinosaurs. *Journal of Vertebrate Paleontology*, 26, 907-921.
- HENDERSON, D. M. 2010. Pterosaur body mass estimates from three-dimensional mathematical slicing. *Journal of Vertebrate Paleontology*, 30, 768-785.

- HENDERSON, D. M. 2018. A buoyancy, balance and stability challenge to the hypothesis of a semi-aquatic Spinosaurus Stromer, 1915 (Dinosauria: Theropoda). *PeerJ*, 6, e5409.
- HENDERSON, D. M. & NICHOLLS, R. 2015. Balance and Strength—Estimating the Maximum Prey-Lifting Potential of the Large Predatory Dinosaur *Carcharodontosaurus saharicus*. *The Anatomical Record*, 298, 1367-1375.
- HENDERSON, D. M. & SNIVELY, E. 2004. Tyrannosaurus en pointe: allometry minimized rotational inertia of large carnivorous dinosaurs. *Proceedings of the Royal Society B: Biological Sciences*, 271, S57-S60.
- HUTCHINSON, J. R. & ALLEN, V. 2009. The evolutionary continuum of limb function from early theropods to birds. *Naturwissenschaften*, 96, 423-448.
- HUTCHINSON, J. R., BATES, K. T., MOLNAR, J., ALLEN, V. & MAKOVICKY, P. J. 2011. A Computational Analysis of Limb and Body Dimensions in *Tyrannosaurus rex* with Implications for Locomotion, Ontogeny, and Growth. *PLoS ONE*, 6, 1-20.
- HUTCHINSON, J. R., NG-THOW-HING, V. & ANDERSON, F. C. 2007. A 3D interactive method for estimating body segmental parameters in animals: Application to the turning and running performance of *Tyrannosaurus rex*. *Journal of Theoretical Biology*, 246, 660-680.
- KARDONG, K. V. 2012. *Vertebrates: Comparative Anatomy, Function, Evolution*, New York, McGraw-Hill.
- MAIDMENT, S. C. R., HENDERSON, D. M. & BARRETT, P. M. 2014. What drove reversions to quadrupedality in ornithischian dinosaurs? Testing hypotheses using centre of mass modelling. *Naturwissenschaften*, 101, 989-1001.
- MALLISON, H. 2010. The digital Plateosaurus I: body mass, mass distribution, and posture assessed using CAD and CAE on a digitally mounted complete skeleton. *Palaeontologia Electronica*, 13, 1-26.
- PAUL, G. S. 1997. Dinosaur Models: The Good, The Bad, and Using Them to Estimate the Mass of Dinosaurs. *Dinofest International Proceedings*, 129-142.
- PICASSO, M. B. J. 2015. Ontogenetic Scaling of the Hindlimb Muscles of the Greater Rhea (*Rhea americana*). *Anatomia, Histologia, Embryologia*, 44, 452-459.
- ROSE, K. A., NUDDS, R. L. & CODD, J. R. 2016. Variety, sex and ontogenetic differences in the pelvic limb muscle architectural properties of leghorn chickens (*Gallus gallus domesticus*) and their links with locomotor performance. *Journal of Anatomy*, 228, 952-964.
- SELLERS, W. I., HEPWORTH-BELL, J., BRASSEY, C. A., EGERTON, V. M., MANNING, P. L., FALKINGHAM, P. L. & BATES, K. T. 2012. Minimum convex hull mass estimations of complete mounted skeletons. *Biology Letters*, 8, 842-845.
- SELLERS, W. I., MARGETTS, L., CORIA, R. A. & MANNING, P. L. 2013. March of the titans: The locomotor capabilities of sauropod dinosaurs. *PLoS ONE*, 8, 1-21.

SELLERS, W. I., POND, S. B., BRASSEY, C. A., MANNING, P. L. & BATES, K. T. 2017. Investigating the running abilities of *Tyrannosaurus rex* using stress-constrained multibody dynamic analysis. *PeerJ*, 5, e3420.

SNIVELY, E., O'BRIEN, H., HENDERSON, D. M., MALLISON, H., SURRING, L. A., BURNS, M. E., HOLTZ, J. T. R., RUSSELL, A. P., WITMER, L. M., CURRIE, P. J., HARTMAN, S. A. & COTTON, J. R. 2018. Lower rotational inertia and larger leg muscles indicate more rapid turns in tyrannosaurids than in other large theropods. *PeerJ Preprints*, 6, e27021v1.

CHAPTER 6 - DISCUSSION

6.1. Overview

This thesis set out to address the following key objectives:

- 1) Assess the absolute accuracies of three commonly used methods for determining centre of mass position, and their applicability to biological specimens.
- 2) Investigate the integumentary changes which occurred in bird-line archosaurs with the advent of feathers, in the context of impact on whole body centre of mass position.
- 3) Explore links between centre of mass position and locomotor behaviours across Aves.
- 4) Establish and apply a new methodology for the estimation of centre of mass position in fossil archosaurs, grounded in an extensive extant dataset.

In summary, this thesis found that:

- 1) The accuracy and repeatability of the scales and digital methods for CoM estimation were high, but they each posed unique challenges when applied to biological specimens (Chapter 2).
- 2) The development of a feathered integument in bird-line archosaurs resulted in a marked ventral CoM shift, of equivalent magnitude to that made by the air cavities (Chapter 3).
- 3) Flying birds were found to have a more dorsally positioned CoM, however this difference was not statistically significant after accounting for phylogeny (Chapter 4).
- 4) The CoM estimates produced for fossil taxa using the new method were different from those of previous studies, and with larger error bars (Chapter 5).

6.2. Methods for CoM estimation

6.2.1. Physical methods for CoM estimation

Chapter 2 successfully established the absolute accuracies of three commonly used methods using test objects with standard geometries. Substantial differences were detected between the two physical methods tested. Suspension performed poorly (error range 8.2 - 38.5mm; Figure 2.8, Table 2.3), while the scales method was found to be highly accurate (less than 1.5mm error; Figure 2.5, Table 2.3). This study highlighted the importance of doing reversed repeats when using the scales method, otherwise the CoM positions derived are inaccurate (Figure 2.5, Table 2.3). These reversed repeats have been done by some previous studies (e.g. Henderson, 2003), but not all (e.g. Clemente, 2014, Henderson, 2006). However, it was identified that application of the scales method to biological specimens would pose difficulties. Primarily, there were practical difficulties when assessing dorso-ventral CoM position for irregularly shaped biological specimens, which would require construction of a custom rig for each specimen/segment being tested. The suspension method was found to have relatively low accuracy, regardless of the number of repeats performed (Figure 2.8, Table 2.3). This to some extent contradicts previous studies which found satisfactory levels of accuracy (e.g. 10mm in Nauwelaerts et al. (2011)) in their variants of the suspension method. Due to the nature of the suspension method, it is likely to contain higher methodological error between runs and between investigators. The high variation identified in this method highlights this (Figure 2.8). Any future work seeking to use a suspension based method should therefore quantify and seek to minimise inherent methodological and inter-investigator errors. Chapter 2 concludes that the scales method is the most accurate and repeatable physical method for quantifying 2D CoM (Figure 2.5, Table 2.3), and can be applied with confidence in future studies of *ex vivo* biological specimens. However it has some limitations when applied to quantify 3D CoM in biological specimens.

6.2.2. Digital method for CoM estimation

Chapter 2 also assessed the accuracy of a digital method for CoM estimation. This was also found to be highly accurate (within 2.4mm; Figure 2.5, Table 2.3), comparable to that of the scales method. This study identified the fundamental method as accurate (in agreement with Allen et al. (2009)), but identified some issues when it is applied to biological specimens. For example, a digital model requires the investigator to assign density values to body segment volumes in order to calculate segment masses. Decisions must be made on the value(s) to be applied, and whether application should be heterogeneous or homogeneous across body segments. The accuracy of the digital model is therefore dependent, to some extent, on the availability of density data appropriate to the biological specimen under study.

There are currently no published segment specific density data for birds, and previously published studies have used a wide range of values (see Table 2.2). A sensitivity analysis assessing the impact of current uncertainty about density data found only small differences (maximum of 3.58mm), provided that reasonable data are assigned to models (Table 2.4, Figure 2.6). Chapter 2 proposed that segment-specific density should be collected in birds to assess the variability present across segments, and in particular to assess potential differences across birds with different body plans and/or life habits. In Chapter 4, segment specific density data were collected from five bird specimens (Supplementary Information 4.2). Average segment densities were applied to all bird models in order to derive CoM estimates based on heterogeneous application of bird segment-specific data, as opposed to the horse and human segment density data used in the sensitivity analysis of Chapter 2. The maximum absolute difference between the heterogeneous and homogeneous CoMs in Chapter 4 was found to be 7mm (for the emu, the largest specimen in the dataset; Figure 4.10). For the three specimens featured in Chapter 2, the maximum difference between

heterogeneous and homogeneous CoMs was small (maximum of 2.61mm; Figure 4.10), within the bounds of the sensitivity analysis of Chapter 2 ($\pm 3.58\text{mm}$; Table 2.4). This indicates that the bird segment density data produce similar CoM estimates to the various non-bird based datasets. This effect of density was deemed to be acceptable for the purposes of this thesis. However, other studies requiring more accurate segment mass properties for birds, or those seeking to identify smaller differences between specimen CoMs, may wish to use bird specific density data. In this case, the segment density dataset established here should ideally be expanded to cover a wider variety of birds, as the comparisons of known versus predicted mass properties in Chapter 4 suggest these density data vary in their suitability across bird species (Figure 4.11).

The digital method used in Chapter 2 offers numerous additional benefits over previously discussed physical methods, including ease of data sharing and manipulation (e.g. for sensitivity analyses); and the use of medical imaging to create models enables visualisation and incorporation of internal structures (e.g. for assessment of air cavities). Chapter 2 concluded that this digital method can be applied with confidence in order to estimate CoM position in extant taxa, though it suggested that additional density data for birds would be useful to ensure the accuracy of models. Subsequent chapters build on this work with the digital method.

6.2.3. Exploring refinements of digital methods - integument

Having demonstrated high levels of accuracy and repeatability in the digital method, this thesis proceeded to examine the impact on predicted CoM position of adding more detail to models. Chapter 3 specifically tackled the impact of integumental changes through Archosauria from scaly skin in crocodylians to a feathered covering in birds. This study found that CoM position was notably affected by the explicit inclusion of a feathered integument

in models, an effect not seen for scaly integument (Figure 3.4). This disparity in integument effect was demonstrated by application of a feathered and scaly integument to the *Microraptor* model. Here, a scaly integument shifted CoM by less than 53% of the shift exerted by the feathered integument (minimum model: 1.57 versus 2.98mm, maximum model: 1.19 versus 3.11mm; Supplementary Text 3.2).

Though the addition of integument had little impact on cranio-caudal CoM position in birds, a feathered integument shifted whole body CoM ventrally in birds & feathered fossil taxa (*Yixianornis* and *Microraptor*). This ventral CoM shift may have facilitated the early development of flight by providing greater inherent stability during volant behaviours (Thomas and Taylor, 2001). This is the first time integument has been explicitly included in models of modern birds and extinct bird-line theropods, an application enabled by the novel dataset on integument mass properties presented in Chapter 3. In several of the extant models, the impact of integument on CoM position was found to be as great as the effect of air cavities (Figure 3.4, Supplementary Text 3.2), which are included as standard in majority of models, raising questions about the ‘standard’ digital modelling procedure. I conclude that future studies should assess the accuracy required from their CoM estimates before deciding on the level of detail to include in their models, a process that can be assisted by the various datasets presented in this thesis. If a research question is likely to be highly sensitive to small changes in CoM position, then air cavities and integument should be explicitly included.

The novel dataset on integument mass properties presented in Chapter 3 represents a sizeable improvement on existing knowledge, but has several limitations. This dataset was comprised of a relatively large number of individuals (49), but these represent a limited number of species (33) and orders (e.g. for birds: 27 individuals, from 17 species, across 10 orders). Additionally, the ‘reptile’ cohort was dominated by lizards (13 lizard versus 9

crocodylian individuals, from 11 lizard versus 5 crocodylian species). This focus on integument from small bodied lizards may not be the best proxy for extinct archosaur species, though the aquatic adapted skin of crocodylians may also be unsuitable. The considerable dataset on integument mass properties is commendable given the time intensive nature of the data collection, with numerous samples taken from each specimen. Modifications to simplify the integument extraction methodology, and to minimise the destructive nature of the testing, have the potential to enable more specimens to be added in future work of this nature.

These data on integument mass properties were also applied to models of extinct taxa in Chapter 3 (Figures 3.4 and 3.5). However, this application was limited, due to use of the models of Allen et al. (2013). These models were originally generated used a manual shape fitting method - ‘maximal’ and ‘minimal’ skin outlines were created around the original 3D skeleton, based qualitatively on knowledge of musculature in extant taxa. The predicted CoMs for these models therefore have considerable error margins, which recognise this subjectivity and uncertainty. In order to increase the confidence around any conclusions drawn from CoM data in extinct taxa, a more objective method is needed for the generation of skin outlines. Conclusions about extinct taxa are further hindered by a current lack of understanding of the links between CoM and locomotor behaviours in extant taxa, particularly in volant behaviours. These links should be quantified in extant birds, before drawing any conclusions about specific locomotor behaviours in extinct, transitional species (discussed below in Section 6.3). Additionally, the amount of variation observed here in bird CoMs and the effect of integument, suggests that use of single individuals are not enough to accurately capture CoM position for an extant group the size of Aves or Crocodylia (as in Allen et al. (2013)). I therefore conclude that more models of extant species, in addition to improved methods for producing extinct models (discussed below in Section 6.4), are

required to assess any evolutionary changes in body plan and CoM position across Archosauria.

6.3. CoM position and locomotion

Having explored methods for determining CoM position in extant taxa, Chapter 4 applied a digital method to 27 extant birds. The primary objective of this chapter was to explore links between body plan, as reflected by CoM position, and locomotor style. Previous studies have found significant differences in the relative investment in forelimb versus hindlimb musculature in birds reliant on terrestrial or volant locomotor behaviours (Heers and Dial, 2015). I hypothesised that these differences would also be detectable at the whole body level, through whole body CoM position. However, Chapter 4 found no statistically significant differences in whole body CoM position between the locomotor groups identified here (Figure 4.3). Substantial variation was detected within the groups here. This is potentially a result of the broad locomotor categories used here (terrestrial, volant or diving), it may be possible to detect significant differences in CoM position if more refined categories were used. However, more specimens would be needed for each of the more specific locomotor groups in order to perform any meaningful statistical tests. Additionally, more samples would help to provide greater coverage of the range of body plans and locomotor types present across Aves. Though the majority of avian orders are represented here, they are each represented by only one specimen, when there is undoubtedly considerable variation present within orders. The degree of CoM variation present within species is also yet to be quantified. It is possible that the axial anatomy of specimens is masking significant differences in the mass properties of the fore- and hindlimbs in taxa with different locomotor specialities. Due to its considerable contribution to whole body mass, the torso segment in particular has the potential to obscure any slight differences in CoM position resulting from differences in limb morphology. Future work on this project is planned to examine linear

proportions and mass properties on a segment-by-segment basis. This will provide a more detailed representation of limb morphology, and may enable more subtle differences between locomotor groups to be elucidated.

Prior to phylogenetic correction of the dataset, significant differences were detected between locomotor groups in the dorso-ventral direction (Figure 4.3). The cause of these differences was explored using segment mass properties - mass, CoM and first mass moments (FMMs). All mass properties for the hindlimb were found to be strongly correlated with dorso-ventral whole body CoM position across all specimens (Table 4.3). This partially supports the hypothesis that limb morphology is driving differences in CoM position, though the differences in whole body CoM were not statistically significant (PGLS, p value > 0.07). This non-significant difference indicated that volant species generally possessed a more dorsal CoM than their terrestrial counterparts (Figure 4.3). A more dorsally positioned CoM is closer to the axis of rotation about the wings, providing greater manoeuvrability in flight, while a more ventral CoM provides greater inherent stability (Thomas and Taylor, 2001). The species included in the volant group in this study use different flight styles - from the soaring buzzard to the continuous flapping of the hummingbird. In a similar way that birds balance these conflicting demands as a result of wing aspect ratios, these species may also have different preferences for the stability versus manoeuvrability benefits resulting from dorso-ventral CoM position.

This study represents a significant step forward in terms of filling the gap in knowledge surrounding the links between CoM and locomotion in living birds. This chapter sought to link whole body CoM position to locomotor behaviour, in order to aid interpretation of CoM position in fossil species. Though the absence of a statistically significant difference in CoM position between locomotor groups was unexpected, it is useful to know that despite a wide

range of body plans and locomotor adaptations present within Aves, all possess fundamentally similar CoMs. This result perhaps underlines the need for caution when interpreting differences in CoM position in extinct species.

6.4. Improving CoM estimation in extinct taxa

Chapter 5 sought to develop a new method using mathematical shape fitting techniques to improve current estimates of CoM position in fossil taxa. This was achieved using a large dataset of living animals to quantify the relationship between skeletal and skin volume in body segments, producing quantitative relationships (Figure 5.1) which formed the basis of CoM predictions for extinct taxa (Figure 5.3). This study found that different body segments possessed significantly different ratios of skeletal to skin volume and therefore heterogeneous segment expansions were required across the body (Figure 5.1, Supplementary Information 5.2). This highlighted a problem with the use of previously established methods, which were originally designed for body mass estimation (e.g. Sellers et al., 2012) and assume a homogeneous expansion, when estimating whole body CoM (e.g. Bates et al., 2016, Sellers et al., 2017). Significant differences were also found between the bird and ‘reptile’ (i.e. crocodylian and lepidosaur) groups in the majority of segments (7 out of 11). That such differences are present between these relatively closely related groups suggests that application of mammal based expansion factors to extinct archosaurs is not the best approach (e.g. Bates et al., 2016, Sellers et al., 2017). However, the applicability of mammal versus bird versus reptile based expansion factors may arguably differ depending on the body plan of the specimen of interest. Large bodied, quadrupedal mammals with columnar limb postures may be good proxies for sauropods (Bates et al., 2016, Sellers et al., 2013), but are unlikely to be good analogues for large bodied, bipedal theropods (Sellers et al., 2017).

Contrary to initial expectations, the method established in Chapter 5 produces CoM positions that are notably different from those of Allen et al. (2013) (which used a subjective, manual shape fitting approach), and the margins of error are greater in all cases (Figure 5.3). This is particularly evident in the four long tailed taxa, mainly due to the large ‘all species’ expansion factor which was applied to the tail segments of all fossil models (Figure 5.1D, Figure 5.3). Nevertheless, the new methodology developed here offers numerous benefits over that of Allen et al. (2013), the most important being a quantitative grounding, based on closely related extant taxa. This not only enables quantification of likely CoM positions, but by assessing the variation present within extant species it can be used to inform appropriate error margins. This is in contrast to the manual shape fitting method of Allen et al. (2013), where maximum and minimum skin outlines were created subjectively. The considerable error margins calculated for the new method suggest that some previous approaches have been overly conservative in the past when predicting the potential biological variability present in skin outlines (Allen et al., 2013); a problem which can be avoided by grounding estimations in data from living species. This suggests that the biological conclusions drawn by previous studies should be viewed with caution. The substantial margins of error present around the CoM positions predicted here indicate the substantial biological variability present in skeleton to skin ratio, even within groups which are relatively closely related. This casts further doubts on the validity of assuming extinct dinosaurs had skeleton to skin ratios equivalent to modern mammals (e.g. Bates et al., 2016, Sellers et al., 2017). However, it should be noted that some of these previous studies studying CoM evolution through time using mathematical shape fitting methods (Bates et al., 2016) have included large error margins around CoM estimates in order to better acknowledge the uncertainty present, even when using a quantitative basis for reconstructions. This is the approach which should be adopted moving forward, in order to acknowledge the maximum error present in reconstructions of mass properties in fossil species. The CoM positions predicted and the

associated error bars must then be used together to inform any conclusions about the biology of the specimens of interest.

The new method developed in Chapter 5 incorporates the best features of previous digital methods (easy to share and manipulate data; grounded in an extant dataset enabling well defined error margins; and the objective generation of segment mass properties), and also adds new features (an extensive dataset of closely related taxa; and segment specific relationships which are designed to estimate CoM). However, further work is required in order for this method to be confidently applied to series of fossil taxa to investigate trends in CoM position through time. Before any application, the dataset used here should be expanded. Though 48 specimens represents by far the largest dataset for a volumetric study of this kind to date, it is a small number of species to capture the full extent of the variation present within archosaurs and lizards. The absence of large bodied, mature ratite specimens is a particular problem. Additionally, better representation of groups whose members display considerable variation in body plan, such as the Galliformes, would also increase the robustness of the resulting relationships. It may also be worthwhile to explore other options for generating skeleton volumes. Though convex hulls are easy to objectively generate, they include considerable empty space around many bones, a factor which may be adversely affecting the relationships between skeletal and skin volume. For example, using alpha shapes would generate more realistic values for bone volume, which may result in tighter fitting relationships. However, the subjectivity within the alpha shape method would pose additional problems which would require addressing.

6.5. References

- ALLEN, V., HUTCHINSON, J. R., BATES, K. T. & LI, Z. 2013. Linking the evolution of body shape and locomotor biomechanics in bird-line archosaurs. *Nature*, 497, 104-107.
- ALLEN, V., PAXTON, H. & HUTCHINSON, J. R. 2009. Variation in center of mass estimates for extant sauropsids and its importance for reconstructing inertial properties of extinct archosaurs. *Anatomical Record*, 292, 1442-1461.
- BATES, K. T., MANNION, P. D., FALKINGHAM, P. L., BRUSATTE, S. L., HUTCHINSON, J. R., OTERO, A., SELLERS, W. I., SULLIVAN, C., STEVENS, K. A. & ALLEN, V. 2016. Temporal and phylogenetic evolution of the sauropod dinosaur body plan. *Royal Society Open Science*, 3, 150636.
- CLEMENTE, C. J. 2014. The evolution of bipedal running in lizards suggests a consequential origin may be exploited in later lineages. *Evolution*, 68, 2171-2183.
- HEERS, A. M. & DIAL, K. P. 2015. Wings versus legs in the avian bauplan: Development and evolution of alternative locomotor strategies. *Evolution*, 69, 305-320.
- HENDERSON, D. M. 2003. Effects of stomach stones on the buoyancy and equilibrium of a floating crocodilian: A computational analysis. *Canadian Journal of Zoology*, 81, 1346-1357.
- HENDERSON, D. M. 2006. Burly gaits; centers of mass, stability, and the trackways of sauropod dinosaurs. *Journal of Vertebrate Paleontology*, 26, 907-921.
- NAUWELAERTS, S., ALLEN, W. A., LANE, J. M. & CLAYTON, H. M. 2011. Inertial properties of equine limb segments. *Journal of Anatomy*, 218, 500-509.
- SELLERS, W. I., HEPWORTH-BELL, J., BRASSEY, C. A., EGERTON, V. M., MANNING, P. L., FALKINGHAM, P. L. & BATES, K. T. 2012. Minimum convex hull mass estimations of complete mounted skeletons. *Biology Letters*, 8, 842-845.
- SELLERS, W. I., MARGETTS, L., CORIA, R. A. & MANNING, P. L. 2013. March of the titans: The locomotor capabilities of sauropod dinosaurs. *PLoS ONE*, 8, 1-21.
- SELLERS, W. I., POND, S. B., BRASSEY, C. A., MANNING, P. L. & BATES, K. T. 2017. Investigating the running abilities of *Tyrannosaurus rex* using stress-constrained multibody dynamic analysis. *PeerJ*, 5, e3420.
- THOMAS, A. L. R. & TAYLOR, G. K. 2001. Animal flight dynamics I. Stability in gliding flight. *Journal of Theoretical Biology*, 212, 399-424.

CHAPTER 7 - CONCLUSION

The key theme running throughout this thesis was methods for CoM estimation. Chapter 2 successfully tested a number of different methods for CoM determination in whole biological specimens. Digital modelling and the scales methodology were both found to be highly accurate and repeatable, but the digital method offered significant logistical benefits for application to biological specimens. Proceeding with a digital modelling approach, the impacts of different modelling assumptions and levels of model detail were assessed using extensive datasets and in some cases, previously unavailable data (e.g. on integument mass properties). The errors associated with modelling assumptions (e.g. the inclusion of air cavities or integument) were identified as being small. These data can be used to inform the level of detail required by future studies using digital modelling in extant taxa. Following on from work modelling CoM position in extant taxa, Chapter 5 sought to develop an improved methodology for estimating CoM in fossil species. An extensive dataset of extant sauropsids was used to quantify skeleton to skin volume ratio, forming the foundation of a new volumetric modelling method. The estimates produced by this method for a sample of dinosaur taxa were found to disagree with previously published work, in addition to being accompanied by larger error margins.

This thesis also sought to quantify links between CoM and locomotion in Chapter 4, with the aim of enabling better interpretation of the biological meaning behind predictions of CoM in extinct taxa. However, contrary to my hypotheses, no significant differences were found in CoM position between birds of different locomotor types. The substantial scatter present in the three locomotor groups identified here speak to the considerable variation present in the avian body plan. Though 27 avian orders were sampled, this is a relatively small sample to cover the full extent of body plan variation across Aves. Additionally, this sample was not

large enough to enable statistical investigation of potential differences between more specific locomotor groups. Future work plans to investigate the links between segment proportions and locomotor type in birds, potentially forming an alternative basis for reconstructing locomotor behaviours in extinct species.

In summary, this thesis successfully explored methodologies for CoM estimation, concluding that digital approaches offered good levels of accuracy alongside practical benefits, making it the most suitable approach for application to extant taxa. Methodological variations on this method were then explored to investigate the extent of the impact of factors such as air cavities and integument on whole body CoM in birds. Having quantified the associated errors, the digital methodology was applied to a range of species across Aves, but was unsuccessful in establishing statistically significant links between whole body CoM position and locomotor type. Finally, a new method was developed for estimating CoM position in fossil taxa. This new method offered greater objectivity than previously published methods, and a considerable quantitative grounding in data from extant taxa. However, the resulting error bars were substantial, and predicted CoM differed considerably to previously published estimates. The implications of this new method on the biological conclusions of previous studies is yet to be understood, however the results of previous studies should be interpreted with caution. This thesis provides the foundation for further work to continue to build towards better methods for CoM estimation in extinct taxa, and more confident biological interpretations of any resulting predictions.

THESIS REFERENCES

- ALEXANDER, D. E., GONG, E., MARTIN, L. D., BURNHAM, D. A. & FALK, A. R. 2010. Model tests of gliding with different hindwing configurations in the four-winged dromaeosaurid *Microraptor gui*. *Proceedings of the National Academy of Sciences of the United States of America*, 107, 2972-2976.
- ALEXANDER, R. M. 1983. *Animal Mechanics*, London, Blackwell Scientific.
- ALEXANDER, R. M. 1985. Mechanics of posture and gait of some large dinosaurs. *Zoological Journal of the Linnean Society*, 83, 1-25.
- ALEXANDER, R. M. 2006. Dinosaur biomechanics. *Proceedings of the Royal Society B: Biological Sciences*, 273, 1849-1855.
- ALLEN, V., ELSEY, R. M., JONES, N., WRIGHT, J. & HUTCHINSON, J. R. 2010. Functional specialization and ontogenetic scaling of limb anatomy in Alligator mississippiensis. *Journal of Anatomy*, 216, 423-445.
- ALLEN, V., HUTCHINSON, J. R., BATES, K. T. & LI, Z. 2013. Linking the evolution of body shape and locomotor biomechanics in bird-line archosaurs. *Nature*, 497, 104-107.
- ALLEN, V., PAXTON, H. & HUTCHINSON, J. R. 2009. Variation in center of mass estimates for extant sauropsids and its importance for reconstructing inertial properties of extinct archosaurs. *Anatomical Record*, 292, 1442-1461.
- AMIT, T., GOMBERG, B. R., MILGRAM, J. & SHAHAR, R. 2009. Segmental inertial properties in dogs determined by magnetic resonance imaging. *Veterinary Journal*, 182, 94-99.
- AMMANN, G. A. 1937. Number of Contour Feathers of *Cygnus* and *Xanthocephalus*. *The Auk*, 54, 201-2.
- ANDERSON, J. F., HALL-MARTIN, A. & RUSSELL, D. A. 1985. Long-bone circumference and weight in mammals, birds and dinosaurs. *Journal of Zoology*, 207, 53-61.
- ANDRADA, E., NYAKATURA, J. A., BERGMANN, F. & BLICKHAN, R. 2013. Adjustments of global and local hindlimb properties during terrestrial locomotion of the Common Quail (*Coturnix coturnix*). *Journal of Experimental Biology*, 216, 3906-3916.
- ATTWELLS, R. L., BIRRELL, S. A., HOOPER, R. H. & MANSFIELD, N. J. 2006. Influence of carrying heavy loads on soldiers' posture, movements and gait. *Ergonomics*, 49, 1527-1537.
- BASU, C., FALKINGHAM, P. L. & HUTCHINSON, J. R. 2016. The extinct, giant giraffid *Sivatherium giganteum*: Skeletal reconstruction and body mass estimation. *Biology Letters*, 12.
- BATES, K. T., BENSON, R. B. J. & FALKINGHAM, P. L. 2012. A computational analysis of locomotor anatomy and body mass evolution in Allosauroidea (Dinosauria: Theropoda). *Paleobiology*, 38, 486-507.
- BATES, K. T., FALKINGHAM, P. L., BREITHAUPT, B. H., HODGETTS, D., SELLERS, W. I. & MANNING, P. L. 2009a. How big was 'Big Al'? Quantifying the effect of soft tissue and

- osteological unknowns on mass predictions for *Allosaurus* (Dinosauria, Theropoda). *Palaeontologia Electronica*, 12, 1-33.
- BATES, K. T., FALKINGHAM, P. L., MACAULAY, S., BRASSEY, C. & MAIDMENT, S. C. R. 2015. Downsizing a giant: re-evaluating *Dreadnoughtus* body mass. *Biology Letters*, 11, 20150215.
- BATES, K. T., MANNING, P. L., HODGETTS, D. & SELLERS, W. I. 2009b. Estimating Mass Properties of Dinosaurs Using Laser Imaging and 3-D Computer Modelling. *PLoS ONE*, 4, 1-26.
- BATES, K. T., MANNION, P. D., FALKINGHAM, P. L., BRUSATTE, S. L., HUTCHINSON, J. R., OTERO, A., SELLERS, W. I., SULLIVAN, C., STEVENS, K. A. & ALLEN, V. 2016. Temporal and phylogenetic evolution of the sauropod dinosaur body plan. *Royal Society Open Science*, 3, 150636.
- BATES, K. T., SELLERS, W. I., MANNING, P. L. & MARGETTS, L. 2010. Sensitivity analysis in evolutionary robotic simulations of bipedal dinosaur running. *Journal of Vertebrate Paleontology*, 30, 458-466.
- BLACKBURN, T. M. & GASTON, K. J. 1994. The Distribution of Body Sizes of the World's Bird Species. *Oikos*, 70, 127-130.
- BRAMWELL, C. D. & WHITFIELD, G. R. 1974. Biomechanics of *Pteranodon*. *Philosophical Transactions of the Royal Society of London B: Biological Sciences*, 267, 503-581.
- BRAND, T. S., JORDaan, J. W., BHIYA, C. S. & AUCAMP, B. B. 2010. Effect of slaughter age and sex on the production output of South African Black ostriches. *British Poultry Science*, 51, 510-514.
- BRASSEY, C. A. & GARDINER, J. D. 2015. An advanced shape-fitting algorithm applied to quadrupedal mammals: improving volumetric mass estimates. *Royal Society Open Science*, 2.
- BRASSEY, C. A., HOLDAWAY, R. N., PACKHAM, A. G., ANNÉ, J., MANNING, P. L. & SELLERS, W. I. 2013. More than One Way of Being a Moa: Differences in Leg Bone Robustness Map Divergent Evolutionary Trajectories in Dinornithidae and Emeidae (Dinornithiformes). *PLoS ONE*, 8, 1-10.
- BRASSEY, C. A., MAIDMENT, S. C. R. & BARRETT, P. M. 2015. Body mass estimates of an exceptionally complete Stegosaurus (Ornithischia: Thyreophora): comparing volumetric and linear bivariate mass estimation methods. *Biology Letters*, 11, 1-5.
- BRASSEY, C. A., O'MAHONEY, T. G., CHAMBERLAIN, A. T. & SELLERS, W. I. 2018. A volumetric technique for fossil body mass estimation applied to *Australopithecus afarensis*. *Journal of Human Evolution*, 115, 47-64.
- BRASSEY, C. A., O'MAHONEY, T. G., KITCHENER, A. C., MANNING, P. L. & SELLERS, W. I. 2016. Convex-hull mass estimates of the dodo (*Raphus cucullatus*): application of a CT-based mass estimation technique. *PeerJ*, 4, e1432.
- BRASSEY, C. A. & SELLERS, W. I. 2014. Scaling of convex hull volume to body mass in modern primates, non-primate mammals and birds. *PLoS ONE*, 9, 1-12.

- BRODKORB, P. 1955. Number of feathers and weights of various systems in a bald eagle. *The Wilson Bulletin*, 67, 142.
- BRUDERER, B., PETER, D., BOLDT, A. & LIECHTI, F. 2010. Wing-beat characteristics of birds recorded with tracking radar and cine camera. *Ibis*, 152, 272-291.
- BUCHNER, H. H. F., SAVELBERG, H. H. C. M., SCHAMHARDT, H. C. & BARNEVELD, A. 1997. Inertial properties of Dutch Warmblood horses. *Journal of Biomechanics*, 30, 653-658.
- CAMPIONE, N. E. 2017. Extrapolating body masses in large terrestrial vertebrates NICOLÁS E. CAMPIONE EXTRAPOLATING BODY MASSES. *Paleobiology*, 43, 693-699.
- CAMPIONE, N. E. & EVANS, D. C. 2012. A universal scaling relationship between body mass and proximal limb bone dimensions in quadrupedal terrestrial tetrapods. *BMC Biology*, 10, 1-22.
- CAMPIONE, N. E., EVANS, D. C., BROWN, C. M. & CARRANO, M. T. 2014. Body mass estimation in non-avian bipeds using a theoretical conversion to quadruped stylopodial proportions. *Methods in Ecology & Evolution*, 5, 913-923.
- CARRANO, M. T. & BIEWENER, A. A. 1999. Experimental alteration of limb posture in the chicken (*Gallus gallus*) and its bearing on the use of birds as analogs for dinosaur locomotion. *Journal of Morphology*, 240, 237-249.
- CHANDLER, R. F., CLAUSER, C. E., MCCONVILLE, J. T., REYNOLDS, H. M. & YOUNG, J. W. 1975. Investigation of Inertial Properties of Human Body Segments. *AMRL Technical Report No. 74-137, Aerospace Medical Research Laboratories, Wright-Patterson Airforce Base, OH*.
- CHATTERJEE, S. & TEMPLIN, R. J. 2007. Biplane wing planform and flight performance of the feathered dinosaur *Microraptor gui*. *Proceedings of the National Academy of Sciences of the United States of America*, 104, 1576-1580.
- CHRISTIANSEN, P. & BONDE, N. 2002. Limb proportions and avian terrestrial locomotion. *Journal fur Ornithologie*, 143, 356-371.
- CLEMENTE, C. J. 2014. The evolution of bipedal running in lizards suggests a consequential origin may be exploited in later lineages. *Evolution*, 68, 2171-2183.
- CLEMENTE, C. J., BISHOP, P. J., NEWMAN, N. & HOCKNULL, S. A. 2018. Steady bipedal locomotion with a forward situated whole-body centre of mass: the potential importance of temporally asymmetric ground reaction forces. *Journal of Zoology*, 304, 193-201.
- CLOSE, R. A. & RAYFIELD, E. J. 2012. Functional morphometric analysis of the furcula in Mesozoic birds. *PLoS ONE*, 7, e36664.
- COLBERT, E. H. 1962. The Weights of Dinosaurs. *American Museum Novitates*, 2076, 1-16.
- COLLINS, K. E., KIEPPER, B. H., RITZ, C. W., MCLENDON, B. L. & WILSON, J. L. 2014. Growth, livability, feed consumption, and carcass composition of the Athens Canadian

- Random Bred 1955 meat-type chicken versus the 2012 high-yielding Cobb 500 broiler. *Poultry Science*, 93, 2953-2962.
- COOPER, S. 2002. Seasonal metabolic acclimatization in mountain chickadees and juniper titmice. *Physiological and Biochemical Zoology: Ecological and Evolutionary Approaches*, 75, 386-395.
- CROMPTON, R. H., LI, Y., ALEXANDER, R. M., WANG, W. & GUNTHER, M. M. 1996. Segment inertial properties of primates: New techniques for laboratory and field studies of locomotion. *American Journal of Physical Anthropology*, 99, 547-570.
- DAAN, S., MASMAN, D. & GROENEWOLD, A. 1990. Avian basal metabolic rates: their association with body composition and energy expenditure in nature. *American Journal of Physiology: Regulatory, Integrative & Comparative Physiology*, 28, R333.
- DEMPSTER, W. T. 1955. Space Requirements of the Seated Operator. *WADC Technical Report No. 55-159, Wright Air Development Centre, Wright-Patterson Airforce Base, OH*.
- DEMPSTER, W. T. & GAUGHRAN, G. R. L. 1967. Properties of body segments based on size and weight. *American Journal of Anatomy*, 120, 33-54.
- DESROCHERS, D. W., SILBERNAGLE, M. D., NADIG, A. & REED, J. M. 2010. Body size, growth, and feather mass of the endangered Hawaiian moorhen (*Gallinula chloropus sandvicensis*). *Pacific Science*, 64, 327-333.
- DIAL, K. P. 2003. Wing-assisted incline running and the evolution of flight. *Science*, 299, 402-404.
- DUNCKER, H. R. 1971. The lung air sac system of birds. A contribution to the functional anatomy of the respiratory apparatus. *Advances in Anatomy, Embryology and Cell Biology*, 45, 7-171.
- DYKE, G., PALMER, C., NAISH, D., GANAPATHISUBRAMANI, B., DE KAT, R. & VAN DER KINDERE, J. 2013. Aerodynamic performance of the feathered dinosaur *Microraptor* and the evolution of feathered flight. *Nature Communications*, 4, 1-9.
- ESHBACH, O. W., TAPLEY, B. D. & POSTON, T. R. 1990. *Eshbach's Handbook of Engineering Fundamentals*, New York, Wiley.
- FARLOW, J. O., SMITH, M. B. & ROBINSON, J. M. 1995. Body Mass, Bone "Strength Indicator" and Cursorial Potential of *Tyrannosaurus rex*. *Journal of Vertebrate Paleontology*, 15, 713-725.
- FEDAK, M. A., HEGLUND, N. C. & TAYLOR, C. R. 1982. Energetics and mechanics of terrestrial locomotion. II. Kinetic energy changes of the limbs and body as a function of speed and body size in birds and mammals. *Journal of Experimental Biology*, 97, 23-40.
- FIELD, D. J., LYNNER, C., BROWN, C. & DARROCH, S. A. F. 2013. Skeletal correlates for body mass estimation in modern and fossil flying birds. *Plos One*, 8, e82000-e82000.
- GATESY, S. M. 1990. Caudofemoral musculature and the evolution of theropod locomotion. *Paleobiology*, 16, 170-186.

- GATESY, S. M. 1999. Guineafowl hind limb function. II: Electromyographic analysis and motor pattern evolution. *Journal of Morphology*, 240, 127-142.
- GATESY, S. M., BÄKER, M. & HUTCHINSON, J. R. 2009. Constraint-based exclusion of limb poses for reconstructing theropod dinosaur locomotion. *Journal of Vertebrate Paleontology*, 29, 535-544.
- GATESY, S. M. & BIEWENER, A. A. 1991. Bipedal locomotion: effects of speed, size and limb posture in birds and humans. *Journal of Zoology*, 224, 127-147.
- GATESY, S. M. & DIAL, K. P. 1996. Locomotor modules and the evolution of avian flight. *Evolution*, 50, 331-340.
- GATESY, S. M. & MIDDLETON, K. M. 1997. Bipedalism, flight, and the evolution of theropod locomotor diversity. *Journal of Vertebrate Paleontology*, 17, 308-329.
- GOETZ, J. E., DERRICK, T. R., PEDERSEN, D. R., ROBINSON, D. A., CONZEMIUS, M. G., BAER, T. E. & BROWN, T. D. 2008. Hip joint contact force in the emu (*Dromaius novaehollandiae*) during normal level walking. *Journal of Biomechanics*, 41, 770-778.
- GREGORY, W. K. 1905. The Weight of the Brontosaurus. *Science*, 22, 572.
- GROSSI, B., IRIARTE-DÍAZ, J., LARACH, O., CANALS, M. & VÁSQUEZ, R. A. 2014. Walking like dinosaurs: Chickens with artificial tails provide clues about non-avian theropod locomotion. *PLoS ONE*, 9.
- HARTMAN, F. A. 1961. *Locomotor Mechanisms of Birds*, City of Washington, Smithsonian Miscellaneous Collections.
- HEERS, A. M. & DIAL, K. P. 2015. Wings versus legs in the avian bauplan: Development and evolution of alternative locomotor strategies. *Evolution*, 69, 305-320.
- HENDERSON, D. M. 1999. Estimating the masses and centers of mass of extinct animals by 3-D mathematical slicing. *Paleobiology*, 25, 88-106.
- HENDERSON, D. M. 2003. Effects of stomach stones on the buoyancy and equilibrium of a floating crocodilian: A computational analysis. *Canadian Journal of Zoology*, 81, 1346-1357.
- HENDERSON, D. M. 2004. Tipsy punters: Sauropod dinosaur pneumaticity, buoyancy and aquatic habits. *Proceedings of the Royal Society B: Biological Sciences*, 271, S180-S183.
- HENDERSON, D. M. 2006. Burly gaits; centers of mass, stability, and the trackways of sauropod dinosaurs. *Journal of Vertebrate Paleontology*, 26, 907-921.
- HENDERSON, D. M. 2010. Pterosaur body mass estimates from three-dimensional mathematical slicing. *Journal of Vertebrate Paleontology*, 30, 768-785.
- HENDERSON, D. M. 2018. A buoyancy, balance and stability challenge to the hypothesis of a semi-aquatic Spinosaurus Stromer, 1915 (Dinosauria: Theropoda). *PeerJ*, 6, e5409.

- HENDERSON, D. M. & NICHOLLS, R. 2015. Balance and Strength—Estimating the Maximum Prey-Lifting Potential of the Large Predatory Dinosaur *Carcharodontosaurus saharicus*. *The Anatomical Record*, 298, 1367-1375.
- HENDERSON, D. M. & SNIVELY, E. 2004. Tyrannosaurus en pointe: allometry minimized rotational inertia of large carnivorous dinosaurs. *Proceedings of the Royal Society B: Biological Sciences*, 271, S57-S60.
- HOBBS, S. J., RICHARDS, J. & CLAYTON, H. M. 2014. The effect of centre of mass location on sagittal plane moments around the centre of mass in trotting horses. *Journal of Biomechanics*, 47, 1278-1286.
- HOPPS, E. C. 2002. Information on waterfowl feather characteristics. *Transactions of the Illinois State Academy of Science*, 95, 229-237.
- HUTCHINSON, J. R. 2004a. Biomechanical modeling and sensitivity analysis of bipedal running ability. I. Extant taxa. *Journal of Morphology*, 262, 421-440.
- HUTCHINSON, J. R. 2004b. Biomechanical modeling and sensitivity analysis of bipedal running ability. II. Extinct taxa. *Journal of Morphology*, 262, 441-461.
- HUTCHINSON, J. R. 2011. On the inference of function from structure using biomechanical modelling and simulation of extinct organisms. *Biology Letters*, 8, 115-118.
- HUTCHINSON, J. R. & ALLEN, V. 2009. The evolutionary continuum of limb function from early theropods to birds. *Naturwissenschaften*, 96, 423-448.
- HUTCHINSON, J. R., BATES, K. T., MOLNAR, J., ALLEN, V. & MAKOVICKY, P. J. 2011. A Computational Analysis of Limb and Body Dimensions in *Tyrannosaurus rex* with Implications for Locomotion, Ontogeny, and Growth. *PLoS ONE*, 6, 1-20.
- HUTCHINSON, J. R., NG-THOW-HING, V. & ANDERSON, F. C. 2007. A 3D interactive method for estimating body segmental parameters in animals: Application to the turning and running performance of *Tyrannosaurus rex*. *Journal of Theoretical Biology*, 246, 660-680.
- JETZ, W., THOMAS, G. H., JOY, J. B., HARTMANN, K. & MOOERS, A. O. 2012. The global diversity of birds in space and time. *Nature*, 491, 444-448.
- JONES, T. D., FARLOW, J. O., RUBEN, J. A., HENDERSON, D. M. & HILLENIUS, W. J. 2000a. Cursoriality in bipedal archosaurs. *Nature*, 406, 716-718.
- JONES, T. D., FARLOW, J. O., RUBEN, J. A., HENDERSON, D. M. & HILLENIUS, W. J. 2000b. Cursoriality in bipedal archosaurs. *Nature*, 406, 716.
- KAMBIC, R. E., BIEWENER, A. A. & PIERCE, S. E. 2017. Experimental determination of three-dimensional cervical joint mobility in the avian neck. *Frontiers in Zoology*, 14.
- KARDONG, K. V. 2012. *Vertebrates: Comparative Anatomy, Function, Evolution*, New York, McGraw-Hill.

- KILBOURNE, B. M. 2013. On birds: Scale effects in the neognath hindlimb and differences in the gross morphology of wings and hindlimbs. *Biological Journal of the Linnean Society*, 110, 14-31.
- KIM, E. J., WOLF, M., ORTEGA-JIMENEZ, V. M., CHENG, S. H. & DUDLEY, R. 2014. Hovering performance of Anna's hummingbirds (*Calypte anna*) in ground effect. *Journal of The Royal Society Interface*, 11, 20140505.
- KLAASSEN, M. 1995. Moult and basal metabolic costs in males of two subspecies of stonechats: the European *Saxicola torquata rubicula* and the East African *S. t. axillaris*. *Oecologia*, 104, 424-432.
- KOEHL, M. A. R., EVANGELISTA, D. & YANG, K. 2011. Using physical models to study the gliding performance of extinct animals. *Integrative And Comparative Biology*, 51, 1002-1018.
- KRINGS, M., NYAKATURA, J. A., BOUMANS, M. L. L. M., FISCHER, M. S. & WAGNER, H. 2017. Barn owls maximize head rotations by a combination of yawing and rolling in functionally diverse regions of the neck. *Journal of Anatomy*, 231, 12-22.
- LEESON, S. & WALSH, T. 2007. Feathering in commercial poultry I. Feather growth and composition. *World's Poultry Science Journal*, 60, 42-51.
- LEPHART, S. A. 1984. Measuring the inertial properties of cadaver segments. *Journal of Biomechanics*, 17, 537-543.
- LILL, A., BOX, J. & BALDWIN, J. 2006. Do metabolism and contour plumage insulation vary in response to seasonal energy bottlenecks in superb fairy-wrens? *Australian Journal of Zoology*, 54, 23-30.
- LINDHE NORBERG, U. M. 2002. Structure, form, and function of flight in engineering and the living world. *Journal of Morphology*, 252, 52-81.
- LONGRICH, N. R., VINTHER, J., MENG, Q., LI, Q. & RUSSELL, A. P. 2012. Primitive wing feather arrangement in *Archaeopteryx lithographica* and *Anchiornis huxleyi*. *Current Biology*, 22, 2262-2267.
- LOVERRO, K. L., BROWN, T. N., COYNE, M. E. & SCHIFFMAN, J. M. 2015. Use of body armor protection with fighting load impacts soldier performance and kinematics. *Applied Ergonomics*, 46, 168-175.
- LOVVORN, J. R. & JONES, D. R. 1991. Body mass, volume, and buoyancy of some aquatic birds, and their relation to locomotor strategies. *Canadian Journal of Zoology*, 69, 2888-2892.
- MACAULAY, S., HUTCHINSON, J. R. & BATES, K. T. 2017. A quantitative evaluation of physical and digital approaches to centre of mass estimation. *Journal of Anatomy*, 231, 758-775.
- MAIDMENT, S. C. R., HENDERSON, D. M. & BARRETT, P. M. 2014. What drove reversions to quadrupedality in ornithischian dinosaurs? Testing hypotheses using centre of mass modelling. *Naturwissenschaften*, 101, 989-1001.

- MAINA, J. N. 2017. Functional Design of the Mature Avian Respiratory System. In: MAINA, J. N. (ed.) *The Biology of the Avian Respiratory System: Evolution, Development, Structure and Function*. Cham: Springer International Publishing.
- MALLISON, H. 2010. The digital Plateosaurus I: body mass, mass distribution, and posture assessed using CAD and CAE on a digitally mounted complete skeleton. *Palaeontologia Electronica*, 13, 1-26.
- MALLISON, H. 2014. Osteoderm distribution has low impact on the centre of mass of stegosaurs. *Foss. Rec.*, 17, 33-39.
- MARTIN-SILVERSTONE, E., VINCZE, O., MCCANN, R., JONSSON, C. H. W., PALMER, C., KAISER, G. & DYKE, G. 2015. Exploring the relationship between skeletal mass and total body mass in birds. *PLoS ONE*, 10, e0141794.
- MCGOWAN, C. 1979. Selection Pressure for High Body Temperatures: Implications for Dinosaurs. *Paleobiology*, 5, 285-295.
- MORRIS, C. A., HARRIS, S. D., MAY, S. G., JACKSON, T. C., HALE, D. S., MILLER, R. K., KEETON, J. T., ACUFF, G. R., LUCIA, L. M. & SAVELL, J. W. 1995. Ostrich slaughter and fabrication: 1. Slaughter yields of carcasses and effects of electrical stimulation on post-mortem pH. *Poultry science*, 74, 1683-1687.
- MOTANI, R. 2001. Estimating body mass from silhouettes: Testing the assumption of elliptical body cross-sections. *Paleobiology*, 27, 735-750.
- MYERS, M. J. & STEUDEL, K. 1997. Morphological conservation of limb natural pendular period in the domestic dog (*Canis familiaris*): Implications for locomotor energetics. *Journal of Morphology*, 234, 183-196.
- NAUWELAERTS, S., ALLEN, W. A., LANE, J. M. & CLAYTON, H. M. 2011. Inertial properties of equine limb segments. *Journal of Anatomy*, 218, 500-509.
- NAVEENA, B. M., SEN, A. R., MUTHUKUMAR, M., GIRISH, P. S., PRAVEEN KUMAR, Y. & KIRAN, M. 2013. Carcass characteristics, composition, physico-chemical, microbial and sensory quality of emu meat. *British Poultry Science*, 54, 329-336.
- NIGG, B. M. & HERZOG, W. 2007. *Biomechanics of the musculo-skeletal system*, West Sussex, John Wiley & Sons.
- NUDDS, R. L. & DYKE, G. J. 2010. Narrow primary feather rachises in *Confuciusornis* and *Archaeopteryx* suggest poor flight ability. *Science*, 328, 887-889.
- NYAKATURA, J. A., ALLEN, V. R., LAUSTRÖER, J., ANDIKFAR, A., DANCZAK, M., ULLRICH, H. J., HUFENBACH, W., MARTENS, T. & FISCHER, M. S. 2015. A three-dimensional skeletal reconstruction of the stem amniote *Orobates pabsti* (Diadectidae): Analyses of body mass, centre of mass position, and joint mobility. *PLoS ONE*, 10, e0137284.
- NYAKATURA, J. A., ANDRADA, E., GRIMM, N., WEISE, H. & FISCHER, M. S. 2012. Kinematics and center of mass mechanics during terrestrial locomotion in Northern Lapwings (*Vanellus vanellus*, Charadriiformes). *Journal of Experimental Zoology Part A: Ecological Genetics and Physiology*, 317, 580-594.

- OSTROM, J. H. 1974. *Archaeopteryx* and the origin of flight. *Quarterly Review of Biology*, 49, 27-47.
- ÖZKAYA, N., NORDIN, M., GOLDSHEYDER, D. & LEGER, D. 2012. Statics: Systems in Equilibrium. *Fundamentals of Biomechanics: Equilibrium, Motion, and Deformation*. New York, NY: Springer New York.
- PADIAN, K. & CHIAPPE, L. M. 1998. The origin and early evolution of birds. *Biological Reviews of the Cambridge Philosophical Society*, 73, 1-42.
- PARK, S. B., KIM, S. Y., HYEONG, J. H. & CHUNG, K. R. 2014. A study on the development of image analysis instrument and estimation of mass, volume and center of gravity using CT image in Korean. *Journal of Mechanical Science and Technology*, 28, 971-977.
- PAUL, G. S. 1997. Dinosaur Models: The Good, The Bad, and Using Them to Estimate the Mass of Dinosaurs. *Dinofest International Proceedings*, 129-142.
- PAXTON, H., TICKLE, P. G., RANKIN, J. W., CODD, J. R. & HUTCHINSON, J. R. 2014. Anatomical and biomechanical traits of broiler chickens across ontogeny. Part II. Body segment inertial properties and muscle architecture of the pelvic limb. *PeerJ*, 2, e831.
- PEYER, K. E., MORRIS, M. & SELLERS, W. I. 2015. Subject-specific body segment parameter estimation using 3D photogrammetry with multiple cameras. *PeerJ*, 3, e831.
- PICASSO, M. B. J. 2015. Ontogenetic Scaling of the Hindlimb Muscles of the Greater Rhea (*Rhea americana*). *Anatomia, Histologia, Embryologia*, 44, 452-459.
- POWERS, D. R. & NAGY, K. A. 1988. Field metabolic rate and food consumption by free-living Anna's hummingbirds (*Calypte anna*). *Physiological Zoology*, 61, 500-506.
- RAYNER, J. M. V. 1988. Form and Function in Avian Flight. In: JOHNSTON, R. F. (ed.) *Current Ornithology*. Boston, MA: Springer US.
- REID, B. & WILLIAMS, G. R. 1975. The Kiwi. In: KUSCHEL, G. (ed.) *Biogeography and Ecology in New Zealand*. Dordrecht: Springer Netherlands.
- REILLY, S. M., WILLEY, J. S., BIKNEVICIUS, A. R. & BLOB, R. W. 2005. Hindlimb function in the alligator: Integrating movements, motor patterns, ground reaction forces and bone strain of terrestrial locomotion. *Journal of Experimental Biology*, 208, 993-1009.
- REN, L. & HUTCHINSON, J. R. 2008. The three-dimensional locomotor dynamics of African (*Loxodonta africana*) and Asian (*Elephas maximus*) elephants reveal a smooth gait transition at moderate speed. *Journal of the Royal Society Interface*, 5, 195-211.
- ROSE, K. A., NUDDS, R. L. & CODD, J. R. 2016. Variety, sex and ontogenetic differences in the pelvic limb muscle architectural properties of leghorn chickens (*Gallus gallus domesticus*) and their links with locomotor performance. *Journal of Anatomy*, 228, 952-964.
- RUBENSON, J. & MARSH, R. L. 2009. Mechanical efficiency of limb swing during walking and running in Guinea Fowl (*Numida meleagris*). *Journal of Applied Physiology*, 106, 1618-1630.

- SALES, J., HORBAŃCZUK, J., DINGLE, J., COLEMAN, R. & SENSIK, S. 1999. Carcase characteristics of emus (*Dromaius novaehollandiae*). *British Poultry Science*, 40, 145-147.
- SALES, J., NAVARRO, J. L., BELLIS, L., MANERO, A., LIZURUME, M. & MARTELLA, M. B. 1997. Carcase and component yields of rheas. *British Poultry Science*, 38, 378-380.
- SAVILE, O. 1957. Adaptive evolution in the avian wing. *Evolution*, 11, 212-224.
- SCHORGER, A. W. 1966. *The Wild Turkey. Its History and Domestication.*, Norman, University of Oklahoma Press.
- SELLERS, W. I., HEPWORTH-BELL, J., BRASSEY, C. A., EGERTON, V. M., MANNING, P. L., FALKINGHAM, P. L. & BATES, K. T. 2012. Minimum convex hull mass estimations of complete mounted skeletons. *Biology Letters*, 8, 842-845.
- SELLERS, W. I., MARGETTS, L., CORIA, R. A. & MANNING, P. L. 2013. March of the titans: The locomotor capabilities of sauropod dinosaurs. *PLoS ONE*, 8, 1-21.
- SELLERS, W. I., POND, S. B., BRASSEY, C. A., MANNING, P. L. & BATES, K. T. 2017. Investigating the running abilities of *Tyrannosaurus rex* using stress-constrained multibody dynamic analysis. *PeerJ*, 5, e3420.
- SMITH, N. C., JESPERS, K. J. & WILSON, A. M. 2010. Ontogenetic scaling of locomotor kinetics and kinematics of the ostrich (*Struthio camelus*). *Journal of Experimental Biology*, 213, 1347-1355.
- SNIVELY, E., O'BRIEN, H., HENDERSON, D. M., MALLISON, H., SURRING, L. A., BURNS, M. E., HOLTZ, J. T. R., RUSSELL, A. P., WITMER, L. M., CURRIE, P. J., HARTMAN, S. A. & COTTON, J. R. 2018. Lower rotational inertia and larger leg muscles indicate more rapid turns in tyrannosaurids than in other large theropods. *PeerJ Preprints*, 6, e27021v1.
- SPRINGS, E. & LEACH, D. 1986. Standardised technique for determining the centre of gravity of body and limb segments of horses. *Equine Veterinary Journal*, 18, 43-49.
- SUMMERS, R. W., UNDERHILL, L. G., NICOLL, M., RAE, R. & PIERSMA, T. 1992. Seasonal, size- and age-related patterns in body-mass and composition of purple sandpipers *Calidris maritima* in Britain. *Ibis*, 134, 346-354.
- SWANSON, D. L. 1991. Seasonal adjustments in metabolism and insulation in the dark-eyed junco. *Condor*, 538-545.
- TAYLOR, G. K. & THOMAS, A. L. R. 2002. Animal flight dynamics II. Longitudinal stability in flapping flight. *Journal of Theoretical Biology*, 214, 351-370.
- TOBALSKE, B. W. 2007. Biomechanics of bird flight. *Journal of Experimental Biology*, 210, 3135.
- THOMAS, A. L. R. & TAYLOR, G. K. 2001. Animal flight dynamics I. Stability in gliding flight. *Journal of Theoretical Biology*, 212, 399-424.

- TSERVENI, A. S. & YANNAKOPOULOS, A. L. 1988. Specific gravity, carcass fat and prediction of fatness in quail carcasses. *The Journal of Agricultural Science*, 111, 95-98.
- VERSTAPPEN, M., AERTS, P. & VAN DAMME, R. 2000. Terrestrial locomotion in the black-billed magpie: Kinematic analysis of walking, running and out-of-phase hopping. *Journal of Experimental Biology*, 203, 2159-2170.
- VILENSKY, J. A. 1979. Masses, centers-of-gravity, and moments-of-inertia of the body segments of the Rhesus Monkey (*Macaca mulatta*). *American Journal of Physical Anthropology*, 50, 57-65.
- WALTER, R. M. & CARRIER, D. R. 2002. Scaling of rotational inertia in murine rodents and two species of lizard. *Journal of Experimental Biology*, 205, 2135-2141.
- WANG, X. & CLARKE, J. A. 2015. The evolution of avian wing shape and previously unrecognized trends in covert feathering. *Proceedings of the Royal Society B: Biological Sciences*, 282.
- WANG, X., NUDDS, R. L. & DYKE, G. J. 2011. The primary feather lengths of early birds with respect to avian wing shape evolution. *Journal of Evolutionary Biology*, 24, 1226-1231.
- WARHAM, J. 1977. Wing loadings, wing shapes, and flight capabilities of procellariiformes. *New Zealand Journal of Zoology*, 4, 73-83.
- WETMORE, A. 1936. The number of contour feathers in passeriform and related birds. *The Auk*, 53, 159-169.
- WILLEY, J. S., BIKNEVICIUS, A. R., REILLY, S. M. & EARLS, K. D. 2004. The tale of the tail: Limb function and locomotor mechanics in Alligator mississippiensis. *Journal of Experimental Biology*, 207, 553-563.
- WITMER, L. M. 1995. The Extant Phylogenetic Bracket and the importance of reconstructing soft tissues in fossils. In: THOMASON, J. J. (ed.) *Functional Morphology in Vertebrate Paleontology*. Cambridge: Cambridge University Press.
- WOLF, P., RABEHL, N. & KAMPHUES, J. 2003. Investigations on feathering, feather growth and potential influences of nutrient supply on feathers' regrowth in small pet birds (canaries, budgerigars and lovebirds). *Journal of Animal Physiology and Animal Nutrition*, 87, 134-141.
- XU, X., ZHOU, Z., WANG, X., KUANG, X., ZHANG, F. & DU, X. 2003. Four-winged dinosaurs from China. *Nature*, 421, 335-340.
- YOUNG, J. W., PATEL, B. A. & STEVENS, N. J. 2007. Body mass distribution and gait mechanics in Fat-tailed Dwarf Lemurs (*Cheirogaleus medius*) and Patas Monkeys (*Erythrocebus patas*). *Journal of Human Evolution*, 53, 26-40.